Russian Original Vol. 31, No. 2, August, 1971
Translation published March, 1972

NE
RS

SOVIET ATOMIC ENERGY

АТОМНАЯ ЭНЕРГИЯ
(ATOMNAYA ÉNERGIYA)

TRANSLATED FROM RUSSIAN

CONSULTANTS BUREAU, NEW YORK

SOVIET ATOMIC ENERGY

Soviet Atomic Energy is a cover-to-cover translation of *Atomnaya Énergiya*, a publication of the Academy of Sciences of the USSR.

An arrangement with Mezhdunarodnaya Kniga, the Soviet book export agency, makes available both advance copies of the Russian journal and original glossy photographs and artwork. This serves to decrease the necessary time lag between publication of the original and publication of the translation and helps to improve the quality of the latter. The translation began with the first issue of the Russian journal.

Consultants Bureau journals appear about six months after the publication of the original Russian issue. For bibliographic accuracy, the English issue published by Consultants Bureau carries the same number and date as the original Russian from which it was translated. For example, a Russian issue published in December will appear in a Consultants Bureau English translation about the following June, but the translation issue will carry the December date. When ordering any volume or particular issue of a Consultants Bureau journal, please specify the date and, where applicable, the volume and issue numbers of the original Russian. The material you will receive will be a translation of that Russian volume or issue.

Subscription
$67.50 per volume (6 Issues)
2 volumes per year
(Add $5 for orders outside the United States and Canada.)

Single Issue: $30
Single Article: $15

CONSULTANTS BUREAU, NEW YORK AND LONDON

227 West 17th Street
New York, New York 10011

Davis House
8 Scrubs Lane
Harlesden, NW10 6SE
England

Published monthly. Second-class postage paid at Jamaica, New York 11431.

SOVIET ATOMIC ENERGY

A translation of *Atomnaya Énergiya*
Translation published March, 1972

Volume 31, Number 2 August, 1971

CONTENTS

CONTENTS

(continued)

CONTENTS

(continued)

The Russian press date (podpisano k pechati) of this issue was 8/4/1971. Publication therefore did not occur prior to this date, but must be assumed to have taken place reasonably soon thereafter.

OPTIMIZATION STUDIES OF FAST REACTORS

A. M. Kuz'min, Yu. V. Silaev,
V. V. Orlov, and V. V. Khromov

UDC 621.039.526

The selection of optimum characteristics of nuclear reactors requires involved considerations of thermophysical, safety, hydraulic, and other questions and is a complex multiparameter problem. When many parameters or equations are required for a fast reactor of the BN-350 type [1] a solution can be obtained by using the optimization procedure for fast reactors given by Khromov et al. [2].

Description of the Algorithm of the Program. The optimization complex includes neutron physics, safety, and thermotechnical reactor calculations and solves the following problem. Find the value of the control vector $\mathbf{u}\{u_1; u_2; \ldots u_q; , , , u_k\}$, satisfying the relation

$$u_{min} \leqslant u \leqslant u_{max} \tag{1}$$

for which some reactor characteristic $F_0(\varphi, \mathbf{u})$ has its optimum value (henceforth we will consider the minimum of F_0) and constraints on other quantities $F_\nu(\varphi, \mathbf{u})$ of the form

$$F_\nu(\varphi, \mathbf{u}) \leqslant A_\nu \quad (\nu = 1, 2, \ldots, p) \tag{2}$$

are satisfied under the condition that the reactor state variables $\varphi(r)\{\varphi^{(1)}; \varphi^{(2)}; \ldots \varphi^{(m)}\}^{(2)}$, such as neutron flux, temperature distribution, etc., satisfy known equations, and the quantities u_{min}, u_{max}, and A_ν are assumed known.

The constant thermal power of the reactor W, the form and properties of the nuclear fuel, coolant, and other reactor materials, the coolant temperature at the reactor outlet T_{out}, the fuel cycle parameters, the operating characteristics of the reactor including the time of fuel reprocessing, the load factor of the reactor, etc., are also assumed given.

The following parameters can be taken as components u_q of the control vector $\mathbf{u}$, where the subscript i distinguishes those parameters which can vary from one reactor region to another: the core height H, the height of the fuel element void for the collection of gaseous fission products $H_{g.p.}$, the thickness of individual reactor zones ΔR_i, the outside diameter of an unclad fuel rod $d_i^{(T)}$, the fuel element cladding thickness Δ_i^{cl}, the relative pitch of the triangular fuel element lattice h_i, the coolant velocity in a channel of the i-th zone for maximum heat release rate v_i^0, the fuel enrichment x_i, the relative fraction of absorbers for compensating reactivity ε_i^a, and the volume fraction of the fuel assembly wall in the reactor $\varepsilon_{a.w.}$.

The neutron physics calculations are performed in the two-group diffusion approximation for a one-dimensional cylindrical reactor with cross sections averaged over an 18-group neutron spectrum in each reactor zone, and the axial neutron leakage is taken into account by the parameter $\varkappa^2 = \pi^2/(H + 2\delta_{eff})^2$. The averaged microscopic cross sections and the effective and reflector savings δ_{eff} are calculated with the 18-4RZ-15 two-dimensional program [3].

The heat engineering calculation is restricted to an estimate of the maximum fuel element cladding temperatures, taking account of hot spots, and to a determination of the average temperature rise of the coolant in the reactor $\overline{\Delta T}_{cool}$. The calculation is performed under the assumption that there is no axial heat flow in the fuel elements. The calculation of the reliability of the fuel element cladding is carried out under the assumption that the fuel does not exert pressure on the cladding in the swelling process [4]. The maximum stress σ_a in a fuel assembly wall for a pressure drop Δp of the coolant over the height of the reactor is determined under the assumption that the thickness of an assembly is very much less than its dimension under the key.

Translated from Atomnaya Énergiya, Vol. 31, No. 2, pp. 83-88, August, 1971. Original article submitted July 22, 1970.

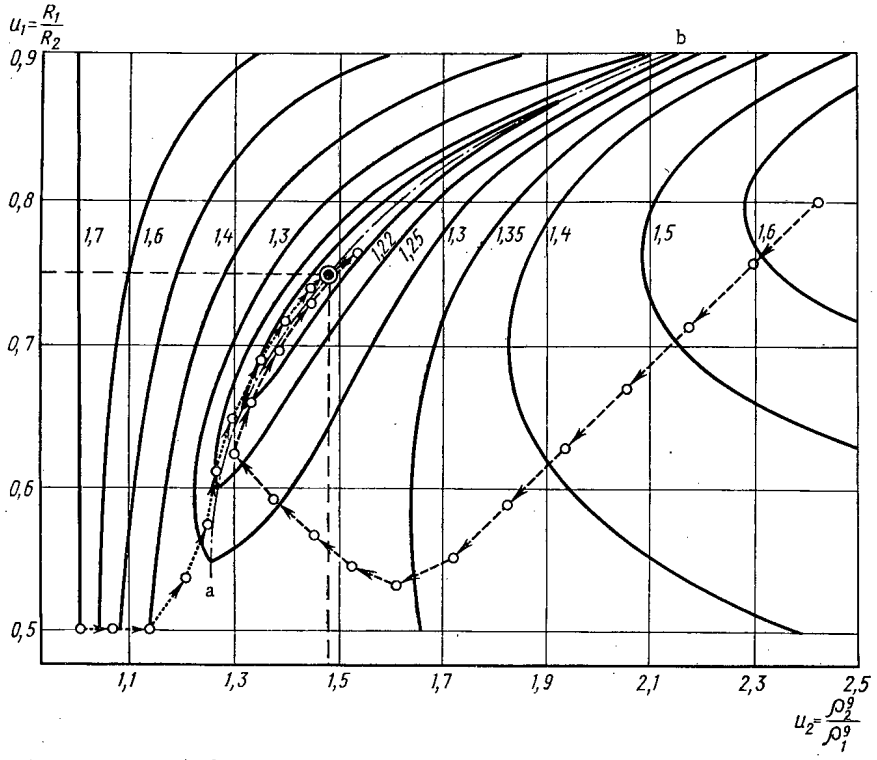

Fig. 1. Curves of K_r = const and gradient search for the minimum of the coefficient of nonuniformity of heat release. a-b is the projection of the crest of the surface $K_r(u_1, u_2)$ on the u_1-u_2 plane.

The program includes algorithms for thermophysical and safety calculations which permit the solution of optimization problems taking account of the constraints:

$$T_c^{max} \leqslant T_c^{per}; \quad \xi_{cl}^{max} \leqslant \xi_{cl}^{per},$$
$$T_{cl}^{max} \leqslant T_{cl}^{per}; \quad \sigma_a^{max} \leqslant \sigma_a^{per}, \tag{3}$$

where T_c^{per}, T_{cl}^{per}, ξ_{cl}^{per}, and σ_a^{per} are respectively the values of the maximum permissible temperatures at the center and in the cladding of a fuel element, the strain in the cladding, and the stress in an assembly. The program uses an iteration method based on perturbation theory and linear programming to search for the optimum variant automatically. The algorithm of the method is described in [5]. The problem admits a solution when the number of constraints of type (2) does not exceed 36 and the number of control parameters is not more than 34. This permits a search for optimum compositions of four radial zones of a fast reactor, taking account of their thermal, safety, and physical characteristics.

The program can calculate the breeding ratio in U^8-U^5 and U^8-Pu^9 fuel cycles, taking account of higher isotopes corresponding to the so-called average isotopic composition with the densities $\langle \rho^j \rangle_i$ of fissionable elements defined by the relation

$$\langle \rho^j \rangle_i = \frac{1}{T_{a_i}} \int_0^{T_{a_i}} \rho_i^j(t)\, dt, \tag{4}$$

where T_{a_i} is the operating period of the i-th reactor zone. In this case the densities $\rho_i^j(t)$ are found from the solution of the burnup equation under the assumption that the one-group microscopic capture and fission cross sections do not change during reactor operation. The change in the heat release distribution with reactor operating time between refuelings is estimated from the envelope of the heat release distributions calculated before refueling, after refueling, and in the middle of the interval between refuelings. These calculations give the factor k_T by which the coolant flow rate through the reactor must be increased. This factor is assumed constant during the several steps in the search for the optimum.

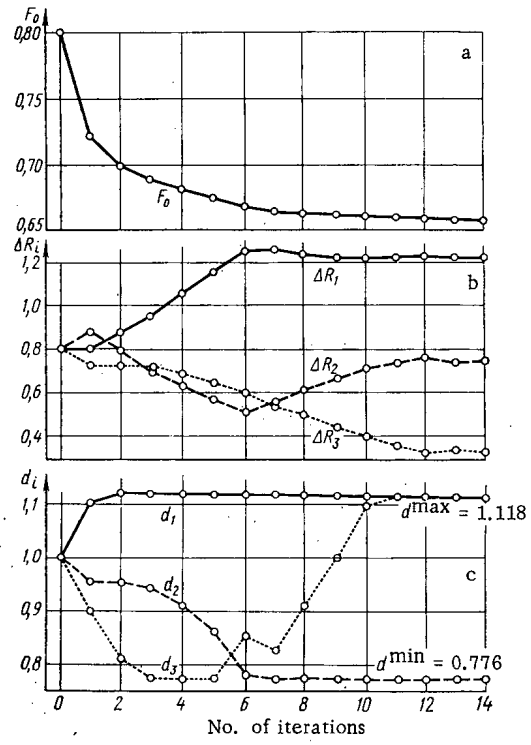

Fig. 2. Convergence of iteration process in the problem of the maximum power of a three-zone fast reactor: a) change of functional F_0 being minimized in iteration process; b) change of reactor zone thicknesses in iteration process; c) change in diameter d_i of fuel elements in iteration process.

TABLE 1. Results of Solving the Problem of Maximum Reactor Power

Parameters	Composition				Results from [8]
	2-zone	3-zone	4-zone	3-zone	
F_0	0,6711	0,6653	0,6652	0,6653	—
ΔR_1	1,297	1,274	0,733	**1,269**	1,26
ΔR_2	1,108	0,793	0,538 } 1,271	0,779	0,78
ΔR_3	—	0,338	0,785	0,357	0,365
ΔR_4	—	—	0,349		
d_1	1,118	1,118	1,118	1,118	1,118
d_2	0,776	0,776	1,118	0,776	0,776
d_3	—	1,118	0,776	1,118	1,118
d_4	—	—	1,118		
N		45		65	—

Problems of the Best Flattening of the Heat Release Distribution. The ROKBAR iteration algorithm for seeking the optimum variant is very similar to the method of steepest descent [6]. Just as in the method of steepest descent the optimum is sought along the gradient of the function. This is illustrated in Fig. 1 which shows the solution of the problem of finding the minimum of the coefficient of nonuniformity of heat release K_r in a one-dimensional cylindrical reactor with two core zones surrounded by a reflector. The control parameters are $u_1 = R_1/R_2$, $u_2 = \rho_2^0/\rho_1^9$, and it is required that

$$0.5 \leqslant u_1 \leqslant 0.9; \quad 1.0 \leqslant u_2 < \infty, \tag{5}$$

where R_i is the radius of the i-th zone and ρ_i^9 is the density of fissionable material in the i-th zone (i = 1, 2). The solid curves of Fig. 1 are obtained from the condition K_r = const, and the dashed lines correspond to the ROKBAR program gradient descent from two different points: 1) $u_1 = 0.5$, $u_2 = 1.0$; 2) $u_1 = 0.8$, $u_2 = 2.4$. In both cases the program at each iteration was chosen so as to reach the crest a-b most rapidly and then to descend along the crest to the point $u_1 = 0.75$, $u_2 = 1.47$ corresponding to the smallest value of K_r.

It is interesting that in this problem the minimum K_r is reached at the point where the first derivatives of K_r with respect to each of the controls are discontinuous. Classical methods of the calculus of variations cannot be used in this case although the optimum lies within the considered range of values of the controls (5).

It is instructive to compare the results of the ROKBAR iteration solution of a problem with the analytic solution obtained by using the Pontryagin maximum principle [7]. Such a comparison has been made for the problem of maximum power of a gas-cooled cylindrical reactor in which the diameter d(r) of a fuel channel can vary. This problem was solved in [8] by the Pontryagin maximum principle for a positive material buckling of the fuel element lattice. It is easy to see that the statement of the problem given in

TABLE 2. Basic Parameters of Reactors Optimized with Respect to the Consumption of Plutonium G and the Doubling Time T_2

T_0, yr	Minimum with respect to consumption of plutonium			Minimum with respect to doubling time
	0	2,5	6,0	
G, kg/MW	1,83	1,49	0,92	—
T_2, yr	13,8	12,5	11,4	10,2
Q, kW/liter	930	880	800	550
P_f, kg	1065	1150	1290	1820
$P_f\left(1+\frac{T_{rc}}{T_a}\right)$	1830	1860	1930	2390
K_r	1,29	1,27	1,28	1,25
BRC	0,518	0,564	0,625	0,802
BR	1,23	1,25	1,27	1,32
$\varepsilon_{a.w.}$	0,105	0,107	0,110	0,103
$H_{g.p.}$, m	0,256	0,288	0,300	0,571
H, m	0,798	0,787	0,764	0,950
ΔR_1, m	0,548	0,594	0,621	0,731
ΔR_2, m	0,435	0,422	0,461	0,442
d_T, mm	3,0	3,32	3,76	5,22
h	1,26	1,23	1,19	1,16
x_1	0,169	0,158	0,147	0,121
x_2	0,206	0,194	0,176	0,146
$v^0_{1,2}$, m/sec	10,0	10,0	10,0	8,77

this paper is equivalent to the following. Find, in relative units, the zone thicknesses ΔR_i and the fuel element diameters d_i which minimize the functional

$$F_0 = \frac{\Phi_0}{\int_0^{2.405} d(r)\,\Phi(r)\,dr}$$

and satisfy the conditions

$$0 \leqslant \Delta R_i \leqslant 2.405; \quad 0.776 \leqslant d_i \leqslant 1.118, \tag{6}$$

where $\Phi(r)$ is the one-group neutron flux at point r in the reactor.

The problem was solved with the ROKBAR program for two-, three-, and four-zone reactors and for various numbers of nodes N of the finite-difference mesh used in determining the neutron fluxes and importances. Table 1 gives the results of the comparison and Fig. 2 shows the convergence of the iteration search for the optimum in a three-zone reactor.

From an analysis of the results shown in Table 1 the following conclusions can be drawn:

1) as in [8] the three-zone reactor turns out to be optimum; the four-zone arrangement chosen initially goes over into a three-zone reactor in the iteration process;

2) as the number of nodes N of the finite-difference mesh is increased, the numerical solution becomes more accurate and approaches the analytic solution obtained by using the Pontryagin maximum principle.

Problems in the Minimum Consumption of Plutonium to Ensure a Given Rate of Development of Nuclear Power. As a more complicated example let us consider the problem of the minimum consumption of plutonium under constraints (3). The calculation of G, the consumption of plutonium per MW (e), for a given rate of growth of nuclear power T_0, leads to the expression

$$G = \frac{P_f}{W_{el}}\left(1+\frac{T_{rc}}{T_a}\right)\left(1-\frac{T_0}{T_2}\right), \tag{7}$$

where P_f is the critical mass of the reactor, W_{el} is its electric power, T_a is the operating time of the fuel elements, T_{rc} is the time of chemical reprocessing of the core fuel elements, and T_2 is the doubling time for a system of breeders operating simultaneously. The doubling time is calculated by the formula obtained from the general expression proposed by Usachev [9]. The problem is solved for a cylindrical sodium-cooled reactor with two core zones surrounded by blankets. The fuel is a mixture of UO_2 and PuO_2 with 15% porosity, and the maximum burnup is 100 kg of fission products per metric ton of fuel. Stainless steel is used as structural material and for fuel element cladding. The time of chemical reprocessing of blanket fuel elements T_{rb} is taken as one year, and that for the core fuel elements T_{rc} as half a year with a 2% loss of fuel. The thermal conductivity of the fuel is taken as 1.8 kcal/m · h · °C. The strength and thermophysical properties of steel, sodium, and fuel are basically the same as those for the BN-350 reactor [1]. The ranges of variation of the control parameters were chosen as follows:

$$\left.\begin{array}{c} 0.01\ \text{m} \leqslant H_{g.p.} \leqslant 2.0\ \text{m}; \\ 0.2\ \text{m} \leqslant H \leqslant 2.0\ \text{m}; \quad 0.0^{3}1 \leqslant \varepsilon_{a.w.} \leqslant 0.2; \\ 0.1\ \text{m} \leqslant \Delta R_i < \infty; \quad 0.0^{2}3\ \text{m} \leqslant d_i^{T} < \infty; \\ 1.15 \leqslant h_i < \infty; \\ 0 \leqslant v_i \leqslant 10\ \text{m/sec}; \quad 0.0^{2}1 \leqslant x_i \leqslant 1.0; \\ (i = 1, 2). \end{array}\right\} \tag{8}$$

For technical reasons the dimensions of the fuel elements and the relative lattice spacing were taken the same for both core regions with Δ_i^{cl} = 0.4 mm. The void for the collection of gaseous fission products was

at the lower axial blanket where the coolant temperature is minimum. The limiting temperature at the center T_c, and in the cladding T_{cl} of a fuel element, the limiting stress in the assembly wall σ_a, and the maximum permissible strain in the fuel element cladding ξ_{cl} were taken as

$$T_c^{per} = 2450^\circ C; \quad \sigma_a^{per} = 18 \text{ kg/mm}^2;$$
$$T_{cl}^{per} = 725^\circ C; \quad \xi_{cl}^{per} = 0.2\%.$$

The problem was solved for a reactor with a core power W = 2250 MW (t) (1000 MW (e)) and a coolant outlet temperature T_{out} = 560°C for various rates of development of nuclear power. The problem of the minimum doubling time of the same reactor was solved simultaneously.

In minimizing G and T_2 the coefficient k_T, which characterizes the variation in the heat release distribution, was taken as 1.15, and the breeding ratio of the core BRC and of the reactor BR were calculated without taking account of higher isotopes. The calculated results are given in Table 2.

It is clear from Eq. (7) that for a doubling time T_2 which is large in comparison with T_0 the optimum with respect to the consumption of plutonium G is determined by the optimum of the product $P_f(1 + T_{rc}/T_a)$ which characterizes the amount of fuel in a fuel cycle (reactor and fuel reprocessing apparatus). For rates of development comparable in magnitude with the doubling time the optimum with respect to G is given by $1 - T_0/T_2$ and the parameters of such reactors should not be greatly different from the parameters obtained in optimizing with respect to T_2.

The following conclusions can be drawn from the results of the calculations.

1. The requirement of minimum consumption of plutonium leads to the development of reactors with large thermal stresses. In this case the maximum temperatures at the center and in the cladding of a fuel element, and the maximum stress in an assembly wall reach their limiting values, and the permissible strain in the fuel element cladding is close to the limit. The average rise in coolant temperature is ΔT_{cool} = 185-190°C.

2. With increasing T_0 the characteristics of an optimum reactor approach the characteristics of a reactor optimized with respect to doubling time, as one should expect. In this case the average power density $\overline{Q}$ decreases, the breeding ratio and the critical mass $\overline{P}_f$ increase, and the diameter of the fuel elements increases with a decrease in enrichment and the volume fraction of the coolant.

It is interesting to note that in the present problem the consumption of plutonium G as a function of the controls has a very flat optimum. This is confirmed by recalculating G for another fixed rate of development T_0.

The solutions of our problems and those published in [10] have shown that the ROKBAR program is a reliable and effective instrument for seeking optimum compositions of fast reactors.

In conclusion the authors thank A. P. Rudik for helpful advice and comments which were taken into consideration in performing the work.

LITERATURE CITED

1. A. I. Leipunskii et al., Atomnaya Énergiya, 25, 380 (1968).
2. V. V. Khromov et al., in: Nuclear Reactor Physics [in Russian], Vol. 2, Atomizdat, Moscow (1970), p. 3.
3. A. M. Kuz'min and V. V. Khromov, in: Engineering-Physics Problems of Nuclear Reactors [in Russian], L. N. Yurova (editor), Atomizdat, Moscow (1966), p. 33.
4. Yu. I. Likhachev and V. V. Vakhromeeva, in: State and Prospects of Constructing Atomic Energy Power Plants with Fast Reactors (SMEA Materials Symposium) [in Russian], Obninsk (1968), p. 508.
5. V. V. Khromov et al., Atomnaya Énergiya, 27, 186 (1969).
6. H. Kelley, in: Optimization Methods with Applications to the Mechanics of Space Flight [Russian translation], Nauka, Moscow (1965), p. 244.
7. L. S. Pontryagin et al., Mathematical Theory of Optimum Processes [in Russian], Fizmatgiz, Moscow (1961).
8. T. S. Zaritskaya and A. P. Rudik, Atomnaya Énergiya, 23, 218 (1967).

9. A. I. Leipunskii et al., Paper No. P/369, Presented by the USSR at the Third International Conference on the Peaceful Uses of Atomic Energy [in Russian], Geneva (1964).
10. A. M. Kuz'min et al., in: Nuclear Reactor Physics [in Russian], Vol. 2, Atomizdat, Moscow (1970), p. 17.

SOME CHARACTERISTICS OF SELF-OSCILLATORY REGIMES OF A BOILING WATER REACTOR

B. V. Kebadze and V. I. Plyutinskii

UDC 621.039.514:621.039.524.44

By now many articles have been published on the determination of the limits of stability of a boiling water reactor in the linear approximation. At the same time for a reactor that is susceptible to resonance instability the processes occurring near the limit of stability are of considerable interest [1, 2]. The object of the present study is to elucidate the characteristics of a boiling water reactor with its own circulating heat-transfer agent in the self-oscillatory regime by experiments and computations.

One of the objectives in the experiments carried out on the reactor VK-50 [3] was to study the nature of the appearance and development of self-oscillations and also the dependence of their amplitude and frequency on the basic parameters of the reactor (power, pressure of the heat-transfer agent, etc.).

For recording the oscillations of the neutron flux fast-response automatic recorders (ÉPP-09M with scale coverage in 1 sec, "Rapidgraph" galvanometer with 0-15 Hz frequency band) with additional ionization chambers were used over and above the regular automatic power recorder. For regulating the average power a signal proportional to the current of the ionization chamber was fed to a filter with a time constant of 10 sec and then to one of the tracks of the automatic recorder. The changes in the pressure of the heat-transfer agent in the reactor were also recorded simultaneously. The observations of the temperature of the heat-transfer agent in the descending part were obtained from the readings of a multipoint automatic recorder. In the experiments, as also in operating conditions, the power regulator was not used. The pressure regulator before the turbine was also not connected.

In the investigated regimes it was not possible to obtain a stationary regime with appreciable amplitude of the oscillations. The nature of the self-oscillatory regime is shown in Fig. 1. The upper and the lower envelopes of the oscillations of the neutron flux are shown in the upper part of the figure. The initial state of the reactor corresponds to a thermal power $N_T \approx 103$ MW and a pressure of the heat-transfer agent $p \approx 39$ abs. atm. The positive reactivity is introduced at $t = 1.5$ min; the vapor valve at the exit from the reactor is opened simultaneously. After some time, during which the pressure drops, the amplitude of the oscillations of the neutron flux begins to increase. After attaining a maximum the oscillations get damped and thereafter maintain a cyclic behavior with a period of about 7 min. The envelopes of the self-oscillations were obtained by averaging the maximum and the minimum readings of the recorder over 10 periods of "fast" oscillations. The frequency of the fast oscillations, which is determined by averaging over 20 periods, has a small range of variation, 0.67-0.70 Hz. The cyclic variations of the amplitude of the oscillations are accompanied by oscillations in the pressure of the heat-transfer agent with the same period but a certain phase lag, and also by variations of the average power of the reactor and the temperature of the heat-transfer agent in the descending part.

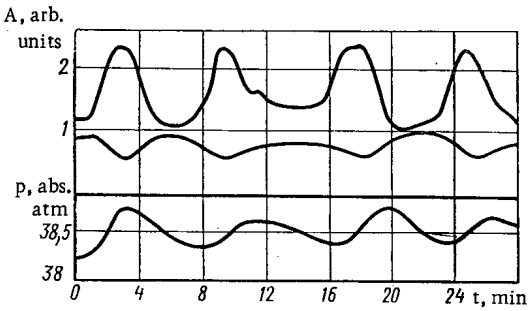

Fig. 1. Cyclic nature of the self-oscillatory regime.

In leading the reactor into the self-oscillatory regime and the attempts to stabilize it, it was found that an increase of the average power of the reactor by 3-4 MW by rapid displacements of the compensators does not by

Translated from Atomnaya Énergiya, Vol. 31, No. 2, pp. 89-92, August, 1971. Original article submitted July 10, 1970; revision submitted December 30, 1970.

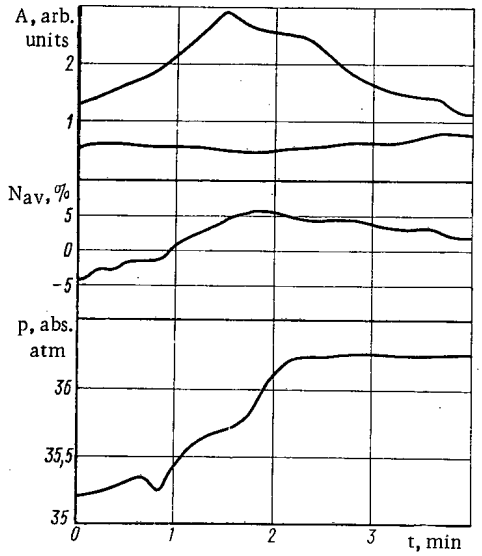

Fig. 2. Variation of the amplitude of oscillations of some parameters in the presence of perturbation in pressure.

itself lead to any noticeable increase in the amplitude of the oscillations; in some regimes the amplitude even decreases. Only with a subsequent change in the pressure of the heat-transfer agent or an increase of the flow rate of the water supply for maintaining the water level in the reactor does the amplitude increase noticeably. The behavior of the envelopes of the oscillations of the neutron flux A and the average power N_{av} in the transition regime, caused by the pressure increase due to closing the vapor valve at the exit from the reactor, is shown in Fig. 2. The amplitude of the oscillations of the neutron flux at first increases with the pressure and the average reactor power; then it drops to a value somewhat lower than the initial.

These experiments demonstrate the complex dynamic interaction of the reactor parameters (average power, pressure of the heat-transfer agent, its enthalpy at the entrance to the active zone) and the fast oscillations; in particular, slow oscillations of the parameters appear simultaneously with the fast oscillations. In order to explain the observed phenomena, first the amplitude of the fast oscillations was computed as a function of these parameters and then the stability of the parameters in the low-frequency range was investigated taking into consideration the change in the amplitude of the fast oscillations and the corresponding variations of the constant component of the reactivity, which lead to a shift of the average power.

The amplitudes of the oscillations were computed by the method of harmonic balance. The feedback equations were assumed to be linear in the water-vapor content and the fuel temperature. A transfer function of the feedback, obtained from the computation of the dynamic power reactivity coefficient from the theory of perturbations taking account of the spatial (height) distribution of the parameters, was used for determining the amplitude of the oscillations. A single-group modified equation, defining the distribution of the neutron flux, was considered for obtaining the increment of the reactivity. Applying the theory of perturbations to this equation a frequency-dependent expression for the reactivity was obtained in terms of the increments of the thermophysical parameters of the active zone:

$$\delta\rho(s) = \int_0^H \varkappa(z)\,\Phi_T^2(z)\,\delta\theta_{bl}(s, z)\,dz + \int_0^H L(z)\,\Phi_T^2(z)\,\delta\gamma_{mix}(s, z)\,dz, \qquad (1)$$

where Φ_T is the flux of thermal neutrons, z is the spatial coordinate, s is the parameter in Laplace transform, $\delta\gamma_{mix}(s, z)$ is the increment of the density of the vapor–water mixture, $\delta\theta_{bl}(s, z)$ is the increment of the temperature of the fuel block, and $\varkappa(z)$, L(z) are certain nuclear-physical parameters of the active zone obtained from averaged space-power variable two-group constants. For determining $\delta\gamma_{mix}(s, z)$ and $\delta\theta_{bl}(s, z)$ the basic equations are the equations of heat conductivity for a three-layer cylindrical fuel element and the equations of conservation of mass and energy for the heated channel with appropriate initial and boundary conditions. In the nonstationary equation for the heat-transfer agent the interphase slippage of the water vapor is disregarded. Changing over to the equations for the increments and carrying out linearization and Laplace transformation with the initial and the boundary conditions we obtain the transfer function from the reactor power to the parameters $\delta\gamma_{mix}$, $\delta\theta_{bl}$. With the use of Eq. (1) we obtain the feedback transfer function; for subsequent computations the imaginary and the real parts of this function are approximated by second degree polynomials.

The periodic solutions of the equations of motions were obtained by the method of successive approximations [1]. The relation between the amplitudes of the harmonics of the reactivity a_k and power A_k is given by

$$W\mathbf{n}^l = \boldsymbol{\rho} + W_\rho \mathbf{n}^{l-1}, \qquad (2)$$

where $\boldsymbol{\rho}$, $\mathbf{n}^l$ are vectors composed of the coefficients a and A_k; W_ρ is a matrix with elements $w_{ij} = a_{j-i}$; W is a diagonal matrix with elements $w(ki\omega)$ corresponding to the inverse of the amplitude-phase characteristic (APC) of a zero power reactor; l is the number of the approximation. The amplitude of the

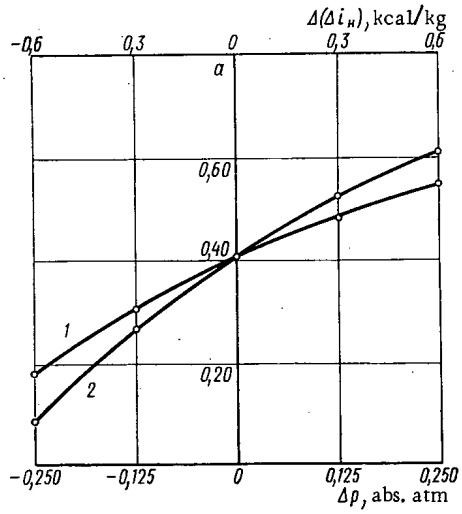

Fig. 3

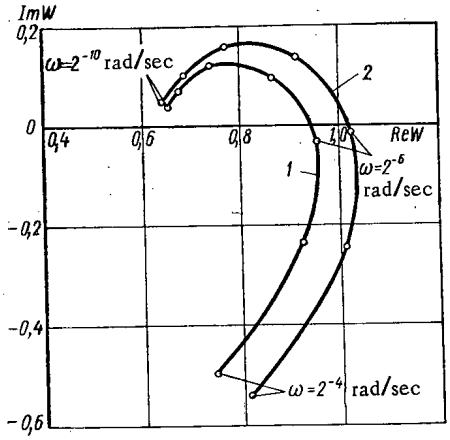

Fig. 4

Fig. 3. Dependence of the amplitude of the first harmonic of the reactivity a on the pressure of the heat-transfer agent (1) and its underheating at the entrance to the reactor (2).

Fig. 4. Amplitude-phase characteristic of an open system with slowly varying parameters without (1) and with (2) self-oscillations taken into consideration.

oscillations and the constant component of the reactivity a_0 were computed on a computer. In view of the intense damping of the higher harmonics in the feedback circuit a filter hypothesis was used. This procedure yields a good convergence for the values of the amplitude of the first harmonic of the reactivity smaller than 0.7β, which corresponds to the amplitude of the oscillations of the first harmonic of power equal to ~60% of the average power level. Figure 3 presents some results of the computations of the oscillations amplitude for the variation of the individual parameters in the neighborhood of the regime with N_T = 100 MW, p = 35 abs. atm and for underheating of the heat-transfer agent at the entrance to the active zone Δi_H = 7.8 kcal/kg. The wide range of variation of the amplitude for inappreciable variations of the pressure and underheating of the heat-transfer agent to enthalpy saturation at the entrance to the active zone is in agreement with the experiment. The increase in the amplitude of the oscillations with the increase in underheating is in good agreement with the deterioration of the reactor stability observed in the experiment on increasing underheating. The computations also confirm the weak dependence of the amplitude of the oscillations on the average power at constant pressure and underheating of the heat-transfer agent (±7-8% for a variation of power by ±5%). In practice, during the experiments it is not possible to vary only one of the reactor parameters for a long time. Thus, in the steady-state regime due to the weak dependence of the flow rate of the heat-transfer agent on the power, an increase in the reactor power is accompanied by an increase in underheating; this leads to a deterioration of the stability and an increase in the amplitude of the oscillations, noticed in the experiments as well as in the computations [3]. Similarly an increase in the pressure of the heat-transfer agent with constant enthalpy at the entrance to the active zone is accompanied by an increase in underheating, which destabilizes the reactor and increases the amplitude of the oscillations. However, as the thermal wave propagates along the descending part and the volume under the reactor, the underheating returns practically to its previous value and the amplitude of the oscillations decreases (Fig. 2). Since the steady-state regimes with different pressures differ little in underheating, the end result of an increase in the pressure is to stabilize the reactor [3].

The variation of the amplitude of the fast oscillations with the variation of the reactor parameters affects the low-frequency processes as a result of the shift of the average power and the subsequent change in the thermal parameters. With a view to improving the temporal (frequency) interrelations of the parameters and to explain, in particular, the slow cyclic variations of the amplitude of the oscillations, we investigated the low-frequency dynamics of the reactor. In the framework of a simplified model we investigated the processes of generation of water vapor in the rising part and condensation in the descending part, the dynamics of the pressure in the reactor and in front of the turbine, and the propagation of the thermal perturbation in the descending part and in the volume under the reactor for constant rate of circulation [4].

The active zone of the reactor was taken as an inertialess unit, since here the time constants of the processes are much smaller than the time scales of the changes in the pressure and enthalpy of the heat-transfer agent in the region under the reactor. The active zone is characterized by the reactivity coefficients with respect to power, the enthalpy of the heat-transfer agent at the entrance, and pressure, obtained from static computations of the reactor based on the theory of perturbations. The role of the self-oscillations is taken into consideration through the change in the constant component of the reactivity corresponding to the change in the amplitude of the oscillations on varying the reactor parameters. The change in the constant component of the reactivity due to the nonlinear static dependence of the reactivity on power is also taken into consideration. The effect of the self-oscillations may be estimated by comparing the reactivity coefficients with respect to pressure K_p and underheating of the heat-transfer agent $K\Delta i_H$ disregarding the self-oscillations

$$K_{\Delta i_H} = -0.007\ (\text{kcal/kg})^{-1}; \quad K_p = 0.016\ \text{abs. atm}^{-1},$$

and with the self-oscillations taken into consideration

$$K^A_{\Delta i_H} = -0.008\ (\text{kcal/kg})^{-1}; \quad K^A_p = 0.017\ \text{abs. atm}^{-1}.$$

The system of equations for the increment of the parameters, obtained after linearization and Laplace transformation, was put in the form of a directional graph [5]. The APC obtained from the graph of an open system was computed on a computer. The APC of an open system without and with the self-oscillations taken into consideration are presented in Fig. 4. In spite of the fact that the sum effect of the variation of pressure and enthalpy of the heat-transfer agent at the entrance to the active zone is positive, the reactor is statically stable in the linear approximation, since the amplification factor of an open system at zero frequency is less than unity. The system has a resonance at $\omega \approx 2^{-6}$ rad/sec, which is determined by the dynamic interaction of pressure within the reactor and the enthalpy at the entrance to the active zone; the change of the enthalpy, caused mainly by the quantity $\partial i'/\partial p$, is characterized by a lag in reference to the pressure change.

Curve 2 in Fig. 4 represents the destabilizing effect of the self-oscillations on the behavior of the slowly varying parameters of the system: the APC intersects the real axis beyond the point (1; 0), which indicates the instability of the system in the linear approximation taking the fast oscillations into consideration. The period corresponding to the resonance frequency (T = 6.8 min) is close to the period of the variation in the amplitude of the oscillations (T = 7 min). As seen from Fig. 4, the effect of the self-oscillations on the characteristic of an open system is weak; however, the fact that the slow oscillations in the experiment are always accompanied by fast oscillations confirms their destabilizing effect on a system with slowly varying parameters.

The following conclusions can be drawn on the basis of the discussion presented above.

1. The inference regarding probable change in the amplitude of oscillations on changing the reactor power and the pressure of the heat-transfer agent, made on the basis of the investigations of stationary regimes, cannot be extended to transition regimes, where the effect may be opposite.

2. The computations of the amplitudes of oscillations and the experiments indicate a "soft" regime of excitation of oscillations. The change in the amplitude of the oscillations from the noise level to a value hindering the normal operation of the reactor corresponds to a small variation of the thermophysical parameters.

3. The self-oscillations have a destabilizing effect on the low-frequency characteristic of the reactor; in some cases this leads to slow cyclic variations of the amplitude of oscillations and of the thermophysical parameters of the reactor.

The authors are grateful to V. A. Afanas'ev for assistance in organizing and conducting the experiments, and also to L. A. Adamovskii and V. A. Zhukova for helping in computations.

LITERATURE CITED

1. B. Z. Torlin, At. Énerg., 18, 463 (1965).
2. V. P. Gorbunov, A. V. Kryanev, and S. B. Shikhov, At. Énerg., 27, 48 (1969).
3. V. A. Afanas'ev et al., At. Énerg., 24, 363 (1968).

4. A. Ya. Kramerov and Ya. V. Shevelev, Engineering Computations of Nuclear Reactors [in Russian], Atomizdat, Moscow (1965).
5. L. Robisho, M. Buaver, and Zh. Rober, Directional Graphs and Their Application to Electrical Circuits and Machines [Russian translation], Énergiya, Moscow (1964).

DISSOCIATION OF URANIUM OXIDES

I. S. Kulikov

UDC 541.451:541.123

Oxides are known in the uranium–oxygen system in the condensed (UO, U_2O_3, UO_2, U_4O_9, U_2O_5, U_3O_8, and UO_3) and gaseous (UO, UO_2, and UO_3) states. However, the oxides UO and U_2O_3 are not cited on the phase diagram of [1]. Thermodynamic data on oxides of uranium, contained in the handbooks [2-7], differ substantially.

In the analysis cited below, data on U, UO_2, UO_g, and $UO_{2,g}$ [6], $UO_{3,g}$ [7], UO [2], U_3O_8 and UO_3 [2, 3], and U_4O_9 [5] were taken as the basis. The oxides U_3O_7 and U_2O_5 fall at the boundaries of the region of homogeneity of the compounds U_4O_9 and U_3O_8.

Let us consider the dissociation of uranium dioxide as the most studied stable oxide in the indicated system. In the gas phase we should consider the probability of the presence of the following components: U, UO, UO_2, UO_3, O, and O_2. For the summary pressure above uranium oxides, let us write:

$$\Sigma P_{U_xO_y} = P_U + P_{UO} + P_{UO_2} + P_{UO_3} + P_O + P_{O_2}. \quad (1)$$

Moreover, for uranium dioxide we can write the following equations:

$$P_U = \frac{K_{UO_2} P^0_{UO_2}}{P^2_O}; \quad P_{UO} = \frac{K_{UO_2} P^0_{UO_2}}{K_{UO} P_O};$$

$$P_{UO_3} = \frac{K_{UO_2} P^0_{UO_2}}{K_{UO_3}} P_O; \text{ and } P_{O_2} = \frac{1}{K_{O_2}} P^2_O.$$

Substituting them into Eq. (1), we obtain:

$$\Sigma P_{UO_2} = \frac{K_{UO_2} P^0_{UO_2}}{P^2_O} + \frac{K_{UO_2} P^0_{UO_2}}{K_{UO} P_O} + P^0_{UO_2} + \frac{K_{UO_2} P^0_{UO_2}}{K_{UO_3}} P_O + P_O + \frac{1}{K_{O_2}} P^2_O. \quad (2)$$

To calculate the minimum of the total pressure, let us take the first derivative of ΣP_{UO_2} with respect to P_O:

$$\frac{\partial}{\partial P_O}(\Sigma P_{UO_2}) = -\frac{2K_{UO_2} P^0_{UO_2}}{P^3_O} - \frac{K_{UO_2} P^0_{UO_2}}{K_{UO} P^2_O} + \frac{K_{UO_2} P^0_{UO_2}}{K_{UO_3}} + 1 + \frac{2}{K_{O_2}} P_O \quad (3)$$

and, setting it equal to zero, we obtain

$$2K_{UO_2} P^0_{UO_2} + \frac{K_{UO_2} P^0_{UO_2}}{K_{UO}} P_O = P^3_O \left(\frac{K_{UO_2} P^0_{UO_2}}{K_{UO_3}} + 1 \right) + \frac{2}{K_{O_2}} P^4_O. \quad (4)$$

The fact that this is a minimum can be ascertained by calculating the second derivative of the total pressure.

Equation (4) can also be obtained from the equation of the balance in the presence of congruent dissociation of uranium dioxide:

$$2P_U + P_{UO} = P_{UO_3} + P_O + 2P_{O_2}. \quad (5)$$

Replacing P_U, P_{UO}, P_{UO_3}, and P_{O_2} in terms of the dissociation constants and substituting them into Eq. (5), we obtain Eq. (4). From this it follows that in the dissociation of congruent chemical compounds, the total pressure is a minimum.

Translated from Atomnaya Énergiya, Vol. 31, No. 2, pp. 93-98, August, 1971. Original article submitted April 20, 1970; revision submitted December 15, 1970.

TABLE 1. Thermodynamic Constants, Partial Pressures, and Composition of the Vapor Phase above Uranium Dioxide

Parameters	Temperature, °K								
	1000	1406	1873	2000	2500	2750	3000	4000	4124
$-\lg P^0_U$	18,002	10,892	6,757	5,970	3,654	2,812	2,111	0,175	0,000
$-\lg P^k_O$	33,650	21,755	14,237	12,820	8,649	7,153	5,883	—	—
$-\lg K_{O_2}$	19,612	12,142	7,258	6,356	3,684	2,710	1,898	0,340	0,543
$-\lg K_{UO}$	34,629	22,689	15,171	13,741	9,495	7,851	6,626	2,965	2,618
$-\lg K_{UO_2}$	64,380	42,084	28,066	25,411	17,545	14,667	12,263	5,583	4,975
$-\lg K_{UO_3}$	(87,239)	(55,589)	(36,588)	(32,904)	22,037	18,085	(14,792)	(5,737)	(4,920)
$-\lg P^0_{UO_2}$	20,921	12,318	7,165	6,199	3,407	2,420	1,614	—	—
$-\lg P_O$	26,308	16,593	10,718	9,593	6,288	5,138	4,092	—	—
$-\lg P_{O_2}$	33,033	21,043	14,178	12,830	8,892	5,566	6,286	—	—
$-\lg P_U$	32,686	21,217	13,795	12,424	8,376	6,811	5,693	—	—
$-\lg P_{UO}$	24,365	15,121	9,342	8,276	5,169	4,098	3,159	—	—
$-\lg P_{UO_3}$	24,370	15,136	9,361	8,299	5,203	4,140	3,177	—	—
$-\lg \Sigma_{UO_2}$	20,921	12,316	7,158	6,182	3,392	2,402	1,585	—	—
Composition, vol. %									
UO_2	99,4	99,69	98,70	98,36	96,66	95,96	94,44	—	—
UO	0,03	0,16	0,65	0,82	1,67	2,02	2,67	—	—
UO_3	0,03	0,15	0,62	0,78	1,54	1,84	2,57	—	—
$-\lg a_U$	14,684	10,325	7,038	6,454	4,722	3,999	3,582	—	—

TABLE 2. Partial Pressures and Composition of the Gas Phase above the System $U-UO_2$

Parameters	Temperature, °K						
	1000	1406	1873	2000	2500	2750	3000
$-\lg P^0_U$	18,002	10,892	6,757	5,970	3,654	2,812	2,111
$-\lg P^0_{UO_2}$	20,921	12,318	7,165	6,199	3,407	2,420	1,614
$-\lg P^k_{O_2,\ UO_2}$	47,687	31,368	21,216	19,284	13,614	11,565	9,868
$-\lg P^k_O$	33,650	21,755	14,237	12,820	8,649	7,153	5,883
$-\lg P_{UO}$	17,023	9,958	5,823	5,049	2,808	2,114	1,368
$-\lg P_{UO_3}$	31,713	20,298	12,880	11,526	7,564	6,186	4,968
$-\lg \Sigma P_{U-UO_2}$	16,980	9,910	5,758	4,973	2,663	1,884	1,126
Composition, vol. %							
U	9,48	10,4	10,0	10,0	10,2	11,8	10,33
UO_2	0,01	0,4	3,9	5,9	18,1	29,1	32,46
UO	90,51	89,2	86,1	84,1	71,7	59,1	57,20

The dissociation constants K_{UO}, K_{UO_2}, and K_{O_2} under saturated vapor pressure $P^0_{UO_2}$ were calculated according to the data of [6]. For the dissociation constant of gaseous uranium trioxide, let us use the approximate equation derived earlier [8]:

$$R \ln K_4 = -\frac{D_0 + 7280}{T} + 76 + 4.5 \cdot 10^{-5} \cdot D_0. \quad (6)$$

According to the data of [9], for the reaction:

$$2UO_{2,g} = UO_g + UO_{3,g}; \quad \Delta H^0_{298} = 28 \text{ kcal}$$

Considering the data of [6], for $D_{O,UO}$ and D_{O,UO_2}, we obtain D_{O,UO_3} = 489.9 kcal/mole. Substituting D_{O,UO_3} into Eq. (6), we obtain:

$$\lg K_{UO_3} = -\frac{108\,670}{T} + 21.431. \quad (7)$$

From Table 1 it is evident that the transition of uranium dioxide into the gaseous state occurs chiefly by sublimation and partly by disproportionation according to the reaction

$$2UO_2 = UO + UO_{3,g}.$$

The activities of uranium are considerably less than one. This is evidence of gaseous dissociation of uranium dioxide. We obtain the summary pressure of the gaseous components above uranium dioxide in the form of the following equations:

$$\lg \Sigma P_{UO_2}\,\text{atm} = -\frac{29\,830}{T} + 8.909\ (1000 - 1406^\circ\text{K}); \tag{8}$$

$$\lg \Sigma P_{UO_2}\,\text{atm} = -\frac{28\,396}{T} + 7.879\ (1406 - 3000^\circ\text{K}). \tag{9}$$

The boiling point of uranium dioxide, according to Eq. (9), is equal to 3604°K. However, considering that Eq. (9) was derived for solid uranium dioxide, this value of the boiling point must be somewhat low.

In the calculation of the composition of the vapor phase above the uranium–uranium dioxide system (Table 2), we used the same thermodynamic constants.

From Table 2 it follows that the basic reaction between uranium and uranium dioxide is the formation of gaseous uranium monoxide, i.e., $U + UO_2 = 2UO_g$.

For the summary pressure of the vapor phase above the uranium–uranium dioxide system, we obtain the following equations:

$$\lg \Sigma P_{U-UO_2} = -\frac{24\,484}{T} + 7.504\ (1000 - 1406^\circ\text{K}); \tag{10}$$

$$\lg \Sigma P_{U-UO_2} = -\frac{23\,244}{T} + 6.622\ (1406 - 3000^\circ\text{K}). \tag{11}$$

We obtain a pressure of 1 atm above the uranium–uranium dioxide system at 3510°K according to Eq. (11).

Using the data of [2] to determine the value of ΔG^0_T of the formation of UO_2, let us attempt to solve the problem of the thermal stability of uranium monoxide in the condensed state.

Table 3 presents the results of calculations of the equilibrium pressures of molecular and atomic oxygen and the saturated vapor pressure of uranium monoxide above the system U–UO. The pressures of uranium monoxide above the uranium–uranium dioxide system are cited for comparison. It is evident that the saturated vapor pressures of UO are higher than the pressures of uranium monoxide above the system $U-UO_2$. Consequently, uranium monoxide is metastable above 1000°K. This is also evidenced by a comparison of the equilibrium pressures of oxygen (see Table 2).

However, the difference in the pressures of uranium monoxide and oxygen above the systems under consideration decreases with decreasing temperature. As was shown by an analysis of the data of Tables 2 and 3, at the temperature 877°K and below, stable uranium monoxide may appear. But this conclusion is insufficiently reliable, since the changes in the parameters are commensurate with the errors in the determination of the quantities compared.

The oxide U_4O_9 is isolated in pure form only at temperatures below 1000°C. At temperatures above 1500°K it forms solutions with UO_2 and U_3O_8. The formation of U_4O_9 from uranium dioxide and oxygen $8UO_2 + O_2 = 2U_4O_9$ is accompanied by a thermal effect, equal to 86.6 kcal/mole at 298°K. The approximate

TABLE 3. Equilibrium Pressures of Oxygen and Saturated Vapor Pressure of Uranium Monoxide above the System U–UO

Parameters	Temperature, °K					
	1000	1406	1873	2000	2500	3000
$-\lg P^k_2$	47,531	30,889	20,571	18,643	12,758	(8,874)
$-\lg P^k_O$	33,572	21,516	13,915	12,500	8,221	(5,386)
$-\lg P^0_{UO}$	16,945	9,719	5,501	4,729	2,380	(0,871)
$-\lg P_{UO}(U-UO_2)$	17,023	9,958	5,823	5,049	2,808	1,368

TABLE 4. Partial Pressures and Composition of the Gas Phase in the Dissociation of U_4O_9 (Approximate calculation)

Parameters	Temperature, °K						Note
	1000	1300	1406	1873	2000	2500	
$-\lg P_{O_2}$	10,400	6,279	5,269	2,295	1,759	0,277	According to Eq. (13)
$-\lg P_O$	15,006	9,895	8,701	4,777	4,058	1,978	—
$-\lg P^k_{O_2,\ U_4O_9}$	43,563	31,667	28,468	19,114	17,337	12,132	—
$-\lg P^k_{O,\ U_4O_9}$	31,988	22,5888	20,305	13,186	11,846	7,908	—
$-\lg A_U$	37,288	28,562	26,099	18,921	17,525	13,337	—
$-\lg P_U$	55,290	40,874	36,991	25,678	23,495	16,991	—
$-\lg P_{UO}$	35,667	25,744	23,003	15,284	13,812	9,474	—
$-\lg P_{UO_2}$	20,921	14,231	12,309	7,169	6,200	3,402	—
$-\lg P_{UO_3}$	13,069	8,398	7,235	3,421	2,765	0,888	—
$-\lg \Sigma P_{U_4O_9}$	10,396	6,274	5,264	2,262	1,716	0,174	—
$-\lg P_{O_2}$	—	4,9—5,6	—	—	—	—	Experimental data according to [1]
Composition, vol. %							
O_2	99,1	98,86	98,89	92,8	90,6	79,1	—
UO_3	0,9	0,75	1,07	6,9	8,9	19,3	—

equation for evaluating the partial pressure of oxygen according to the thermal effect of dissociation, derived earlier [8], takes the following form:

$$R \ln P_{O_2} = -\frac{\Delta H^0_{298}}{T} + 34 + 5.8 \cdot 10^{-5} \Delta H^0_{298} + (6.6 \cdot 10^{-5} \Delta H^0_{298} - 13.2) \frac{T - 1000}{2000}. \quad (12)$$

In the dissociation of the oxide U_4O_9 to uranium dioxide and oxygen, using Eq. (12), we can obtain

$$\lg P_{O_2} = -\frac{18\,930}{T} - 0.82 \cdot 10^{-3} T + 9.348. \quad (13)$$

We calculate the standard pressure of oxygen in the formation of the oxide U_4O_9 from uranium and oxygen from the following equation:

$$\lg P^k_{O_2,\ U_4O_9} = \frac{1}{9} (8 \lg P^k_{O_2,\ UO_2} + \lg P_{O_2}),$$

where $P^k_{O_2, UO_2}$ is the oxygen pressure, calculated according to the free energy of formation of uranium dioxide from the components in the standard states; P_{O_2} is the oxygen pressure in the dissociation of the oxide U_4O_9 to UO_2 according to the reaction:

$$2U_4O_9 = 8UO_2 + O_2.$$

Table 4 presents the partial pressures of the components of the gas phase above the system U_4O_9—UO_2, assuming the existence of pure phases. The experimental data of [1] at the temperature 1300°K for U_4O_9 were obtained in the range from 4.9 to 5.6 for $-\log P_{O_2}$, which is somewhat higher than the data obtained by calculation. However, the discrepancies are small, considering the approximate nature of Eq. (13).

We obtain the summary pressures of the gas phase above U_4O_9 in the form of the following equations:

$$\lg \Sigma P_{U_4O_9} = -\frac{17\,773}{T} + 7.377 \ (1000 - 1406^\circ K); \quad (14)$$

$$\lg \Sigma P_{U_4O_9} = -\frac{16\,354}{T} + 6.358 \ (1406 - 2500^\circ K). \quad (15)$$

The gas phase above U_4O_9 contains uranium trioxide, together with oxygen.

The data of Table 4 are applicable only for the pure phase of U_4O_9. However, at 1500°K and above, UO_2 and U_4O_9 form a continuous series of solutions [1]. Therefore, when the condensed phase is impoverished in oxygen, from U_4O_9 to UO_2, the partial pressures of oxygen should be reduced, which agrees with the

TABLE 5. Thermodynamic Constants and Partial Pressures of the Components above U_3O_8

Parameters	Temperature, °K					
	1000	1300	1406	1500	1873	2000
$-\Delta G^0_{T,\ U_4O_9}$, cal	884727	847551	842063	807143	737074	713851
$-\Delta G^0_{T,\ U_3O_8}$, cal	691500	643400	626134	611000	550625	520500
$-\Delta G^0_{T,\ diss.\ U_3O_8}$, cal	44728	12376	13931	9027	−3490	−13821
$-\lg P_{O_2}$, atm	9,776	2,075	2,011	1,315	−0,407	−1,510
$-\lg P^*_{O_2}$, atm	6,80	2,90	2,00	1,40	−0,70	−1,20
$\Delta G^{0*}_{T,\ diss.\ U_3O_8}$, cal	31110	17250	12670	9600	−6000	−11000
$-\lg P^k_{O_2,\ U_3O_8}$, atm	37,787	27,045	24,335	22,259	16,246	14,221
$-\lg a_U$	41,316	32,192	29,780	27,812	22,596	20,560
$-\lg P_U$, atm	59,318	44,504	40,672	37,662	29,353	26,530
$-\lg P^*_O$, atm	13,406	8,205	7,071	6,055	3,265	5,578
$-\lg P_{UO_3}$, atm	11,697	6,598	6,026	4,811	2,560	1,360

*Corrected according to the curve.

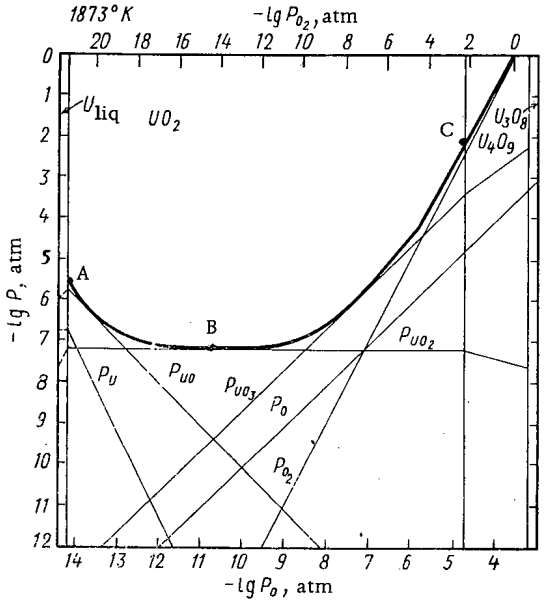

Fig. 1. Total and partial pressures of the components above uranium oxides at 1873°K as a function of the oxidation potential of the gas phase.

experimental data of Aronson and Bell [1]. According to the latter, when O/U is lowered from 2.33 to 2.018 at 1300°K, P_{O_2} is reduced from $8 \cdot 10^{-6}$ to 10^{-9} atm.

The boiling points of phases of variable compositions $UO_{2,33}-UO_2$ should change from 2572 to 3600°K as the oxygen content is lowered. The oxide U_3O_8 has an interval of homogeneity $UO_{2,62}-UO_{2,67}$ [1]. The results of a calculation of the dissociation of this oxide to U_4O_9 and oxygen are cited in Table 5.

The decomposition point of the pure oxide U_3O_8, according to the data of our calculation, is equal to 1726°K. According to the data of [3], the decomposition point of U_3O_8 is 1950°K. This discrepancy is quite regular, if we consider the formation of solutions of U_3O_8 and U_4O_9.

Uranium trioxide forms a continuous series of solid solutions with U_3O_8. The free energy change for the dissociation reaction $6UO_3 = 2U_3O_8 + O_2$ was calculated according to the data of [2, 3].

The partial pressure of oxygen in the dissociation of the pure oxide UO_3 can be described in a first approximation by the equation:

$$\lg P_{O_2,\,atm} = -\frac{9480}{T} + 9.125\,(298 - 925^\circ K). \qquad (16)$$

The decomposition point of uranium trioxide, according to Eq. (16), is equal to 1037°K, and according to the data of [10] 925°K.

Figure 1 presents the dependence of the total and partial pressures of the components above oxides of uranium on the oxidation potential of the gas phase. Uranium dioxide exists in a broad range of oxidation potentials and is the only congruent uranium oxide. The minimum of the total pressure above uranium dioxide during dissociation, noted in Fig. 1 by the point B, is greatly blurred, in view of the fact that the basic component of the gas phase under these conditions is uranium dioxide. However, the position of the point of the maximum is rather accurately calculated, since the constant quantity, the pressure of gaseous molecules of uranium dioxide, does not enter into Eqs. (4) and (5).

From the data of Fig. 1 it follows that uranium dioxide predominates as the basic component of the gas phase above the system $U-UO_2$. When the oxidation potential is further increased, uranium trioxide becomes the basic component of the gas phase. In the region of equilibrium of uranium dioxide with the

oxide U_4O_9, and all the more under the conditions of the equilibrium $U_4O_9-U_3O_8$, the basic component of the gas phase is molecular oxygen.

As the results of a thermodynamic analysis of the dissociation of uranium oxides, the following was revealed.

1. Of the variety of oxides of uranium, the only congruently dissociating oxide is uranium dioxide, which exists in a broad range of oxidation potentials. In the thermal decomposition, uranium dioxide sublimes with partial disproportionation to gaseous uranium monoxide and trioxide.

2. The existence of uranium monoxide in the condensed state is observed only at low temperatures at equilibrium with pure uranium.

3. The oxides UO_3, U_3O_8, and U_4O_9 decompose successively, liberating oxygen.

LITERATURE CITED

1. V. S. Emel'yanov and A. I. Evstyukhin, The Metallurgy of Nuclear Fuel [in Russian], Atomizdat, Moscow (1968), p. 116.
2. U. D. Veryatin et al., Thermodynamic Properties of Inorganic Substances. Handbook [in Russian], Atomizdat, Moscow (1965).
3. K. E. Wicks and F. E. Block, Thermodynamic Properties of 65 Elements, Their Oxides, Halides, Carbides, and Nitrides [in Russian], Metallurgiya, Moscow (1965).
4. M. K. Karapet'yants and M. L. Karapet'yants, Basic Thermodynamic Constants of Inorganic and Organic Substances [in Russian], Khimiya, Moscow (1968).
5. A. N. Krestovnikov et al., Handbook for Calculations of the Equilibria of Metallurgical Reactions [in Russian], Metallurgizdat, Moscow (1963).
6. H. Schick, Thermodynamics of Certain Refractory Compounds, Academic Press, New York–London (1966).
7. V. I. Vedeneev et al., Cleavage Energies of Chemical Bonds. Ionization Potentials and Electron Affinity. Handbook [in Russian], Izd-vo AN SSSR, Moscow (1962).
8. I. S. Kulikov, Thermal Dissociation of Compounds [in Russian], Metallurgiya, Moscow (1969).
9. G. De-Maria et al., J. Chem. Phys., 32, No. 5, 1373 (1960).
10. L. Brewer et al., Thermodynamic Properties and Equilibria at High Temperatures of Uranium Halides, Oxides, Nitrides, and Carbides. AEC MDDC-1543, September 20, 1945, p. 84.

RADIOCHEMICAL DETERMINATION OF THE ABSOLUTE YIELDS OF FRAGMENTS OF THE FISSION OF Pu^{241} AND Pu^{239} BY SLOW NEUTRONS

A. V. Sorokina, N. V. Skovorodkin,
S. S. Bugorkov,* A. S. Krivokhatskii,
and K. A. Petrzhak

UDC 539.173:543.53

In a radiochemical study of the absolute yields of fission fragments, the basic difficulty is to determine the amount of fission in the irradiated sample. The number of fissions can either be calculated according to the neutron flux and effective cross-section of fission, using, for example, the formalism of Westcott [1] for the calculation, or it can be measured experimentally.

In this work the number of fissions in targets used for radiochemical analysis was calculated according to the number of tracks in mica detectors from fragments of the fission of an exactly known fraction of a fissioning substance, applied on mica, which were irradiated simultaneously with the working target in a special collector.

Natural mica, muscovite, preliminarily annealed at the temperature 600°C and etched in concentrated HF, was used as the fragment detectors. After such treatment, the tracks from fragments of the spontaneous fission of uranium, contained in the mica, take the form of rounded rhombi, differing sharply in external form, dimensions, and depth from the tracks of forced fission; they do not interfere with the count of the latter and at the same time aid in the exact focusing on the surface of the mica.

A known amount of a solution of plutonium, which was produced by diluting the initial plutonium solution, from which the working targets were prepared for the determination of the yields, with 2 N nitric acid, was applied on detectors, discs of mica 20-24 mm in diameter. The dilution and application were carried out by a weight method. To prevent drops of the solution from spreading over the surface of the mica, a thermal gradient was used to dry it: the mica was heated on a plate, placed on a support with an opening in the center. A drop of the solution was applied in the center of the mica above the opening. As a result of the poorer thermal conductivity of mica, the temperature in the central portion above the opening was somewhat lower than near the edge of the mica, and this is sufficient to maintain a drop of solution weighing

*Deceased.

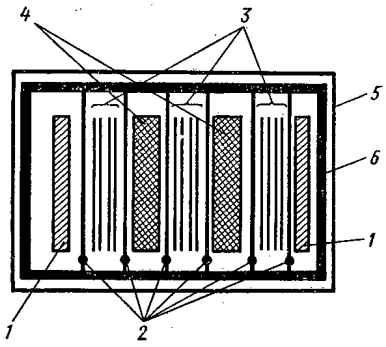

Fig. 1. Arrangement of the working targets and detectors in the assembly for irradiations: 1) target of gold; 2) mica partitions; 3) mica detectors; 4) working target with plutonium; 5) aluminum foil beaker; 6) mica lining.

Translated from Atomnaya Énergiya, Vol. 31, No. 2, pp. 99-102, August, 1971. Original article submitted July 22, 1970.

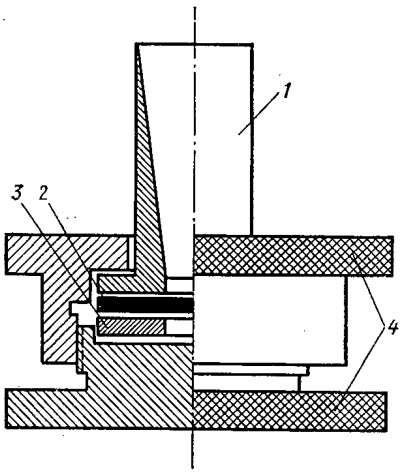

Fig. 2. Instrument for etching of irradiated micas: 1) Teflon beaker; 2) mica; 3) Teflon gasket; 4) band.

up to 70 mg in the center of the disc. After the mica with the applied plutonium was dried, it was covered with mica from the same lot.

Mica detectors with applied plutonium were packed together with the working targets into aluminum foil beakers. Mica on which 2 N HNO_3 was applied was placed in the same assembly to consider the background from this solution. The inner surface of the beaker was covered with mica to exclude contact of the mica detectors with aluminum. The detectors and working targets were also separated by a mica lining. The entire assembly was clamped between two aluminum discs (Fig. 1).

The samples were irradiated in the reactor of the A. F. Ioffe Physicotechnical Institute in a neutron flux for which the cadmium ratio for gold proved equal to 4.26. The absorption of neutrons in the working targets, measured according to the difference of the specific number of tracks in mica detectors, arranged between the working targets and from their outer sides, was less than 0.5%.

After irradiation, the mica was exposed for 2-3 weeks and etched in 28% HF for 6-8 h at room temperature in a special instrument (Fig. 2). The mica was clamped between a Teflon gasket and the beaker into which the acid was poured. The access of the acid to the opposite side of the mica was excluded; therefore, the tracks were etched only on one side of the mica and on a definite area, limited by the diameter of the opening of the beaker, which substantially facilitates the subsequent count of the tracks under a microscope. After the end of the etching, the etched portion was outlined with a needle, and the number of tracks on the outlined area was counted with an MBI-9 microscope at a magnification of 300 power.

The background, i.e., the number of tracks from uranium fission fragments contained in the mica, was determined for each mica according to peripheral regions on the outlined area far from the central zone with the layer of plutonium. It was 5-7% of the initial number of tracks. The background from a solution of 2 N HNO_3 was 1.5-3.0% of the total number of tracks. Each mica was examined by two coworkers; the discrepancy of the results did not exceed 1.5%.

The efficiency of the recording of fragments by the mica was determined according to two sources of Cf^{252}, prepared by the method of aggregate recoil. The number of spontaneous fissions in these sources was measured with an argon-filled ionization chamber with a grid. For the conditions of treatment and etching of the mica selected, the efficiency of recording of fragments was 96.7%, while the mean square error of ten measurements was 0.62%.

The number of fissions in the working target was calculated on the basis of the number of tracks of the fragments registered by the detector, and the fraction of the fissioning substance applied to it. Thus, there was no longer any need to precisely measure the amount of the fissioning substance on all the targets. The mean square error of a determination of the number of fissions in the working targets was 2-3%, considering all errors: for dilution and application of the solutions, count of the number of tracks, and determination of the efficiency of the mica.

This method of measurement of the number of fissions was used for radiochemical determination of the absolute yields of Mo^{99}, Ce^{141}, Ce^{144}, and Ba^{140} in the fission of Pu^{239} and Pu^{241} by slow neutrons. The working targets were dissolved in 6 M HCl in the presence of carriers: barium, cerium, and molybdenum, 10, 3, and 1 mg, respectively. All the elements were isolated from one sample. The separation and purification were carried out chiefly by ion-exchange methods. Columns 6 mm in diameter and 100 mm high were used. Barium and cerium were separated from molybdenum and most of the plutonium by sorption of the latter on the anion-exchange resin Dowex 1 $\times$8 from 6 M HCl [2]. Hydroxides were coprecipitated with carbonates from the eluates containing barium and cerium and partially plutonium, using NaOH and Na_2CO_3. The precipitate was dissolved in HNO_3, and barium and cerium were separated by precipitation of $Ba(NO_3)_2$ with fuming nitric acid, cooling in ice. The $Ba(NO_3)_2$ precipitate was dissolved in water, reprecipitated twice more, and barium and strontium separated with ammonium acetate on the cation-exchange resin

TABLE 1. Absolute Cumulative Yields of the Fragments of the Fission of Pu^{239} and Pu^{241} by Slow Neutrons

isotopes	Absolute yields, %			
	Pu^{239}		Pu^{241}	
	this work	other studies	this work	other studies
Mo^{99}	6,17±0,19	6,44 [12] * 5,9 [14]† 6,10 [15]	6,15±0,16	6,00 [13]† 6,17 [16] *
Ba^{140}	—	5,58 [11] * 5,16 [17] †	5,64±0,11	6,21 [17]† 5,78 [18] * 5,86 [16] *
Ce^{141}	5,18±0,13	5,75Z [14]† 5,23 [11] * 5,1 [15]	4,81±0,14	5,11 [13]† 4,84 [18] *
Ce^{144}	3,85±0,09	3,84 [11] * 4,09 [14]† 3,82 [20] * 3,79 [15]	4,08±0,14	4,13 [16] * 4,07 [18] * 4,08 [19] *

* The yield of the stable isotopes of the indicated masses were measured by a mass spectrometric method with an error in the region of light masses no more than 3-4%, and in the region of heavy masses no more than 2%.

† The yields were determined by a radiochemical method with an error of 4-5%.

Dowex 50 × 8 [3]. The chemical yield of barium was determined by a gravimetric method according to $BaSO_4$ or $BaCrO_4$.

The solutions remaining after the precipitation of barium nitrate were combined, diluted with water to 8 N HNO_3, the Pu(IV) was stabilized, and it was extracted from the solution by sorption on the anion-exchange resin Dowex 1 × 8 [4]. The eluate, containing cerium, was immediately sent to another column, filled with the same resin, mixed with PbO_2 powder. In 7-8 N nitric acid, PbO_2 oxidized cerium to the tetravalent state, and cerium was absorbed by the anion-exchange resin [5]. Cerium was desorbed with 0.5 M HCl with several drops of H_2O_2. From the solution obtained we precipitated $Ce(OH)_3$ with NaOH. The precipitate was washed, dissolved in HNO_3, and cerium fluoride precipitated for additional purification. The chemical yield of cerium was determined colorimetrically according to the color of Ce(IV) in alkaline medium in the presence of Trilon B [6] in comparison with standard solutions of the same concentration as the test solutions. The error in the determination of the chemical yield of cerium was estimated at 2-3%, although the convergence of the results was better.

Molybdenum was desorbed from the resin with 3 M HCl. Then it was freed of antimony by sorption of the latter on the cation-exchange resin KU-2 from 12 M HCl [7]. The eluate was evaporated, the residue dissolved in NaOH, and $La(OH)_3$ precipitated twice by adding lanthanum. The precipitate was discarded, and the alkaline solution neutralized with concentrated HCl to a neutral reaction according to phenolphthalein, an equal volume of concentrated HCl was added, and the cycle of anion-exchange purification of molybdenum was repeated. The desorption of molybdenum from the resin was carried out with 1 M HCl. Under these conditions, technetium is not desorbed [2]. The chemical yield of molybdenum was determined colorimetrically according to the color of the complex of Mo(V) with thiocyanate. Ascorbic acid was used as the reducing agent [8]. Just as for cerium, standard solutions of molybdenum were prepared in approximately the same concentration as the test solutions, and they were subjected to colorimetry simultaneously.

The activity of preparations of cerium, molybdenum, and barium was measured in a propane flow-through $4\pi\beta$-counter. Aliquot portions of solutions of cerium, molybdenum, and barium were applied on gold-plated collodion films and dried. The density of the films was no more than 15 $\mu g/cm^2$; the amount of dry substance on the film did not exceed 30 $\mu g/cm^2$, and in the case of Mo^{99}, 5 $\mu g/cm^2$.

Ba^{140} was measured at equilibrium with La^{140}. Filters 6 and 250 mg/cm^2 thick were used to measure the activities of Ce^{141} and Ce^{144}. Only the β particles of Pr^{144}, according to which the activity of Ce^{144} was calculated, passed through the 250 mg/cm^2 filter. The activity of Ce^{141} was determined according to the difference of the activities measured through the 6 and 250 mg/cm^2 filters, considering the coefficients of

TABLE 2. Absolute Yields of Rare Earth Elements and Yttrium in the Fission of Pu^{239} and Pu^{241} by Slow Neutrons

Isotope	Pu^{239}		Pu^{241}	
	relative yield	absolute yield, %	relative yield	absolute yield, %
La^{141}	1,22	4,70±0,26	1,10	4,50±0,17
Ce^{141}	1,32	5,09±0,14	1,17	4,78±0,18
Ce^{143}	1,04	3,99±0,21	0,952	3,88±0,16
Pr^{143}	1,11	4,27±0,17	1,06	4,31±0,15
Ce^{144}	1,00	3,85±0,09	1,00	4,08±0,14
Pr^{145}	0,919	3,54±0,16	0,739	3,01±0,14
Nd^{147}	0,553	2,13±0,09	0,574	2,34±0,09
Pm^{147}	0,555	2,14±0,13	0,577	2,35±0,12
Nd^{149}	0,296	1,14±0,08	0,361	1,47±0,06
Pm^{149}	0,338	1,30±0,05	0,373	1,52±0,08
Pm^{151}	0,192	0,741±0,036	0,207	0,846±0,050
Sm^{153}	0,0960	0,370±0,015	0,128	0,522±0,022
Eu^{155}	0,0443	0,171±0,019	0,0568	0,231±0,022
Sm^{156}	0,0313	0,121±0,005	0,0401	0,163±0,007
Eu^{156}	0,0322	0,124±0,005	0,0417	0,170±0,006
Eu^{157}	0,0198	0,0764±0,0037	0,0319	0,130±0,006
Gd^{159}	0,00561	0,0216±0,0007	0,0113	0,0462±0,0018
Tb^{161}	0,00134	0,00515±0,00020	0,00200	0,00815±0,00032
Y^{91}	0,639	2,46±0,08	0,409	1,67±0,06

absorption of the β particles of Ce^{141} and a mixture of Ce^{144} and Pr^{144} [9]. The activity of Mo^{99} was calculated according to the method of least squares from the curve of the increase in the activity of Tc^{99m} in Mo^{99}. The activity measurements were begun 0.5-1.0 h after the removal of Tc^{99m}.

Table 1 presents the calculated absolute cumulative yields and mean square errors of four to seven experiments; the data of other authors are also cited for comparison.

In the calculation of the yields of fragments of the fission of Pu^{241}, the contribution from the fission of Pu^{239}, contained in the samples, was also considered; it came to 4-7% of the total number of fissions. The values of the cross-sections of the fission of Pu^{239} and Pu^{241} by neutrons of the reactor spectrum were taken from [10], while the yield of Ba^{140} for Pu^{239} was taken from [11]. In all cases the calculation was performed, just as in [9], considering the yields of the predecessors in the chains.

We earlier determined the cumulative yields of the rare earth elements and Y^{91} relative to the cumulative yield of Ce^{144} in the fission of Pu^{239} and Pu^{241} by slow neutrons [9]. The absolute yields of these elements, calculated on the basis of the absolute yield of Ce^{144}, determined in this work, are cited in Table 2.

The negligible changes in the values of the relative yields in comparison with the same data of [9] are explained by the fact that Table 2 includes the results of still another experiment. The values of the yields of Sm^{156}, Eu^{156}, and Sm^{156*} were recalculated, using the half-life of Sm^{156} (9.4 ± 0.1) h.

LITERATURE CITED

1. C. Westcott, W. Walker, and T. Alexander, Report No. 202, Presented by Canada at the Second International Conference on the Peaceful Uses of Atomic Energy (Geneva, 1958).
2. E. Huffman, R. Oswalt, and L. Williams, J. Inorg. Nucl. Chem., 3, 49 (1956).
3. O. M. Lilova and B K. Preobrazhenskii, Radiokhimiya, 2, 731 (1960).
4. J. Ryan and E. Wheelwright, J. Indian Engng. Chem., 51, 60 (1959).
5. F. Moor, Analyt. Chem., 39, 1874 (1967).
6. A. K Babko and O. M. Eremenko, Zh. Analiticheskoi Khim., 13, 206 (1958).
7. A. I. Kalinin, R. A. Kuznetsov, and V. V. Moiseev, Radiokhimiya, 4, 565 (1962).
8. A. I. Lazarev and V. I. Lazareva, Zavod. Lab., 24, 798 (1958).
9. N. V. Skovorodkin et al., Radiokhimiya, 12, 487 (1970).
10. C. Bigham, CRRP-1183 (AECL-1910), 1964 (cited according to BNL-325 (1965)).
11. H Fickel and R. Tomlinson, Canad. J. Phys., 37, 926 (1959).
12. H. Fickel and R. Tomlinson, Canad. J. Phys., 37, 916 (1959).
13. I. Croall and H. Willis, AERE-R-6154 (1969).

*As given in Russian original – Consultants Bureau.

14. I. Croall et al., AERE-R-5086 (1967).
15. S. Katcoff, Nucleonics, 18, 201 (1960).
16. F. Lisman, W. Maeck, et al., Idaho Nuclear Corporation Report IN 1277 (TID-4500) (1969) (cited according to [13]).
17. A. Okazaki and W. Walker, Canad. J. Phys., 43, 1036 (1965).
18. H. Farrar et al., Canad. J. Phys., 42, 2063 (1964).
19. B. Rieder et al., USAEC Document GEAP-5505 (1967) (cited according to [13]).
20. B. Rieder and M. Meek, USAEC Report APED-5398A (1968).
21. C. Lederer, J. Hollander, and I. Perlman, Table of Isotopes, Sixth Edition, Wiley, New York (1967).

MEASUREMENT OF FISSION CROSS SECTIONS OF U^{235} AND Pu^{239} IN A NEUTRON SPECTROMETER BY MEANS OF THE MODERATION TIME

A. E. Samsonov, Yu. Ya. Stavisskii,
V. A. Tolstikov, and V. B. Chelnokov

UDC 539.125.5.164.07

Using a neutron spectrometer, we have measured the fission cross sections of U^{235} and Pu^{239} by means of the moderation time in lead [1, 2]. The energy range of the spectrometer permitted us to find the relative energy dependence of the cross section from about 50 keV to thermal energies. The energy dependence curves of the cross sections were normalized by means of the thermal fission cross section.

Method of Measurement of Cross Section

At the base of the measurement channel of the lead moderator (Fig. 1) we measured the count rate of a fission chamber containing a layer of the test substance, as a function of the moderation time $J_f(t)$ and the neutron density $J_B(t)$, with the aid of a detector with an efficiency proportional to 1/v (a BF_3 counter). Then, as shown in [2],

$$\frac{J_f(t)}{J_B(t)} = \text{const} \int N(E, t)\, v\sigma_f(E)\, dE = k_f \langle \sigma_f(E)\sqrt{E} \rangle = k_f \sigma_f(\bar{E})\sqrt{\bar{E}}\,(1+\delta), \tag{1}$$

where v is the mean velocity of the neutrons at the time of moderation t, $\sigma_f(E)$ is the fission cross section for nuclei of the test substance, $\langle \sigma_f(E)\sqrt{E} \rangle$ is the average over the neutron spectrum of N(E, t) in the moderator at time t, δ is a small correction term representing the replacement $\langle \sigma_f(E)\sqrt{E} \rangle \rightarrow \sigma_f(\bar{E})\sqrt{\bar{E}}$ and depending on the width of the neutron energy spectrum N(E, t) and the energy dependence of the test cross section $\sigma_f(E)$, and k_f is a normalizing factor.

The mean neutron energy $\bar{E}$ (keV) and the moderation time t (μsec) are connected [2] by the relation

$$\bar{E} = \frac{183}{(t+0.3)^2}. \tag{2}$$

If we can neglect the correction term δ, then the expression for the cross section in terms of the neutron energy takes the form

$$\sigma_f(\bar{E}) = \frac{J_f(t)}{J_B(t)} \cdot \frac{1}{k_f \sqrt{\bar{E}}}. \tag{3}$$

The energy dependence of the cross section can be normalized [2] from resolved resonances with known parameters [3] or from the thermal cross section. However, the poor resolution of the spectrometer does not always permit us to resolve resonances in the measured cross section with reliably measured parameters. Furthermore, if the measured cross sections have low resonances with energies of the order of a few tens of electron volts, then the statistical accuracy of measurements in the thermal region becomes inadequate, partly owing to the marked fall in neutron density in the moderator [2],

$$J_B(t) = \text{const}\, t^{-0.35} e^{-t/T}, \tag{4}$$

where T is the mean lifetime of the neutrons ($\sim$890 μsec) in the lead prism, and partly owing to the long times, relative to a neutron burst ($\sim$2000 μsec), to which in this case the thermal region corresponds (1/v law).

Translated from Atomnaya Énergiya, Vol. 31, No. 2, pp. 103-106, August, 1971. Original article submitted August 31, 1970.

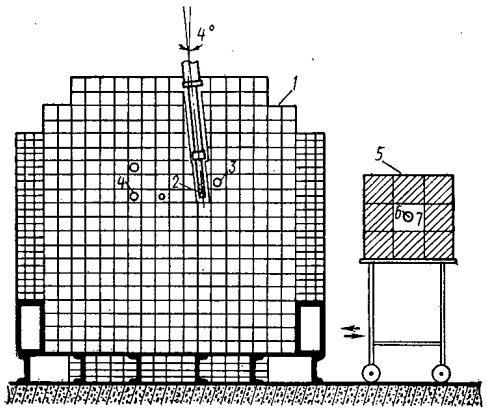

Fig. 1. Diagram of main prism of lead moderator and graphite prism for normalization of cross section curves by means of thermal value. 1) Prism of lead moderator; 2) position of zirconium–tritium target; 3) channel in which fast neutron bursts are registered; 4) main measurement channel; 5) graphite prism; 6) measurement channel of graphite prism; 7) hole in graphite moderator.

TABLE 1. Thermal Cross Sections (in b) Used for Normalization with the Aid of Measurements in a Graphite Prism

	U^{235}	Pu^{239}
$\sigma_f (E=0{,}0253$ eV)	580,2±1,8 [16]	741,6±3,1 [16]
f	0,977 [17]	1,052 [17]
$\bar{\sigma}_f^{th}$	566,8	740,6

An adequately intense thermal neutron spectrum can be obtained in a graphite prism placed near the main prism of the lead moderator (see Fig. 1). Since the thermal neutron density is greater in the graphite prism than in the lead moderator, for the same times relative to a neutron burst we can reliably normalize the data from the thermal cross section.

Method of Normalization by Means of Thermal Cross Section in Graphite Prism

For normalization by the thermal cross section we constructed a graphite prism, 120 × 60 × 60 cm in size. By means of a boron detector we investigated the dependence of the neutron density $J_f^{th}(t)$ in the graphite prism in terms of the time relative to a neutron burst. The results of $J_B^{th}(t)$ measurements show that $\ln J_B^{th}(t)$ has a linear graph which is established at time $t > 1000$ μsec after the formation of an equilibrium spectrum. In this time range the integral neutron density in the graphite prism is about 10 times greater than in the measurement channel of the lead prism.

In the graphite prism we also investigated the dependence of the count rate of the fission chamber, $J_f^{th}(t)$. Then by analogy with Eq. (1) we have

$$\frac{J_f^{th}(t)}{J_B^{th}(t)} = k_f \langle \sigma_f(E^{th}) \sqrt{E^{th}} \rangle, \tag{5}$$

whence we get an expression for the normalization factor from measurements in the graphite prism:

$$k_f = \frac{J_f^{th}(t)}{J_B^{th}(t)} \cdot \frac{1}{\bar{\sigma}_f^{th} \sqrt{\bar{E}^{th}}}, \tag{6}$$

where $\bar{\sigma}_f^{th}$ is the thermal cross section averaged over the Maxwell spectrum in the graphite prism with mean energy $\bar{E}^{th}$.

Measurements and Treatment of Results

We investigated the energy dependence $\sigma_f(E)$ for U^{235} with the aid of a fission chamber containing 15 mg of $UO_2(NO_3)_2$, and the dependence $\sigma_f(E)$ for Pu^{239} with fission chambers containing 1.6 and 12.4 mg of PuO_2. The chambers were filled with a mixture of argon (200 mm Hg) and carbon dioxide (10 mm Hg).

We investigated the time dependence of the detector counts with the aid of a 256-channel analyzer [4].

As a result of the measurements we made a correction for deviation of $\sigma_{B^{10}}(n, \alpha)$, the cross section of boron, from the 1/v law at energies E > 1 keV. This correction was based on an expression which fairly accurately represents the energy dependence of $\sigma_{B^{10}}(E)$ [5]:

$$\sigma_{B^{10}} \text{ (barn)} = \frac{610.3}{\sqrt{E \text{ (eV)}}} - 0.286, \tag{7}$$

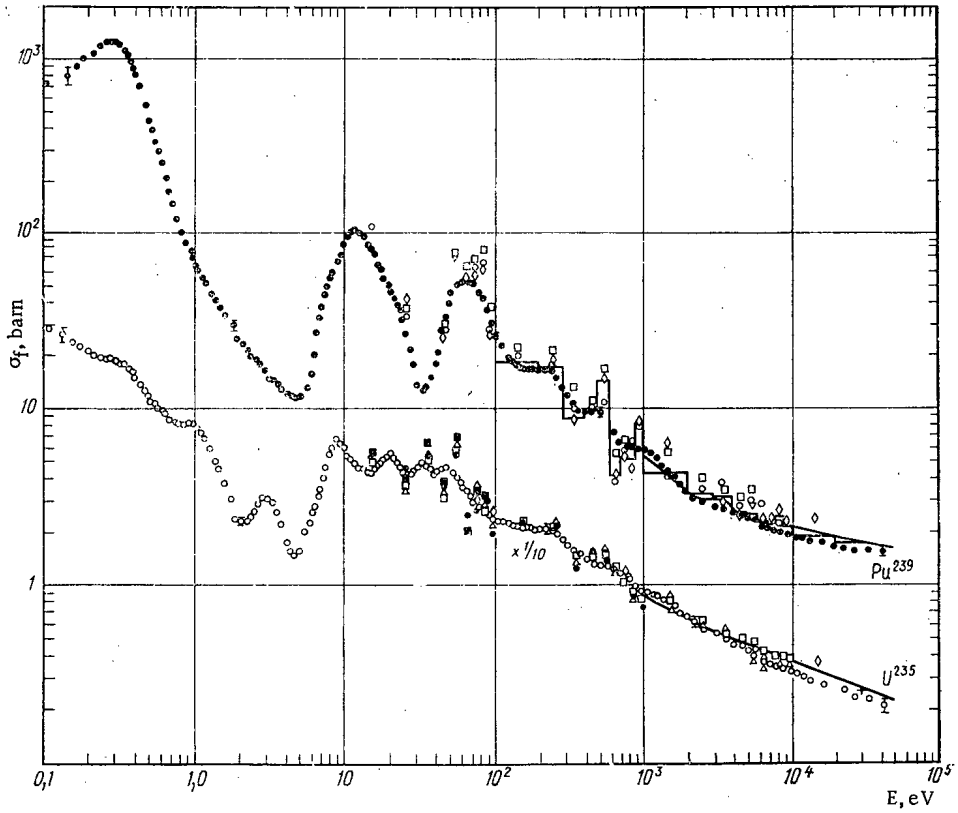

Fig. 2. Energy dependence of fission cross sections of U^{235} and Pu^{239}. Pu^{239}: ●) present authors; ○) [6]; □) [7]; ◇) [8]; ——) [9]; histogram) [5]. U^{235}: ○) present authors; □) [10]; ■) [11]; +) [12]; △) [8]; ●) [13]; ◇) [14]; ——) [9].

TABLE 2. Values of Normalizing Factors Calculated for Measurements with Pu^{239} Fission Chamber

Method of calculation	k_f
By means of thermal cross section in graphite prism	0,487±0,015
By means of group of resonances E_0 = 7.85-32.3 eV	0,500±0,057
By means of resonance E_0 = 0.296 eV	0,514±0,051

the values found were 10% at E = 40 keV and 2% at E = 2 keV.

The correction for the weak resolution of the spectrometer, δ, was based on theoretical estimates of the resolution [2]. To find the value of δ we expand $\langle\sigma_f(E)\sqrt{E}\rangle$ in a series in $E-\overline{E}$, and reject all terms after the second:

$$\langle\sigma_f\sqrt{E}\rangle=(\sigma_f\sqrt{E})|_{\overline{E}}+\frac{\overline{E}^2}{2}\cdot\frac{d^2(\sigma_f\sqrt{E})}{dE^2}\Big|_{\overline{E}}\cdot\frac{\Delta\overline{E}^2}{\overline{E}^2}. \quad (8)$$

Clearly the correction δ is the relative value of the second term in the expansion:

$$\delta=\frac{\overline{E}^2}{2\sigma_f}\left(\frac{d^2\sigma_f}{dE^2}+\frac{1}{E}\cdot\frac{d\sigma_f}{dE}-\frac{1}{4}\cdot\frac{\sigma_f}{E^2}\right)\Big|_{\overline{E}}\cdot\frac{\Delta\overline{E}^2}{\overline{E}^2}. \quad (9)$$

If the measured cross section follows the law $\sigma_f \sim 1/v$, then $\delta = 0$; if σ_f = const, then

$$\delta=-\frac{1}{8}\cdot\frac{\Delta\overline{E}^2}{\overline{E}^2}. \quad (9a)$$

The correction in the cross section given by (9) is at most 2% when E ≈ 50 keV, where the resolution of the spectrometer is worst (~70%).

DISCUSSION OF RESULTS

The results of our measurements of the energy dependences of the fission cross sections of U^{235} and Pu^{239} are plotted in Fig. 2. The cross-section ratio $\sigma_f^{Pu^{239}}/\sigma_f^{U^{235}}$ is plotted in Fig. 3.

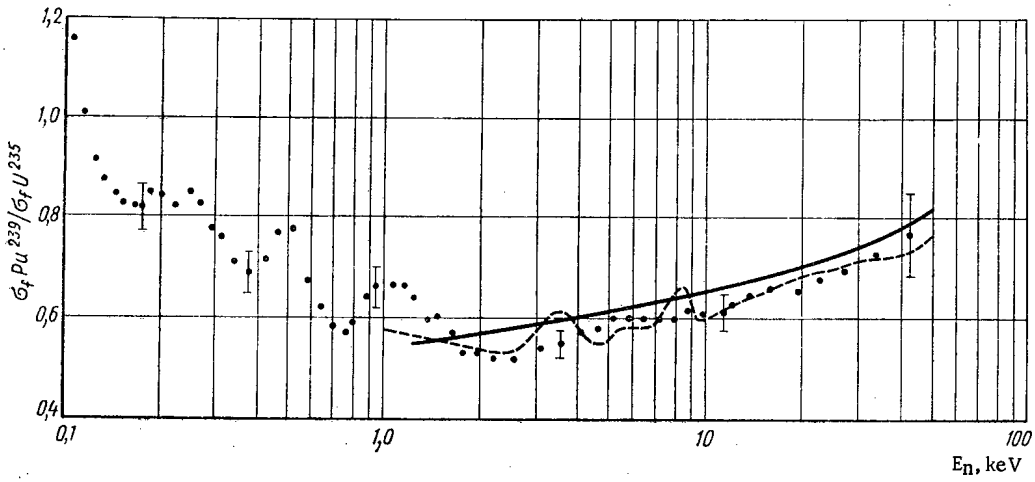

Fig. 3. Energy dependence of cross-section ratio $\sigma_f Pu^{239}/\sigma_f U^{235}$. ●) Present authors' data; ——) [15]; – – –) [9].

The cross sections were normalized with the aid of the thermal spectrum in the graphite prism. The thermal cross sections used to calculate the normalizing coefficient are listed in Table 1. The values of the normalizing factors calculated for the fission cross section of Pu^{239} from the resonance $E_0 = 0.296$ eV and the resolved group of resonances $E_0 = 7.85$–32.3 eV with known parameters [3] agree, within the experimental error, with the values calculated from the thermal cross section (Table 2).

The rms error in the measurement results is due mainly to errors in normalization, statistical errors (~2%), and errors in extrapolation of the time–energy curve (2) to low energies (E < 1 eV) and high energies (E > 10 keV) [2]. Errors in normalization by the thermal cross section are mainly due to statistical error and count instability in the graphite prism, and amount to about 3%.

Note that the effect of diffusion cooling, estimated from the formulas in [18], leads to reduction in the spectral temperature in the graphite prism by about 12°C. From the graphs in [17] it follows that the values of $\bar{\sigma}_f^{th}\sqrt{\bar{E}^{th}}$ used in normalizing the fission cross sections then alter by less than 0.2%.

The results of our measurements of σ_f for U^{235} in the range E > 5 keV diverge from the recommended data in [9] on average by 9–12%; the discrepancy with [12] at 30 keV is about 10%.

At energies of 0.07–10 keV, our results agree within the error of measurement with the averaged selector data in [8, 10, 11, 13, 14], which we assign to the mean value of the energy averaging interval. The discrepancy at energies below 0.07 keV is probably due to the different values of the resolution in our work and in the above-cited papers.

Our results for σ_f for Pu^{239} at energies E < 6 keV agree with the averaged data in [5] and the recommended data in [9].

At E > 6 keV we observe a systematic deviation from the data in [5, 9], averaging 12–15%. The discrepancy with the averaged data of selector experiments [6–8] is probably due partly to insufficient resolution in our method of measurement in comparison with these experiments.

The values obtained for σ_f^9/σ_f^5 agree with the averaged values in [19]. The agreement with the recommended values of Hart [9] is much better. The recommended results of Davey [15] seem somewhat too high in comparison with our own experimental data.

LITERATURE CITED

1. A. A. Bergman et al., First Geneva Conference (1955), Vol. 4, Izd-vo AN SSSR, Moscow (1957), p. 166.
2. F. L. Shapiro, Trudy FIAN, 24, 3 (1964).
3. J. Stehn et al., Neutron Cross Sections, BNL-325, Suppl. 2, 2nd ed. (1965).
4. I. V. Shtranikh, A. M. Klabukov, and A. E. Samsonov, Trudy FIAN, 42, 69 (1968).
5. Materials of Conference of Experts of International Atomic Energy Agency [Russian translation], Winfrith (1969).

6. L. Bollinger et al., Second Geneva Conference (1958), Vol. 2, Atomizdat, Moscow (1959), p. 123.
7. J. Friedman and M. Platt, BNL-883 (T-357).
8. J. James and M. Schomberg, AERE-M2157, Harwell (1969).
9. W. Hart, UK–USSR Seminar, Paper UK-10, Dubna (June, 1968).
10. A. Michaudon et al., J. de Physique, 21, 429 (1960).
11. T. A. Mostovaya and O. G. Bespalov, Bulletin of Nuclear Data of the Information Center, No. 3, Atomizdat, Moscow (1966). p. 10.
12. G. Knoll and W. Poenitz, J. Nucl. Energy, A/B 21, 643 (1967).
13. M. Yeater et al., Phys. Rev., 104, 479 (1956).
14. Wang Shih-ti et al., in: Physics and Chemistry of Fission, Vol. 1, IAEA, Vienna (1965), p. 287.
15. W. Davey, Nucl. Sci. and Engng., 26, 149 (1966).
16. G. Hanna et al., Atomic Energy Rev., 7, No. 4 (1969).
17. J. Hughes, Effective Neutron Cross Sections [Russian translation], Izd-vo IL, Moscow (1959).
18. A. Weinberg and E. Wigner, The Physical Theory of Nuclear Reactors [Russian translation], Izd-vo IL, Moscow (1961).
19. W. Gilbey and G. Knoll, KFK-450 (October, 1966).

NEUTRON RADIATIVE CAPTURE CROSS SECTIONS IN SILVER, Au^{197}, Th^{232}, AND U^{238}

Yu. Ya. Stavisskii, V. A. Tolstikov, V. B. Chelnokov, A. E. Samsonov, and A. A. Bergman

UDC 539.172.4

The neutron radiative capture cross section in heavy nuclei is of interest in nuclear theory and in reactor construction.

This paper presents measurements of averaged neutron radiative capture cross sections for silver, Au^{197}, Th^{232}, and U^{238} in the energy region below 50 keV which were obtained with a neutron spectrometer using slowing-down time in lead [1, 2].

Normalization of the energy dependence of the cross sections for silver and Au^{197} was carried out by means of resolved low-lying resonances and thermal capture cross sections based on measurements in a graphite prism located close to the main prism of the lead moderator [3]. Normalization of the energy dependence of the cross sections for Th^{232} and U^{238} was carried out by means of low-lying resonances and radiative capture cross sections for silver and Au^{197}. The data presented here is compared with other results.

Method of Measurement

In the working channel of the lead moderator, measurements were made of the dependence on slowing-down time of the prompt radiative capture γ-ray count from the sample, $J_\gamma(t)$, by means of a γ-detector, and of the neutron flux flux, $J_B(t)$, by means of a 1/v counter (BF_3 counter). Then, as was shown in [2],

$$\sigma_c(E) = \frac{\mathcal{J}_\gamma(t)}{\mathcal{J}_B(t)} \cdot \frac{(t+0{,}3)}{k_x}, \quad (1)$$

where $\sigma_c(E)$ is the radiative capture cross section of the sample nuclei, and $k_x(\bar{n}, M, \varepsilon_c)$ is a normalization factor which depends on the effective sample thickness, $\bar{n}$, the monitor count, M, and the detection efficiency for a capture event, ε_c.

The average neutron energy E (keV) and the slowing-down time t (μsec) are connected by the empirical relation [2]

$$E = \frac{183}{(t+0.3)^2}. \quad (2)$$

Detector

A gas proportional counter was used as the detector of prompt capture γ-rays. By surrounding the walls of the counter with lead (having a total thickness $d \geq R_e$, where R_e is the range of the secondary electrons produced by the γ-rays from radiative capture) and filling to high pressure (10 atm of argon + 4% CO_2), it was possible to make the dependence of the γ-ray detection efficiency (ε_γ) on γ-ray energy (E_γ) nearly linear

$$\varepsilon_\gamma \approx \text{const}\, E_\gamma. \quad (3)$$

In this case, the detection efficiency for a radiative capture event is determined only by the total energy of the γ-ray cascade, i.e., by the neutron binding energy in the nucleus B_n (since the kinetic energy of the

Translated from Atomnaya Énergiya, Vol. 31, No. 2, pp. 107-112, August, 1971. Original article submitted December 7, 1970.

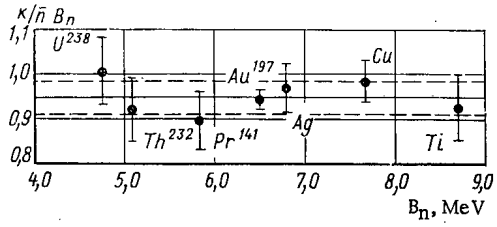

Fig. 1. Dependence of the adjusted normalization factor on B_n for the various samples measured with a proportional gamma counter.

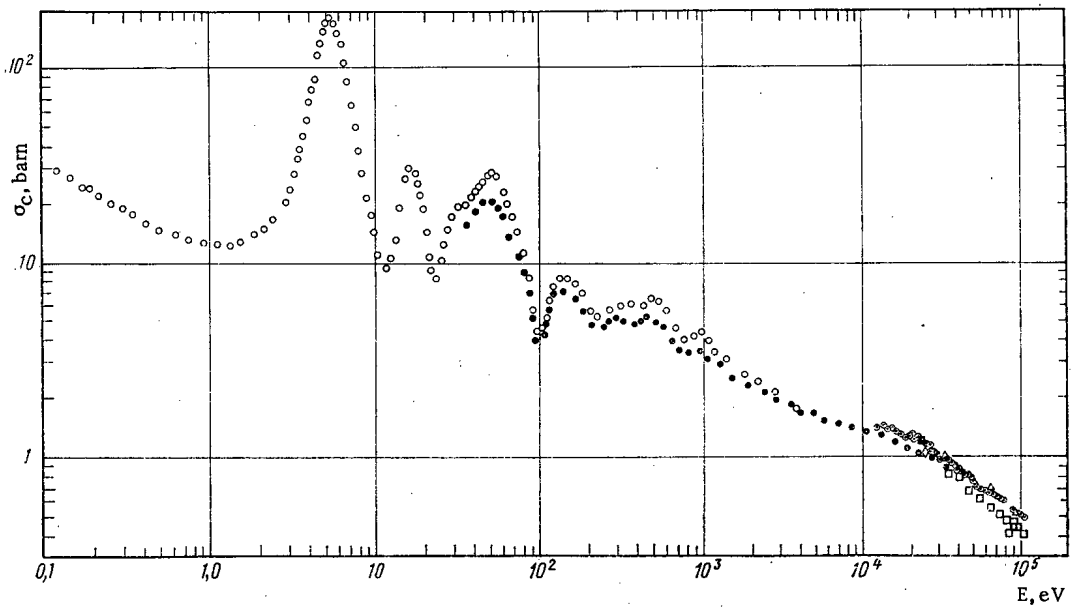

Fig. 2. Energy dependence of the radiative capture cross section in silver: ●, ○) this work; ◇) [12]; □) [24]; ⊙) [25]; ■) [26]; △) [27].

TABLE 1. Values of Normalization Factors

Sample	Method	k_x
Silver, $\bar{n}$ = 2,2 × 10^{21} atom /cm²	Resonance Ag^{109}, E_0 = 5,19 eV	1,392±0,089
	Thermal cross section σ_c^{Th} = 63,6±0,6 barn [7]	1,465±0,030
Au^{197}, $\bar{n}$ = 1,8 × 10^{21} atom /cm²	Resonance Au^{197} E_0 = 4,906 eV	1,104±0,066
	Thermal cross section σ_c^{Th} = 98,8 ±0,3 barn [7]	1,096±0,025
Th^{232}, $\bar{n}$ = 1,0 × 10^{21} atom /cm²	Resonance Th^{232} E_0, 21,78 and 23,45 eV	0,467±0,036
	Au^{137}, $\bar{n}$ = 6,0 × 10^{20} atom/cm²	0,477±0,028
U^{238}, $\bar{n}$ = 1,3 × 10^{21} atom /cm²	Resonance U^{238} E_0 = 6,67 eV	0,621±0,077
	Au^{197}, $\bar{n}$ = 6,0 × 10^{20} atom/cm²	0,582±0,038

neutron can be neglected)

$$\varepsilon_c \approx \text{const}\, B_n, \qquad (3a)$$

and does not depend on changes in the γ-ray spectrum from resonance to resonance [4].

The accuracy of Eq. (3a) can be evaluated through measurements of the various samples on a proportional gamma counter. Since the normalization factor k_x (calculated from resonances of known parameters [5] or from the thermal cross section [3, 5] and adjusted for sample thickness $\bar{n}$ and neutron flux) depends only on the detection efficiency for a capture event, it is possible to determine the dependence $\varepsilon_c(B_n)$.

Normalization factor values obtained by gamma counter measurements of the various samples are shown in Fig. 1. A least-squares analysis of the results yields a value $k_x/\bar{n}B_n = 0.945 \pm 0.037$; it then follows that Eq. (3a) is satisfied with an accuracy of ±4% for the gamma detector used in the measurements.

Measurements and Analysis of Results

Sample measurements were made with a neutron burst frequency f equal to 625 and 312.5 Hz. The duration of the neutron burst was kept to a minimum (~0.5 μsec) in those sets of measurements where it was important to obtain data on the energy dependence of the cross sections in the keV energy region (at small slowing-down times).

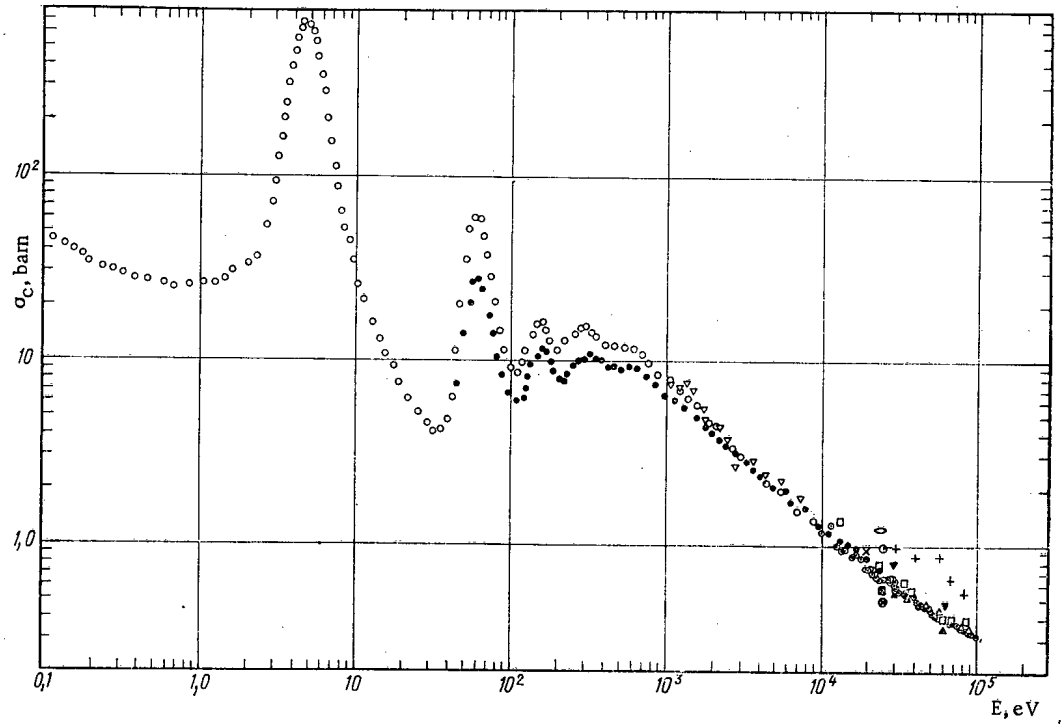

Fig. 3. Energy dependence of the radiative capture cross section in Au^{197}: ●, ○) this work; □) [30]; △) [31]; ◑) [33]; ×) [32]; ⊙) [34]; ■) [12]; ▲) [35]; ▼) [36]; ▽) [37]; +) [18]; ×) [10].

The amplification channel of the gamma counter combined a UIS-2 nonoverloading amplifier with a "Siren" discriminator amplifier. The time dependence of the detector counts was investigated with a 256-channel analyzer from the Measurement and Detection Center of FIAN [6].

In measurements of the effect of capture in the sample and of the spectrometer γ-background (without sample), the detector activation was maintained at saturation (the counter was irradiated for ~10 min before the beginning of each set of measurements), which made it possible to neglect it in the analysis of the results. Measurements of the effect were alternated with measurements of the natural γ-background of the samples (thorium and uranium). Correction for the contribution from the natural γ-background, which was constant for equal time intervals over the entire time range, to the total count was made by simple subtraction. Sample activation was determined from the ratio of the counts obtained for measurements in the gamma counter to the counts obtained from measurements in a boron detector, where there is no activation, in the analyzer channels corresponding to energy regions in which the cross section under study follows the 1/v law:

$$\frac{J'_\gamma - a}{J'_B} = \frac{J''_\gamma - a}{J''_B} = \text{const.} \tag{4}$$

It is then easy to obtain an expression for the determination of the activation correction:

$$a = J'_\gamma - J'_B \frac{(J'_\gamma - J''_\gamma)}{(J'_B - J''_B)}. \tag{5}$$

Evaluation of other corrections and possible errors in measurement, made in accordance with [5], leads to an insignificant error (less than 1-1.5%) in the cross sections investigated.

Normalization of the energy dependence of the cross sections was made by means of resolved resonances with known parameters [5] and by means of thermal capture cross sections obtained by measurements in a graphite prism located near the main prism of the lead moderator [3]. In addition, measurements with a gamma detector for which Eqs. (3) and (3a) were satisfied permitted normalization by means of measurements of samples for which the radiative capture cross sections were reliably known. Then if the investigated and standard samples had identical geometries

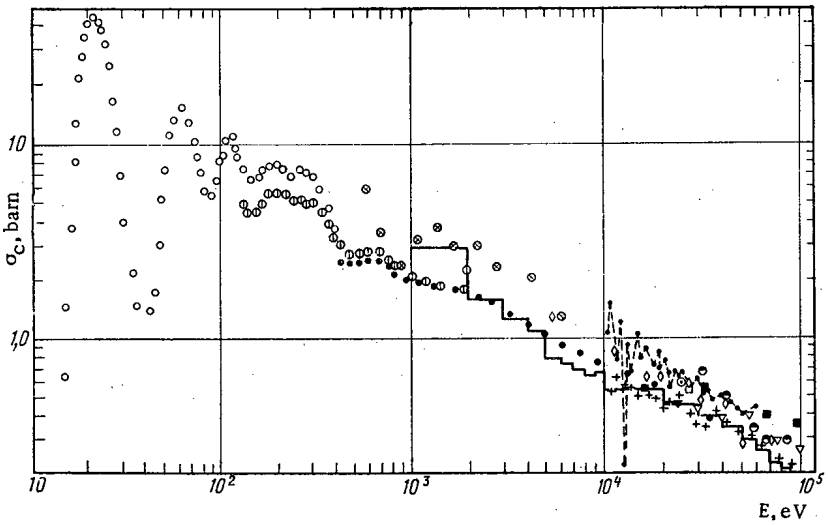

Fig. 4. Energy dependence of the radiative capture cross section in Th^{232}: ●, ⊕, ○) this work; ■) [9]; ▽) [18]; ◇) [20]; ◓) [19]; □) [26]; ▼) [10]; ⊙) [12]; ⊗) [13]; +) [14]; – – –) [15]; ——) [16].

$$k_x = k_{st}\frac{\bar{n}_x M_x \varepsilon_c^x}{\bar{n}_{st} M_{st} \varepsilon_c^{st}} = k_{st}\frac{\bar{n}_x M_x B_n^x}{\bar{n}_{st} M_{st} B_n}, \qquad (6)$$

where k_x, n_x, M_x, ε_c^x, and B_n^x are respectively the normalization factor, sample thickness, monitor count, detection efficiency for a capture event, and nuclear binding energy for the sample under study, and k_{st}, n_{st}, M_{st}, ε_c^{st}, and B_n^{st} are the same quantities for the standard. Normalization factor values obtained from measurements of the samples under study are shown in Table 1. The errors shown are the results of statistics and the inaccuracy of the resonance parameters used [7].

DISCUSSION OF RESULTS

Silver. The energy dependence of $\sigma_c(E)$ for silver was measured with samples containing the natural mixture of isotopes having two effective thicknesses: $4.3 \cdot 10^{21}$ and $2.2 \cdot 10^{21}$ atom/cm^2 (● and ○ respectively in Fig. 2).

The data obtained in this work is in agreement with measurements made with the slowing-down-time spectrometer previously [5] (normalization by means of the resonance at $E_0 = 5.19$ eV). The agreement with other data shown in Fig. 2 is good; it is within the limits of experimental error.

Au^{197}. The energy dependence of $\sigma_c(E)$ for Au^{197} was measured with samples of two effective thicknesses: $1.8 \cdot 10^{21}$ and $6.0 \cdot 10^{20}$ atom/cm^2 (● and ○ respectively in Fig. 3).

The data obtained in this work is also in agreement with previously obtained results from the slowing-down-time spectrometer [8] (normalization by means of the resonance at $E_0 = 4.9$ eV). The agreement with other work, mainly using time of flight, is good.

Th^{232}. The energy dependence of $\sigma_c(E)$ for Th^{232} was measured with ThO_2 samples of three effective thicknesses: $9.6 \cdot 10^{21}$, $4.0 \cdot 10^{21}$, and $1.0 \cdot 10^{21}$ atom/cm^2 (●, ◓, and ○ respectively in Fig. 4).

The data from [9-16] is presented in original form while that from [17-20] was renormalized as described below. By way of warning, we point out that we did not have numerical data available from [9, 13-16]. The appropriate information was taken from figures in the publications mentioned.

In [20], the cross section σ_c for Th^{232} was measured by the activation technique. In calculating the cross section from the experimental data, the authors used a γ-ray yield $K = 0.9$ quanta/decay for γ-rays with an energy $E_\gamma = 311$ keV. According to the decay scheme for Pa^{233}, however, only a fraction $K_1 = 0.36$ of the β decays yields quanta with an energy of 311 keV, and a fraction $K_2 = 0.59$ of the β decays yields quanta with an energy of 311 keV in cascade with quanta of lower energies. Obviously, only $K_2/2$ of the quanta arrive at the crystal unaccompanied by cascade quanta, and will be recorded in the 311 keV photopeak. The remaining half of these quanta must be recorded in the sum peak of the cascade. However, the

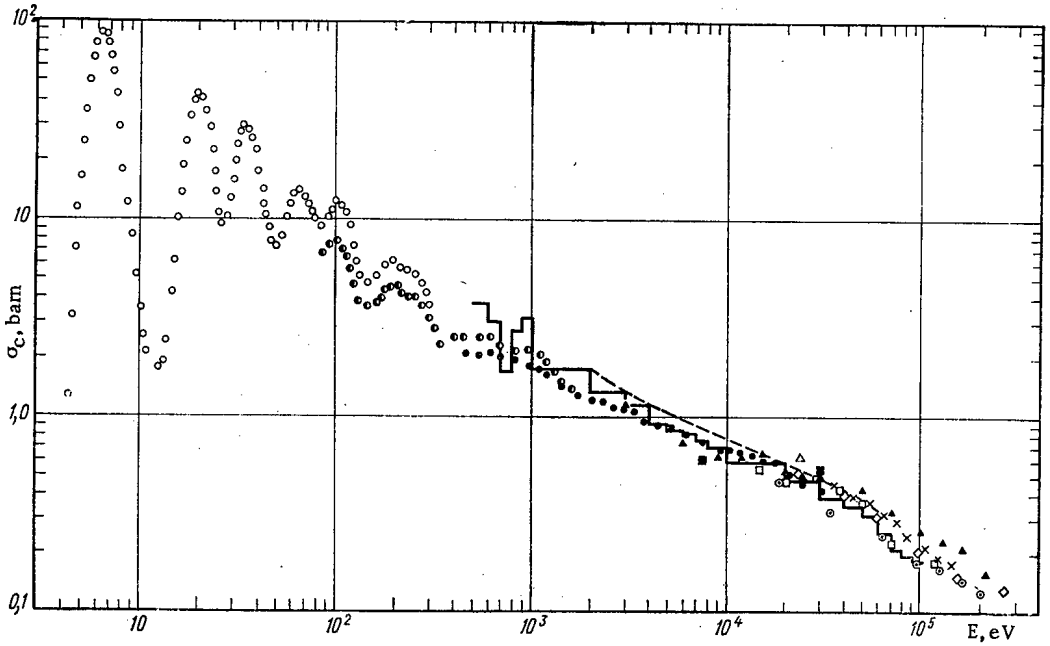

Fig. 5. Energy dependence of the radiative capture cross section in U^{238}: ●, ◐, ○) this work; △) [26]; □) [20]; ▲) [38]; ——) [16]; ⊙) [27]; ■) [39]; ◇) [40]; ×) [41]; – – –) [42];

softer quanta are more strongly absorbed in the sample and in the crystal housing; consequently, there is an additional fraction of γ rays with E_γ = 311 keV which will be recorded in the 311-keV photopeak. Therefore the true fraction of γ rays per β decay event lies between the values $K_1 + K_2/2$ and $K_1 + K_2$. As an estimate, one can take $K = (K_1 + 3K_2/4) \pm k_2/4$. Then the adjusted cross section will be 560 ± 150 mb.

The data from [17] was renormalized by using $\sigma_c(E)$ for I^{127} taken from the curve in the atlas [7]. In addition, the more recently recommended value of 6.2 b [7] was used in place of $\sigma_c^{Th} = 5.6$ b.

In [19], the behavior of the cross section σ_c for Th^{232} was measured with respect to the cross section for the $B^{10}(n, \alpha)$ reaction. These results were reviewed and joined with σ_c (24 keV) = 615 mb [12]. The results in [18] were renormalized by taking into account new fission cross sections taken from [22].

Our data in the energy region above 5 keV is in agreement within the limits of experimental error with the main part of previously published work. In this region, and also in the region below 5 keV, there are significant disagreements with [13, 16]. It is difficult to point out the reasons for such discrepancies without having more detailed information. It is necessary to point out, however, that in comparing data from different authors, it is important to consider differences in resolution and sample thickness (blocking effect).

U^{238}. The energy dependence of the cross section $\sigma_c(E)$ for U^{238} was measured with U_3O_8 samples of three effective thicknesses: $7.1 \cdot 10^{21}$, $3.9 \cdot 10^{21}$, and $1.3 \cdot 10^{21}$ atom/cm^2 (●, ◐, and ○ respectively in Fig. 5).

Preliminary data on the neutron radiative capture cross section of U^{238} was published earlier [23]. In this work, this data is brought to final form after refinement of the experimental constants associated with the normalization of the energy dependence of the cross section.

In Fig. 5, our data is compared with other results, which are presented in original form with the exception of [19] where the data was renormalized to the value σ_c = 439 mb (E = 24 keV). One should also keep in mind that the results in [16] were obtained with a U^{238} sample thinner than ours ($1.3 \cdot 10^{21}$ atom/cm^2) and therefore the blocking effect should be weaker.

In conclusion, the authors express their gratitude to I. M. Frank and I. Ya. Barit for offering the opportunity to make measurements with the slowing-down-time spectrometer, to F. L. Shapiro for his interest and for valuable discussions, to I. V. Shtranikh for arranging the work at the Measurement and Detection Center, to Yu. A. Dmitrenko, V. M. Polyakov, and their associates in the electronics group for help with the measurements, and to I. V. Syutkina and E. N. Zhukova for help in analysis of the results.

LITERATURE CITED

1. A. A. Bergman et al., Papers from International Conference on Peaceful Uses of Atomic Energy (Geneva, 1955), Vol. 4 [in Russian], Izd-vo AN SSSR, Moscow (1957), p. 166.
2. F. L. Shapiro, Trudy FIAN SSSR, 24, 3 (1964).
3. A. E. Samsonov et al., At. Énerg., 31, 103 (1971).
4. M. Moxon et al., UK/USSR Seminar, Paper UK/22, Dubna (1968).
5. Yu. P. Popov, Trudy FIAN SSSR, 24, 111 (1964).
6. I. V. Shtranikh et al., ibid., 42, 69 (1968).
7. D. Hughes et al., Neutron Cross Sections, Suppl. to BNL-325, 2nd ed. (1960); J. Stehn et al., ibid., Vol. III (1965); M. Goldberg et al., ibid., Vol. II (1966).
8. V. A. Konks et al., ZhÉTF, 46, 80 (1964).
9. BNL-325, 2nd ed., 7 (1958) (Los Alamos data).
10. A. Chaubey and M. Sehgal, Nucl. Phys., 66, 267 (1965).
11. R. Schuman, Wash-1127 (1969).
12. T. S. Belanova et al., At. Énerg., 19, 3 (1965).
13. R. Block and G. Slaughter, ORNL-2910, 35 (1960).
14. M. Moxon and C. Chaffey (1963) (see [4]).
15. R. Macklin and J. Gibbons (1964) (see [4]).
16. M. Moxon, Dissertation, London University (1968).
17. Yu. Ya. Stavisskii and V. A. Tolstikov, At. Énerg., 10, 508 (1961).
18. J. Miskel et al., Phys. Rev., 128, 2717 (1962).
19. V. A. Tolstikov et al., At. Énerg., 15, 414 (1963).
20. R. Macklin et al., Phys. Rev., 107, 504 (1957).
21. B. S. Dzhelepov, P. K. Peker, and V. S. Sergeev, Decay Schemes of Radioactive Nuclei [in Russian], Izd-vo AN SSSR, Moscow–Leningrad (1963).
22. W. Hart, AHS B (S), R-124 (1967).
23. A. A. Bergman et al., Second International Conference on Nuclear Data, Paper CN-26/78, Helsinki (1970).
24. V. N. Kononov et al., Nuclear Data for Reactors, 1, 469 (1967).
25. D. Kompe, Fast Reactor Physics, 1, 67 (1968).
26. H. Schmitt and C. Cook, Nucl. Phys., 20, 202 (1960).
27. I. Bergqvist, Arkiv Fys., 23, 425 (1963).
28. W. Poenitz, J. Nucl. Energy, 20, 825 (1966).
29. T. Ryves et al., J. Nucl. Energy, 20, 248 (1966).
30. K. Harris et al., Nucl. Phys., 69, 37 (1965).
31. W. Poenitz et al., J. Nucl. Energy, 22, 505 (1968).
32. R. Booth et al., Phys. Rev., 112, 226 (1958).
33. V. N. Kononov et al., At. Énerg., 5, 564 (1958).
34. K. Beckurts et al., Fast Reactor Physics, 1, 67 (1968).
35. R. Macklin et al., Phys. Rev., 129, 2695 (1963).
36. L. Weston et al., Phys. Rev., 123, 949 (1961).
37. R. Block et al., Neutron Time-of-Flight Methods (Saclay Conference) (1961), p. 203.
38. E. Bilpuch et al., Ann. Phys., 10, 455 (1960).
39. E. Arai et al., Nucl. Sci. Engng., 26, 573 (1960).
40. H. Menlove and W. Poenitz, Nucl. Sci. Engng., 33, 24 (1968).
41. Yu. G. Penitkin et al., Second International Conference on Nuclear Data, Paper CN-26/77, Helsinki (1970).
42. W. Davey, Nucl. Sci. Engng., 39, 337 (1970).

EXPERIMENTAL INVESTIGATION OF THE FEASIBILITY OF INCREASING THE CAPACITY OF INDIUM – GALLIUM CIRCUITS

G. I. Kiknadze, V. S. Bedbenov, R. B. Lyudvigov, and L. G. Sharimanova

UDC 621.039.55

The great interest in liquid-metal radiation circuits with indium–gallium and indium–gallium–tin alloys is associated with the possibility of creating high-power γ-radiation sources [1]. The radiation capacity of such installations depends in a considerable measure on the kind of activity generators in which neutron fluxes, leaking out of the nuclear reactor core, are directly converted into pure γ-radiation.

Up until recently, such generators consisted of single "thick" ($\Sigma_a d \sim 1$)* blocks of indium γ-carrier located in the reactor reflector [2-5].

The high absorption of thermal and resonance neutrons in such activity generators causes drastic disturbance of the neutron flux, the self-shielding factor is very low, and the total number of absorbed neutrons is small in comparison with the total leakage of core neutrons into the reflector.

At the same time, the specific radiation power of the γ-carrier $A = \overline{\Phi}\Sigma_a\Gamma$ [6] (where $\overline{\Phi}$ is the average neutron flux that activates the carrier and Γ is the energy released in the decay of one carrier nucleus) determines the maximum possible overall capacity of any radiation circuit R:

$$R \approx \overline{\Phi}\Sigma_a\Gamma \frac{V_{ag}V_{ir}}{V_{ag}+V_{ir}+V_{rc}} = A \frac{V_{ag}V_{ir}}{V_{ag}+V_{ir}+V_{rc}}, \quad (1)$$

where V_{ag}, V_{ir}, and V_{rc} are the volumes of the γ-carrier in the activity generator, irradiator, and radiation circuit respectively. The factor $\overline{\Phi}\Sigma_a\Gamma$ in (1) corresponds to saturation activity of the γ-carrier and depends solely on the average flux of neutrons generating radioactive nuclei.

Obviously, the main factor in increasing the total radiation circuit capacity is the neutron flux $\overline{\Phi}$ which determines the magnitude of A for a given species of γ-carrier nuclei.

The method suggested in [7] has been used to calculate the thermal neutron distribution in indium γ-carrier blocks in a graphite reflecting layer $\sqrt{\tau}$†. The layer touches the core border. Figure 1 shows the thermal neutron distribution in indium γ-carrier blocks numerically calculated by solving the one-velocity kinetic Boltzmann equation by the spherical harmonic method in the P_3 approximation. An analysis of these curves for absorbing blocks λ_a/n (n = 0.5, 1, 2, 4, 8, 16) thick indicates that the thermal-neutron self-shielding factor of the block can be substantially increased by using "thin" ($\Sigma_a d \approx 0.1$) indium γ-carrier layers. (For example, if $\lambda_a/16$, the thermal neutron flux that activates the γ-carrier is nearly equal to the undisturbed flux.) On the other hand, the influence function, calculated for thin indium layers spaced at $\sim\lambda_{tr}$‡ in a moderator block with continuously distributed thermal neutron sources, indicates the advisability of using multilayer activity generator systems. Thus, the interlayer influence function of an

*Where Σ_a is the macroscopic absorption cross section of thermal neutrons in the indium γ-carrier. $\Sigma_a d = 1$ when $d = \lambda_a$, λ_a being the mean absorption path of thermal neutrons in the γ-carrier.

† τ denotes the neutron age in the moderator.

‡ λ_{tr} is the transport mean free path of neutrons in the moderator.

Translated from Atomnaya Énergiya, Vol. 31, No. 2, pp. 113-118, August, 1971. Original article submitted August 6, 1970; revision submitted January 4, 1971.

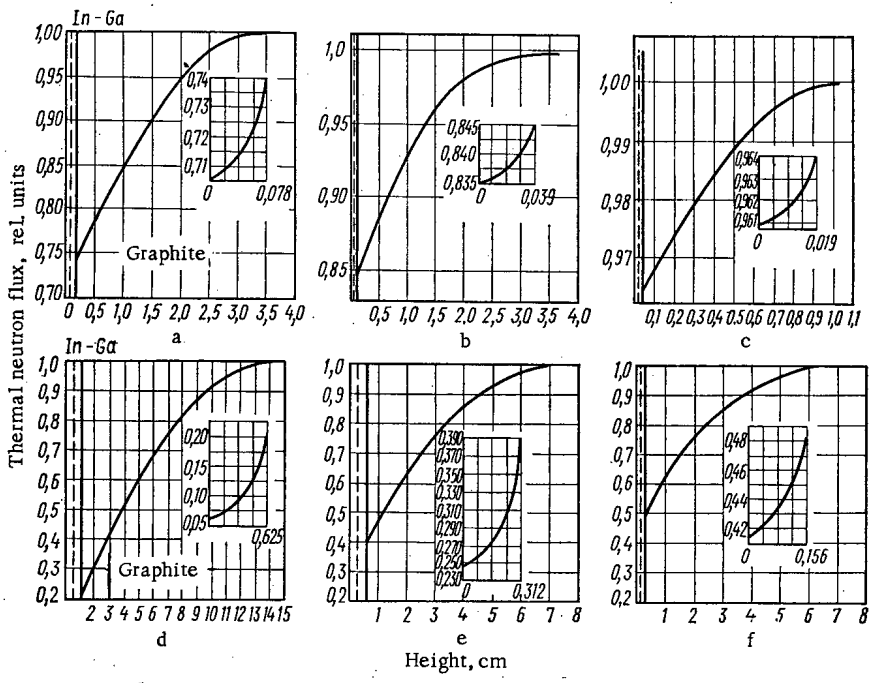

Fig. 1. Thermal neutron distribution in an indium–gallium–graphite system (inserts show thermal neutron distribution within the indium absorber layer): a) $\lambda_a/4 = 0.156$ cm; b) $\lambda_a/8 = 0.078$ cm; c) $\lambda_a/16 = 0.039$ cm; d) $2\lambda_a = 1.25$ cm; e) $\lambda_a = 0.625$ cm; f) $\lambda_a/2 = 0.312$ cm.

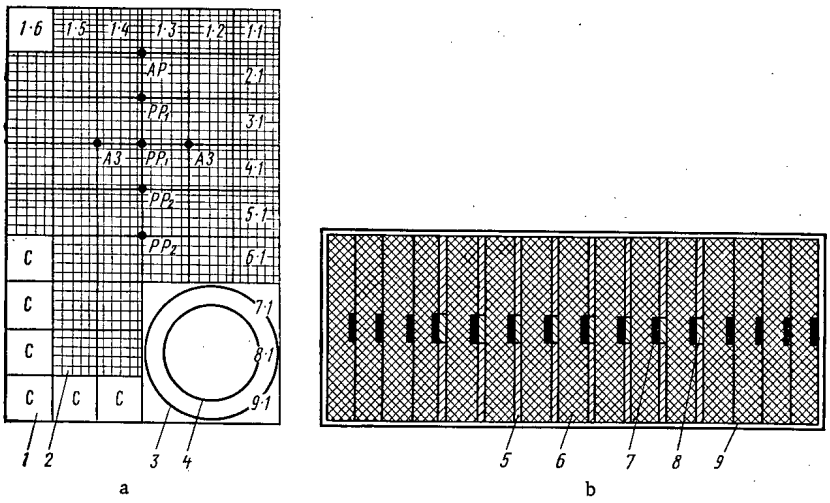

Fig. 2. Location of vertical channel in nuclear reactor core (a) and graphite assembly of eight-layer activity generator model (b): 1) graphite; 2) fuel; 3) 180 mm channel; 4) 120 mm assembly; 5) $\lambda_a/8$ indium foil; 6) 2 cm graphite layer; 7) copper monitor; 8) indium sample; 9) aluminum assembly jacket; PP_1, PP_2, AP) reactor control rods.

activity generator consisting of alternating layers of indium γ-carriers $\lambda_a/16$ thick spaced at 2 cm in a graphite reflector $\sqrt{\tau}$ thick amounts to about 5%.

To verify these results, the Physics Institute of the Academy of Sciences of the Georgian SSR conducted an experimental analysis of neutron flux distributions in various heterogeneous assemblies that served as activity generator models.

TABLE 1. Activity Generator Characteristics

Number of model	Location of indium absorber in the graphite assembly model	Relative specific activity of indium in the models normalized for monitor count rate	Average relative specific activity of indium in assembly models	Average specific activity of indium in generator models normalized for average indium activity in generator model having a single indium layer with a thickness λ_a	Ratio of average thermal neutron flux in the various activity generator models to the undisturbed thermal neutron flux in graphite assembly*	Ratio of average thermal neutron flux in the various activity generator models to the average thermal neutron flux in a generator model having a single indium layer with a thickness λ_a
I	One indium layer λ_a thick at the center of graphite assembly. The indium layer consists of eight indium foils $\lambda_a/8$ thick each	78±3,9; 68±3,4; 65±3,3; 60±3,0; 66±3,3; 64±3,2; 68±3,4; 75±3,7;	68±3,4	1	0,37±0,02	1
II	Eight layers of indium $\lambda_a/8$ thick each spaced symmetrically with respect to the assembly center at 20 mm intervals	136±6,8; 119±6,0; 110±5,5; 110±5,5; 99±5,0; 85±4,3; 91±4,5; 97±4,8;	105,9±5,3	1,56±0,16	0,58±0,03	1,57±0,16
III	Eight layers of indium $\lambda_a/4$ thick each spaced symmetrically with respect to the center at 20 mm intervals. Each $\lambda_a/4$ layer consists of two $\lambda_a/8$ indium foils	65±3,2; 48±2,4; 45±2,5; 44±2,2; 49±2,4; 39±2,0; 41±2,0; 40±2,0; 40±2,0; 45±2,3; 36±1,8; 40±2,0; 41±2,0; 42±2,1; 38±1,9; 42±2,1;	43,4±2,2	0,64±0,07	0,23±0,01	0,62±0,06
IV	One $\lambda_a/2$ layer of indium at the center of the graphite assembly. The layer consists of eight $\lambda_a/16$ indium foils	137±7,0; 123±6,2; 115±5,8; 120±6,0; 128±6,4; 126±6,3; 125±6,3; 128±6,4;	125,3±6,3	1,84±0,18	0,66±0,03	1,78±0,18
V	Eight $\lambda_a/16$ indium layers symmetrically spaced with respect to the center at 20 mm intervals	259±13,0; 248±12,5; 247±12,4; 244±12,2; 240±12,0; 236±11,8; 241±12,0; 242±12,1;	244,6±12,3	3,6±0,36	0,37±0,04	2,35±0,24

* As the average thermal neutron flux in activity generator models having a single γ-carrier layer λ_a and $\lambda_a/2$ thick is taken the neutron flux averaged over the measured thermal neutron distribution in the layer. Within the limits of experimental accuracy, the average thermal neutron flux in models with $\lambda_a/4$, $\lambda_a/8$, and $\lambda_a/16$ γ-carrier layers is taken to be the neutron flux measured on the layer surface.

The experiments described below were an attempt to find a range of optimum parameters of various dense indium–graphite lattices serving as activity generator models.

EXPERIMENTAL METHOD

The model assemblies were cylinders consisting of alternating graphite discs and indium foils of various thickness and spacing. The diameter and total height of all assemblies was 120 and 320 mm, respectively.

The assembly construction, made up of individual graphite discs 20 mm thick and of thin indium foil with a thickness $\lambda_a/8 = 125$ mg/cm^2 (0.0173 cm) and $\lambda_a/16$ mg/cm^2 (0.0086 cm), made it possible to vary both the lattice spacing and the thickness of indium layers by varying the number of foils in a layer. We have studied six different configurations of heterogeneous assemblies simulating six different activity generator models (see Table 1).

For plotting the neutron flux distributions in the assemblies and to find the specific activity (specific radiation capacity) stored in the foils, the assemblies were irradiated in a vertical channel 180 mm in diameter placed at the edge of the core of the IRT nuclear reactor in Tbilisi [8] (see Fig. 2a).

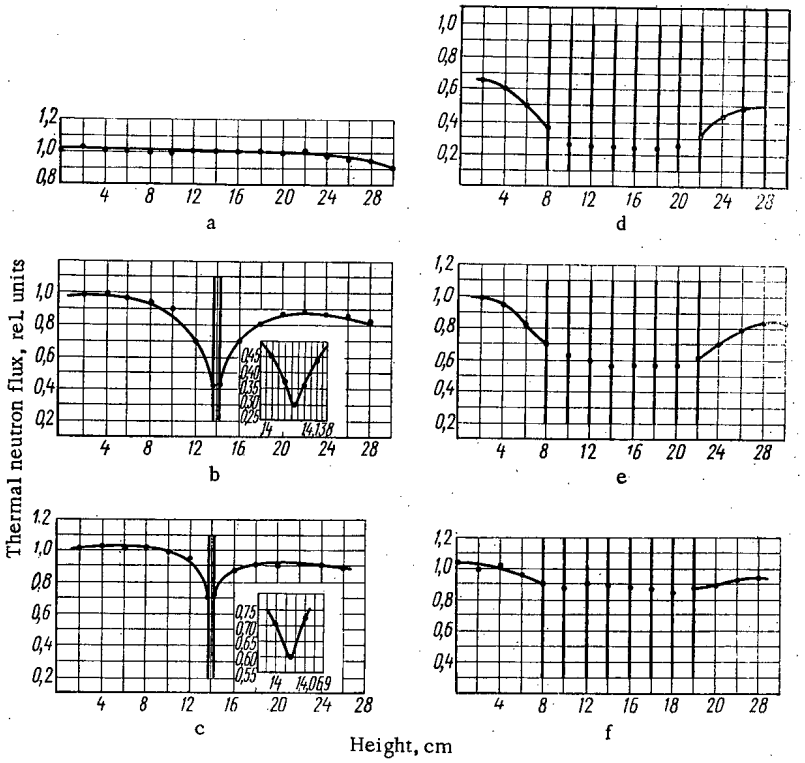

Fig. 3. Thermal neutron flux distribution: a) in graphite block without absorber; b) in single-layer model of activity generator with λ_a layer of γ-carrier; c) in single layer generator model with $\lambda_a/2$; d) in eight-layer generator model with $\lambda_a/4$; e) in eight-layer generator model with $\lambda_a/8$; f) in eight-layer model with $\lambda_a/16$.

To allow for reactor power fluctuations, monitors of 10 mg/cm^2 metal gold foil were placed in all assemblies at a distance 60 cm from their top. All measurements were normalized for the counting rate of this monitor. The distribution of thermal neutrons over the height of heterogeneous indium–graphite assemblies was measured by activating 20 mg/cm^2 pure copper foils placed between graphite discs at 20 mm intervals (see Fig. 2b).

The specific activity in the indium absorber layers was determined by measuring the radioactivity of indium samples in the form of discs 10 mm in diameter cut from the center of irradiated $\lambda_a/8$ and $\lambda_a/16$ foils. The measurements were made with the aid of a pulse-height analyzer and a scintillation γ-spectrometer. The measuring error was 4-5%. The thermal neutron flux distribution is shown in Fig. 3.

DISCUSSION OF RESULTS

The distribution of thermal neutron flux in a graphite assembly without γ-carrier (Fig. 3a) indicates that the neutron production density in the assembly is constant over a length of 26 cm ($\sim\sqrt{2\tau}$ for graphite) as predicted by the Fermi age theory. The relative thermal neutron flux determined in this assembly and normalized for the monitor count rate has been assumed as the average undisturbed flux Φ_0 in all subsequent measurements. In plotting the thermal neutron distributions in the investigated activity generator models, the relative flux has been obtained by similar normalization. This makes it possible to compare the results obtained in different models by relating it to a unit ordinate corresponding to the undisturbed flux in the chosen relative units.

Figure 3b shows the thermal neutron distribution in a single-layer activity generator model with a γ-layer λ_a thick (model I in Table 1). The disturbance of the neutron flux by the absorber is high and the average thermal neutron flux in the γ-carrier layer is $0.37\overline{\Phi}_0$.

A comparison of the curves in Fig. 3b and e shows that the average thermal neutron flux in the case of a single γ-carrier layer is 1.56 times lower than in the eight-layer model with the same total thickness of γ-carrier* (models I and II in Table 1). The specific radiation power of the eight-layer model is 1.6 times the radiation power in a single layer of the same total thickness.

The curve in Fig. 3d shows the thermal neutron flux distribution in a heterogeneous system of eight indium layers (model III in Table 1) of a total thickness equal to $2\lambda_a$. The average specific activity of indium foils as well as the relative average thermal neutron flux in this model is 35-40% lower than in a single-layer system consisting of an indium block λ_a thick (model I in Table 1). The total indium activity is ~1.25 times the total activity in model I.

If the indium foils were placed in the moderator not as a heterogeneous system, as in model III, but as a single indium block of equivalent thickness, the total indium activity would amount to ~ 0.85 and not 1.25 (relative units) (see Fig. 1).

The thermal neutron flux distribution in a single $\lambda_a/2$ indium block (model IV) is shown in Fig. 3c. The disturbed flux at the distribution minimum amounts to $0.6\overline{\Phi}_0$ and the average flux in the layer is $\overline{\Phi} \approx 0.66\overline{\Phi}_0$.

A comparison of the specific activity of single-layer models (I and IV in Table 1, Fig.3b and c) shows that the specific activity of the γ-carrier in a $\lambda_a/2$ layer is 1.84 times than in a λ_a layer.

The average thermal neutron flux, which determines the γ-carrier specific activity, in a $\lambda_a/2$ layer is 1.78 times the flux in a λ_a layer. Thus, the generation of radioactive nuclei in the γ-carrier layers of such thickness takes place as a result of absorption of mainly thermal neutrons.

The specific activity of model V, stored in eight indium layers $\lambda_a/16$ thick each and spaced in the graphite at intervals of the order $0.7\lambda_{tr}$, cannot be ascribed entirely to In^{116} generation by thermal neutrons. This is indicated by the data in Table 1 in which the ratio of average thermal neutron fluxes is 2.35 in the chosen system of relative units, while the ratio of specific activities is ~3.6. Such a discrepancy can be explained only if the contribution of resonance neutrons into the generation of In^{116} nuclei is allowed for. In fact, the resonance integral, calculated in accordance with [9], is ~600 b for thin indium layers such as $\lambda_a/16$ layers and barely 100 b for λ_a layers. This fact can be of great importance in reactors in which the fraction of fast and resonance neutrons in the leakage spectrum is considerable. In such reactors it is possible to design activity generators in which the thickness of moderator layers between γ-carrier layers with high self-shielding factors for resonance electrons is such that groups of fast neutrons can achieve an age equivalent to indium resonance energies. In such a case it is possible to obtain considerable gain in specific and total capacity of the radiation circuit.

The practically continuous distribution of thermal neutron sources in the investigated graphite structure (see Fig. 3a) makes it possible to compare the theoretical and experimental values of thermal neutron fluxes in thin γ-carrier layers. In particular, the distribution curve in Fig. 1c indicates that the average thermal neutron flux in a $\lambda_a/16$ layer is $\sim 0.963\overline{\Phi}_0$. Taking into account the influence function of such layers spaced at 20 mm intervals in a graphite moderator we arrive at a figure of $\sim 0.9\overline{\Phi}_0$ for the thermal neutron flux in the assembly. The experimental value of thermal neutron flux is $\sim 0.88\overline{\Phi}_0$.

LITERATURE CITED

1. A. P. Aleksandrov, At. Énerg., 25, 356 (1968).
2. Yu. S. Ryabukhin et al., Industrial Use of Large Radiation Sources (Abstract of Reports of the USSR Delegation), Vol. 2, IAEA, Vienna (1963), p. 175.
3. É. L. Andronikashvili et al., At. Énerg., 13, 342 (1962).
4. G. I. Kiknadze et al., At. Énerg., 19, 176 (1965).
5. G. I. Kiknadze et al., Abstracts of Reports of the Conference of Young Scientists on Radiation Chemistry and Radiobiology [in Russian], Obninsk (1969), p. 140.
6. Yu. S. Ryabukhin and A. Kh. Breger, At. Énerg., 5, 533 (1958).
7. R. Murray, Nuclear Reactor Physics [Russian translation], Gosatomizdat, Moscow (1959).

*Neutron fluxes measured on the surface of indium foils are taken as the average thermal-neutron flux in $\lambda_a/16$, $\lambda_a/8$, and $\lambda_a/4$ layers. The error in the average flux in such layers is quite small and does not exceed 5% because of low flux depression.

8. V. V. Goncharov et al., Nuclear Reactors and Nuclear Power Engineering (Reports of Soviet Scientists at the Second Geneva Conference) [in Russian], Gosatomizdat, Moscow (1959), p. 243
9. V. V. Orlov, T. V. Golashvili, and A. I. Baskin, in: Neutron Physics [in Russian], Gosatomizdat, Moscow (1961).

DOSIMETRIC PROPERTIES OF BORON NITRIDE

G. A. Lubyanskii, V. V. Styrov, and V. A. Sokolov

UDC 539.16.08

The development of new and effective thermoluminescence dosimeters is closely associated with the study of radiation processes in solids [1]. An investigation of the dosimetric properties of compounds of the type of A(III) and B(V), which is now being paid considerable attention, is of interest. In this work we investigated the thermoluminescence and dosimetric properties of one of the representatives of this type of compound, boron nitride (BN).

EXPERIMENTAL

Samples. Boron nitride, synthesized according to the method described in [2],* possesses a hexagonal lattice with parameters corresponding to the literature data [3]. Spectral analysis for impurities indicated the presence (in wt. %) of: Al < 10^{-4}, Mg < 10^{-4}, Ca < 10, Ag < 10^{-4}, Si < 10^{-3}.

Samples activated by manganese, europium, and samarium were also produced. Boric acid served as the flux. The charge was calcined at 750°C for 1 h and at 1400°C for 30 min in a stream of ammonia. The samples were used in the form of powders; in individual cases tablets were prepared by pressing at a pressure of 450 kg/cm^2.

Experimental Method. The thermoluminescence of boron nitride was investigated after irradiation of the samples at room temperature with γ-quanta on an RKh-γ-30 apparatus and with thermal neutrons in the vertical channel of the nuclear reactor of the Institute of Physics of the Academy of Sciences of the Latvian SSR.

The apparatus for recording thermoluminescence curves, consisting of heating and recording units, permitted the use of higher rates of heating (3.6-9.1 deg/sec) and ensured constancy of the selected system. The sample was applied directly on a constantan plate, heated by current, with a depression for the luminophore, in a thin dense layer in the form of a weighed sample (30 mg) or in the form of a tablet (60 mg). The thermoluminescence curves were recorded with an FÉU-39 with an SZS-14 filter, cutting out thermal radiation. The time of recording of one curve was 40 sec. The emission spectra were measured on apparatuses of P. Stuchka Latvian State University and A. F. Ioffe Physicotechnical Institute of the Academy of Sciences of the USSR.†

Thermoluminescence of Boron Nitride Irradiated by γ-Quanta

Curves of Thermoluminescence and Spectra. The absorbed dose was varied from 10 to $3 \cdot 10^8$ rad. The experiments indicated that without preliminary irradiation, both of inactivated and of activated BN, no thermoluminescence is detected. However, at a dose of 10 rad, a thermoluminescence peak already appears at a temperature of 125°C (rate of recording 9.1 deg/sec); Beginning with a dose of $5 \cdot 10^2$ rad, a second peak appears at the temperature 425°C. When the dose is further increased, the second (high-temperature) peak becomes dominant, and the light sum luminescing in it constitutes 95% of the total stored light sum.

*We should like to express our great gratitude to G. V. Samsonov and M. D. Lyutoi for providing boron nitride.

†We should like to thank V. Ya. Grabovskii and L. S. Druskina for providing these apparatuses and for their practical aid in conducting the experiment.

Translated from Atomnaya Énergiya, Vol. 31, No. 2, pp. 119-122, August, 1971. Original article submitted July 30, 1970; revision submitted October 5, 1970.

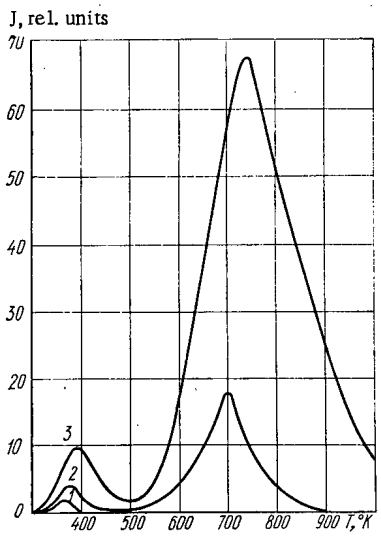

Fig. 1

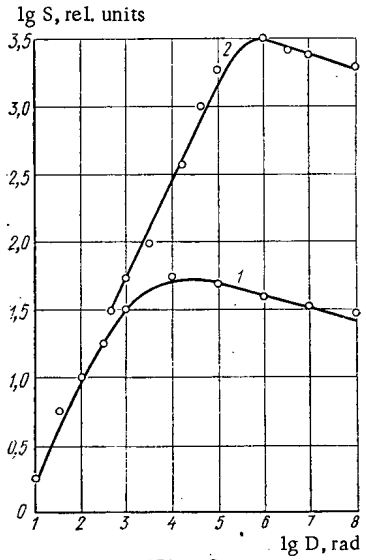

Fig. 2

Fig. 1. Curves of the intensity J of thermoluminescence of hexagonal BN at various temperatures and absorbed doses: 1) 10^2 rad; 2) 10^3 rad; 3) 10^5 rad.

Fig. 2. Value of the stored light sum of hexagonal BN as a function of the dose D of γ-radiation for the first (1) and second (2) thermopeaks. The relative units of the light sum are different for the two curves.

The dynamics of the curves of thermoluminescence of BN is shown as a function of the absorbed dose in Fig. 1. For various samples of inactivated BN (samples of a different origin, in addition to those indicated in the experimental section, were also investigated), the first peak lies in the interval 110-150°C, the second in the interval 425-490°C. From Fig. 2 it is evident that the stored light sum in the first peak increases nonlinearly with the dose, and a deviation from linearity already occurs at relatively low doses (10^3 rad). At the same time, the stored light sum in the second peak increases as a linear function of the dose all the way up to 10^5 rad. In the same dose interval, the thermoluminescence intensity is approximately proportional to the irradiation dose.

At a dose of $5 \cdot 10^6$ rad, the stored light sum reaches a maximum value and gradually drops when the dose is further increased. Moreover, the maximum of this peak is shifted in the direction of high temperatures with the dose. Thus, at a dose of $2.4 \cdot 10^8$ rad, it corresponds to a temperature of 510°C.

The emission spectrum of the thermoluminescence of inactivated BN lies in the blue-green region. In both thermopeaks, radiation with wavelengths λ = 380-520 nm is observed. (The position of the maximum of the spectrum for various samples varies in the region 388-429 nm.)

Boron nitride, activated by manganese (1 mole %), exhibits three thermopeaks. The first thermopeak is situated at the same temperature (110-150°C) as the temperature of inactivated BN. The second is situated at the temperature 250-270°C, and the third at 375-440°C.

The activator thermopeak (250-270°C) begins to appear at a dose of $5 \cdot 10^2$ rad; the stored light sum corresponding to it is approximately proportional to the dose of irradiation up to 10^6 rad. At very high doses, $2.4 \cdot 10^8$ rad, this thermopeak disappears. The activator thermopeak has somewhat lower intensity than the high-temperature peak of inactivated BN at equal doses.

The emission spectrum of the thermoluminescence in the activator thermopeak takes the form of a band with maximum at λ = 497 nm to 518 nm.

In the case of activation of boron nitride by europium (0.1 mole %) and samarium (0.5 mole %), no activator peaks were detected, but a high-temperature thermopeak appears at a somewhat lower temperature (by 60-70°C) than for inactivated BN.

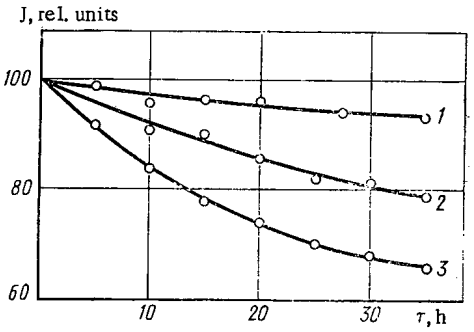

Fig. 3. Loss of the stored light sum S of the high-temperature peak of hexagonal BN as a function of the duration of storage at various temperatures.

From the results cited it follows that inactivated BN contains at least two varieties of traps, the depth of which were determined from the thermoluminescence curves according to the Urbach formula and the Lushchik equation [4] and are 0.7-0.8 eV for the first thermopeak, and 1.4-1.6 eV for the second thermopeak.

We should mention the high reproducibility of the results from sample to sample in a lot and from lot to lot for the same method of synthesis of BN from raw material of the same quality: ±5% for the position of the maximum of the thermopeaks, ±10% for their intensities.

The method of synthesis and purity of the starting materials appreciably influences the curve of thermoluminescence, especially the light sum. Thus, BN synthesized from cp raw material stored an order of magnitude smaller light sum than BN synthesized from very pure raw materials. We observed the same tendency for a shift in the thermopeaks of BN, synthesized according to the method of [2], after its supplementary calcination in air. Thus, after 20 h of calcination at 1300°C, the maximum of the first peak was shifted from 120 to 140°C, and that of the second from 480 to 400°C; there was a redistribution of the intensities of the peaks in favor of the low temperature peak.

With respect to sensitivity to the dose, BN is only two to three times inferior to LiF. Let us note that the activator peak of BN–Mn, possessing linear dose characteristics and favorably situated in the temperature scale, is also convenient for purposes of dosimetry.

Conservation of Stored Light Sum. We verified the ability of boron nitride to conserve the light sum at different temperatures. The results are cited in Fig. 3. It is evident that in a period of 10 h at room temperature, BN loses approximately 3% of the light sum (curve 1), while at 50 and 68°C it loses 8 and 17%, respectively (curves 2 and 3). Dosimetric information with respect to the second thermopeak is preserved (by approximately 30%) for 90 days (dose of irradiation 10^5 rad).

At a low dose rate of the irradiation of boron nitride for a long time, there are practically no losses of light sum. Thus, in an experiment during which BN was irradiated for ten days at a dose rate of 0.6 rad/h, the stored light sum proved close to the calculated. This property permits the use of BN for dosimetric purposes, including low dose rates.

Dependence of the Sensitivity on the γ-Radiation Energy. The storage of the light sum in the irradiation of inactivated BN with γ-quanta of Co^{60} with energies equal to 1.17 and 1.33 MeV, and Tu^{170} with E_γ = 0.084 MeV, was compared. It was established that in these cases neither the shape of the thermoluminescence curve nor the dose characteristics depend on E_γ.

Boron nitride, as a dosimetric material, possesses tissue equivalence: the effective atomic numbers of soft biological tissue (7.42) and BN (6.8) almost coincide.

Possibility of Repeated Use. In the dosimetric respect it is important that a sample does not experience irreversible changes after complete deexcitation of the stored light sum, and return to the initial state. The reproducibility of the thermoluminescence curves was verified in the case of repeated (five times) irradiation of the same sample with the same dose. After each irradiation, as a result of one temperature cycle, the thermoluminescent emission entirely disappeared. When irradiation was repeated, the intensity of the thermopeaks and their positions were almost unchanged. This shows the possibility of the repeated use of BN as a dosimeter without special intermediate treatment.

Resistance to Interference. In thermoluminescence dosimetry, the source of interference, especially at low doses, may be chemiluminescence and triboluminescence, which give a false signal. We did not detect any emission of nonirradiated BN during heating in air. Triboluminescence also was not detected. To verify this, the same sample was irradiated with the same dose twice, and the second time the powder was mixed before heating. No differences in the thermoluminescence curves were detected.

We also verified whether the light sum is stored when BN is irradiated with sunlight. It was found that in the case of 5 h exposure, the first thermopeak is detected for inactivated BN (at the temperature

TABLE 1. Dosimetric Properties of BN in Neutron Irradiation

Sample	Flux, neutrons/cm^2																							
	10^{10}				10^{11}				10^{12}				10^{13}				10^{14}				10^{15}			
	J_1	t_1	J_2	t_2	J_1	t_1	J_2	t_2	J_1	t_1	J_2	t_2	J_1	t_1	J_2	t_2	J_1	t_1	J_2	t_2	J_1	t_1	J_2	t_2
BN, cubic	4	120	—	—	6	150	—	—	10	160	—	—	12	163	—	—	16	165	—	—	25	165	—	—
BN, hexagonal	2	150	40	500	6	150	70	510	11	150	155	520	22	151	170	522	8	150	180	522	3	155	7	520
BN – Mn, 1 mole %	102	85	126	260	133	107	132	282	25	150	165	365	22	150	42	315	9	165	47	387	2	164	14	390
BN – Eu, 0.1 mole %	10	118	63	401	20	120	74	405	130	137	129	412	133	152	183	362	80	155	43	387	13	147	180	370

Note: J_1 and J_2 are the intensities of the first and second thermopeaks, rel. units; t_1 and t_2 are the temperatures corresponding to them, °C; rate of heating 9.1 deg/sec.

150°C), equivalent to an absorbed dose of γ-radiation of 3 rad. In the case of 20 h exposure, the intensity of this peak reached a level equivalent to 7 rad.

BN activated by manganese proved even most sensitive to daylight. In the case of a 5 h exposure, it exhibited a thermopeak at the temperature 110°C, equivalent to a dose of 4.5 rad; in the case of 20 h exposure, it exhibited two thermopeaks, and the high-temperature peak at the temperature 260°C corresponded to a dose of 12 rad.

Thus, a dosimeter based on BN must be protected from the action of sunlight.

Thermoluminescence of Boron Nitride Irradiated with Thermal Neutrons

The experimental results are presented in Table 1. It is evident from it that cubic BN exhibits thermoluminescence with one peak, the intensity of which increases nonlinearly with the thermal neutron flux. In this case, the temperature corresponding to the maximum of the thermoluminescence curve is shifted from 120 to 165°C.

Hexagonal BN, in the case of irradiation with thermal neutrons, just as in the case of irradiation with γ-quanta, possesses two peaks of thermoluminescence, lying at the temperatures 150-155°C and 500-525°C, respectively. Probably the centers of capture responsible for these peaks are of the same nature as in irradiation with photons, although in the case of neutron irradiation the peaks are somewhat shifted in the high-temperature direction. These centers of capture existed before irradiation and did not appear as a result of it. In addition, irradiation induces color centers in BN, which in the presence of large fluxes ($> 10^{14}$ neutrons/cm^2) becomes evident, since the color of the sample changes from white to brownish. However, no new peak of thermoluminescence appears in this case, and the intensity of the old ones, on the contrary, decreases. At a flux of $\sim 10^{17}$ neutrons/cm^2, thermoluminescence disappears entirely. The coloration of BN may be explained by the formation of F-centers [5, 6].

Hexagonal BN, activated with manganese and europium, also possesses two thermopeaks, the positions of which, as can be seen from Table 1, differ from the thermopeaks characteristic of inactivated BN. For example, the high-temperature peak corresponds to considerably lower temperatures at the same doses. The dependence of the temperature of the maximum on the neutron flux in this case is sharper.

Let us note also that the dosimetric information is well preserved during neutron irradiation. Thus, 16 days after irradiation, the light sum is still 80% of the original value. A comparison of the efficiency of BN as a dosimeter in irradiation with γ-quanta and neutrons shows that the intensity of the thermopeaks at a γ-irradiation dose of 1 rad is approximately six times as great as at a dose of 1 rem of irradiation with thermal neutrons. Thus, BN can serve as an effective dosimeter of γ-irradiation.

In conclusion, let us express our sincere gratitude to Z. A. Grant and K. K Shvarts for their useful advice and their aid in conducting this work.

LITERATURE CITED

1. K. K. Shvarts et al., Thermoluminescence Dosimetry [in Russian], Znanie, Riga (1968).
2. G. A. Meerson et al., Ogneupory, No. 2, 72 (1955).
3. G. V. Samsonov et al., Boron, Its Compounds and Alloys [in Russian], Izd-vo AN UkrSSR, Kiev (1960).
4. Ch. B. Lushchik, Dokl. Akad. Nauk SSSR, 101, 641 (1955).
5. M. B. Khusidman and B. N. Sharupin, Radiokhimiya, 9, 279 (1967).
6. M. B. Khusidman and V. S. Neshpor, Teor. i Éksperim. Khimiya, 2, 270 (1967).

A VARIABLE-ENERGY PROTON LINEAR ACCELERATOR

V. A. Bomko, A. P. Klyucharev, and B. I. Rudyak

UDC 621.384.643

The most serious disadvantage of most linear accelerators for ions is that the particle energy cannot be varied. An accelerating structure of Alvarez type [1] takes the form of a cavity loaded by drift tubes and excited in the E_{010} mode; in principle, it does not allow the beam energy to be varied. Particles with intermediate energies can be obtained only by dividing the accelerator into sections, which involves some difficulties and which does not provide smooth energy variation.

There is a long history of attempts to obtain intermediate ion energies from linear accelerators. The Berkeley heavy-ion accelerator uses the fact that a detuned linear-accelerator system can produce a beam containing particles with intermediate energies as well as ones with the maximum energy. Some components of intermediate energies can be isolated by deliberate deviation from normal operation (e.g., by changing the accelerating field distribution and adjusting other elements). Such working conditions are unstable, and the intensity is much less than that for a beam with the full energy. Various explanations have been offered in terms of features of the particular accelerators: large apertures of the drift tubes and grid focussing in the section before the extractor.

A new method of linear ion acceleration has been developed at Kharkov Physicotechnical Institute, which provides smooth energy adjustment (in principle, to any value less than the maximum) without loss of intensity or of monochromaticity.

Principle of Smooth Energy Adjustment

The device uses parts with uniformly distributed accelerating fields of varying length, so the cavity cannot be excited in the E_{010} mode. If the cavity is so excited, such parts cannot be produced. The field distribution can only be distorted (perhaps chaotically) by the perturbing tuned devices normally used to produce acceptable uniformity in the field.

We concluded that excitation in the E_{011} mode (or higher E_{01l} modes) can provide energy adjustment when the frequencies of the individual sections of the accelerator are perturbed by tuned devices. We drew this conclusion about this essentially parasitic wave type from the changes in the field distribution in the cavity.

It is usual to employ a cosine distribution of the high-frequency electric field along the axis (curve 1 of Fig. 1) in order to excite the E_{011} mode in the cavity of a linear accelerator having drift tubes with all the sections tuned to the same resonant frequency. Perturbations at one end of the cavity allow one to shift the nodes in the electric field along the axis, and appropriate turning of the sections allows one to produce parts with uniform fields and sharp cutoff (curve 2 of Fig. 1).

Stepwise energy adjustment is provided on changing the length of a uniform part having ideally steep cutoff, the steps being equal to the energy gain per stage in the accelerating structure. The practical cutoff has a finite slope, which can be varied to provide smooth energy adjustment.

The beam must pass without loss through the part of the accelerating structure where there is no acceleration, which requires a prearranged distribution of the magnetic fields in quadrupole lenses in the drift tubes.

Translated from Atomnaya Énergiya, Vol. 31, No. 2, pp. 123-126, August, 1971. Original article submitted June 8, 1970; revision submitted January 4, 1971.

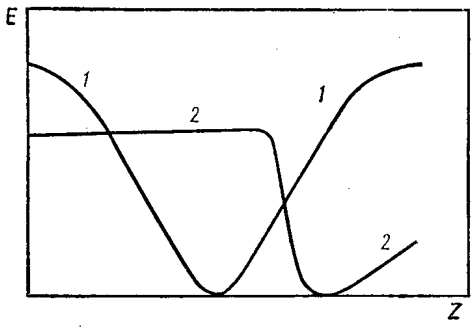

Fig. 1. Field distributions along the accelerator corresponding to E_{011} excitation: 1) all sections tuned to the same frequency; 2) frequencies of sections adjusted to produce a part with a uniform distribution in the accelerating field.

Fig. 2. Disposition of the tuned stub in the cavity.

Field-Shaping Devices

The cutoff must be fairly steep in the parts of uniform distribution but vary in length in order to provide monoenergetic beams accelerated to intermediate energies.

There is another reason why the beam becomes less monoenergetic. If the uniform field distribution is produced by deforming the left branch of the E_{011} wave (Fig. 1), there remains a certain distribution of the electric field from the right branch. This field is especially strong when short parts with uniform fields are produced in order to accelerate particles to energies less than half the maximum energy. These fields have no great effect on the mean energy, which is determined by the left branch; in the right branch, the particles deviate from synchronism, and their energies on average do not alter. However, the residual right-branch E_{011} field increases the energy spread, and it also causes useless dissipation of high-frequency power in the cavity.

One needs very simple adjustment of the accelerator from one output energy to another, and this should provide for automatic control of the adjustment to optimum beam parameters at any intermediate energy as well for programmed variation.

These requirements impose severe demands on the tuned devices. Some currently used tuned devices (cylinders, spheres, plates, etc.) attached to the cavity wall are ineffective when the E_{011} mode is involved, since the fields are then much more stable, and hence they are less sensitive to perturbations introduced into the cavity. Also, they do not allow one to eliminate completely the right-branch field of the E_{011} mode.

All these requirements are met by a stub of variable length attached to the end wall of the cavity; this is also simple and convenient. This new resonant system has effects somewhat similar to those of a half drift tube attached to the end, whose length is also adjustable.

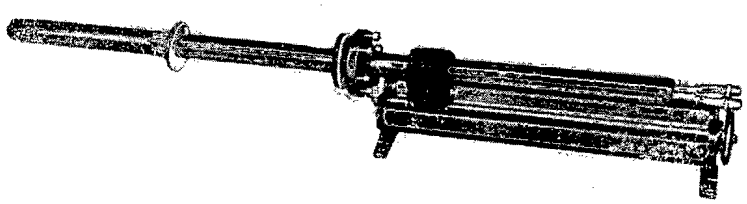

Fig. 3. The tuned device.

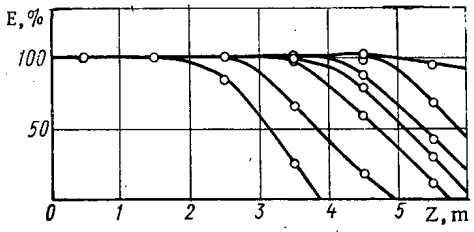

Fig. 4. Distributions of the fields produced along a cavity excited in the E_{011} mode.

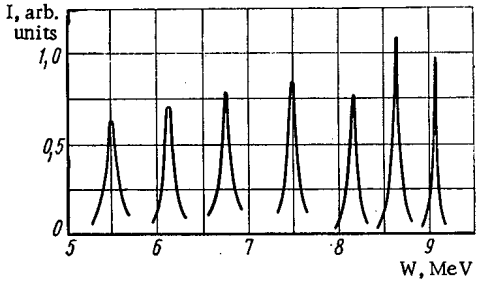

Fig. 5. Energy spectra of accelerated protons.

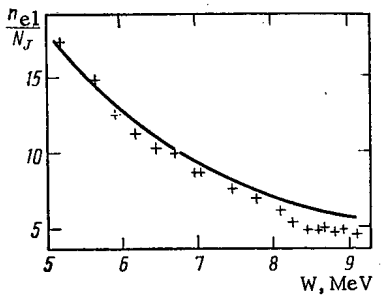

Fig. 6. Elastic-scattering excitation function for protons produced with smooth energy adjustment.

A tuned stub was found to be most effective if placed near the side wall of the cavity (Fig. 2). As the stub is inserted into the cavity, the E_{011} field node shifts along the cavity, and the right-branch field is ultimately eliminated completely. This device is not only effective but also simple in design (Fig. 3); it is convenient to use and provides for automatic smooth energy adjustment.

RESULTS

We examined the energy adjustment on a proton linear accelerator having a maximum energy of 9 MeV and an energy spread of 90 keV [3]. The working wavelength was $\lambda_0 = 2.1$ m, mean electric field along the axis 18.4 kV/cm, cavity length 6 m, injection energy 500 keV, 34 drift tubes, and grid focussing. This accelerator was commissioned in 1966 and since then had worked in the E_{010} mode at 0.2 μA and a utilization factor of 0.1%.

Early in 1969 it was converted to smooth energy adjustment. First we did development tests on methods of producing parts with uniform accelerating fields and variable lengths in the E_{011} mode. We examined the distribution of the loss of high-frequency energy in this method of field shaping, the effects on the cavity Q from various methods of field shaping, and the stability and perturbation sensitivity of the field. We also examined the working characteristics with smooth energy adjustment.

The resonant stub was attached to the end wall of the cavity 10 cm from the side wall. This distance provided adequate performance while eliminating breakdown to the wall.

The resonant stub was used with tuned devices of ordinary type to shape the fields for producing smooth energy adjustment. The stub shifted the E_{011} node through the necessary distance, while lateral tuned devices provided field uniformity and steep cutoff. Figure 4 shows seven accelerating-field distributions along the axis produced in this way.

Appropriate adjustment provided a uniform distribution for the E_{011} left-branch field throughout the length of the accelerator. As we did not know the entire previous history of this distribution, we could not distinguish it from the uniform E_{010} distribution usually obtained. The two uniform distributions all along the cavity produced identical losses of the high-frequency power.

Figure 5 shows examples of the proton energy spectra for energies corresponding to the field distributions of Fig. 4. The energy spread was 50 keV when the protons were accelerated to the maximum energy by an E_{011} field uniform all along the accelerator, which is substantially less than the spread for ordinary E_{010} acceleration. Figure 5 shows that the beam current and energy increase together, which is due to the

use of grid focussing, which was absent on the part where there was no accelerating field and where there was some loss of the particles.

Figure 6 illustrates the scope for use of this method by reference to the excitation function for elastic scattering of protons by Cr^{53} as measured at 60°. The points correspond to the energies used in the experiment.

Since September 1969 the accelerator has been used in experiments involving smooth energy variation from 3 to 9 MeV. The insertion depth of the tuned devices was varied in accordance with a set program without breaking the vacuum and with the high-frequency power on. The power supplies were placed to inject the power near the entry section in order to provide the required levels for the short parts with uniform field distribution.

Prolonged use in the E_{011} mode has shown that this provides not only smooth energy adjustment but also high stability in the beam characteristics. Even when maximum-energy operation is needed, E_{011} working is preferable to the ordinary E_{010} mode.

This method has the advantage that it can be operated on existing linear accelerators without major design changes and hence without additional cost.

LITERATURE CITED

1. L. Alvarez et al., Rev. Sci. Inst., 26, 111 (1955).
2. A. Ghiorso et al., Proceedings of the Linear Accelerator Conference, Los Alamos, 1966.
3. B. I. Rudyak et al., Coll.: Nuclear Physics [in Russian], Kharkov, Izd. FTI AN UkrSSR (1967), p. 25.

DYNAMICS OF COLLISIONS OF CHARGED CLUSTERS ASSOCIATED WITH A SHOCK ACCELERATION MECHANISM

A. G. Bonch-Osmolovskii

UDC 621.384.01

In 1956 Veksler [1] proposed a shock mechanism for accelerating clusters of charged particles, a variant of the general coherent method which he considered there. At the 1959 Geneva Conference on Accelerators, Veksler and Tsytovich [2] presented a brief analysis of shock acceleration, and included the case of collision of charged clusters.

Recently interest has revived considerably in the collective acceleration method [3], on the one hand, and in the question of obtaining large electron currents [4], on the other. There is reason to think that success in this area could bring the accomplishment of shock acceleration considerably closer, since the real problem has become the creation of a heavy cluster with the required parameters.

The present paper deals mainly with certain aspects of collision dynamics of charged clusters and the establishment of the main characteristics of shock acceleration, including the basic parameters of the charged clusters themselves. The generation and prior acceleration of these clusters are not considered here.

Kinematics of Elastic Collision of Two Clusters

Our notation will be: all quantities relating to a heavy cluster will have the numeral 1, and to a light cluster, the numeral 2. For example, M_1, v_1^0, γ_1^0 are the mass, velocity, and energy (in units of Mc^2) before a collision of a heavy cluster; and N_2^e, ν_2, $\gamma_{\perp 2}$ are the number of particles (electrons), the "running" electron, and the transverse energy of the electrons in a light cluster, respectively. The running electron is usually defined by: $\nu = r_0 n$ ($r_0 = e^2/mc^2$, n is the linear density of particle number, and is $N/2\pi R$ for a thin ring of radius R); Quantities before collision have subscript 0, and after collision, no subscript.

We assume that conditions for elastic collision of two clusters are met, and that the collision is head-on (the target parameter is much less than the cluster size). The first assumption will be discussed below.

In the general case we assume that the heavy cluster has velocity v_1^0 and the light cluster v_2^0 before collision, the directions of the velocity vectors being the same, and $v_1^0 > v_2^0$. Then it is easy to show, using relativistic velocity transformation formulas, that the energy of the light cluster after the collision (the precise meaning of the word "after" is elaborated below) will be

$$E_2 = M_2 c^2 \gamma_2^0 \frac{1 - 2\frac{Vv_2^0}{c^2} + V^2/c^2}{1 - V^2/c^2}, \tag{1}$$

where V is the velocity of the system center of gravity (the c-system):

$$V = \frac{M_1\gamma_1^0 v_1^0 + M_2\gamma_2^0 v_2^0}{M_1\gamma_1^0 + M_2\gamma_2^0}. \tag{2}$$

If the condition

$$M_1\gamma_1^0 \gg M_2\gamma_2^0 \tag{3}$$

is satisfied, then $V \approx v_1^0$; and the c-system practically coincides with that in which the heavy cluster is at rest. Then

Translated from Atomnaya Énergiya, Vol. 31, No. 2, pp. 127-132, August, 1971. Original article submitted July 10, 1970.

$$E_2 \approx 2M_2c^2\gamma_1^0 \frac{\gamma_{rel} + \frac{M_2}{M_1}}{1+2\frac{M_2}{M_1}\gamma_{rel}} \tag{4}$$

and

$$\gamma_{rel} = \gamma_1^0\gamma_2^0\left(1 - \frac{v_1^0 v_2^0}{c^2}\right). \tag{5}$$

The quantity γ_{rel} is the energy of the light cluster at infinity in the c-system with condition (3) satisfied. We derive a simpler formula for γ_{rel} in the important practical case when

$$\gamma_1^{0^2} \gg 1; \quad \gamma_2^{0^2} \gg 1; \quad \gamma_1^{0^2} \gg \gamma_2^{0^2}: \tag{6}$$

$$\gamma_{rel} \approx \frac{1}{2}\cdot\frac{\gamma_1^0}{\gamma_2^0}. \tag{7}$$

Now we can see that if a stricter condition than (3) is satisfied, viz.:

$$M_1 \gg 2M_2\gamma_{rel} \tag{8}$$

(here the heavy cluster has practically no energy change in the collision process), then:

$$E_2 \approx 2M_2c^2\gamma_1^0\gamma_{rel}. \tag{9}$$

In the particular case when $v_2^0 = 0$, $\gamma_{rel} = \gamma_1^0$ and

$$E_2 \approx 2M_2c^2\gamma_1^{c^2}. \tag{10}$$

The last formula was given by Veksler [1], and defines the well-known γ^2 effect in elastic collision of relativistic particles.

Under the above conditions, an increase in energy of a light cluster by a factor of γ^2 in the laboratory system during a collision indicates elastic reflection in the c-system of a light cluster from the force center (the heavy cluster), with energy γ at infinity.

Conditions for an Elastic Collision

The above collision kinematics assumes that charged clusters move and interact according to the law applicable to the behavior of elastic spheres of mass M_1 and M_2. We should explain that the conditions for this model are close to the actual picture of charged cluster collision.

Earlier papers on shock acceleration mainly considered neutral clusters with an intense azimuthal current, and interacting by virtue of magnetic repulsion forces (for oppositely directed currents in the clusters). But these currents cannot be maintained by a spatially uniform magnetic field, and, additionally, the magnetic interaction is relatively weak in this case, which is awkward from many points of view. Therefore, the present paper gives attention mainly to interaction of charged clusters.

We consider a light cluster in the form of a thin electron ring with large radius R and small radius a, and a small impurity of ions, the electrons rotating with energy $\gamma_{\perp 2}^0$ (before the collision) in the azimuthal direction. As regards the heavy cluster, we assume only that its characteristic geometrical dimension does not exceed R, and that the rotational energy of the electrons is $\gamma_{\perp 1}^0$. We also assume that it consists entirely of electrons and that its mass satisfies Eq. (8). This last point means that the heavy cluster is at rest in the c-system, and its subsequent motion is not considered.

The large dimension of both clusters is maintained by a uniform magnetic field, so that the currents in the clusters have the same direction.

The chief assumption made in considering shock acceleration is that the distance of closest approach during the collision (in the c-system) is considerably larger than the characteristic dimension R of the clusters. Then the interaction energy of the two clusters can be written approximately in the form

$$W \approx \frac{e^2N_1N_2}{z} - \frac{e^2N_1N_2}{2z}\left(\frac{R}{z}\right)^2. \tag{11}$$

In writing Eq. (11) it is assumed that the currents in the clusters are relativistic during the entire time of collision. The number of ions in the light cluster is small, so that $N_2 \approx N_2^e$. We neglect the second term in Eq. (11), considering that $R \ll z_{min}$.

We now explain the conditions when the changes in the parameters of the light cluster, i.e., the large radius and rotational energy $\gamma_{\perp 2}$, during the collision can be considered small.

The ratio of the additional radial coulomb force due to the heavy cluster to the centrifugal force of the electrons in the light cluster primarily determines the change of light cluster radius as it nears the heavy cluster. This change is small if

$$\frac{eE_r}{F_{\text{center}}} = 2\pi \frac{\nu_1}{\gamma_{\perp 2}} \cdot \frac{R^3}{z_0^3} \ll 1. \tag{12}$$

Here ν_1 is the running electron of the heavy cluster, and z_0 is the least distance between the clusters.

The change in radius R is also related to the change in $\gamma_{\perp 2}$ due to magnetic interaction of the clusters, which can easily be evaluated from the law of conservation of generalized azimuthal momentum of the electrons of the light ring.

Assuming that the change of radius indicated by Eq. (12) is small, we can obtain the following condition for the change in $\gamma_{\perp 2}$:

$$\frac{\Delta\gamma_{\perp 2}}{\gamma_{\perp 2}} \approx \pi \frac{\nu_2}{\gamma_{\perp 2}} \left(\frac{R}{z_0}\right)^3 \ll 1. \tag{13}$$

Thus, if Eq. (12) is satisfied, as we shall assume from now on, the parameters of the light cluster can be considered unchanged during the collision ($\nu_1 \gg \nu_2$).

It is easy to show that the change in the corresponding parameters of the heavy cluster is negligibly small when Eq. (12) is satisfied.

A collision will be truly elastic when the light cluster, during scattering at the heavy cluster in the c-system, loses a negligibly small fraction of its original energy by radiation. It is clear that the known radiation upon coulomb scattering of a charge eN_2 can play the main part under the assumptions made.

Assuming small loss to radiation, we determine the dynamics of motion of the light cluster, and establish criteria for a small loss in radiation.

Taking account of Eqs. (10) and (11), the equation of motion of a light cluster in the field of a heavy one is

$$M_2 \frac{\ddot{z}}{(1-\dot{z}/c)^{3/2}} = \frac{e^2 N_1 N_2}{z^2}. \tag{14}$$

Here M_2 contains both the ordinary and the electromagnetic mass of the light cluster. With renormalization, the mass of the light cluster is:

$$M_2 = m_e \gamma_{\perp 2} N_2^e \left[1 + \frac{\nu_2}{\gamma_{\perp 2}} \left(\ln \frac{8R}{a} - \frac{7}{4}\right)\right] + m_i N_i. \tag{15}$$

Here ν_2 is the running electron of the light cluster, and m_i and N_i are the mass and the number of ions that it contains.

Accounting for conditions at infinity (the total energy of the light cluster is $M_2 c^2 \gamma_{\text{rel}}$), the first integral of Eq. (14) gives the energy conservation law:

$$\frac{M_2 c^2}{\sqrt{1-\beta^2}} = M_2 c^2 \gamma_{\text{rel}} - \frac{e^2 N_1 N_2}{z} \tag{16}$$

and

$$\frac{\dot{z}}{c} = \beta = \frac{\sqrt{\left(M_2 c^2 \gamma_{\text{rel}} - \frac{e^2 N_1 N_2}{z}\right)^2 - M_2^2 c^4}}{M_2 c^2 \gamma_{\text{rel}} - \frac{e^2 N_1 N_2}{z}}. \tag{17}$$

Now it is easy to determine the distance of closest approach of the clusters in the c-system:

$$z_0 = \frac{e^2 N_1 N_2}{M_2 c^2 (\gamma_{\text{rel}} - 1)}. \tag{18}$$

Subsequent integration of Eq. (17) leads to the relation z(t).

A matter of very great interest is the possibility of finding the "collision time" τ_c, defined as twice the time for the light cluster to travel the distance from z_0 to the point where the interaction of the clusters may practically be neglected, i.e., when the light cluster has energy equal to $\varkappa\gamma_{rel}M_2C^2$ ($\varkappa \lesssim 1$). From Eq. (16) we easily obtain

$$\varkappa = 1 - \frac{\gamma_{rel}-1}{\gamma_{rel}} \cdot \frac{z_0}{z}; \quad \frac{1}{\gamma_{rel}} \leqslant \varkappa \leqslant 1. \tag{19}$$

At distances of $z > 10z_0$ following reflection, the energy of the light cluster exceeds 90% of the maximum value.

According to the definition

$$\tau_c = 2\int_{z_0}^{z(\varkappa)} \frac{dz}{\dot{z}} \tag{20}$$

or [using Eqs. (17), (18), and (19)]

$$\tau_c = \frac{2z_0(\gamma_{rel}-1)}{c} \int_{1/\gamma_{rel}}^{\varkappa} \frac{x\,dx}{(1-x)^2\sqrt{\gamma_{rel}^2 x - 1}}. \tag{21}$$

This integral has been calculated, and τ_c is

$$\tau_c = \frac{2z_0}{c(1+\gamma_{rel})}\left[\frac{\sqrt{\gamma^2\ \varkappa^2-1}}{1-\varkappa} + \frac{1}{\sqrt{\gamma_{rel}^2-1}} \ln \frac{\sqrt{\gamma_{rel}^2-1}\sqrt{\gamma_{rel}^2\varkappa^2-1}+\gamma_{rel}^2\varkappa^2-1}{\gamma_{rel}(1-\varkappa)}\right]. \tag{22}$$

In the majority of cases of practical interest, $\gamma_{rel}^0 - 1 \gg 1$; then the term in Eq. (22) containing ln can be neglected, and

$$\tau_c \approx \frac{2z_0}{c} \cdot \frac{\sqrt{\gamma_{rel}^2\varkappa^2-1}}{(1-\varkappa)(1+\gamma_{rel})}; \tag{23}$$

for $\varkappa = 0.1$ $\tau_c \approx 20\ z_0/c$.

We determine one further characteristic of shock acceleration: the "interaction length" is the distance which the heavy cluster traverses during the collision time $\tau_c\gamma_1^0$ (in the laboratory system):

$$L = c\tau_c\gamma_2^0 \approx \frac{2e^2N_1N_2\gamma_1^0}{M_2c^2(\gamma_{rel}^2-1)} \cdot \frac{\sqrt{\gamma_{rel}^2\varkappa^2-1}}{1-\varkappa}. \tag{24}$$

The quantity L is the path length over which the light cluster is accelerated by the electric field of the heavy cluster.

We now estimate the fraction of energy which the charge of the light cluster loses in radiation. It is known [5] that the energy loss in radiation by unit charge is

$$\Delta E = \frac{2e^4}{3m^2\gamma_{\perp 2}^2c^3}\int_{-\infty}^{+\infty} \varepsilon_r^2(z)\,dt = \frac{4e^4N_1^2}{3m^2\gamma_{\perp 2}^2c^3}\int_0^{\infty} \frac{dt}{z^4(t)}. \tag{25}$$

The main part of the radiation spectrum is concentrated in the frequency region $\omega\tau_c \sim 1$; the corresponding wavelengths are considerably greater than the geometrical size R of a cluster, i.e., $\lambda \approx 20\pi z_0 \gg R$. Overestimating the result somewhat, we consider that the radiation of the light cluster is fully coherent, and then

$$\Delta E \approx \frac{4e^6N_2^2N_1^2}{3m^2\gamma_{\perp 2}^2c^3}\int_0^{\infty} \frac{dt}{z^4(t)}. \tag{26}$$

It can be shown that the main part of the loss falls in the relativistic velocity region far from the stop point; the losses near the latter are less by a factor of γ_{rel} than that in the relativistic region. Then we can substitute $z = z_0 + ct$ in the interval, and calculations give

$$\frac{\Delta E}{E} \approx \frac{4}{9} \cdot \frac{N_2}{N_1}(\gamma_{rel}-1)^2\left[1 + \frac{\nu_2}{\gamma_{\perp 2}}\left(\ln\frac{8R}{a} - \frac{7}{4}\right) + \frac{m_i}{m_e\gamma_{\perp 2}} \cdot \frac{N_i}{N_2}\right]^2. \tag{27}$$

Under ordinary conditions $\nu_2/\gamma_{\perp 2} \ll 1$ and $m_i/m_e\gamma_{\perp 2} \cdot N_i/N_2 \sim 1$. Then the criterion for an elastic collision reduces to the condition

$$\frac{N_1}{N_2} \gg (\gamma_{rel}-1)^2. \tag{28}$$

Simultaneous Acceleration of Ions and Electrons of a Light Cluster during Shock Acceleration

As was seen in the previous section, the distance z_0 of closest approach of the clusters in the c-system determines all the important characteristics of shock acceleration. The conditions of the coulomb nature of the interaction and the absence of change in the geometrical dimensions and in the elastic nature of the collision determine z_0 at low values.

For a group acceleration mechanism there must be ions in the acceleration process, contained in the light cluster, and accelerated along with the electrons. This requirement also imposes a limit on the distance of closest approach of the clusters; these conditions prove to be very rigorous.

We assume that the small dimensions a of the cross section of a light cluster (a ring) remain unchanged during the collision, in a coordinate system instantaneously fixed in the light cluster. Then the ion oscillation frequency in this coordinate system is also unchanged and is:

$$\Omega_i^2 = \frac{e^2 N_2 Z}{\pi R a^2 m_i}. \tag{29}$$

The collision process is adiabatic as regards the ion oscillations if the ions make many oscillations about an equilibrium position during the collision time τ_c, i.e., the condition

$$\frac{\Omega_i \tau_c}{\gamma_{rel}} \gg 1 \tag{30}$$

is satisfied. For the parameters of practical interest condition (30) is satisfied, and the problem thus reduces to ion oscillations in the potential well of the light cluster under the action of an external force varying slowly with time.

It is convenient to solve a problem of this type by transforming to an intrinsic (noninertial) coordinate system fixed in the light cluster. The appropriate mathematical tools have been described in [6]. The problem of containing ions in the light cluster resembles that of the accelerated relativistic oscillator [6], with the difference that the acceleration is variable in the instantaneous coordinate system. If the conditions for relativistic motion of ions in the intrinsic coordinate system, $\nu_2 m_e/m_i \ll 1$, and for the deviation of the metric of the intrinsic system from the Gallilean to be small, $e^2 N_1 N_2 a/M_2 c^2 z_0^2 \ll 1$, are satisfied, then the equations of motion of ions in this system will have the form [6]:

$$\frac{d^2 z'}{dt^2} + \Omega_c^2 z' = -\frac{e^2 N_1}{z^2(t)}\left(\frac{Z}{m_i} + \frac{1}{m_e \gamma_{\perp 2}}\right). \tag{31}$$

Taking condition (30) into account, the solution of this equation is the sum of the oscillatory term and the forced term; this gives the deviation of the center of oscillations of the ion from the center of the potential well because of inertia forces. By requiring that this deviation should not exceed, for example, half of the small radius, a, of the light cluster, and putting $Z/m_i \ll 1/m_e \gamma_{\perp 2}$ and $N_i/N_{e2} \cdot m_i/m_e \gamma_{\perp 2} \ll 1$ for simplicity, we obtain the condition for the ions to be contained in the form:

$$\frac{N_1}{N_2} > \frac{m_i}{m_e} \cdot \frac{a\gamma_{\perp 2}}{2\pi R}\left(\frac{\gamma_{rel}-1}{\nu_2}\right)^2. \tag{32}$$

From the above discussion the following conclusions can be drawn.

Conditions have been determined which, on the one hand, ensure maximum efficiency of this method of acceleration, and, on the other hand, allow a very simple mathematical analysis of the acceleration process to be made. Conditions (8) and (28) relate the ratio of the number of particles in the clusters and γ_{rel}, and indicate that N_1 and N_2 must differ by at least two orders of magnitude. The most stringent restrictions, also involving other cluster parameters, are imposed by condition (12) and particularly by (32).

A light cluster can be represented in the form of a thin ring with $R/a \gg 1$, $\gamma_{\perp 2} \geq 10$, and $\nu_2 \approx 1$, which corresponds to number of electrons $N_{e2} \approx 10^{14}$. If we take $\nu_1 = 10$, which corresponds to $N_1 \approx 10^{16}$, conditions (8), (12), and (28) will be satisfied for $\gamma_{rel} \lesssim 5$.

From expression (32), with the chosen parameters, we find that the ratio of the large and small radii of the light cluster must be $\sim 10^2$. Thus, acceleration of this kind of cluster of electrons and ions over a length of ~ 100 m results in the ions acquiring an energy of ~ 300 GeV, assuming, for example, $\gamma_2^0 = 3$ and $\gamma_1^0 = 30$.

Further increase of the energy of the light cluster (or weakening of the restrictions on the shock acceleration parameters) is possible if we obtain compact charged clusters with number of electrons more than 10^{16}.

In conclusion, the author wishes to stress the decisive part played by V. I. Veksler in formulating the problem in the form described here, and also wishes to thank M. L. Iovnovich, K. A. Reshetnikov, and V. P. Sarantsev for useful discussion related to the questions dealt with in this paper.

LITERATURE CITED

1. V. I. Veksler, At. Énerg., 2, 427 (1957).
2. V. Veksler and V. Tsytovich, Proc. Conf. on Accelerators (Geneva, 1959), Vol. 1, Geneva, CERN (1959), p. 160.
3. V. I. Veksler et al., At. Énerg., 24, 317 (1968).
4. W. Link, IEEE Trans. Sci., 14, 777 (1967); F. Ford et al., Bull. Amer. Phys. Soc., 12, 961 (1967).
5. L. D. Landau and E. M. Lifshits, Field Theory [in Russian], Fizmatgiz, Moscow (1962).
6. A. G. Bonch-Osmolovskii et al., Preprint of OIYaI No. 2649-2 (Dubna, 1966).

EXPANDED EXPERIMENTAL POSSIBILITIES OF METHODS BASED ON STUDY OF THE NEUTRON NOISE OF A NUCLEAR REACTOR

V. V. Bulavin

UDC 621.039.512.2

A method is proposed for analyzing the neutron noise of a "zero-power" reactor, based on the assumption of a one-rate "point" kinetic model. In contrast with existing statistical methods based on the same model, this method permits one to obtain in an independent experiment exhaustive information about the physical parameters of the reactor. This is achieved by artificially separating the neutron-detection events in a detector in a steady-state reactor into two groups of events having different effects on the subsequent development of the chain reaction.

We consider a subcritical reactor within which there are two physically different pulse detectors: an absorption detector (e.g., a boron counter) and a fission chamber. We assume that a steady-state neutron flux is maintained in the reactor by a source having an intensity S (neutrons per second) and a Poisson neutron distribution. Retarded neutrons are neglected. According to this model, each neutron in the reactor may disappear as the result of capture or leakage; cause a fission event in the active zone, resulting in the formation of ν neutrons with a probability of $f(\nu)$; be absorbed in the first detector (the boron counter); or be absorbed in the second detector (the fission chamber) during a fission event, resulting in the formation of ν neutrons with a probability of $f_2(\nu)$. We denote by λ_c, λ_f, λ_{d_1}, and λ_{d_2} respectively, the probabilities per unit time for these processes. The total probability per unit time that a neutron will disappear in the reactor is $\lambda_t = \lambda_c + \lambda_f + \lambda_{d_1} + \lambda_{d_2} = 1/l$, where l is the lifetime of instantaneous neutrons. In general we have $f(\nu) \neq f_2(\nu)$, since the fissile isotopes in the reactor and detector may be different. The method proposed here consists of measuring the probability that a neutron is detected by detector j during a time interval $(t, t + \Delta t)$ for a steady-state reactor under the condition that a detection has occurred in detector i at $t = 0$. We denote this probability by $C_{ij}(t)\Delta t$, where i and j may take on the values 1 and 2. Analytic expressions are obtained in the complete article relating $C_{ij}(t)$ to the properties of the medium and detectors:

$$C_{1i}(t) = \lambda_{d_i} B + \lambda_{d_i} A \exp(-\alpha t) \quad (i = 1, 2); \tag{1}$$

$$C_{2k}(t) = \lambda_{d_k} B + \lambda_{d_k} A \exp(-\alpha t) + \lambda_{d_k} \bar{\nu}_2 \exp(-\alpha t) \quad (k = 1, 2), \tag{2}$$

where

$$B = \frac{S}{\alpha}; \quad A = \frac{\lambda_f \overline{\nu(\nu-1)} + \lambda_{d_2} \overline{\nu_2(\nu_2-1)}}{2\alpha};$$

$$\alpha = \lambda_t - \lambda_f \bar{\nu} - \lambda_{d_2} \bar{\nu}_2; \quad \bar{\nu} = \sum_{\nu=0}^{\infty} \nu f(\nu);$$

$$\overline{\nu(\nu-1)} = \sum_{\nu=0}^{\infty} \nu(\nu-1) f(\nu); \quad \bar{\nu}_2 = \sum_{\nu=0}^{\infty} \nu f_2(\nu);$$

$$\overline{\nu_2(\nu_2-1)} = \sum_{\nu=0}^{\infty} \nu(\nu-1) f_2(\nu).$$

The probabilities $C_{ij}(t)$ may be measured by a multichannel time analyzer, as in the Rossi-α experiment. This procedure yields α, λ_{d_1}, λ_{d_2}, S, λ_f, λ_t, and λ_c, if $\bar{\nu}$, $\bar{\nu}_2$, $\overline{\nu(\nu-1)}$, and $\overline{\nu_2(\nu_2-1)}$ are known. These

Translated from Atomnaya Énergiya, Vol. 31, No. 2, p. 133, August, 1971. Original article submitted August 20, 1970.

data may be used to calculate the effective instantaneous-neutron multiplication coefficient $K_m = \overline{\nu}\lambda_f + \overline{\nu}_2\lambda_{d_2}/\lambda_t$. If the fissile isotopes in the active zone and in the detector are the same, we have $f(\nu) = f_2(\nu)$ and thus $K_m = \overline{\nu}(\lambda_f + \lambda_{d_2})/\lambda_t = K_{eff}(1-\beta_{eff})$ and $A = \overline{\nu(\nu-1)}/\overline{\nu} \cdot K_{eff}(1-\beta_{eff})/2\alpha l$, where K_{eff} is the effective neutron multiplication coefficient, and β_{eff} is the effective relative number of retarded neutrons. By measuring probabilities (1) and (2) in a critical reactor ($K_{eff} = 1$), one can determine β_{eff}. This method expands the capability of statistical methods, since it permits a study of the physical properties of media in which neutron multiplication does not occur, and it permits measurement of the average number of secondary neutrons ($\overline{\nu}_2$) which arise during the fission of various isotopes.

DYNAMICS OF NEUTRON KINETICS PROCESSES IN A CIRCULATING-FUEL REACTOR

V. P. Zhukov and R. I. Kreer

UDC 621.039.514

A simplified ("point") dynamic model of neutron kinetics processes in a circulating-fuel reactor is derived under the assumption that the time it takes the fuel to pass through the core is much shorter than the average lifetime of the principal sources of delayed neutrons. The equations of the point model were obtained by integration distributed equations of the original dynamic model (neutron diffusion equations, equations of the concentration of sources of delayed neutrons, separation of sources at the core exit) over the volume of the core of the circulating-fuel reactor. The above assumption is resorted to when there is insufficient connection between the intermediate, entrance, and exit concentrations of the sources of delayed neutrons. The following system of equations of the kinetics of a circulating-fuel reactor is derived:

$$\frac{dn}{dt} = \frac{\delta k - \beta}{l} n + \frac{\Sigma_{f0} l_0}{\Sigma_f l} \sum_i \lambda_i C_i;$$

$$\frac{dC_i}{dt} = \frac{\beta_i \Sigma_f}{l_0 \Sigma_{f0}} n - \lambda_i C_i - \frac{V}{L}(C_{i\,ex} - C_{i\,en});$$

$$C_{i\,en} = \frac{V}{L} C_{i\,sep.\,ex} \left(t - \frac{L_T}{V_T}\right) e^{-\lambda_i \frac{L_T}{V_T}};$$

$$C_{i\,sep.\,ex} = S_i C_{i\,ex}$$

$$C_i = 0.5(C_{i\,en} + C_{i\,ex}),\ i = 1, \ldots, N.$$

Here V and V_T are the fuel velocities in the core and in the fuel return path; L and L_T are the length of the core and the length of the fuel return path; S_i is the separation coefficient; the subscript 0 refers to unperturbed conditions, the subscript "sep" refers to the separator; the rest of the notation retains the usual meanings.

This system of equations was used in an investigation of the dynamic properties of circulating-fuel reactors. The investigation was conducted by analog computer simulation. An estimate of the effectiveness of various modes of perturbations in terms of reactivity δk, fuel velocities V and V_T, and the macroscopic fission cross section Σ_f was made. It was shown that the principal perturbation is the reactivity perturbation. The effect of delay time (in the core and in the fuel return path) and of the degree of separation of the sources of delayed neutrons on the dynamics of the neutron kinetics processes was investigated. Separation of sources of delayed neutrons having the highest value of the product $\beta_i\lambda_i$ is found to exert the greatest influence.

Translated from Atomnaya Énergiya, Vol. 31, No. 2, p. 134, August, 1971. Original article submitted December 8, 1970.

EQUIVALENT SYSTEMS OF KINETICS EQUATIONS FOR A CIRCULATING-FUEL REACTOR*

V. P. Zhukov and R. I. Kreer

UDC 621.039.514

The use of equations of neutron kinetics with all groups of delayed neutrons is not always justified, in some investigations of the dynamics of circulating-fuel reactors, particularly in investigations of a qualitative nature.

The article discusses mathematical descriptions of neutron-kinetics processes in circulating-fuel reactors, utilizing equivalent equations of kinetics which make use of only one group of delayed neutrons. A system obtained in the case of the "point" model of a circulating-fuel reactor [see the preceding abstract] was used as the initial system of equations. Two equivalent parameters are determined when the initial system of equations is replaced by the equivalent system: the decay constant λ and the separation factor α of the equivalent group of sources of delayed neutrons.

The choice of criteria for determining parameters λ and α is studied. The article relies on two criteria: 1) the criterion for approximation of the values $d^2\nu/dt^2|_{t=0}$, $d\nu_{lin}/dt|_{t\to\infty}$; 2) the criterion for approximation of the values $d^2\nu/dt^2|_{t=0}$, $d^3\nu/dt^3|_{t=0}$, where ν and ν_{lin} are the relative deviations of the neutron density in the nonlinear and linear models of the neutron kinetics of a circulating-fuel reactor.

Equations for determining parameters λ and α were derived on the basis of these criteria. Comparison of the results of investigation of the equivalent systems corresponding to these criteria show that best results are obtained when reliance is placed on the first criterion, particularly when investigating circulating-fuel reactors for stability.

THE TRANSFER OF RADIOACTIVE N^{13}, N^{16}, AND F^{18} ALONG THE LOOP OF THE VK-50 BOILING REACTOR†

A. P. Veselkin, V. D. Kizin,
I. G. Kobzar', V. Ya. Kucheryaev,
A. V. Nikitin, L. N. Rozhdestvenskaya,
and Yu. V. Chechetkin

UDC 621.039.5

We conducted an experimental investigation of the distribution of water activation products – the isotopes N^{13}, N^{16}, and F^{18} – along the loop of the VK-50 boiling reactor. Specimens of reactor water and steam condensate from the loop were passed through an ion exchange column. The activity of each isotope was measured in the cationic, anionic, and neutral forms. The isotope N^{16} was separated spectrometrically, and the N^{13} and F^{18} were also separated according to the decay curve and the chemical processing of the specimen.

The measurements showed that the N^{16} in the reactor water contained 10-15% cations, 85-90% anions, and no detectable neutral forms. In the steam the N^{16} is all in cationic form. The distribution of the different forms of N^{13} in the reactor water was analogous.

*Translated from Atomnaya Énergiya, Vol. 31, No. 2, p. 134, August, 1971. Original article submitted December 8, 1970.

†Translated from Atomnaya Énergiya, Vol. 31, No. 2, p. 135, August, 1971. Original article submitted November 16, 1970; revision submitted January 8, 1971.

It was shown earlier that the only compound of nitrogen with oxygen or hydrogen that can pass in substantial quantities from the boiling water into the saturated steam is ammonia in the neutral form NH_3 or $NH_3 \cdot H_2O$. In the VK-50 reactor this takes place under operating conditions, but when the coolant specimen is cooled, the ammonia dissociates and is recorded on the instrument as the cation NH_4^+. The absence of the neutral form N^{16} in the steam, even though it had been detected in the EBWR and HBWR reactors, is apparently due to the lower specific energy release and steam content in the EBWR and HBWR active zones.

Measurements of the activity of the N^{16} in the reactor water and steam as a function of the water level in the reactor showed that the most important role is played by the radioactive decay of nuclei as a result of the variation in the time it takes the coolant to move from the active zone to the input of the sampling lines.

The activity of the N^{16} in the steam is approximately proportional to the square of the reactor thermal power. This agrees with the measurement made on the EBWR reactor but differs from the results obtained on the HBWR.

On the basis of the measurement of N^{16} and N^{13} forms in the coolant of the VK-50 reactor and the apparent distribution coefficients for NH_3, NO_2^-, and NO_3^-, we estimated the apparent distribution coefficient of the total activity of the nitrogen isotopes between the steam and the water. Depending on the parameters of the installation, this coefficient varied from 0.2 to 0.6, with an average value of approximately 0.32.

All of the F^{18} in the reactor water and steam condensate is in the anionic form; the apparent distribution coefficient for this is 0.1-0.2.

MINIMIZING THE RADIAL TEMPERATURE DROP IN CYLINDRICAL DISPERSE FUEL ELEMENTS

Yu. V. Milovanov and R. I. Abramyan

UDC 621.039.516.5

Minimization of the radial temperature drop ΔT in a disperse fuel element requires solution of the variational problem for the radial distribution of the fuel concentration in the element for the minimum ΔT (the fuel concentration $\bar{c}$ averaged over the cross section, the diameter of the element, and its thermal power must remain constant). This problem is solved below for the particular case of a stepped concentration distribution, easily achievable in practice, in which the fuel element is divided into two concentric zones (an inner one and an outer one) having different volume concentrations of fuel, c_1 and c_2, respectively, constant within each zone. Here we have

$$c_1 = c\rho - c_2(\rho - 1), \tag{1}$$

where $\rho = r_2^2/r_1^2$; r_1 is the radius of the inner zone; and r_2 is that of the outer zone.

The calculations are based on a parabolic dependence of the thermal-conductivity coefficient λ on the fuel concentration:

$$\lambda = \lambda'' - a(\lambda'' - \lambda')c + b(\lambda'' - \lambda')c^2, \tag{2}$$

which is a good approximation of the experimental data. Here λ' and λ'' are the thermal-conductivity coefficients of the fuel and matrix, respectively, and a and b are constant coefficients.

It is also assumed that the volume heat evolution q_V is related to the fuel concentration by

$$q_{V1(2)} = Ac_{1(2)} \tag{3}$$

Translated from Atomnaya Énergiya, Vol. 31, No. 2, pp. 135-136, August, 1971. Original article submitted December 23, 1970; abstract submitted March 17, 1971.

(where A is a constant coefficient); this corresponds to the situation in the case of a hard neutron spectrum, i.e., in a fast reactor.

Solution of the differential heat-conduction equation for the two zones of the fuel element leads to the following expression for ΔT:

$$\Delta T \equiv T(0) - T(r_2) = \frac{q_{V1} r_1^2}{4\lambda_1} + \frac{q_{V2}(r_2^2 - r_1^2)}{4\lambda_2} - \frac{(q_{V2} - q_{V1}) r_1^2}{4\lambda_2} \ln \frac{r_2^2}{r_1^2}. \quad (4)$$

Substituting Eqs. (1)-(3) into Eq. (4) and converting the latter to dimensionless form, we find

$$\theta \equiv \frac{\Delta T}{\overline{\Delta T}} = \frac{1 - \bar{c}\left(1 - \frac{\lambda'}{\lambda''}\right)(a - b\bar{c})}{\rho} \left\{ \frac{\rho - \varkappa(\rho - 1)}{1 - \bar{c}\left(1 - \frac{\lambda'}{\lambda''}\right)[\rho - \varkappa(\rho - 1)][a - b\bar{c}(\rho - \varkappa(\rho - 1))]} + \frac{\varkappa(\rho - 1) - \rho(\varkappa - 1)\ln\rho}{1 - \varkappa\bar{c}\left(1 - \frac{\lambda'}{\lambda''}\right)(a - b\bar{c}\varkappa)} \right\}, \quad (5)$$

where $\varkappa \equiv c_2/c$ and $\overline{\Delta T} = \bar{q}_V r_2^2/4\bar{\lambda}$ is the temperature drop in a fuel element having a uniform concentration distribution ($c_1 = c_2 = \bar{c}$). The range of the quantity $\varkappa$ in Eq. (5) is found by solving the physically obvious inequalities $0 \leq c_1 \leq 1$ and $0 \leq c_2 \leq 1$, from which it follows that

$$\left.\begin{matrix} \frac{\rho - 1/\bar{c}}{\rho - 1} \\ 0 \end{matrix}\right\} \leqslant \varkappa \leqslant \left\{\begin{matrix} 1/\bar{c} \\ \frac{\rho}{\rho - 1} \end{matrix}\right. \quad (6)$$

The problem of minimizing ΔT thus reduces to that of finding the minimum value of θ, a function of two independent dimensionless variables ρ and $\varkappa$, by means of variational calculations based on Eq. (5).

The calculated results show that in most cases of practical interest, a minimum ΔT may be achieved without any fuel in the inner zone at all. This inner zone may be either filled with matrix material or left empty (as a compensation volume for swelling and for collecting the gaseous fission products); the two possibilities are equivalent insofar as the temperature distribution is concerned.

MECHANISM UNDERLYING RELEASE OF GASEOUS FISSION FRAGMENTS FROM CERAMIC NUCLEAR FUEL

B. V. Samsonov and A. K. Frei

UDC 621.039.572.034.584.343

The diffusion coefficient of gaseous fission fragments in ceramic nuclear fuel apparently declines when exposures as high as 10^{19} fission events per cm^3 are resorted to [1]. This fall-off is manifested in a decline in the yield of gaseous fission fragments, and is accounted for by the appearance of vacancy pores in the intragrain crystalline structure during the irradiation process, with these pores then entrapping atoms of the fragments migrating within the grains [2].

An attempt was made, on the basis of the experimental data shown plotted in Fig. 1, to determine the concentration and dimensions of those pores.

Calculations show that there are always $3 \cdot 10^{17}$ to 10^{19} free vacancy pores, 10 to 60 Å in diameter, per cm^3 in ceramic fuel (whatever the shape of the fuel), starting with doses $\sim 5 \cdot 10^{18}$ fissions per cm^3. The pores exhibit appreciable mobility and anneal out with an annealing constant $\sim 4 \cdot 10^{-6}$ sec^{-1}. A slight fraction ($\sim 5\%$) of the pores constantly trap fission fragments appearing during the fission process, and these become occupied pores, forming gas bubbles. The mobility of the gas bubbles is incommensurably slower than the mobility of the free pores, so that the former disappear at a constant rate of $\sim 10^{-9}$ sec^{-1}. The

Translated from Atomnaya Énergiya, Vol. 31, No. 2, p. 136, August, 1971. Original article submitted July 10, 1970; abstract submitted March 16, 1971.

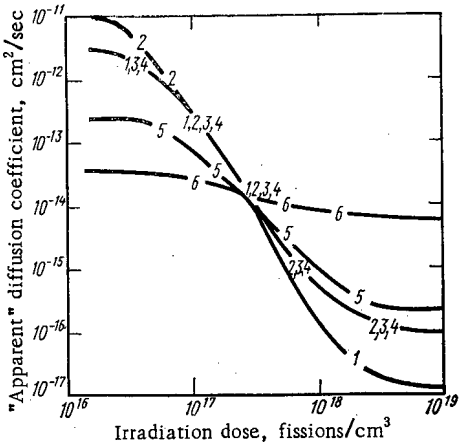

Fig. 1. Nature of change in the "apparent" diffusion coefficient in the case of ceramic fuel: 1) $Xe^{133}UO_2$; 2) $Xe^{133}UC$; 3) $Xe^{133}UC_2$; 4) $Xe^{133}UN$; 5) $Xe^{135}UO_2$, UC, UC_2, UN; 6) Xe^{138}.

mean migration life of atoms of gaseous fission fragments before they impinge upon free pores is 100 sec. The distance separating free pores is in the 50-500 Å range.

Increased swelling, estimated to be 0.20% per each 10^{20} fission events per cm^3, is attributed to a buildup of these gas bubbles in the intragrain structure of the fuel. This state of affairs comes about at temperatures to ~1500°C, and seems to continue so long as the crystalline structure is maintained.

LITERATURE CITED

1. B. V. Samsonov and A. K. Frei, At. Énerg., 30, 358 (1971).
2. B. V. Samsonov and A. K. Frei, At. Tekh. za Rubezhom, No. 8, 31 (1970).

FLUORINATION KINETICS OF Nb_2O_5

É. G. Rakov, D. S. Kopchikhin,
B. N. Sudarikov, and B. V. Gromov

UDC 66.094.402

Niobium is one of the principal materials going into the fabrication of fuel elements [1], and moreover it is a frequently occurring fission fragment element. The behavior of niobium in fluorination processes is consequently of no mean practical interest.

The kinetics of the interaction of pure powdery α-Nb_2O_5 and NbO_2F with elemental fluorine was studied by a gravimetric method over the temperature range 330-430°C. The experiments were conducted with Nb_2O_5 specimens exhibiting a specific surface area 3.45 m^2/g and particle sizes about 50 μ (but 3.11 m^2/g and 40-50 μ respectively in the case of NbO_2F) under conditions eliminating any effect of out-diffusion slowing-down on the process rate.

It was demonstrated, with the aid of chemical analysis and x-ray phase analysis, that two consecutive reactions occur in the fluorination of Nb_2O_5:

$$Nb_2O_5 + F_2 \rightarrow 2NbO_2F + 1/2O_2;$$
$$NbO_2F + 2F_2 \rightarrow NbF_5 + O_2,$$

with the rate of the first reaction being much faster than the rate of the second, and the second acting as the rate-limiting process on the whole. The kinetics of the latter reaction are described by the equation:

Translated from Atomnaya Énergiya, Vol. 31, No. 2, p. 137, August, 1971. Original article submitted October 12, 1970.

$$1-(1-\alpha)^{1/3}=K_1e^{-E/RT}p^n\tau,$$

where α is the degree of reaction response to the time τ, in min; E = 26.2 ± 2.2 kcal/mole is the apparent energy of activation; n = 0.97 ± 0.08 is the order of the reaction with respect to fluorine; p is the pressure exerted by the fluorine, in atm; $k_1 = 5.00 \cdot 10^7$ $min^{-1} \cdot atm^{-1}$ is the preexponential factor.

The NbO_2F isolated from aqueous solutions behaves in a somewhat different fashion. Its fluorination rate is expressed by the equation

$$\lg[\alpha/(1-\alpha)]=k_2e^{-E/RT}p^n\tau,$$

where E = 26.4 ± 2.2 kcal/mole; n = 0.88 ± 0.07; $k_2 = 1.74 \cdot 10^8$ $min^{-1} \cdot atm^{-1}$. The slight discrepancy between the kinetic data for NbO_2F samples obtained by fluorinating Nb_2O_5 and those isolated from aqueous solutions seems to be due to differences in the amount of specific surface area and in the structure of the particles.

Calculations based on the theory of absolute reaction rates enabled us to find that the experimental fluorination rate of Nb_2O_5 at 350°C corresponds to the greatest extent to the theoretically predicted fluorination rate in two instances: 1) when the assumption that the reaction is limited by fluorine adsorption with the formation of a fixed layer of adsorbate holds; 2) when the assumption that the process is governed by the monomolecular reaction between the oxide (oxofluoride) and the fluorine holds.

The picture of the interaction becomes more complicated when elemental fluorine is applied to a mixture of U_3O_8 and Nb_2O_5 than when the individual oxides are fluorinated. Using the necessary auxiliary data from the literature [2-4], we see readily that the heats of the reactions:

$$5UF_6g+2Nb_2O_5cr \rightarrow 4NbF_5g+5UO_2F_2cr;$$
$$UF_6g+2Nb_2O_5cr \rightarrow 4NbO_2Fcr+UO_2F_2cr$$

amount to −31.4 kcal/mole and −55.4 kcal/mole, respectively, at 298°K, which allows us to infer negative values of the isobaric–isothermic potential. This means that it will be predominantly niobium that is removed with the gases at the commencement of the fluorination process, when comparable initial quantities of uranium oxides and niobium oxides are present.

LITERATURE CITED

1. J. Reily et al., Ind. and Engng. Chem., Process Design and Development, 5, 51 (1966).
2. B. N. Sudarikov et al., Trudy MKhTI, No. 51, 194 (1966).
3. M. Kh. Karapet'yants and M. L. Karapet'yants, Basic Thermodynamic Constants of Inorganic and Organic Materials [in Russian], Khimiya, Moscow (1968).
4. É. G. Rakov et al., Trudy MKhTI, No. 65, 46 (1970).

OPERATION OF THE FACILITY FOR DEEP BURIAL OF LIQUID RADIOACTIVE WASTES

V. F. Bagretsov, S. I. Zakharov, and S. V. Metal'nikov

UDC 621.039.717

The preliminary results of the operation of a test-industrial facility for the disposal of deactivated radioactive solutions in deep formations of the earth were communicated in 1967.* An analysis of the performance of the facility during the period 1967-1969 shows that the initial solutions before burial can be

*See S.I. Zakharov et al., in: Disposal of Radioactive Wastes into the Ground, Vienna, IEAE (1967), p. 577.

Translated from Atomnaya Énergiya, Vol. 31, No. 2, pp. 137-138, August, 1971. Original article submitted November 22, 1970; abstract submitted March 29, 1971.

prepared according to one of the following schemes: filtration, lowering of pH to 6-7; an increase of pH to 11.5, setting, filtration, and lowering pH to 6-7; addition of 3.0 mg-eq/liter calcium, an increase of pH to 11.5, setting, filtration, and lowering pH to 6-7; for solutions with a high content of surface-active substances (SAS) it is necessary to add, besides calcium, magnesium (up to 1.5 mg-eq/liter). The last scheme was not used in 1969, since the content of SAS was reduced by a factor of two to three in comparison with the initial period. Accordingly, in 1969 the specific expenditure of reagents (acid from 48 to 10.4 g-eq/m^3, calcium from 3.15 to 1.5 g-eq/m^3) and the quantity of pulp assigned for storage in bulk decreased in 1969 in comparison with 1966.

The main equipment in the facility except the filters, which were cemented by suspensions after six to seven months of operation, functioned normally all these years. For restoring the filtering capability of the charge it was necessary to regenerate the filters with 5% nitric acid solution (consumption of acid 5 m^3 per 1 m^3 sand) twice a year.

After the disposal of 290 thousand m^3 solutions the pressure at the mouth of the hold reached 57 atm while its pickup was probably caused by hydrodynamic factors as well as by silting of the end face zone by soft particles left in the solution.

The most efficient method for controlling the extension of solutions disposed in a reservoir is γ-logging in observational holes. This method cannot be recommended as yet for a qualitative estimate of the filling of the reservoir due to the variability of the specific radioactivity and the radiochemical composition of the disposed solutions. Observations show that the solutions extended from the blower hole to 500-600 m in northwest and southeast directions. A radiochemical analysis of samples of stratified water showed that its activity is mainly due to Sr^{90}, Cs^{137}, and Ru^{106}.

AN ELECTROCHEMICAL METHOD OF DETERMINING THE RADIATION DOSE RATE

G. Z. Gochaliev and S. I. Borisova

UDC 539.12.08

A new type of electrochemical dosimeter has been proposed for the determination of the radiation dose rate according to the currents of electrochemical oxidation or reduction of radiolysis products (RP). In comparison with known samples [1], these detectors possess the following advantages: a larger range of measurements of the dose rate, smaller range with hardness, possibility of use with any type of radiation. The operating principle consists of the fact that in continuous electrochemical oxidation or reduction of RP in a limited volume of solution, some time after the beginning of irradiation, a stationary distribution of the concentration is established, and, consequently, a stationary distribution of the ionization currents of the RP. The stationary currents increase as a linear function of the rate of formation of RP or the dose rate.

Detectors suitable for the determination of the dose rate of soft radiation take the form of cuvettes opened from above, filled with the working solution. The indicator electrode is fastened to the bottom of the cuvette and has an opening opposite the tube soldered to the bottom of the cuvette, communicating with the auxiliary electrode. Detectors in which the working volume of the solution is included in a capillary electrode of platinum were investigated in detail. Diameter of the electrode 2.2 mm, wall thickness 20 μ. The working volume was equal to 0.11 cm^3, and when necessary it could be reduced severalfold. The electrode was welded to the inner surface of a glass tube, sealed from below. At the other end of the electrode, the tube has a partition separating the working volume from the auxiliary electrode. A mercury sulfate

Translated from Atomnaya Énergiya, Vol. 31, No. 2, pp. 138-139, August, 1971. Original article submitted May 20, 1970; abstract submitted April 7, 1971.

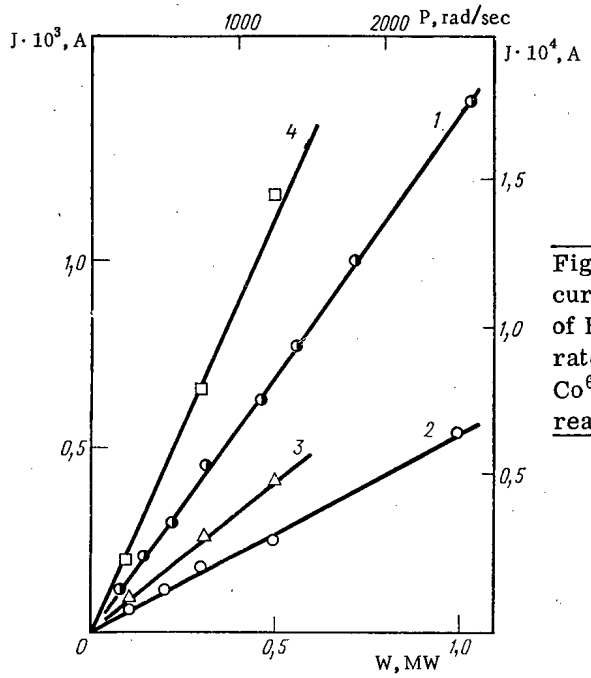

Fig. 1. Dependence of the currents J of the oxidation of H_2 and H_2O_2 on the dose rate P of the γ-radiation of Co^{60} and the power W of the reactor.

electrode served as the reference electrode and simultaneously as the auxiliary electrode. The method of determination of the currents was analogous to that described in [1]. The stationary distribution of the concentration and the stationary currents are described by the following equations:

$$C(r)=\frac{qr_0^2}{4D}\left(1-\frac{r^2}{r_0^2}+\frac{2D}{kr_0}\right);$$

$$J_c=nFqv,$$

where q is the rate of formation of RP; r_0 is the radius of the capillary; r is the distance from the axis of the cylinder; D is the diffusion coefficient; k is the formal rate constant of the electrode reaction; v is the working volume; F is Faraday's number; n is the number of electrons in the electrode reaction.

Figure 1 presents the dependence of the currents of the oxidation of H_2 and H_2O_2 on platinum at a potential 1.1 V (with respect to the hydrogen electrode) on the dose rate of the γ-radiation of Co^{60} (straight line 1) and the reactor power (straight lines 2, 3, and 4). Straight lines 1 and 2 were obtained in 0.5 M H_2SO_4, 3 in 0.5 M H_2SO_4 with an addition of 0.5 M natural Li_2SO_4, 4 in 0.5 M H_2SO_4 with an addition of 0.1 M H_3BO_3, up to 80% enriched with the isotope B_5^{10}.

LITERATURE CITED

1. G. Z. Gochaliev and Ts. I. Zalkind, in: Transactions of the Second All-Union Conference on Radiation Chemistry [in Russian], Izd-vo AN SSSR, Moscow (1962), p. 741; Byulleten' Izobretenii, No. 6 (1961).

DETERMINATION OF THE SPECIFIC ACTIVITY OF γ-EMITTING ISOTOPES IN EXTENDED SOURCES WITHOUT SAMPLE COLLECTION

V. I. Polyakov and Yu. V. Chechetkin

UDC 539.122.164:539.16.08

Approximate analytical expressions for calculating the relative photoefficiency† of the recording by a scintillation γ-spectrometer with a collimator in the determination of the specific activity of isotopes in sources with simple configurations (point, line, plane, plate) of volume and surface cylindrical sources are considered. Thus, for cylindrical sources

$$\varepsilon^*_{V_1}=\frac{\varepsilon\varphi k_1\pi a^4}{4\mu_s L^2}\left[1-\exp\left(-2\mu_s R\right)\right]\exp\left(-\mu_t t\right)\left[1+\frac{4}{\mu_K L}+\frac{4}{\mu_K^2 L^2}\right]\text{when } b<b^V_{gr}\approx\frac{LR}{a}; \tag{1}$$

$$\varepsilon^*_{V_2}=\frac{\varepsilon\varphi k_2\pi a^3 R}{4bL\mu_s}\left[1-\exp\left(-2\mu_s R\right)\right]\exp\left(-\mu_t t\right)\left[1+\frac{3}{\mu_K\sqrt{bL}}+\frac{3}{\mu_K^2 bL}\right]\text{when } b>b^V_{gr}\approx\frac{LR}{a}; \tag{2}$$

$$\varepsilon^*_{S_1}=\frac{\varepsilon\varphi k_1\pi a^4}{4L^2}\left[1+\exp\left(-2\mu_s R\right)\right]\exp\left(-\mu_t t\right)\left[1+\frac{4}{\mu_K L}+\frac{4}{\mu_K^2 L^2}\right]\text{when } b<b^S_{gr}\approx\frac{2LR}{a}; \tag{3}$$

$$\varepsilon^*_{S_2}=\frac{\varepsilon\varphi k_2\pi a^3 R}{2bL}\left[1+\exp\left(-2\mu_s R\right)\right]\exp\left(-\mu_t t\right)\left[1+\frac{3}{\mu_K\sqrt{bL}}+\frac{3}{\mu_K^2 bL}\right]\text{when } b>b^S_{gr}\approx\frac{2LR}{a}, \tag{4}$$

where ε^*_V, ε^*_S are the relative photoefficiency of registration by a scintillation γ-spectrometer with collimator of the radiation of volume and surface cylindrical sources, respectively; ε_φ is the photoefficiency of registration of a crystal for a narrowly collimated beam of γ-quanta; b is the distance from the source to the crystals; $2a$ and L are the diameter and length of the collimator, respectively; 2R and t are the diameter of the cylindrical source and thickness of the wall, respectively; k is a coefficient considering the nonuniformity of the flux from the cylindrical source through the collimator, $k_1 \approx 1$, $k_2 \approx 0.85$ (experimental values); μ_s, μ_t, μ_K are the coefficients of absorption of γ-quanta in the source, shield, and walls of the collimator, respectively.

For an experimental verification of the possibility of using expressions (1)-(4), we used volume cylindrical sources filled with an aqueous solution of a radioactive isotope, and surface cylindrical sources with self-absorption in water and without it, crystals of NaI(Tl) with dimensions 70×70 and 40×40 mm, and collimators 150 and 250 mm long, 5, 10, 20, and 50 mm in diameter. For the entire range of γ-quantum energies considered (0.1-1.5 MeV), distances (25-170 cm), dimensions of sources (diameter 16-255 mm), and collimators, the deviation of the experimental points from the calculated values of the relative photoefficiency of recording lies within the limits of the experimental errors and comprises 10-15%; only at $b \approx b_{gr}$ does the error increase to 40%.

The value of the minimum measurable specific activity of the isotopes is 10^{-7} Ci/liter for volume cylindrical sources and 10^{-9} Ci/cm^2 for surface cylindrical sources. The method of measurement was used to determine the activity of a coolant and to analyze deviations in the circuit of an atomic electric power plant.

†The relative photoefficiency of recording of the radiation of a detector with a collimator is the rate of count of pulses at the peak of total absorption from the source of a unit volume (surface, linear) specific activity.

Translated from Atomnaya Énergiya, Vol. 31, No. 2, p. 139, August, 1971. Original article submitted October 12, 1970.

PORTABLE NEUTRON-IRRADIATION APPARATUS†

V. K. Andreev, B. G. Egiazarov,
L. A. Korytko, and Yu. P. Sel'dyakov

UDC 542.1:541.28

A portable pulsed neutron-irradiation apparatus is described which can carry out the following tasks in the case of natural rock formations: 1) spectrometry of the natural γ-radiation, 2) spectrometry of the γ-radiation from inelastic scattering of fast neutrons (ISFN), 3) spectrometry of the γ-radiation from the radiative capture of neutrons (GRCN), 4) measurement of the temporal distribution of captured γ-radiation, and 5) spectrometry of the induced-activity γ-radiation (IAG) in two situations – during and after irradiation of the medium by means of a pulsed neutron source (for relatively short-lived isotopes). Figure 1 illustrates the operation of the apparatus.

The apparatus consists of a remote unit containing a pulsed neutron source and a scintillation detector, a control and synchronization unit, and a recording device (a pulse analyzer).

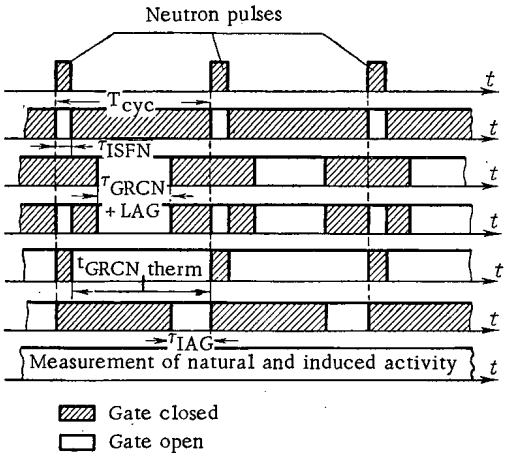

Fig. 1. Operation of the apparatus.

The pulse neutron source provides a neutron output of up to 10^7 neutrons/sec at a pulse repetition frequency of 500-10,000 Hz, and a pulse length of 5-10 μsec. The neutron source may operate continuously.

The control and synchronization unit detects γ-radiation during specified time intervals and synchronizes the operation of the apparatus at the various stages of the measurement. Amplitude-to-time pulse analyzers may be used as recorders.

The apparatus weighs about 12 kg (without the recorder). It draws no more than 20 W. The remote unit is 110 mm in diameter and 1300 mm long.

The complete article contains experimental results illustrating the operation of the apparatus and its capabilities for directly determining the coal content (with a bore model) and the content of the basic rock-forming elements. The results of measurements with a semiconductor γ-detector are also reported.

MEASUREMENT OF BEAM PARAMETERS FOR α-PARTICLES EXTRACTED FROM THE JINR* HEAVY-ION 2 METER ISOCHRONOUS CYCLOTRON‡

V. S. Alfeev, E. D. Vorob'ev,
G. N. Zorin, and Yu. I. Kharitonov

UDC 621.384.02

In this study the energy of α-particles was measured using Rutherford scattering on a thin gold foil (0.25 μ) at an angle of 20° l.s. (laboratory system), since in this region of angles for the Au^{197} (α, α) reaction

*Joint Institute for Nuclear Research.

†Translated from Atomnaya Énergiya, Vol. 31, No. 2, p. 140, August, 1971. Original article submitted November 9, 1970.

‡Translated from Atomnaya Énergiya, Vol. 31, No. 2, pp. 140-141, August, 1971. Original article submitted October 12, 1970.

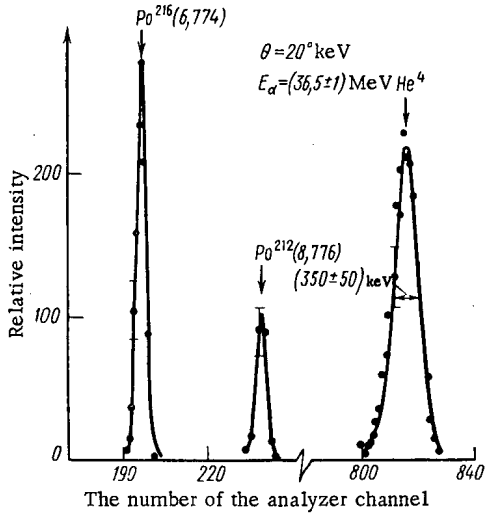

Fig. 1. The energy spectra of the scattered α-particle beam extracted from the JINR U-200 heavy ion 2 meter isochronous cyclotron and the α-calibration lines.

channel, the cross section of elastic scattering of α-particles in the energy range of 30-40 MeV exceeds the cross sections of inelastic processes by several orders of magnitude. The beam, with a geometric radius of 860 mm, was extracted from the JINR U-200 cyclotron using a charge-exchange technique [1].

To detect the α-particles a semiconductor surface barrier detector with a 27 mm^2 cross section was used, which is made from high resistivity silicon and which has certain advantages over a Li-drifted detector [2]. The detector was situated at a 45° angle l.s. relative to the scattered beam, and at a bias of 300 V provided a sensitive layer of ~800 μ, corresponding to the mean free path of α-particles with an energy of ~45 MeV. At 200 V bias on the detector the resolution was equal to 20 keV for a known α-line from Am^{241} (5.482 MeV).

After the removal of the spectrum of scattered α-particles, the scale of the 1024 channel analyzer was determined by a precision pulse generator which was calibrated at the known α-lines from Po^{212} (8.776 MeV) and Po^{216} (6.774 MeV).

The measured energy of α-particles extracted from the U-200 is equal to (36.5 ± 1.0) MeV, and the degree of monochromatism of the α-beam, allowing for the inherent resolution of this procedure, is equal to (350 ± 50) keV, which is 1% of the beam energy (see Fig. 1).

It has been established that one of the basic contributions to resolution is the instability of the high-frequency voltage on the dees of the cyclotron.

As a check on the measurements, a stack of aluminum foils with a common density of (100 ± 4) mg /cm^2 was introduced. The thickness of each foil was 6 μ. The energy of the α-particles after the absorber was equal to 17.5 MeV, which corresponds to an energy of primary α-particles of (36.0 ± 1.4) MeV [3].

The energy measurement by means of absorbers agrees well within the limits of error with the measurements by the precision pulse generator.

LITERATURE CITED

1. I. A. Shelaev et al., Pribory i Tekh. Éksperim., No. 3, 53 (1970).
2. G. Andersson-Lindstroem, Nucl. Instrum. and Methods, 56, 309 (1967).
3. L. Northcliffe, Ann. Rev. Nucl. Sci., 13, 67 (1963).

METHOD OF MEASURING (p, n)-THRESHOLDS FOR THE STUDY OF ACCELERATOR BEAM ANALYZING SYSTEMS

M. I. Afanas'ev, A. L. Bortnyanskii, and A. I. Graevskii

UDC 621.384.6

A system is proposed for automatically recording the yield of nuclear reactions. The energy of the incident particles is changed by modulating the potential on the target. A sawtooth voltage on the target is obtained by means of its charge through capacitive coupling to the beam current and its rapid discharging using a high-voltage relay. As the potential increases, the channels of a pulse-height analyzer are shifted by a current integrator. The yield of the nuclear reaction is registered in the memory of the analyzer synchronously with the increase of the target potential. The analyzer operates in a multi-channel accumulator mode.

A cassette of boron counters in a paraffin moderator was used as a neutron detector. The construction of the chamber permits the detection of the total neutron yield in a cone with an opening angle of 90°; at the same time, the generating cone does not touch the metallic components, which makes it possible to detect all neutrons in the reaction $Al^{27}(p, n)Si^{27}$ in the range ~8 keV above the threshold.

Small leakages in the chamber insulation ($5 \cdot 10^{-9}$ A) permit operation with beam currents up to 10^{-8} A without significant distortions in the form of the excitation function.

A curve is cited to illustrate the relative neutron yield in the $Al^{27}(p, n)Si^{27}$ reaction in the vicinity of the threshold. The scanning range of the target potential is 25 kV.

With the same target chamber insulation, measurements may be taken in an energy range two times greater, by charging the target negatively beforehand. In this case the target potential will increase to zero, and then to the previously given maximum positive potential. The apparatus described permits measurements in the bipolar scanning mode of the target potential. At the same time, before the beginning of each cycle the high-voltage relay connects the target to a rectifier, at the output of which the specific voltage is established.

The excitation function of the $C^{13}(p, n)N^{13}$ reaction near the threshold is presented, which was obtained in the bipolar scanning mode. The scanning amplitude is 25 kV.

Translated from Atomnaya Énergiya, Vol. 31, No. 2, p. 141, August, 1971. Original article submitted November 9, 1970.

EXPANDED CAPACITY RADIATION LOOP AT THE IRT NUCLEAR REACTOR IN TBILISI

G. I. Kiknadze, É. L. Andronikashvili, V. S Bedvenov, I. A. Gassiev, G. V. Zakomornyi, D. M. Zakharov, B. I. Litvinov, R. B. Lyudvigov, L. O. Mkrtichyan, I. A. Natalenko, and L. I. Fel'dman

UDC 621.039.573

The first immersion type RK-P indium–gallium radiation loop was commissioned in 1963 at the nuclear reactor of the Institute of Physics of the Academy of Sciences of the Georgian SSR [1]. In ~30,000 h of steady operation, this facility demonstrated excellent reliability and ease of operation [2].

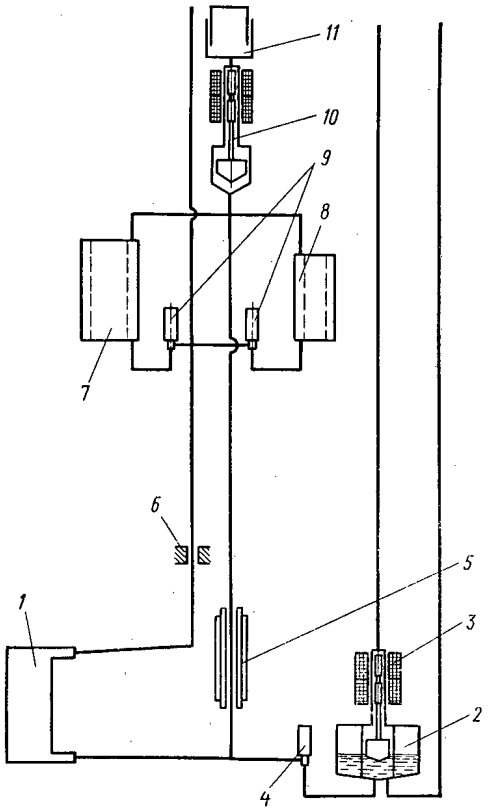

Fig. 1. Basic layout of the RK-PM radiation loop facility: 1) activity generator; 2) overflow tank; 3,10) float level gages; 4,9) globe valves; 5) electromagnetic induction pump; 6) electromagnetic flowmeter; 7,8) large irradiator and small irradiator; 11) gas holder.

The radiation loop was dismantled in 1967 while the reactor was being rebuilt. The entire dismantling operation took 5-6 h. The radiation environment presented no serious hazard to the personnel engaged in the dismantling operation.

After the reactor had been rebuilt and its power output had been brought up to 4-5 MW [3-5], construction work was begun on a modernized RK-PM radiation loop, installation of which was based on the same design principles.

The new radiation loop was built by the end of 1968 and was brought up to rated irradiation conditions in January, 1969. The γ-radiation carrier in this renovated facility was again a binary indium–gallium alloy of eutectic concentration [6]. Contact between the alloy and oxygen present in the atmosphere was prevented by a protective blanket of inert gas.

The layout of the facility is shown in Fig. 1, and a general view of the facility appears in Fig. 2. The components of the facility are combined in the following four principal structural units.

1. The activity generator, comprising a four-layer system of branching slotted channels 3 mm thick and with transverse dimensions 410 ± 500 mm, joined by common collectors (Fig. 3). The layers are separated by graphite slugs 40 mm thick. The casing of the generator and the slotted channels are made of titanium.

The choice of that design reflected the possibility of more complete utilization of leakage neutrons from the reactor, and the possibility of increasing the neutron self-shielding factor in multilayered systems [7, 8].

The total volume of the alloy present in the activity generator is 2.6 liters. Two resistance thermometers were installed in the top and central parts of the activity generator, in titanium wells sunk in the graphite slugs.

Translated from Atomnaya Énergiya, Vol. 31, No. 2, pp. 143-145, August, 1971. Original article submitted August 6, 1970.

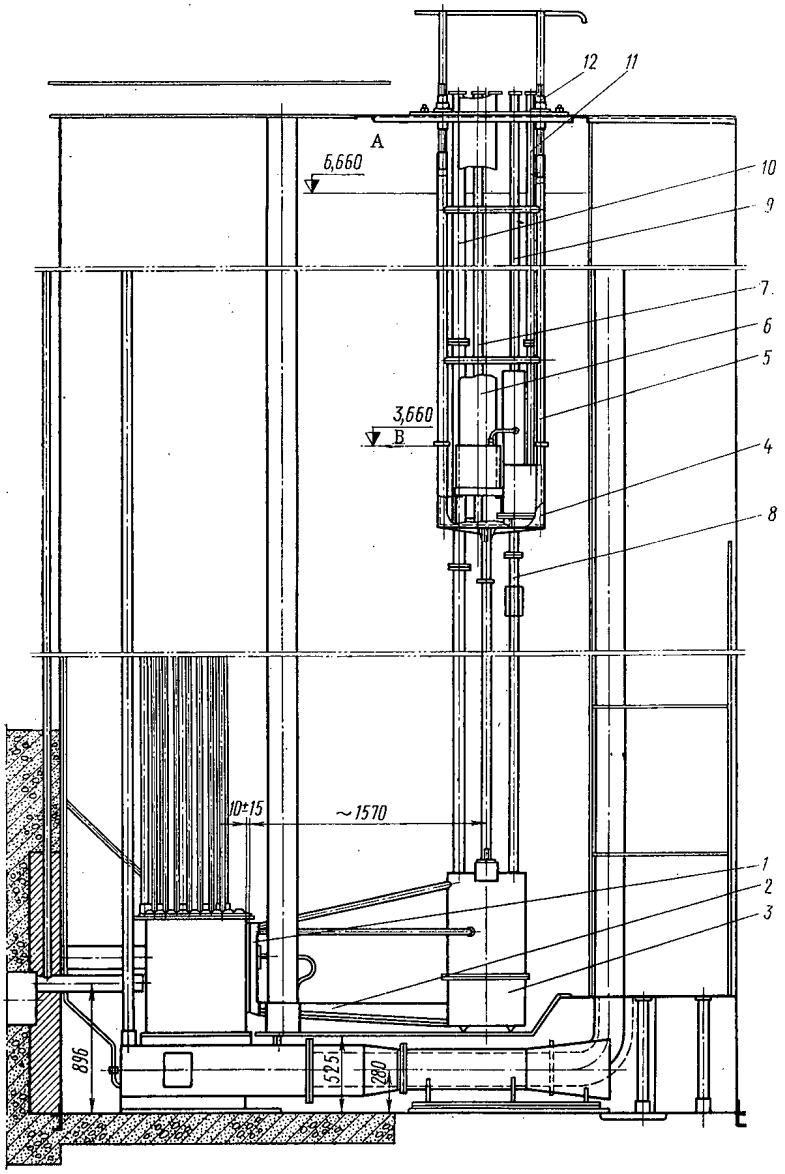

Fig. 2. General view of the RK-PM radiation loop: 1) activity generator; 2) tray under activity generator; 3) underwater chamber; 4) tray with irradiator; 5) tubular girder; 6) central channel of large irradiator; 7) central channel of small irradiator; 8, 9) process channels; 10) channel for electrical cable and drain valve control switch; 11) channel for irradiator globe valves control switch; 12) topside support area; A) water level; B) irradiator positioning level.

A protective pan made of 1Kh18N9T steel is placed under the activity generator and under the feed piping, to help cope with any alloy leakage emergency.

2. The underwater chamber, made of 1Kh18N9T steel, is shaped as a cylinder 520 mm in diameter and 800 mm in height. An electromagnetic linear induction pump and a magnetic flowmeter completely identical to the ones used earlier in the RK-P radiation loop are installed inside the chamber. Also located there are the overflow tank of 15 liters capacity, also made of 1Kh18N9T steel, and provided with a float level gage with a differential-transformer type sensor. The working recorded travel of the sensor float (50 mm) monitors the top half of the tank capacity, and aids in checking on how completely the γ-ray carrier is drained from the loop piping. A stop valve, also located in the underwater chamber, is used to control overflow.

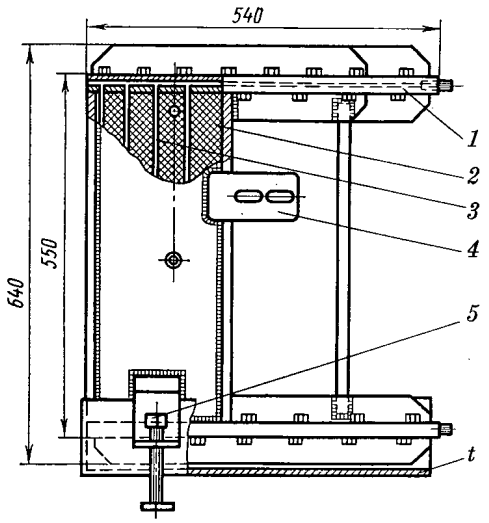

Fig. 3. Activity generator for RK-PM radiation loop: 1) top collector; 2) graphite slug; 3) slotted channel; 4) mounting bracket for generator; 5) reference adjusting screw; 6) tray.

3. The system of two irradiators, the stop valves serving them, and the float level gage are mounted on a rigid tray which is coupled to the bottom of the facility by four standpipes. These standpipes function simultaneously as process lines through which loop piping, electrical cableware, and the remote control switch for the globe valves pass. The irradiators are fabricated in the form of hollow cylinders with the alloy flowing along a helical track between them. The globe valves make it possible to switch either of the irradiators, or both simultaneously, into the circulation system. The irradiators are equipped with central and peripheral channels to facilitate irradiation exposures in a field of pure γ-radiation and dosimetric monitoring of the γ-emission dose rate of the facility.

The float level gage located at the uppermost point of the circulating system makes it possible to measure the amount of γ-ray carrier present in the system, and to reliably record cases of accidental leakage of alloy with a sensitivity of 20 cm^3.

4. The top support area with the pipe-suspension system, forming a rigid girder truss connecting all the units enumerated above in a single structure is shown in Fig. 2. The channels of the irradiators in the irradiation loop, and the channels for the remote control switches actuating the globe valves, are mounted on the top support platform. A system of control adjustment screws on the support platform makes it possible to adjust the activity generator with precision relative to the boundary of the IRT reactor core [9].

The loop control panel is in the form of a memory panel, giving the operating personnel up-to-the-minute information on the performance of the facility.

The instruments mounted on the control panel take care of monitoring the temperature in the activity generator and in the channel for the induction pump, the level of the indium–gallium alloy in the circulating system and in the overflow tank, currents flowing through the windings of the induction pump, the flowrate of γ-ray carrier as it circulates through the system, and the dose rate in the two irradiators.

The emergency and alarm annunciation system (which is transistorized) rings an audible alarm signal and switches on the appropriate alarm bulb on the memory panel of the loop in the event the temperature rises, the flowrate declines, there is leakage of inert gas, the pump malfunctions or shuts off, or the fill level of the alloy declines.

The dose rate of γ-radiation at the center of the loop's large irradiator is ~ 400 r/sec; that at the center of the loop's small irradiator is ~ 500 r/sec, for each MW of reactor power output when the two irradiators are operating simultaneously.

When the large irradiator is shut off, the dose rate in the small irradiator is ≈ 850 r/sec for each MW of reactor power output. The γ-equivalent of the arrangement is 60,000 g-eq Ra per megawatt. The operating flowrate of the γ-ray carrier is ~ 7 cm^3/sec, the duration of a single alloy circulation period is 30 min. The temperature of the γ-ray carrier attains its peak in the activity generator, specifically 63°C when the reactor output is at 1 MW, and 155°C when the reactor output is at 4 MW. The total volume of γ-ray carrier is 13.1 liters, of which 2.6 liters are present in the activity generator, as indicated earlier, 7.5 liters are present in the large irradiator, 2.5 liters in the small irradiator, and 0.5 liters in the piping.

The peak radiation power output of the RK-PM facility, attained when the thermal power output of the IRT reactor is 5000 MW, was 300,000 g-eq Ra.

The RK-PM radiation loop differs from its precursor not only in the significant increase in radiation dose rate, but also in terms of compactness and ease of assembly. A five-man team carried out the rigging and assembly work for the whole facility in the reactor vessel within eight hours.

A large number of exposures have already been performed in the channels of the RK-PM radiation loop in pilot production and research work. The commissioning of this radiation loop has expanded the experimental capabilities of the reactor facility considerably. Radiation loops of this type can be constructed with ease at any existing pool type reactor facility.

LITERATURE CITED

1. G. I. Kiknadze et al., At. Énerg., 19, 176 (1965).
2. E. D. Chistov et al., Nauchnye Raboty Inst. Okhrany Truda VTsSPS, 48, 42 (1967). Safety Institute of the All-Union Council of Trade Unions], 48, 42 (1967).
3. Sh. P. Abramidze et al., Proceedings of the Jubilee Session of the Institute of Physics of the Academy of Sciences of the Georgian SSR devoted to the 50th Anniversary of the October Socialist Revolution, Tbilisi, 1968 [in Russian], Inst. Fiziki Akad. Nauk GruzSSR (1969).
4. Sh. P. Abramidze et al., At. Énerg., 27, 547 (1959).
5. Sh. P. Abramidze et al., Report to the Vth International Conference on the Physics and Engineering of Research Reactors, Warsaw, 1968 [in Russian].
6. G. I. Kiknadze et al., At. Énerg., 19, 178 (1965).
7. G. I. Kiknadze, Doctoral Dissertation [in Russian], Tbilisi (1968).
8. G. I. Kiknadze et al., Report to the IVth Working Conference on the Physics and Engineering of Research Reactors, Budapest, 1965 [in Russian].
9. V. N. Chernyshevich et al., Report to the Vth International Conference on the Physics and Engineering of Research Reactors, Warsaw, 1968 [in Russian].

FABRICATION OF LIQUID-METAL WORKING MATERIALS FOR RADIATION LOOPS

G. I. Kiknadze, D. M. Zakharov, R. B. Lyudvigov, and L. I. Fel'dman

UDC 621.039.573.669.87

The fabrication of liquid-metal γ-ray carriers, for example, indium–gallium or indium–gallium–tin alloys, is one of the principal problems in the design of radiation loops. In each specific case, the procedure followed in the fabrication of these materials may differ in certain technological features of the process, but the following general rules do have to be observed consistently in each instance.

1. Structural materials of high stability to attack by the liquid-metal environment must be used in the melting facility, and most particularly in the piping and parts coming into direct contact with the liquid γ-ray carrier.

This requirement pursues the aim of eliminating any possibility of the γ-ray carrier being contaminated by extraneous elements (as a result of possible dissolution of the structural material in the alloy) or by interaction products forming on the interface between the structural material and the melt. Quartz or titanium single-phase and two-phase alloys (such as VT1-1, VT-6, etc.) can be recommended as suitable structural materials in these applications. The use of titanium is preferred for technological reasons. It would also be desirable to carry out a preliminary passivation of the titanium in air at temperatures 550-570°C for 100 to 150 h. This treatment leads to the formation of a TiO_2 oxide film on the surface of the titanium, thereby preventing any interaction between the titanium and the indium–gallium alloy [1, 2].

2. A special degassing of the metals comprising the charge to the γ-ray carrier is required, during the meltdown and in heating to the specified temperature.

This requirement pursues the aim of lowering the oxygen content and lowering the content of other gases dissolved in the original metals, and also of removing (at least partially) any volatile gallium oxides or indium oxides that may be present. The degassing process must be carried out gradually, by pumping out the vapor phase from the melting vessel into which the charge has been introduced previously, down to a residual pressure of 10^{-3} to 10^{-4} mm Hg over the entire period that the metals are being melted down and heated to the specified temperature. The heating rate is 1.5-2 deg/min.

3. Special attention must be given to isothermal holding of the melt for several hours with bubbling of the inert gas through the melt. The isothermal holding temperature must not be higher than 500°C, and in case titanium is used as the structural material the maximum heating temperature must be lowered to 300°C. Bubbling with inert gas (helium best of all) makes it possible to: a) carefully mix the components of the melt by mechanical means; b) bring the oxide phase present in the bulk of the liquid γ-carrier in the suspended state to the surface of the melt.

Isothermal holding of the liquid phase promotes an equalization of the concentration of the components of the γ-ray carrier throughout the bulk of the melt through intensification of the diffusion processes at work. It should be stressed that bubbling of inert gas through the melt may result in the formation of a finely dispersed phase of black coloration (this means that gallium oxides and indium oxides, or gallium alone, may turn up in the melt [3-5]), and this phase would be present in the suspended state throughout the free space of the melting vessel, gradually settling on the walls and on the surface of the vessel as a "cap" of oxides covering the melt.

Translated from Atomnaya Énergiya, Vol. 31, No. 2, p. 146, August, 1971. Original article submitted August 6, 1970.

4. The next stage is cooling of the liquid-metal γ-ray carrier to temperatures close to room temperature, and careful filtration of the carrier.

The cooling rate is 2-3 deg/min. The filtering system consists of an array of filters featuring a gradual transition from rough clean-up to fine filtering. Stainless steel mesh combined with Petryanov fabric, caprone fabric, and quartz shavings is suitable for filter aids; Schott filters and porous graphite can be used for the fine filtration step.

5. Periodic analysis of samples of the γ-ray carriers for their content of basic components is advised.

Analysis of the γ-ray carrier during the isothermal holding process and during the bubbling process is particularly crucial. A constant level of the concentration of components of the γ-ray carrier with time is an objective indicator of the quality with which the alloy has been prepared, and can serve as a signal to terminate the isothermic holding and bubbling steps. Analysis of the γ-ray carrier for the content of the basic components is also required before the radiation loop is filled with alloy (after the γ-ray carrier has been through the filtering system). This makes it possible to secure reliable information on the composition of the γ-ray carrier fulfilling the functions of a working fluid for the radiation circulation loop.

6. The entire complex of operations involved in preparing the γ-ray carrier and in filling the radiation loop with it must be carried out in the strict absence of any contact between the alloy and oxygen in the air, or moisture.

This stresses the necessity of monitoring the oxygen content and moisture content in an inert gas, and where the need arises taking measures to purify the inert gas. Traces of moisture must be removed from the piping and from the various units involved in the preparation of the alloy.

The principles formulated here were arrived at in the course of work done at the Institute of Physics of the Academy of Sciences of the Georgian SSR [6], and can be considered a basis for the design of equipment intended to prepare large batches of alloy for industrial-scale radiation loops.

The authors express their sincere thanks to B. I. Litvinov for his highly appreciated participation in the design and operation of the facilities for preparing the liquid-metal γ-ray carrier.

LITERATURE CITED

1. L. S. Moroz et al., Titanium and Titanium Alloys [in Russian], Vol. 1, Sudpromgiz, Leningrad (1960).
2. G. I. Kiknadze, D. M. Zakharov, and L. V. Mel'nikova, At. Énerg., 19, 177 (1965).
3. M. Robert, Compt. Rend., 5, 51 (1964).
4. A. G. Godzhello, Trudy Mosk. Energ. Inst., No. 5, 354 (1964).
5. S. P. Yatsenko, G. N. Perel'shtein, and D. V. Lokshin, Trudy Inst. Khimii, Ural'skii Filial Akad. Nauk SSSR, No. 18, Sverdlovsk (1968).
6. I. G. Kiknadze et al., At. Énerg., 19, 176 (1965).

PNEUMATIC IRRADIATION CHANNEL RELOADING SYSTEM FOR THE IRT-M REACTOR

T. S. Ambardanishvili, G. V. Zakomornyi,
G. D. Kiasashvili, G. I. Kiknadze,
B. I. Litvinov, L. O. Mkrtichyan,
and A. M. Uvarov

UDC 621.039.5:621.54

The pneumatic reloading system for the vertical channels of the IRT-M reactor in Tbilisi incorporates the following principal components (Fig. 2).

1. The specimen irradiation channel located in the core or in the reflector is an array of two coaxial tubes of 1Kh18N9T steel, 38 mm and 57 mm in diameters, wall thickness 2 mm and 2.5 mm, respectively. At the blind end of the inner tube in the channel is mounted a special valve normally closed when the channel is being loaded and open under the pressure of the working gas when the channel is being unloaded. This

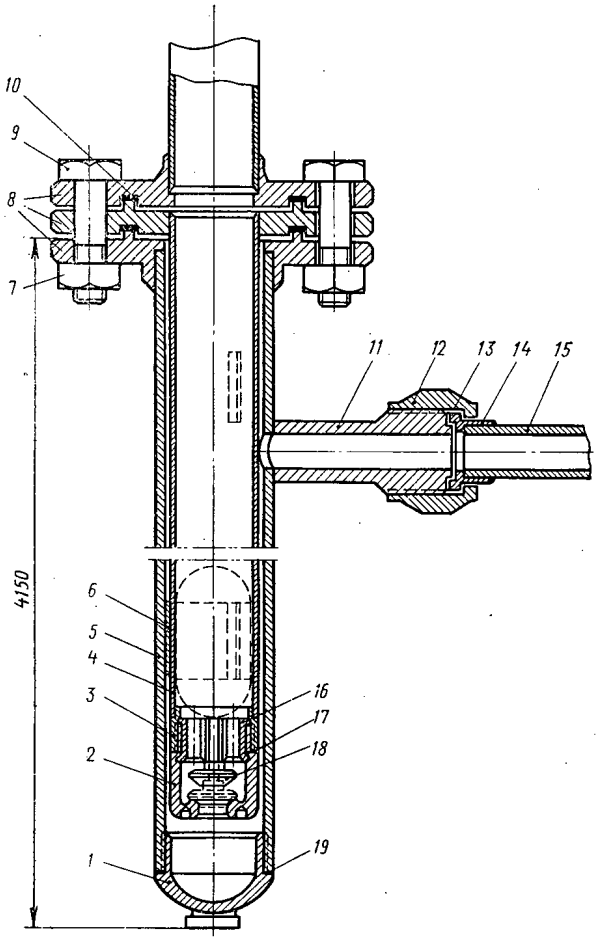

Fig. 1. Irradiation channel: 1) bottom; 2, 3) inserts; 4) channel inner tube; 5) channel body; 6) distance spacer; 7) nut; 8) flange; 9) bolt; 10, 13, 17, 19) washers; 11) pipe connection; 12) union nut; 14) pipe connector; 15) pipe; 16) travel stop; 18) valve.

Translated from Atomnaya Énergiya, Vol. 31, No. 2, pp. 147-150, August, 1971. Original article submitted July 31, 1970.

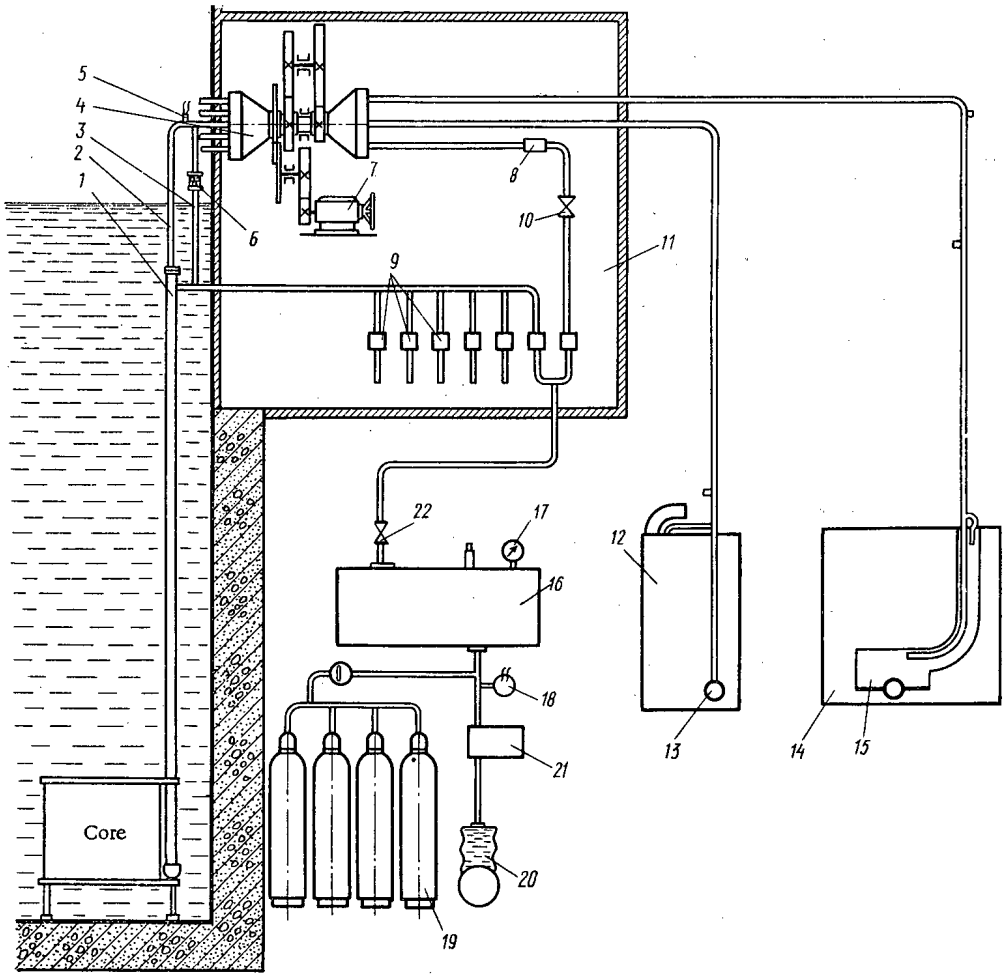

Fig. 2. Pneumatic reloading system of vertical channels of IRT-M reactor: 1) specimen irradiation channel; 2) main tube; 3) air tube; 4) distributor; 5) sensor; 6) bypass valve; 7) motor; 8) charging device; 9) pneumatic valve; 10, 22) globe valves; 11) recess in reactor shielding; 12) reactor hot cave; 13) receiving chamber in reactor hot cave; 14) hot cave for radiochemical laboratory; 15) receiver in hot cave of radiochemical laboratory; 16) receiver tank; 17, 18) pressure gages; 19) high pressure emergency controls; 20) compressor; 21) decontamination unit.

valve also acts as a stop valve converting the channel into a pulsation-dampening volume to allow smooth descent of the specimen during the loading operation. The layout of the channel is shown in Fig. 1.

When a specimen is being loaded into the channel, the excess amount of working gas is dumped through the bypass valve located between the feed line for the working gas and the pneumatic shuttle conveying channel.

An electrical sensor records the entry of the specimen into the zone where it is expedited to the vertical portion of the channel. This sensor then shuts off the system pumping the working gas which transports the loaded specimen through the channel, and records the passage of the specimen in the appropriate cell of the memory panel.

2. The distributor (Fig. 3) is a device providing a combination of any of five channels reserved for the pneumatic shuttle system at the IRT-M reactor in Tbilisi, and one of the three channels reserved for loading of specimens, the path to the radiochemical laboratory, or the path to the operational hot cave in the reactor building.

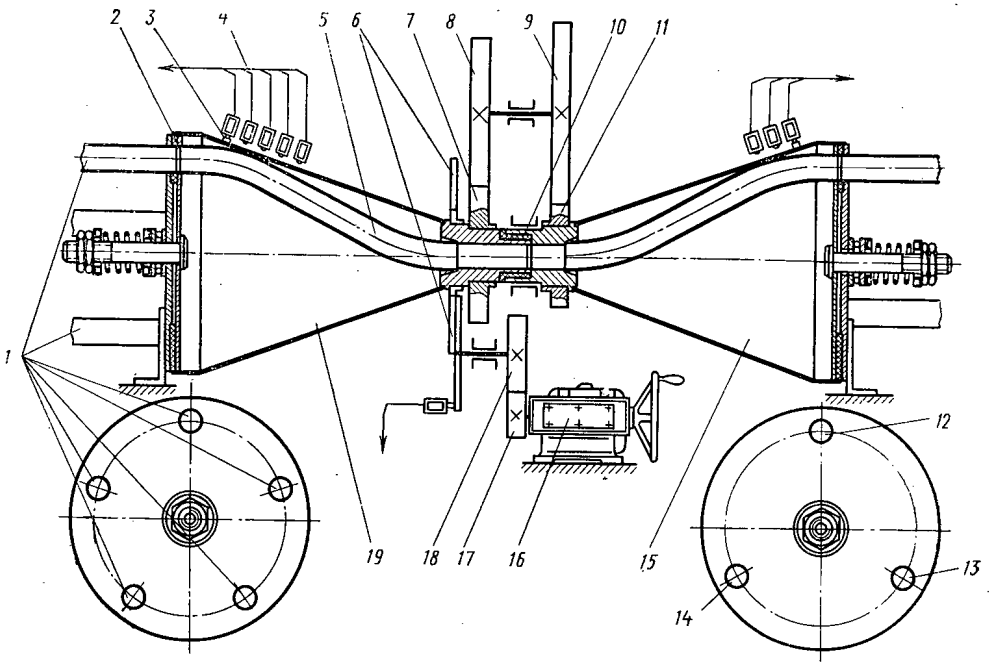

Fig. 3. Distributor: 1) container duct to channels; 2) gasket; 3) hood; 4) electrical microswitches; 5) combination channel; 6) five-groove Maltese cross; 7, 9, 17) gears; 8, 11, 18) driven gears; 10) insert; 12) loading line; 13) radiochemical laboratory line; 14) operational hot cave line; 15) half-body of container duct; 16) electric power drive; 19) channel half-body.

The distributor thus consists of two parts kinematically linked with each other by a system of transmissions.

The two parts of the distributor are brought into action by an electric power drive, with the aid of a five-groove Maltese cross. The combination of the pneumatic shuttle channels and their mutual fixed positions is brought about by using a special sector of a driving disk. Teflon gasketing is used to provide sealing between the five-channel and three-channel parts of the distributor.

The sensors for the combination of channels in the three-channel and five-channel parts of the distributor are microswitches included in the control circuitry of the electric drive. The electric power drive, and with it the combination of channels on the two parts of the distributor, is stopped by a programmed matching of protrusions on the rotating parts with microswitches mounted on the frame of the distributor.

The accuracy with which the reactor channel is matched to one of the three specimen-conveying channels is achieved by using the microswitch to shut off the power drive motor at the instant the Maltese cross is engaged by the sector on the drive disk. The system transmitting motion from the five-channel part of the distributor to the three-channel part is designed such that displacement of the five-channel part by one channel corresponds to displacement of the three-channel part by one channel also, so that the switchover can be accomplished through the action of the same electric power drive.

The distributor is housed in a recess in the biological shield of the reactor, with pressuretight access doors. This recess is hooked up to the special ventilation system (to evacuate the radioactive gas liberated, when specimens are discharged, through possible clearances between the five-channel and three-channel parts).

3. The loading device, acting as a locking mechanism, is accommodated in the same recess in the shield as the distributor. The working gas is fed during the loading operation through the action of electromagnetically actuated valves. The working gas exists from a receiver tank with tank pressure maintained at set level by a compressor. The compressor motor is controlled by using an electrical contact pressure gage which sets the upper and lower pressure limits in the receiver tank. The working pressure in the receiver tank is 4 atm. In case of emergency, there is a reserve supply of working gas available in pressure cylinders, which can be connected up to the receiver tank by opening globe valves.

A container for conveying the specimen is made up of two thread-engaged parts made of aluminum or plastic, and forms a cylinder with spherical ends. The diameter of the container is 32 mm, the length 65 mm.

The pneumatic shuttle control system makes it possible to carry out the following operations:

1) combination of either of five channels in the core and the loading device, either with the discharge lines leading to the radiochemical laboratory or with those leading to the operational hot cave;

2) loading of containers with the test specimens in the five channels;

3) discharge of containers with test specimens to the radiochemical laboratory or to the operational hot cave;

4) interlock against loading of more than one container into any one channel;

5) interlock of loading and unloading until the combining operation has been completed;

6) interlock of distributor motor starting until the end of the loading and unloading operation;

7) air pressure in receiver tank maintained within set range;

8) loading and unloading interlocked when pressure in receiver tank falls below or rises above set range;

9) annunciation of combining of channels for container reloading operations, lowering or raising pressure in receiver tank, and also on movement of container through one of the three conveying lines, by switching on appropriate light bulbs on the front panel of the control desk.

In addition, the pneumatic shuttle control system takes care of restoring the basic signals recorded in the overall system memory, when the electrical power supplies are switched on again after being disconnected or deenergized accidentally.

Measures were taken to decrease the number of contacts and to decrease the amount of current flowing through them, with the object of enhancing system reliability, and this was achieved through the use of transistors and semiconductor diodes.

An indication of container loading into the irradiator channel is achieved through the use of a memory cell in the pneumatic shuttle control system. A twin-coil polarized relay acts as the memory element.

When the container passes by the corresponding load sensor, the circuit supplying one of the relay coils is broken, and the current flowing through the other coil then throws the yoke into the "loaded" position. A green light bulb then goes out and a red bulb goes on on the control panel, and the corresponding transistor is driven to cutoff, thus interlocking any loading of a second container while the channel is "busy."

Electrical sensors feeding information on the progress of the container are located every ten meters along the travel path. Signals from these sensors light up bulbs on the memory panel of the pneumatic shuttle control system, making it possible to pinpoint the position of the container in the event of an accidental shutdown.

It has been proposed to work out a completely noncontacting system using controlled valves, in the future.

The control panel is made in the form of a memory block for the pneumatic shuttle system.

The receiver device placed in the hot receiving cave for reception and forwarding of specimens to the radiochemical laboratory consists of two coaxial tubes (1Kh18N9T steel) 38 mm and 57 mm in diameter, with respective wall thicknesses 2 mm and 2.5 mm. The valve for venting the conveying gas discharges spent gas into the tube space as the container passes by, and the tube space communicates to the hot cave, where the spent gas is drawn into the special ventilation system of the radiochemical laboratory. After the valve has done its work, the vertical portion of the receiving channel becomes converted into a damping volume which lowers the container down smoothly into the hot cave. The container falls into a spherical trap with a swing-out flap cover, and is withdrawn from there by a remote-controlled manipulator.

The basic parameters of the pneumatic shuttle are: operating pressure when container is loaded in 0.5 atm, gas flowrate 20 liters, pressures of 1.0, 1.3, and 1.5 atm for discharge at respective speeds 2, 4, and 6 m/sec; average flowrate of conveying gas over a 100 meter stretch of piping: 310 liters.

GAS EVOLUTION IN THE PRIMARY LOOP OF A PRESSURIZED-WATER REACTOR WITH GAS VOLUME COMPENSATORS

Yu. F. Bodnar'

UDC 621.039.5:629.1

The conditions that guarantee that there will be no gas evolution in the primary loop of a pressurized-water (water-cooled, water-moderated) reactor with gas volume compensators (VC) were considered in [1, 2]. The presented temperature dependence of the solubility of a gas in water for a constant total pressure P_0 taking account of the vapor pressure P_v of the water is correct for a heterogeneous gas–water system [2].

In the primary loop, the only such system is the VC. In the articles indicated above, an estimate of the solubility of the gas in the primary coolant, where there are no gas pockets, was also carried out taking the vapor pressure of water into account. However, there is a basic difference between the concepts of gas solubility in heterogeneous and in homogeneous systems. Therefore, the conclusions drawn concerning the conditions for gas evolution in the primary loop are incorrect.

According to Henry's law, the solubility of a gas in water for given P_0 and T_0 depends on the partial pressure of the gas P_g in the vapor–gas mixture above the level of the water, where, with increasing partial pressure of the gas, its solubility in the water increases [3]. We thus expect that the maximal solubility, for given parameters, will occur for $P_g = P_0$, i.e., when there is no water vapor in the gas phase. Such conditions are possible, e.g., because of the constant exchange of gas above the level of the water.

To confirm the above, we carried out the following experiment. Completely degasified water was poured into an open container, and the temperature was kept at 100°C during the entire experiment – preventing boiling. Measurement of the concentration of nitrogen in water over several hours showed that the nitrogen content is equal to the solubility at 100°C and nitrogen partial pressure of 1 kgf/cm^2. The experiment was conducted at atmospheric pressure. The solubility of nitrogen at 100°C and atmospheric pressure, determined taking into account the partial pressure of the water vapor above the water level, was equal to zero. No evolution of nitrogen within the volume of water was observed.

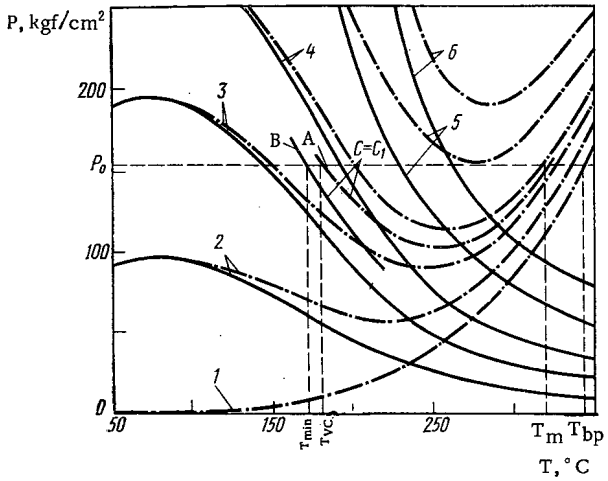

Fig. 1. Temperature dependencies of the partial pressure P_g and also of $P_g + P_v$ for C = const [all concentrations are in liters per kilogram at normal temperature and pressure (NTP)]: 1) C = 0; 2) C = 1; 3) C = 2; 4) C = 3; 5) C = 5; 6) C = 7.

Translated from Atomnaya Énergiya, Vol. 31, No. 2, pp. 150–151, August, 1971. Original article submitted August 3, 1970; revision submitted November 11, 1970.

Hence it follows that the solubility of a gas in a homogeneous system C_{hom} equals the solubility of the gas in a heterogeneous system C_{het} determined for the condition that the partial pressure of the gas above the water level equals the total pressure.

Thus, there should be no evolution of gas bubbles in a homogeneous system for concentration of the gas in water less than C_{hom}. Especially because the formation of centers in the gas phase is limited, for a radius of curvature of the bubble surface less than 10^{-5} cm, the pressure inside them noticeably increases because of the surface-tension forces [4].

The gas concentration in the primary coolant has a definite steady-state value for constant pressure and constant temperature in the VC [2]. Therefore, in order to determine the conditions for gas evolution in the primary loop, it is more convenient to use the temperature dependence of the gas partial pressure for constant gas concentration in water C.

The temperature dependence of the nitrogen partial pressure calculated according to the data of [5, 6] is shown by the continuous lines in Fig. 1. The partial pressure of nitrogen decreases with increasing temperature.

The dot-dash lines show the temperature dependence of the total pressure of the vapor–gas mixture for an equilibrium distribution of gas in the heterogeneous gas–water system at a constant nitrogen concentration in water. The curves have a minimum, which, with increasing nitrogen concentration in water, shifts toward higher temperatures.

The condition for the formation of a gas phase within the water volume is $P_g > P_0$. For a heterogeneous gas–water system, gas will evolve when $P_g + P_v > P_0$.

For a known temperature T_{VC} in the VC and pressure P_0, the nitrogen concentration C_1 in the water found in the VC, and hence also in the primary coolant, is determined from curve A, since for a heterogeneous gas–water system, the condition $P_g + P_v = P_0$ is satisfied. The dependence of the nitrogen partial pressure P_g on the temperature, for a nitrogen concentration in water C_1, is represented by curve B.

From Fig. 1 it follows that evolution of nitrogen inside the volume of water is possible only for $T_{1l} < T_{min}$, where T_{1l} is the temperature of the coolant in the first (primary) loop. Note that $T_{min} < T_{VC}$. For artificial introduction of gas into a homogeneous volume or local boiling of the coolant, a heterogeneous system forms. The conditions for evolution of nitrogen from the water are $T_{1l} < T_{VC}$ and $T_{1l} > T_m$, where T_m is the maximal temperature characterizing the equilibrium state of the heterogeneous system, for a nitrogen concentration in water C_1 and specified parameters. In the temperature range $T_{VC} < T_{1l} < T_m$, the gas in the gas pocket that was formed earlier will go into solution.

It follows that when there is dissolved gas in the water, the boiling point decreases somewhat. When the water boils, the gas that was dissolved in it produces a definite partial pressure P_{1g} in the volume of vapor that forms. We also have that the pressure of the water vapor is $P_{1v} = P_0 - P_{1l}$. Hence, the water will boil at the temperature T_{1s} that corresponds to the saturation state for pressure P_{1v}.

The decrease in boiling point $\Delta T = T_s - T_{1s}$, where T_s is the boiling point of pure water at pressure P_0, was calculated for various nitrogen concentrations in water at pressures 100 and 170 kgf/cm^2. The results can be represented by

$$\Delta T_{100} = 0.090C, \text{ °C};$$
$$\Delta T_{170} = 0.133C, \text{ °C},$$

where C is the concentration of nitrogen in water (liters per kilogram at NTP).

Thus, the condition for the absence of gas evolution in the primary loop of a pressurized-water reactor with gas volume compensators is the maintenance of a temperature in the VC lower than the maximal temperature that is feasible in the primary coolant; also, a temperature regime must be observed that ensures that there will be no local boiling of the water. In order to dissolve the vapor–gas pockets that were formed earlier, it is necessary to reduce the temperature in the loop for a short time down to a value slightly less than T_m.

LITERATURE CITED

1. V. S. Sysoev, At. Énerg., 26, 461 (1969).
2. N. V. Bychkov and A. I. Kasperovich, At. Énerg., 28, 145 (1970).

3. V. A. Kirillin and A. E. Sheindlin, Thermodynamics of Solutions [in Russian], Gosénergoizdat, Moscow–Leningrad (1956).
4. A. I. Rusanov, Phase Equilibria and Surface Phenomena [in Russian], Khimiya, Leningrad (1967), p. 165.
5. H. Pray et al., Ind. Engng. Chem., 44, 1146 (1952).
6. T. Andersen, Trans. Amer. Nucl. Soc., 10, 507 (1967).

EFFECT OF REACTOR ON CORROSION CRACKING OF ALLOY AMg6M

Kh. B. Krast and A. V. Byalobzheskii

UDC 621.039

It is well known that the hardness and brittleness of metals increase under the influence of reactor radiation as a result of increased internal stresses [1]. At the same time it was shown [2] that a relaxation of the microstresses occurs, for example, in uranium under the effect of the neutron flux. These phenomena, which are observed also for nickel and zirconium, are explained by the diffusion of the defects under the influence of the stress field.

Based on this an assumption was made that the reactor radiation must also affect corrosion under stress. Due to the lack of published information the experimental procedure had to be worked out anew.

The experiments were carried out on the reactor IRT-2000 [3]. In view of the impossibility of carrying out experiments at constant load the method of constant deformation was used, for which samples in the form of loops [4] made from a 1.5 mm thick sheet of alloy AMg6M was used. The blank was 160 × 15 mm in dimensions [5].

Before the experiment the samples were subjected to artificial aging for 24 h at a temperature of 170°C. The position of the sample in the experimental unit is shown in Fig. 1. After bending the sample into the loop a slit of 0.2-0.3 mm remained between the ends; this would not lead to any noticeable change in the stress. An electric current from a 6 V source was applied to insulated contacts built-in in the sample. When the sample disintegrated, the contacts were closed due to the presence of a spring and a signaling device for the current was switched on (a lamp, a bell, or such things).

After checking several solutions recommended for rapid determination of the susceptibility of alloys to corrosion cracking [5] a solution consisting of 0.25 N NaCl + 0.2 N CH_3COONa + 0.05 N CH_3COOH (pH = 5.15) was chosen, which did not cause ordinary corrosion. The volume of the solution was 150 ml. The results of the experiments are presented in Table 1. As evident from the table, the time taken before the

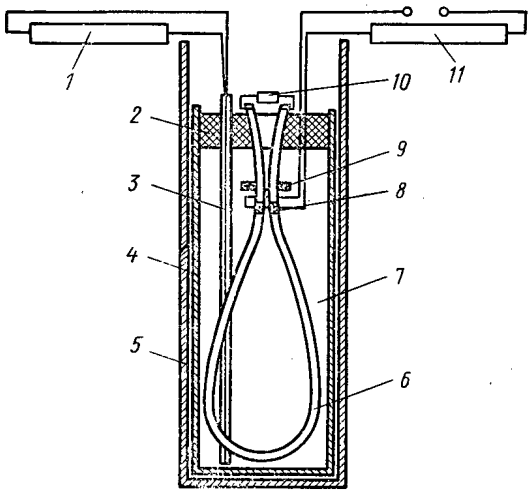

Fig. 1. Experimental unit for experiments on corrosion cracking in reactor: 1) potentiometer; 2) plug; 3) thermocouple in glass tube; 4) quartz test tube; 5) polyethylene container; 6) sample loop; 7) solution; 8) insulated contacts; 9) clamp; 10) spring; 11) signaling device for current.

Translated from Zhurnal Atomnaya Énergiya, Vol. 31, No. 2, pp. 151-153, August, 1971. Original article submitted September 14, 1970; revision submitted February 1, 1971.

TABLE 1. Effect of Neutron Irradiation on Corrosion Cracking (Intensity of radiation 10^{12} neutron/cm^2 · sec)

Conditions of irradiation	Duration of the experiment under irradiation, h	Temperature, °C	pH at the end of the experiment	Time taken before disintegration (average for three samples), h
Without irradiation	—	53	5,2	5—7,5
Irradiation of the sample in solution	11,12*, 11	50—55	6,4	120—140
	11	50—55	6,4	120—140
	36	50—55	6,4	450
Irradiation of the solution alone	11†	50—55	6,4	6—10
	11‡	53	7,1	5—6
Irradiation of the sample alone	11	53	5,2	150

* Without irradiation with subsequent irradiation for 11 h.

† Thermal power of the reactor 1500 kW.

‡ Thermal power of the reactor 2200 kW.

disintegration increases sharply on irradiation of the corroding system in the reactor. The pH of the system also changes simultaneously. It was established from experiments that without irradiation the change in pH was 0.1-0.2 units in 300 h.

Solutions of different compositions were irradiated in order to find out the reasons for the change in the pH of the mixture. These experiments showed that the pH of sodium acetate solution changed most appreciably. Thus the pH of 0.2 N solution before irradiation was 8.1 and after irradiation it was 9.45. The increase in the alkalinity of the sodium acetate solution obviously determines the increase in the pH of the solution as a whole. The reason for the increase in the pH of the acetate solution is not definitely known. Perhaps it is related to the intensification of the process of hydrolysis of the acetate under the action of the isotope Na^{24}.

The slowing down of cracking (see Table 1) is caused not by the change in the composition of the corrosion solution under the action of the reactor radiation, but by the action of the radiation on the metal leading to a relaxation of the existing stresses. Actually, if the unirradiated metallic loop is placed in a preirradiated solution, a slowing down of the process of its cracking is not observed. On the other hand a preirradiation of the metallic sample in air leads to a slowing down of its cracking even in an unirradiated solution. The slowing down of cracking is caused by neutron irradiation, since test experiments with γ-radiation of 600 rad/sec did not show any noticeable effect on corrosion cracking.

It must be mentioned that the inferences made on the basis of the present work pertain only to the investigated form of mechanical stresses. In the presence of stresses, less liable to relaxation, the results may be different.

In conclusion the authors express their sincere thanks to A. A. Tsvetaev and E. M. Zaretskom for help in setting up the experiments and for taking part in the discussion of the obtained results.

LITERATURE CITED

1. D. M. Skorov (editor), Metallography of Reactor Materials [in Russian], Part 2, Gosatomizdat, Moscow (1962).
2. S. T. Konobeevskii, Effect of Radiation on Materials, Atomizdat, Moscow (1967).
3. Kh. B. Krast et al., At. Énerg., 27, 286 (1969).
4. I. L. Rozenfel'd and K. A. Zhigalova, Fast Methods of Corrosion Tests of Metals [in Russian], Metallurgiya, Moscow (1966), p. 283.
5. T. M. Sigalovskaya and E. M. Zaretskii, Zashchita Metal., 3, 730 (1967).

RELATION BETWEEN SOLUTIONS OF THE NONSTATIONARY AND QUASICRITICAL TRANSPORT EQUATIONS

B. D. Abramov

UDC 621.039.51.12

There are two types of equations describing noncritical reactors in the one-velocity approximation: 1) a nonstationary transport equation taking account of delayed neutrons

$$\frac{1}{v}\cdot\frac{\partial\psi}{\partial t}=-\Omega\nabla\psi-\Sigma\psi+\frac{1}{4\pi}(\Sigma_s+b_0\nu\Sigma_f)\int d\Omega'\psi+\sum_{i+1}^{m}\lambda_i N_i;$$

$$\frac{\partial N_i}{\partial t}=-\lambda_i N_i+\frac{1}{4\pi}b_i\nu\Sigma_f\int d\Omega'\psi;\ i=1,\ 2,\ \ldots,\ m\ , \tag{1}$$

where $\psi(\mathbf{r}, \Omega, t)$ is the neutron flux and $N_i(\mathbf{r}, t)$ is the concentration of the precursors of delayed neutrons of group i; 2) a quasicritical equation of the form

$$\Sigma\psi=-\Omega\nabla\psi+\frac{c\Sigma}{4\pi\eta}\int d\Omega\psi, \tag{2}$$

where η is some parameter related to k_{eff}.

In general the relation between the solutions of these equations is rather complicated. From several papers [1, 2] devoted to this problem it follows that a simple relation exists only for reactors that are slightly noncritical.

Our procedure leads to a very simple relation in the one-velocity approximation even for a homogeneous bare reactor that is far from critical.

We seek a solution of Eq. (1) in the form $\psi(\mathbf{r}, \Omega, t) = e^{\alpha t}\varphi(\mathbf{r}, \Omega)$. Then we obtain

$$\left(\frac{\alpha}{v\Sigma}+1\right)\Sigma\varphi=-\Omega\nabla\varphi+\frac{c\Sigma}{4\pi}\frac{\left(\frac{\alpha}{v\Sigma}+1\right)}{\xi(\alpha)}\int d\Omega'\varphi, \tag{3}$$

where

$$\xi(\alpha)=\frac{\left(\frac{\alpha}{v\Sigma}+1\right)}{1-\sum_{i=1}^{m}\frac{\alpha\beta_i}{\alpha+\lambda_i}};\quad c=\frac{\Sigma_s+\nu\Sigma_f}{\Sigma};\quad \beta_i=\frac{b_i\nu\Sigma_f}{\Sigma_s+\nu\Sigma_f}. \tag{4}$$

Introducing the notation $\mathbf{r}' = \mathbf{r}(1 + \alpha/v\Sigma)$ and $\varphi(\mathbf{r}) \equiv \varphi(\mathbf{r}'/[1 + (\alpha/v\Sigma)]) = \bar{\varphi}(\mathbf{r}')$, we transform Eq. (3) to the form

$$\Sigma\bar{\varphi}=-\Omega\nabla\bar{\varphi}+\frac{c\Sigma}{4\gamma\xi(\alpha)}\int d\Omega'\bar{\varphi}. \tag{5}$$

The solutions of Eqs. (2) and (5) agree if $\eta = \xi(\alpha)$ and at some boundary $\mathbf{L} = \mathbf{R}(1 + \alpha/v\Sigma)$ with normal $\mathbf{n}$ both solutions satisfy the boundary condition

$$\psi(\mathbf{L}, \Omega)=\bar{\varphi}(\mathbf{L}, \Omega)=0,\ (\Omega\mathbf{n})<0, \tag{6}$$

i.e., the equation

Translated from Atomnaya Énergiya, Vol. 31, No. 2, pp. 153-154, August, 1971. Original article submitted July 31, 1970.

$$\psi(\mathbf{r}', \Omega) = \overline{\varphi}(\mathbf{r}' \Omega) = \varphi(\mathbf{r}, \Omega) \tag{7}$$

will be satisfied, where $\varphi(\mathbf{r}, \Omega)$ as a function of $\mathbf{r}$ satisfies the boundary condition

$$\varphi(\mathbf{R}, \Omega) = 0, \quad (\Omega \mathbf{n}) < 0. \tag{8}$$

Denoting the eigenfunctions of Eqs. (3) and (2) with boundary condition (8) corresponding to the eigenvalues α_i and η_k by $\varphi_i(\mathbf{r}, \Omega; \mathbf{R})$ and $\psi_k(\mathbf{r}, \Omega; \mathbf{R})$ respectively, we see that if

$$\xi(\alpha_i) = \eta_k \tag{9}$$

is satisfied the relation

$$\varphi_i(\mathbf{r}, \Omega; \mathbf{R}) = \psi_k\left[\mathbf{r}\left(1+\frac{\alpha}{v\Sigma}\right), \Omega; \mathbf{R}\left(1+\frac{\alpha}{v\Sigma}\right)\right] \tag{10}$$

holds. In a similar way it is shown that

$$\psi_k(\mathbf{r}, \Omega; \mathbf{R}) = \varphi_i\left(\frac{\mathbf{r}}{1+\frac{\alpha_i}{v\Sigma}}, \Omega; \frac{\mathbf{R}}{1+\frac{\alpha_i}{v\Sigma}}\right). \tag{11}$$

Since for a given η_k Eq. (9) has (m + 1) roots α_i, it follows from Eq. (11) that the neutron distribution function in a quasicritical reactor (a solution of Eq. (2)) corresponding to the eigenvalue η_k is geometrically similar to the distribution functions corresponding to the eigenvalues α_i in (m + 1) nonstationary reactors of the same composition and form but different dimensions if the eigenvalues α_i and η_k are related by Eq. (9). On the other hand only one quasicritical reactor can be associated with each nonstationary reactor in this sense.

There is a simple relation between the spectra of the eigenvalues of these problems also. If the solution of Eq. (2) leads to a relation between the eigenvalues η_k and $\mathbf{R}$ of the type

$$F(\eta_k, \mathbf{R}) = 0, \tag{12}$$

where F is some functional relation, then it is easy to show that the eigenvalues α_i of the nonstationary Eq. (3) will be the roots of the equation

$$F\left[\xi(\alpha_i), \mathbf{R}\left(1+\frac{\alpha_i}{v\Sigma}\right)\right] = 0, \tag{13}$$

if Eq. (9) is satisfied.

We note that the eigenvalues of these problems are real [3]; we assume that $\alpha > -v\Sigma$.

Thus the true neutron distribution in a nonstationary reactor, i.e., a solution of Eq. (3), can be determined from a solution of the quasicritical Eq. (2) written for a reactor of a different size. The inverse procedure is possible also.

The author thanks G. Ya. Rumyantsev for valuable comments and his attention to the work.

LITERATURE CITED

1. L. N. Usachev, Proceedings of the First International Conference on the Peaceful Uses of Atomic Energy, Vol. 5, Geneva (1955), p. 503.
2. A. Henry, Nucl. Sci. and Engng., 20, 338 (1964).
3. J. Mika, Nukleonik, 9, 46 (1967).

MOMENTS OF THE NEUTRON DENSITY DISTRIBUTION FUNCTION

T. E. Zima, A. A. Kostritsa, and E. I. Neimotin

UDC 621.039

Finding the moments of the neutron density distribution function N by Marshak's method [1] does not require a knowledge of the function N or its Fourier transform $\tilde{N}$. It is sufficient to know the values of the Fourier transform and its derivatives at the origin. This method is ordinarily used to determine moments of the P_1-approximation to the distribution function. We interest ourselves in the moments of the exact function N.

Let us consider first the one-velocity kinetic equation for the distribution function $N(x, \mu, t)$ in plane one-dimensional geometry with a localized pulsed neutron source

$$\frac{\partial N}{\partial t}+v\mu\frac{\partial N}{\partial x}+v\Sigma N=\frac{v\Sigma_s}{2}\sum_j \mu_j P_j(\mu)\int P_j(\mu')\,N(x,\mu',t)\,d\mu'+\frac{S}{2}\delta(x)\,\delta(t-t_0). \tag{1}$$

In writing Eq. (1) it was assumed that the scattering function $\mu_g(\Phi)$ can be represented by a finite sum of Legendre polynomials:

$$\mu_g(\Phi)=\sum_j \mu_j P_j(\cos\Phi). \tag{2}$$

Here Φ is the angle between the neutron velocity vectors before and after scattering; μ is the cosine of the angle between the neutron velocity vector and the x axis; Σ is the total cross section; and Σ_s is the scattering cross section. We assume also that $\mu_k > \mu_{k+1}$.

We introduce the Fourier transform of the function:

$$\tilde{N}(q,\mu,t)=\int_{-\infty}^{+\infty} N(x,\mu,t)\,e^{iqx}\,dx. \tag{3}$$

By using the equation for the Fourier transform obtained from Eq. (1) it can be shown that the total number of neutrons in an unbounded medium varies according to the well-known law

$$\int_{-\infty}^{+\infty}\int_{-1}^{+1} N(x,\mu,t)\,dx\,d\mu=\left[\int_{-1}^{1}\tilde{N}(q,\mu,t)\,d\mu\right]_{q=0}=\tilde{N}_0(q=0)=S\vartheta(t-t_0)\,e^{-v\Sigma_a(t-t_0)}, \tag{4}$$

where

$$\vartheta(t-t_0)=\begin{cases}1 & \text{for } t\geqslant t_0;\\ 0 & \text{for } t<t_0.\end{cases} \tag{5}$$

Simple calculations give the value of the second derivative of $\tilde{N}_0=\int\tilde{N}(q,\mu,t)d\mu$ at the origin in the plane of the complex variable q and then the second spatial moment of the neutron distribution function $\overline{x^2}$ as a function of time:

$$\overline{x^2}=\frac{2v}{3\Sigma_s\left(1-\frac{\mu_1}{3}\right)}\left\{t-t_0-\frac{1}{v\Sigma_s\left(1-\frac{\mu_1}{3}\right)}\left[1-e^{-v\Sigma_s\left(1-\frac{\mu_1}{3}\right)(t-t_0)}\right]\right\}. \tag{6}$$

In principle there is no difficulty in finding higher moments.

By integrating $\tilde{N}_0(q=0)$ and $(\partial^2\tilde{N}_0/\partial q^2)_{q=0}$ with respect to t_0 from $-\infty$ to t we can find $\overline{x^2_{st}}$ for a stationary source:

Translated from Atomnaya Énergiya, Vol. 31, No. 2, pp. 154-156, August, 1971. Original article submitted August 3, 1970.

$$\overline{x_{st}^2} = \frac{2}{3} \cdot \frac{1}{\Sigma\Sigma_a \left(1 - \frac{\mu_1}{3} \frac{\Sigma_s}{\Sigma}\right)}. \tag{7}$$

It is worth noting that the second moment of the exact function and its value in the P_1-approximation agree if by the P_1-approximation we understand the full form of the differential equation obtained. Thus, for example, in the telegraphic equation it is necessary to take account of the time derivative of the source. The diffusion equation with the first time derivative gives the familiar relation $\overline{x^2} = 2D(t - t_0)$.

Higher moments are obtained differently. Earlier we found the moments of the distribution function for certain problems in the theory of entrainment of neutrons by a moving medium. In a similar way it is possible to study the effect of an acceleration of the system on neutron transport.

Bucci [2] noted a possible effect of large accelerations of the system on the critical state of a reactor. Kostritsa and Neimotin [3] considered the effect of a sudden acceleration of the system on the density of a neutron gas in a medium with a uniform distribution of sources.

Let the acceleration w be along the x axis. Then the term in the kinetic equation taking account of the effect of inertial forces can be written in the form

$$w\nabla_v N = w\mu \frac{\partial N}{\partial v} + \frac{w}{v}(1 - \mu^2) \frac{\partial N}{\partial \mu}. \tag{8}$$

For simplicity let us assume that the scattering is isotropic. Then the kinetic equation for a problem with a stationary source has the form

$$v\mu \frac{\partial N}{\partial x} + w\mu \frac{\partial N}{\partial v} + w \frac{1 - \mu^2}{v} \cdot \frac{\partial N}{\partial \mu} + v\Sigma N = \frac{v\Sigma_s}{2} \int_{-1}^{+1} N \, d\mu + \frac{S\delta(v - v_0)}{2v_0^2} \delta(x), \tag{9}$$

where $N = N(x, \mu, v)$. In spite of the monoenergetic nature of the source v has a spectrum because of the inertial forces. It is difficult to determine N or even its Fourier transform $\tilde{N}$ in Eq. (9). Let us take $\Sigma_a = 1/vT$ and $\Sigma_s = 1/v\tau$, where T and τ are constants, and find the moments of the distribution function

$$\bar{x} = \frac{\int dx \int v^2 dv \int d\mu x N(x, \mu, v)}{\int dx \int v^2 dv \int d\mu N(x, \mu, v)} = \frac{w T \tau}{1 + \frac{\tau}{T}}; \tag{10}$$

$$\overline{x^2} = \frac{\int dx \int v^2 dv \int d\mu x^2 N(x, \mu, v)}{\int dx \int v^2 dv \int d\mu N(x, \mu, v)} = \overline{x_{w=0}^2} \left[1 + \frac{3\bar{x}w}{v_0^2} \left(1 + \frac{2}{3} \cdot \frac{1 + 3\frac{\tau}{T}}{1 + \frac{\tau}{T}}\right)\right], \tag{11}$$

where

$$\overline{x_{w=0}^2} = \frac{2}{3} \cdot \frac{v_0^2 T \tau}{1 + \frac{\tau}{T}}. \tag{12}$$

Thus the neutron distribution becomes asymmetric with respect to the plane x = 0 when there is an acceleration. We note that $\bar{x}$ and $\overline{x^2}$ can be obtained from the solution of Eq. (9) in the P_1-approximation. The value of $\bar{x}$ agrees with Eq. (10), and $\overline{x^2}$ differs from (11) by a small quantity. The drift velocity v_{dr} can be found from the relation $\bar{x} = v_{dr}T$.

The same result can be obtained from the solution of Eq. (9) for monoenergetic sources uniformly distributed in an infinite medium if N is written in the form

$$N = \sum_{n=0}^{\infty} f_n(v) P_n(\mu) \tag{13}$$

and we limit ourselves to the P_1-approximation in considering the infinite system of differential equations

$$w \frac{k+1}{2k+3} \cdot \frac{df_{k+1}}{dv} + w \frac{k}{2k-1} \cdot \frac{df_{k-1}}{dv} + \frac{w}{v} \frac{(k+1)(k+2)}{2k+3} f_{k+1} - \frac{w}{v} \cdot \frac{k(k-1)}{2k-1} f_{k-1}$$
$$+ v\Sigma f_k = \left[v\Sigma_s f_0 + \frac{S}{2v_0^2} \delta(v - v_0)\right](2k+1)\delta_{k0}. \tag{14}$$

Having determined the neutron density and current we obtain the expression

$$v_{dr} = \frac{w\tau}{\zeta\left(1 + \frac{\tau}{T}\right)}, \tag{15}$$

where ζ takes on various values for different types of dependence of the cross sections on the neutron velocity:

$$\zeta=\begin{cases} 1 \text{ for } \Sigma_s \sim \frac{1}{v} \text{ and } \Sigma_a \sim \frac{1}{v}; \\ \approx 3 \text{ for } \Sigma_s = \text{const}, \ \Sigma_a = \text{const}; \\ \approx 2.4 \text{ for } \Sigma_s = \text{const}, \ \Sigma_a \sim \frac{1}{v}. \end{cases} \tag{16}$$

Let us consider how an acceleration might manifest itself in actual neutron experiments. The quantities v_{dr}, $\overline{x}$, and the corrections to $\overline{x^2}$ are small for thermal neutrons and accelerations of the order of the acceleration due to gravity g. For $w \gtrsim 100$ g one might expect changes in the operation of a thermal reactor [3]. Since $v_{dr} \sim w l_s / v_0$, where l_s is the scattering mean free path, the drift velocity may be a few centimeters per second for ultracold neutrons* diffusing in a tube a few centimeters in diameter. If the lifetime of the ultracold neutrons is taken into account $\overline{x}$ and the correction to $\overline{x^2}$ will be significant.

The authors thank F. L. Shapiro and E. P. Shabalin for valuable comments.

LITERATURE CITED

1. R. Meghreblian and D. Holmes, Reactor Analysis, McGraw-Hill, New York (1960).
2. P. Bucci, Atomkerenergie, Vol. 11/12, 435 (1966).
3. A. A. Kostritsa and E. I. Neimotin, Izv. AN KazSSR, Ser. Fiz.-Mat., No. 2, 39 (1969).

*The effect of a gravitational field on ultracold neutrons was first studied by F. L. Shapiro and co-workers [OIYaI Preprint RZ-5392 (1970)].

SPONTANEOUSLY FISSIONING ISOMERS OF URANIUM, PLUTONIUM, AND AMERICIUM FROM NEUTRON REACTIONS

Yu. P. Gangrskii, T. Nad', I. Vinnai,* and I. Kovach*

UDC 539.173.7

At the present time more than 20 spontaneously fissioning isomers from uranium to berkelium are known. Most of these isomers have lifetimes in the nanosecond range and can be studied by the time-of-flight method [1]. We use this method to investigate spontaneously fissioning isomers formed in fast neutron reactions. A schematic diagram of the experimental arrangement is shown in Fig. 1. A beam of neutrons falls on a target surrounded by a mica–muscovite dielectric ring detector. The target is 1 cm in diameter and the outside diameter of the detector is 6 cm. The relative positions of the target and mica are such that prompt fission fragments cannot strike the mica. Fragments are recorded only when recoil nuclei undergo spontaneous fission more than 1 mm from the target. From the angle and the coordinate of the track left in the mica by the fragment it is possible to determine the distance the recoil nucleus traveled before decay. This distance determines the lifetime of the fissioning nucleus since the velocity of the recoil nucleus is known from the kinematics of the reaction.

This procedure gets rid of the background of fragments arising from the spontaneous fission of the target material or from fissions induced by thermal neutrons after the beam of the bombarding particles is shut off. Therefore the targets can be made of isotopes with a short spontaneous fission half-life (even isotopes of plutonium and curium) or of materials having a large cross section for fission by thermal neutrons (odd isotopes of uranium and plutonium). At the same time the use of neutrons to obtain spontaneously fissioning isomers imposes special requirements on the cleanliness of the target surfaces since the momentum of a recoil nucleus is small and any contamination of the surface significantly reduces the reaction yield. In addition the dielectric detectors for recording fragments must have a low uranium and thorium

*Members of the staff of the Central Institute of Physical Studies, Budapest.

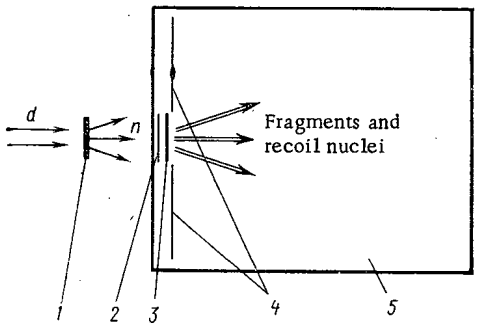

Fig. 1

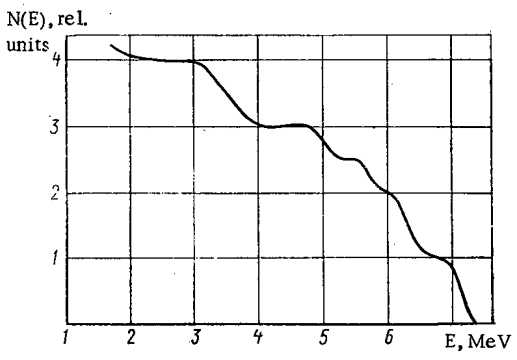

Fig. 2

Fig. 1. Schematic diagram of experimental arrangement. 1) T or Be target; 2) aluminum foil; 3) thorium, uranium, plutonium, or americium target; 4) mica ring detector; 5) vacuum chamber.

Fig. 2. Calculated spectrum of neutrons from the irradiation of a thick beryllium target by 3 MeV deuterons.

Translated from Atomnaya Énergiya, Vol. 31, No. 2, pp. 156-157, August, 1971. Original article submitted February 16, 1971.

TABLE 1. Cross Sections for the Formation of Spontaneously Fissioning Isomers

Reaction	$\sigma_i \times 10^{-28}$, cm^2	$\sigma_g \times 10^{-24}$, cm^2	$\frac{\sigma_i}{\sigma_g} \times 10^{-4}$
$Th^{232}(n, 2n)Th^{231}$	$\leqslant 0{,}09$	$1{,}56 \pm 0{,}16$	$\leqslant 0{,}06$
$U^{235}(n, 2n)U^{234}$	$\leqslant 0{,}09$	$0{,}65 \pm 0{,}28$	$\leqslant 0{,}15$
$U^{238}(n, n')U^{238}$	$1{,}4 \pm 0{,}5$	$0{,}80 \pm 0{,}30$	1,8
$U^{238}(n, 2n)U^{237}$	$\leqslant 0{,}13$	0,78	$\leqslant 0{,}17$
$Pu^{239}(n, 2n)Pu^{238}$	$\leqslant 0{,}06$	0,20	$\leqslant 0{,}3$
$Pu^{242}(n, n')Pu^{242}$	$0{,}9 \pm 0{,}3$	0,94	0,95
$Am^{243}(n, n')Am^{243}$	$0{,}2 \pm 0{,}1$	0,74	0,27
$Am^{243}(n, 2n)Am^{242}$	$0{,}6 \pm 0{,}3$	0,36	1,6

content since these detectors are irradiated by practically the same neutron flux as the target.

Spontaneously fissioning isomers were obtained by using neutrons from the reaction H^3 + d with deuteron energies of 200 keV, and Be^9 + d with 3 MeV deuterons and thick beryllium targets. The neutrons were obtained from an NG-200 neutron generator and from the ÉG-5 electrostatic generator of the Institute of Physical Studies at Budapest. Figure 2 shows the neutron spectrum obtained in the Be^9 + d reaction. This spectrum was computed from the geometry of the experiment and the known cross sections and angular distributions of the neutrons [2]. These neutrons are produced mainly in the (n, n') reaction since the (n, γ) cross section is appreciably smaller. The neutron spectrum for the H^3 + d reaction is a relatively narrow line at 14.7 MeV arising mainly from the (n, 2n) reaction. The neutron flux was determined from the activation of an aluminum foil of the same size as the target irradiated by neutrons. The target thicknesses were as a rule greater than the range of the recoil nuclei. Therefore the thickness of the layer of material from which the recoil nuclei were ejected was calculated by using the familiar theory of the transmission of heavy charged particles through matter [3]. For 14 MeV neutrons the thickness of this layer was 10 $\mu g/cm^2$. These calculations were confirmed by measuring the yield of recoil nuclei in the reactions Cu^{65}(n, 2n)Cu^{64} and Ta^{181}(n, 2n)Ta^{180m}; the measured and calculated yields agreed within the limits of error (20%).

The cross section for the formation of a nucleus in the isomeric state was determined from the number of tracks obtained in mica, the neutron flux through the target, and the calculated effective layer of target material. The efficiency of counting fragments depends on the half-life of the isomer formed in the reaction. This efficiency has a maximum value of 40% for half-lives of 100 nsec and drops to less than 5% for half-lives less than 5 nsec and greater than 1 μsec since in this case the recoil nucleus either decays on the target surface or moves a long way from the detector. Therefore in order to increase the yield of fragments when studying long-lived isomers a recoil nuclei collector was placed 1 cm from the target.

The cross sections σ_i were measured and the upper limits for five (n, 2n) reactions and three (n, n') reactions leading to spontaneously fissioning isomers were determined. In the latter case the average cross sections were found for neutron energies from the reaction threshold of about 3 MeV to 7.6 MeV. The results are shown in Table 1. It can be seen from the table that the cross sections for the formation of spontaneously fissioning isomers in the (n, n') and (n, 2n) reactions are of the same order of magnitude. The isomers U^{234} ($T_{1/2}$ = 34 nsec) obtained in the (n, γ) reaction [4], and Pu^{238} ($T_{1/2}$ = 6.5 nsec) obtained in the (α, 2n) reaction [5] were not observed. Table 1 also gives the (n, 2n) and (n, n') cross sections for reactions leading to the ground state σ_g, and the isomer ratios σ_i/σ_g. The values of σ_g for Th^{232}, U^{235}, and U^{238} are known, and for the other nuclei they were calculated by using the statistical model of the nucleus and taking account of the competition between neutron evaporation and fission [6]. The average cross section for the (n, n') reaction in the 0-7.6 MeV range was calculated with the neutron spectrum of Fig. 2. It was assumed that the (n, n') reactions take place only via the compound nucleus. Table 1 shows that the isomer ratios are $\sim 10^{-4}$, which is close to the values obtained for the Am^{242} isomer in charged particle and neutron reactions [7].

In conclusion the authors thank G. N Flerov for his constant attention to the work, and I. Veresh for his help in irradiating the targets.

LITERATURE CITED

1. Yu. P. Gangrskii et al., ZhÉTF Pis. Red., 4, 429 (1966).
2. R. Siemssen et al., Nucl. Phys., 69, 209 (1965).
3. J. Linhard et al., Mat. Fys. Medd. Dan. Vid. Selsk., 33, No. 14 (1963).
4. A. Elwyn and A. Ferguson, Nucl. Phys., A148, 337 (1970).
5. S. Burnett et al., Phys. Lett., 31B, 523 (1970).
6. R. Vandenbosch et al., Phys. Rev., 111, 1358 (1958).
7. G. N. Flerov et al., Yadernaya Fizika, 6, 17 (1967).

YIELDS OF Be^7 IN THE IRRADIATION OF LITHIUM AND BORON WITH PROTONS AND DEUTERONS AND THAT OF BERYLLIUM WITH PROTONS, DEUTERONS, AND α-PARTICLES

P. P. Dmitriev, N. N. Krasnov,
G. A. Molin, and M. V. Panarin

UDC 621.039.573

The isotope Be^7 ($T_{1/2}$ = 53 days) decomposes by electron capture and is a monochromatic γ-emitter with E_γ = 478 keV. It is finding wide use in various fields of scientific research. The published data on the yields of Be^7 [1-9] are contradictory and incomplete (see Table 1).

In this work we investigated the dependences of the yield of Be^7 on the energy of the bombarding particles in the irradiation of thick targets of lithium and boron with protons and deuterons and that of beryllium with protons, deuterons, and α-particles. The energy of accelerated ions differed somewhat in individual irradiations. The largest values of the particle energy were: $E_p = 22.7 \pm 0.35$ MeV, $E_d = 22.8 \pm 0.35$ MeV, and $E_\alpha = 45.7 \pm 0.7$ MeV. Table 1 presents the energies of the particles after their passage through a monitor foil. To obtain the yield of Be^7 as a function of the particle energy we used copper retarding foils. The scintillation γ-spectrometer was calibrated with respect to photoefficiency with the aid of standard γ-emitters of the International Atomic Energy Agency. The yield of γ-quanta with energy 478 keV was assumed equal to 12.3 quanta per 100 disintegrations of Be^7. The accuracy of the values obtained for the yields of Be^7 is ±13%. The details of the method of measuring the yields were outlined in [10, 11].

TABLE 1. Characteristics of Various Methods of Producing Be^7

Method of production	Reaction of formation	Energy threshold of reaction, MeV	Content of initial isotope, %	Published data on yields		
				particle energy, MeV	yield, $\mu Ci/\mu A \cdot h$	literature
Li + p	$Li^6(p\gamma)$	—	7,52	22,1	245	This work
				8	77	[1]
				12	256 *	[2]
	$Li^7(pn)$	1,88	92,47	17,1	254	[3]
				20	166	[4]
				22	170	[5]
Li + d	$Li^6(dn)$	—	7,52	22,2	119	This work
				13	2	[5]
				13,5	76	[6]
	$Li^7(d2n)$	4,97	92,48	15	48	[1]
				19	2	[7]
				25	70	[8]
				30	150	[9]
B + p	$B^{10}(p\alpha)$	—	18,8	22,2	54	This work
	$B^{11}(p\alpha n)$	11,78	81,2	12	37 *	[2]
B + d	$B^{10}(d\alpha n)$	1,39	18,8	22,2	38	This work
	$B^{11}(d\alpha 2n)$	16,12	81,2			
Be + p	$Be^9(pt)$	13,4	100	22,4	10,6	The same
Be + d	$Be^9(dtn)$	17,4	100	22,4	0,68	" "
Be + α	$Be^9(\alpha\alpha 2n)$	29,6	100	43	2,3	" "
	$Be^9(\alpha He^6)$	28,4				

*Obtained by integration of the excitation functions.

Translated from Atomnaya Énergiya, Vol. 31, No. 2, pp. 157-159, August, 1971. Original article submitted September 14, 1970.

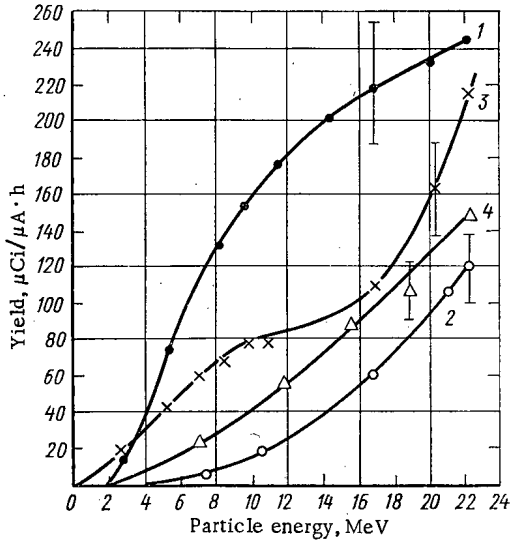

Fig. 1

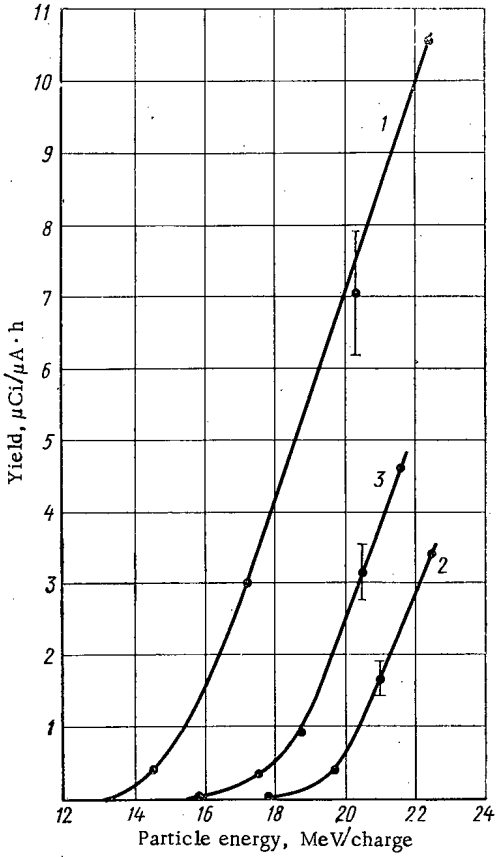

Fig. 2

Fig. 1. Dependence of the yield of Be^7 on the energy of the bombarding particles in the irradiation of thick targets of lithium and boron with protons and deuterons: 1) Li + p; 2) Li + d; 3) B + p (increased fourfold); 4) B + d (increased fourfold).

Fig. 2. Dependence of the yield of Be^7 on the energy of the bombarding particles in the irradiation of thick targets of beryllium with protons, deuterons, and α-particles: 1) Be + p; 2) Be + d (increased fivefold); 3) Be + α (increased twofold).

Metallic lithium is inconvenient as a material for irradiation (rapid oxidation, necessity of using thick layers); therefore the salt Li_2SO_4 was irradiated. The ranges of the particles in Li_2SO_4 and the factor for conversion of the yield of Be^7 for Li_2SO_4 to the yield of Be^7 in pure lithium were calculated according to the method outlined in [12, 13]. The conversion factor proved equal to 7.24. Samples of boron and beryllium were prepared for irradiation from the pure elements. Table 1 presents the basic characteristics of the investigated methods of producing Be^7, the yields at the maximum energy obtained in this work, and the data from the studies of other authors. The yield of Be^7 as a function of the particle energy for the five investigated methods of production is presented in Figs. 1 and 2. In this work the yields of Be^7 in the irradiation of boron and beryllium were measured for the first time.

As can be seen from the results obtained, the most effective methods for the production of Be^7 are the irradiation of lithium with protons and deuterons.

The authors would like to thank Z. P. Dmitriev and G. N. Grinenko for their aid in the work and V. G. Vinogradov for his radiochemical isolations of Be^7 from certain samples.

LITERATURE CITED

1. I. Gruverman and P. Kruger, Intern. J. Appl. Rad. and Isotopes, 5, 21 (1959).
2. S. P. Kalinin, A. A. Ogloblin, and Yu. M. Petrov, At. Énerg., 2, 171 (1957).
3. G. Gleason, J. Gruverman, and J. Need, Intern. J. Appl. Rad. and Isotopes, 13, 223 (1962).
4. I. Martin et al., Nucleonics, 13, No. 3, 28 (1955).
5. I. F. Kolosova and I. V. Kolosov, At. Énerg., 15, 422 (1963).

6. K. Wagner, Kernenergie, 6, 122 (1963).
7. W. Garrison and J. Hamilton, Chem. Rev., 49, 237 (1951).
8. H. Moeken, Production of Radioisotopes with Charged Particles (Dissertation), Amsterdam (1957).
9. A. Aten and J. Halberstadt, Philips Techn. Rev., 16, No. 1 (1954).
10. N. N. Krasnov and P. P. Dmitriev, At. Énerg., 21, 52 (1966).
11. P. P. Dmitriev, I. O. Konstantinov, and N. N. Krasnov, ibid., 22, 310 (1967).
12. N. N. Krasnov, ibid., 26, 284 (1969).
13. G. Friedlander, J. Kennedy, and J. Miller, Nuclear Chemistry and Radiochemistry [Russian translation], Mir, Moscow (1967), p. 102.

STUDY OF THE WEAK α-ACTIVITIES OF THE VOLATILE FRACTIONS OF LEAD – ZINC ORE BY THE α – X COINCIDENCE METHOD

V. Kush, V. I. Chepigin,
G. M. Ter-Akop'yan, and S. D. Bogdanov

UDC 543.53

During the last few decades many articles have been published on the identification of very weak, long-living α-emitters in ores and minerals, the energies of these emitters not falling within the framework of existing classifications [1-13].

The publication of theoretical papers discussing the possible existence of long-lived heavy nuclei with atomic numbers between 110 and 114 [14] has intensified interest in the unidentified weak α-emitters in nature.

The results of investigations into weak α-activity and (to a certain extent) chemical data strongly suggest the existence of α-active, very heavy elements in nature; however, existing experimental methods are as yet incapable of yielding unequivocal results. In the present investigation we used the method of α–X coincidences in order to identify the atomic number of the isotopes under consideration.

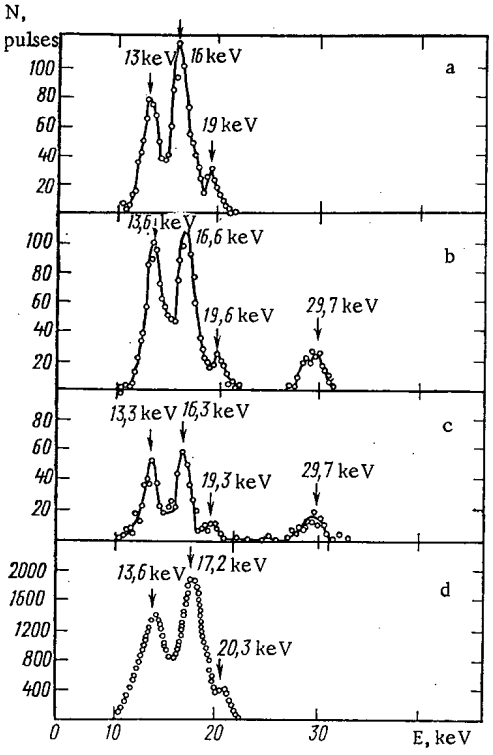

Fig. 1. X-ray spectrum of sources: uranium (a), Np^{237} (b), test sample (c), and Pu^{238} (d). An Si(Li) detector was employed.

The volatile fraction of a lead–zinc concentrate was subjected to the chemical processing normally used for the separation of osmium. The volatile products obtained from the dust were condensed in a liquid nitrogen trap and dissolved in nitric acid containing hydrogen peroxide. After heating to 110°C and further condensation, the most volatile products collected on the substrate contained α-activity with an intensity of 4 decays/min per milligram.

After a 20 h measurement with a surface-barrier Si–Au detector, we obtained an α-spectrum in which one line with an energy of 4.78 MeV appeared quite clearly.

In subsequent measurements we used a coincidence spectrometer. The x-radiation was measured with Si(Li) detector having an effective layer thickness of 2.4 mm, cooled to −110°C. For recording the α-particles we used a surface-barrier Si–Au detector with an area of 3.2 cm^2. The coincidence circuit only allowed recording by the Si(Li) detector when an α-particle pulse with an energy of over 4 MeV appeared. The correct working of the spectrometer and the efficiency of the coincidence recording were verified by using a source containing natural uranium.

The resolving power of the x-ray spectrometer on subjecting to a week's exposure was 2.5 keV or better.

The first series of measurements indicated the presence of an emitter emitting α-particles in an excited state,

Translated from Atomnaya Énergiya, Vol. 31, No. 2, pp. 159-161, August, 1971. Original article submitted August 17, 1970; revision submitted November 10, 1970.

TABLE 1. Intensity Ratio for the Test Sample and Np^{237}

Intensity ratio	Test sample	Np^{237}	With correction	Np^{237} calculation [15]
$f_\alpha/f_{\alpha-x}$	10,8±1,0	8,5±0,9	10,9±1,1	9,2
$f_\alpha/f_{\alpha-\gamma}$	60±8	55±10	65±12	64,5
$f_{\alpha-x}/f_{\alpha-\gamma}$	6,4±1,0	8,5±1,0	6,4±1,0	7,1

Note: The quantity f_α is the number of recorded α particles; $f_{\alpha-x}$ and $f_{\alpha-\gamma}$ are the numbers of x-ray and γ-radiation quanta recorded in coincidence with α-particles.

so that four lines in the 10-30 keV range appeared in our spectrum. On the basis of the energy of the two strongest lines (L_α, L_β) we were able to establish that the atomic number of the unknown element was $Z = 93 \pm 1$.

In the second series of measurements, we decided to compare the spectrum of our own source with those of existing α-emitters in this range of Z. This method eliminates calculation of the recording efficiency. Figure 1 shows the x-ray spectra of uranium, Np^{237}, Pu^{238}, and our own source; on the basis of these results we concluded that the α-activity discovered belonged to Np^{237}.

Table 1 indicates the x-ray line intensities of the Np^{237} and those of our own source. The intensity ratio of the individual lines confirms our identification, and so does the ratio of the coincidence intensity to the α-count rate. The slightly higher value of the intensity of the L series obtained for the calibrated Np^{237} sample is associated with the presence of a trace of Pu^{239} in this. The amount of impurity was such that the intensity of the Pu^{239} decays equalled half the neptunium intensity. In the fourth column of Table 1 we show the intensities of the L lines of the calibrated source, corrected to allow for the plutonium impurity.

The discovery of Np^{237} in a lead–zinc concentrate is not to be regarded as extraordinary. Estimates based on the enrichment factors achieved during the processing of the original ore show that in the original concentrate the neptunium content was no greater than 10^{-11} wt. %. Traces of neptunium of this order are in accordance with the proportion of technogenic neptunium in the Earth.

The data here presented may well turn the attention of authors studying weak α-activity in the Earth's rocks to the possible masking of the present effect (or even its simulation) by technogenic neptunium. The weak activities and the great thickness of the samples employed lead to large statistical errors and also to the broadening of the spectrum. If we also consider possible apparatus instability, such as is liable to occur in measurements extending over many days (this may be illustrated by Cherdyntsev's results [7]), it becomes perfectly clear that the three factors, taken together, may introduce a serious error into the measurement of α-particle energy. The insufficiently accurate determination of energy and the lack of information relating to lifetimes may give rise to unjustified conclusions. The use of the method of α–X coincidences, in our own opinion, eliminates this possibility.

In conclusion, the authors wish to thank G. N. Flerov for proposing this problem and for interest in its progress; they are also grateful to O. D. Maslov for help in the work.

LITERATURE CITED

1. J. Joly, Naturwiss., 12, 693 (1924).
2. M. Ziegert, Z. Phys., 46, 668 (1928).
3. J. Schintelmeister, Sitzungsber. Österr. Akad. Wiss., 144, No. 11a, 475 (1935).
4. G. Seaborg and I. Perlman, J. Amer. Chem. Soc., 70, 1571 (1948).
5. D. Peppard, J. Amer. Chem. Soc., 74, 60 (1952).
6. V. V. Cherdyntsev and V. F. Mikhailov, Geokhimiya, 1, 1 (1963).
7. V. V. Cherdyntsev et al., Geokhimiya, 4, 395 (1968).
8. R. Cherry, K. Richardson, and J. Adams, Nature, 202, 639 (1964).
9. R. Gentry, Appl. Phys. Letters, 8, 65 (1966).
10. R. Gentry, Bull. Amer. Phys. Soc., 12, 32 (1967).
11. C. Levine and G. Seaborg, J. Amer. Chem. Soc., 73, 3278 (1951).

12. W. Davis and J. McWherter, Geochim. Cosmochim. Acta, 26, 681 (1962).
13. H. Meier et al., J. Naturforschung, 25, 79 (1970).
14. Yu. A. Muzychka, V. V. Pashkevich, and V. M. Strutinskii, Joint Institute for Nuclear Research, R7-3733, Dubna (1968); S. Nilsson et al., Nucl. Phys., A115, 545 (1968).
15. C. Lederer, J. Hollander, and I. Perlman, Table of Isotopes, J. Wiley (1967).

NEUTRON-RESONANCE APPARATUS WITH A CENTRAL SOURCE ARRANGEMENT

B. S. Vakhtin and E. M. Filippov

UDC 543.53

In studies [1-2] results are presented of research into the application of the neutron-resonance method for the determination in specimens of silver, gold, indium, rhodium, boron, and other elements. The neutron source was located in a moderator outside the specimen.

The authors of this study developed a neutron-resonance apparatus (NRA) with a central source arrangement (Fig. 1) for a rapid determination of boron. The feasibility of using the NRA for determining high concentrations of boron is established in [3]. The neutron source in the NRA is situated inside a cylindrical activator, which is, in turn, inside a cylindrical cassette surrounded by the moderator. The induced activity of the activator develops through neutrons which have lost their energy in the moderator and passed through the specimen. The apparatus consists of a block moderator 1, which is a plastic cube with a 50 cm edge. In the block is a horizontal canal in which a carriage 2, also made of plastic, is placed. A vertical canal lined with cadmium (~1 mm) passes through the middle of the carriage where a cylindrical cassette 3 with the specimen is placed. The distance between the walls of the cassette (the thickness of a layer of the specimen) is 5 mm; the height of the cassette is 95 mm. The cylindrical activator 4 is made from silver foil 0.1 mm thick. Its diameter is ~49 mm; its height is 85 mm. A circular cadmium disk

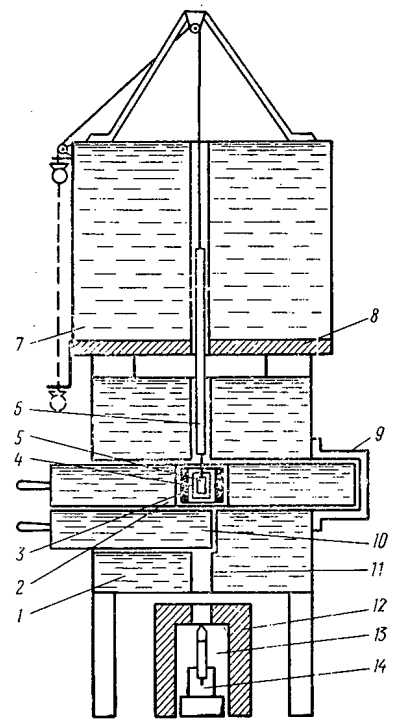

Fig. 1. Diagram of the NRA with a central source arrangement.

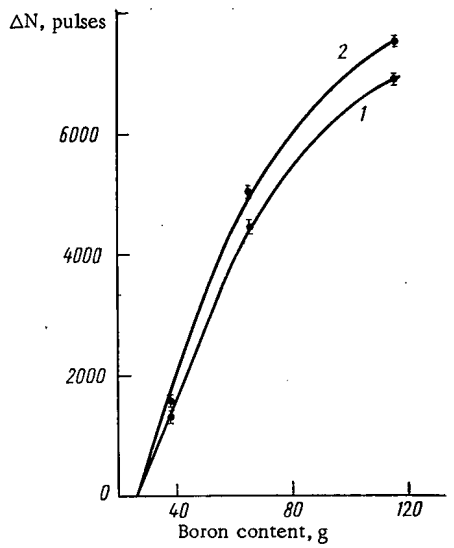

Fig. 2. Dependence of the counting rate of resonance neutrons on the boron content in a measurement with one source inside the cassette (1) and with 2 sources outside the cassette in the moderator (2).

Translated from Atomnaya Énergiya, Vol. 31, No. 2, pp. 161-163, August, 1971. Original article submitted October 14, 1970; revision submitted December 17, 1970.

TABLE 1. Values of Relative Root Mean Square Error in the Determination of the Counting Rate under Different Geometric Measurements

Type of product; boron content,%	Weight of the specimen, g	Boron content, g	Error in the counting rate measurement	
			one source inside the activator	two sources outside the activator
Crystalline boron (98)	116,6	114,1	1,25	1,35
Microcrystalline boron (98)	38,6	37,8	7,1	6,8
Brown boron (94,66)	67,3	63,7	2,0	2,1

1 mm thick with a 0.1 mm silver coating is in the lower part of the carriage canal. The disk has an opening slightly larger than the diameter of the activator and is the mount for the cassette. An analogous disk is placed on top of the cassette. The vertical canal in the block moderator serves as a passage for the neutron source 5, which is mounted on a sliding tube 6. In the "off" position the neutron source (plutonium–beryllium with a yield of $4.3 \cdot 10^6$ neutron/sec) is placed in a protective paraffin block 7. Lead 8 is used to protect the detector from radiation. A stop 9 fixes the carriage in an "on" position. The activator mount 10, a plastic bar, is found under the carriage. The mount, when at the extreme right (see Fig. 1) serves as a support for the activator; moving it to the left frees the activator which, by its own weight, feeds through the canal 11 into the measuring cell 12 and is put onto the detector 13. The detector (3 STS-6 type counters) is held firm in a collar 14 which can be removed from the cell.

The operating sequence of the NRA is as follows. The neutron source is placed in the upper position with the mount on the extreme right. The cassette with the specimen and the activator are inserted in the carriage canal, the cadmium disk is set in, and the carriage moved to the right to the catch in the stop. The source is placed in the lower "on" position (inside the activator), and this moment is considered the beginning of the irradiation time t_0. After time t_0 the source is removed, the mount is moved 5-6 cm to the left, and the activator goes into the measuring cell. After a pause t_p (the end of irradiation to the beginning of measurement) the scalar PP-12 is switched on, and in the course of time t_i the induced activity of the activator is measured. Time t_0 consisted of 2 min, t_p of 8 sec, and t_i of 100 sec.

Products with an 86-98% boron content were used as specimens (see Table 1). The results of the determination of boron in the specimens are presented in Fig. 2. Here the dependence of the difference ΔN in the counting rates on the boron content is given, with the counting rate from the specimen containing 86% boron serving as the minuend. The error in the counting rate measurement (see Table 1) is several percent in the duration of the complex cycle of measurements, which is equal to several minutes. In order to compare the accuracy obtained in a given geometric measurement with the accuracy in the case when the neutron source is outside the cassette, the NRA was reconstructed: positions 7 and 8 were eliminated (see Fig. 1), and the neutron sources (2 with a common yield of $8.6 \cdot 10^6$ neutron/sec) were placed in the central part of the block moderator. The operating sequence differed from that described above in that the beginning t_0 was considered to be the moment of the placement of the cassette with the activator in the irradiation position. The times t_0, t_p, and t_i were the same. The results of the measurements are presented in Fig. 2 (curve 2) and in Table 1. The drawing and the table clearly demonstrate the advantage of the geometry with the source placed inside the activator, since the errors of the measurements in both cases are roughly identical, and the activity of the neutron source can be decreased twofold, if it is positioned inside the activator.

In conclusion the authors are grateful to Yu. G. Fadeev and G. A. Sychev for their participation in the construction of the apparatus.

LITERATURE CITED

1. B. S. Vakhtin and E. M. Filippov, Geol. i Geofiz., No. 2, 72 (1970).
2. R. G. Gambaryan, E. V. Rogov, and A. S. Shtan', At. Énerg., 25, 237 (1968).
3. B. S. Vakhtin and E. M. Filippov, Geol. i Geofiz., No. 2, 101 (1968).

LONGITUDINAL STABILITY OF A BEAM IN A LINEAR INDUCTION SYSTEM

V. K. Grishin

UDC 621.384.65

Various methods for producing intense accelerated-particle beams are currently under study. One promising system in this regard is the linear induction accelerator (LIA), whose simplicity and reliability open up new application possibilities [1, 2]. In this case, however, longitudinal beam instability arises at high currents and disrupts the beam homogeneity.

The accelerating system of an LIA is a set of annular inductors with a ferromagnetic core. The particles move in a ferromagnetic channel, and the permeability of the material is $\mu \gg 1$. Even at comparatively low velocities the conditions for the Cerenkov instability hold [3]: $\mu\beta^2 > 1$, where β is the ratio of the particle velocity v to the speed of light c in vacuum. This can be seen from the following simple physical considerations. When local density perturbations arise, an additional field is excited whose Coulomb component corresponds to dissipation of the current inhomogeneity, and whose vortex induction part corresponds to an increase in this inhomogeneity. When $\mu\beta^2 > 1$, the latter phenomenon predominates, and the beam loses its longitudinal stability.

For some specific results, we consider an infinite system of annular LIA inductors arranged along the z axis. The state of the beam in this system may be described by a kinetic equation giving the change in the particle density F in phase space of the coordinate z and the longitudinal momentum P_z:

$$\frac{\partial F}{\partial t}+e\mathscr{E}\frac{\partial F}{\partial P_z}+v\frac{\partial F}{\partial z}=0. \tag{1}$$

It is assumed here that particles with charge e move along the z axis in the accelerator channel at velocity v; their motion is affected by the longitudinal electric field $\mathscr{E}$. Neglecting transverse motion (this is valid in a consideration of longitudinal perturbations whose length is much greater than the transverse dimensions of the beam), and assuming it to be stable, we can state that F is equal to the linear current density of particles with velocity v. The total beam current is

$$J=e\int_{-\infty}^{\infty} vF\,dP_z. \tag{2}$$

The intrinsic field of the beam is governed by the interaction of particles with the ferromagnetic environment. The Coulomb components may be neglected under the condition $\mu\beta^2 \gg 1$ [4], while the vortex component may be described by means of the ordinary concept of self-induction of the annular system [5]:

$$\mathscr{E}_F \approx -\frac{\bar{\mu}l_0}{c^2}\cdot\frac{\partial J}{\partial t}, \tag{3}$$

where $\bar{\mu}l_0$ is the average self-induction coefficient per unit length of the system. At a perturbation wavelength much greater than the transverse dimensions of the inductors (for a more detailed discussion of the inductor construction see [2]), we have $l_0 \simeq 2\ln R/r$, where R and r are the maximum and minimum inductor radii. The field $\mathscr{E}_F$ is essentially constant over the chamber cross section.

Under the assumption that $F = F(z-vt)$, we have

$$\mathscr{E}_F=\bar{\mu}l_0\frac{\partial}{\partial z}\int_{-\infty}^{\infty}\beta^2F\,dP_z. \tag{4}$$

Translated from Atomnaya Énergiya, Vol. 31, No. 2, pp. 163-164, August, 1971. Original article submitted July 23, 1970.

Small perturbations in the homogeneous infinite beam are described by

$$F \approx F_0(P_z) + f(t, P_z, z), \tag{5}$$

where $f \ll F_0$. Obviously, F_0 does not produce a field, and the linearized kinetic equation becomes, after a Fourier z transformation and a Laplace time transformation,

$$pf_k + ik\bar{\bar{\mu}}l_0 \frac{\partial F}{\partial P_z} \int_{-\infty}^{\infty} \beta^2 f_k \, dP_z + ikvf_k = f_0, \tag{6}$$

where f_0 is the initial perturbation (the external field is neglected).

According to the standard procedure for analyzing a kinetic equation [6], the asymptotic behavior of the perturbation is described by that root p of the equation

$$1 = ik\bar{\bar{\mu}}l_0 e^2 \int_{-\infty}^{\infty} \frac{\beta^2 \frac{\partial F_0}{\partial P_z}}{p + ikv} dP_z, \tag{7}$$

which has the maximum real part.

As an example, we consider the distribution

$$F_0 = \begin{cases} J/(2ev_0\Delta) & \text{for } |P_z - P_0| \leq \Delta, \\ 0 \end{cases} \tag{8}$$

where v_0 is the average velocity of the beam. Then it follows from Eq. (7) that ($\beta \sim 1$)

$$p = -ikv_0 + kc(\Lambda - (\Delta\beta)^2)^{1/2}, \tag{9}$$

where $\Lambda = \bar{\mu}l_0 J(1-\beta^2)^{3/2}/J_A$, $J_A = mc^3/e \approx 17{,}000$ A, and $\Delta\beta$ is the velocity scatter in the beam. It follows from Eq. (9) that the beam remains stable (Re p → 0) only at small currents. For the distribution [7]

$$F_e = \frac{J}{e\pi v_0} \cdot \frac{P_1}{(P_z - P_0)^2 + P_1^2}, \tag{10}$$

we have Re p = kc($\sqrt{\Lambda} - \Delta\beta$), and the same conclusion follows.

In practice the strong dispersion of the magnetic permeability of the material should be taken into account. For a perturbation wavelength of the order of 1-3 m, the permeability does not exceed 10^2-10^3 [2]. Then with J = 200 A, the instability growth time for a beam having electrons with an energy of 1-10 MeV is

$$\tau = \frac{1}{\mathrm{Re}\, p} \sim (0.1 - 3) \cdot 10^{-8} \text{ sec};$$

i.e., the instability grows over a distance of a few meters. In a real system of course one must take into account the loss in the core (the imaginary part of μ) and the effect of the accelerating field, which, without qualitatively changing the phenomenon, limits the perturbation growth, since Re p depends strongly on the particle energy.

A real result of the longitudinal beam instability will be the excitation of the intrinsic field of the beam (or amplification of the field of inhomogeneities introduced during injection), which may significantly disrupt the energetic homogeneity of the particles [5].

The author thanks A. A. Kolomenskii for discussion of the results.

LITERATURE CITED

1. N. Christofilos, Proceedings of the International Conference on High-Energy Accelerators, Dubna, 1963 [in Russian], Gosatomizdat, Moscow (1964), p. 1073.
2. A. I. Anatskii et al., At. Énerg., 21, 439 (1966).
3. A. I. Akhiezer and Ya. B. Fainberg, Zh. Éksp. Teor. Fiz., 21, 1262 (1951); Ya. B. Fainberg, At. Énerg., 11, 313 (1961).

4. L. Ginzburg and I. M. Frank, Dokl. Akad. Nauk SSSR, 56, 699 (1947).
5. V. K. Grishin, Pribory i Tekh. Éksperim., No. 5, 35 (1970).
6. L. D. Landau, Zh. Éksp. Teor. Fiz., 16, 574 (1946).
7. A. A. Kolomenskii and A. N. Lebedev, At. Énerg., 7, 549 (1959).

ABSOLUTE MEASUREMENT OF PARTICLE-BEAM INTENSITY BY A FLUCTUATION METHOD

Yu. P. Lyakhno and V. A. Nikitin

UDC 539.16.08

The number of particles produced at a thin target by a stable particle beam from a pulsed accelerator fluctuates (from pulse to pulse) about an average value according to a Poisson law. Here the relative deviation or the so-called variation coefficient in the number of particles is $v(n) = 1/\sqrt{\bar{n}}$, where $\bar{n}$ is the average number of particles produced at the target during a single accelerator pulse. This means that a direct measurement of the beam intensity may be replaced by measurement of the variation coefficient. The variation coefficient of the number of particles may be measured by means of a relative detector. We assume that we have carried out m relative measurements $x_1, x_2, \ldots, x_m$ which are proportional to the values n: $n_1, n_2, \ldots, x_m$ of the random quantity. Then the average value of the relative measurements is $\bar{x} = \sum_{i=1}^{m} x_i = (1/m) \sum_{i=1}^{m} kn_i = k\bar{n}$, while the dispersion is $D(x) = (1/m) \sum_{i=1}^{m} (x_i - \bar{x})^2 = (1/m) \sum_{i-1}^{m} (kn_i - k\bar{n})^2 = k^2 D(n)$, where k is the proportionality coefficient between x_i and n_i. According to the definition of the variation coefficient [1], we have

$$v(x) = \frac{\sqrt{D(x)}}{\bar{x}} = \frac{\sqrt{D(n)}}{\bar{n}} = v(n). \quad (1)$$

Thus the procedure described here permits us to use a relative detector to carry out absolute measurements of the intensity of particle beams without the use of a calibration if the distribution of the number of secondary particles from pulse to pulse is known. The intensity of these beams may exceed the detection capabilities of particle detectors and may reach up to intensities measurable by means of integrating devices (calorimeters, Faraday cups, etc.).

The particles incident on the target sometimes have a large probability for interacting with it. In this case the number of secondary particles fluctuates according to a binomial distribution [1], and the variation coefficient is $v(n) = \sqrt{(1-p)/\bar{n}}$, where p is the probability that a secondary particle will be created by the incident particle. For a known probability p, measurement of the number of particles $\bar{n}$ may thus replace a measurement of v(n).

Using Eq. (5.3.78) in [1], we can show that the statistical error in measurements by this procedure is the same as during a direct count of particles for the case $m > 50$ and $p \ll 1$.

When the number of secondary particles is measured by this procedure in practice, however, three types of errors must be taken into account. First, the intensity of the particle beam incident on the target from the accelerator always fluctuates; this increases the measured variation coefficient in the number of secondary particles. This increase may be easily taken into account by measuring the fluctuation in the intensity of the incident beam by means of a second detector, which may also be a relative one. Second, the detector itself may respond differently to particles incident on it. The corrections to the measured variation coefficient caused by these detection fluctuations may be made by calculating them or by measuring them [2] for one of n detected particles and for a given detector; then we use the mathematically rigorous relation [1] $v_{det} = v'_{det}/\sqrt{\bar{n}}$, where v'_{det} is the relative detection fluctuation for a single particle, and v_{det} is that part of the measured variation coefficient due to detection fluctuations. Third, the measuring system, which may consist of a photomultiplier, amplifier, and pulse analyzer, also introduces errors into the experimental results.

Translated from Atomnaya Énergiya, Vol. 31, No. 2, pp. 164-165, August, 1971. Original article submitted August 17, 1970.

These errors may be easily taken into account by measuring them by means of standard light flashes [3].

The detection fluctuations and the fluctuations in the number of secondary particles are not correlated. Correlations between errors of the detection system and the value of x can usually be neglected.

Since none of these errors will change the average number of secondary particles during a measurement, we can use the rule for summing the dispersions of random quantities [1] to write the measured variation coefficient as

$$v_m^2 = v^2(n) + v_\gamma^2 + v_{det}^2 + v_{sys}^2, \quad (2)$$

where v_{sys} is the relative error of the measurement system, and v_γ is the relative fluctuation intensity of the incident particle beam.

This procedure has been used to measure the intensity of the hardened bremsstrahlung used in pulse-chamber experiments (~300 photons/pulse). Bremsstrahlung beams having intensities greater than 500 photons/pulse were measured simultaneously by a thick-walled ionization chamber; the experimental results found by the two methods agreed within 15%.

LITERATURE CITED

1. I. V. Dunin-Barkovskii and N. V. Smirnov, Probability Theory and Mathematical Statistics [in Russian], Gostekhteorizdat, Moscow (1955).
2. J. R. Bishop, Onde Électr., No. 421 (1962).
3. A. F. Pavlov, Pribory i Tekh. Éksperim., No. 1, 210 (1964).

ORIGIN OF ACCELERATED ATOMS ACCOMPANYING A PLASMA BLOB

K. B. Kartashev, V. I. Pistunovich,
V. V. Platonov, and E. A. Filimonova

UDC 533.98

According to the observations of several authors, there are fast atoms of the working gas in the fast plasma blob generated by a coaxial plasma gun, in addition to the accelerated ions. In [1] the density of accelerated hydrogen atoms in the interelectrode space was estimated by means of an optical interferometer. In [2], where the working gas was xenon, the density of accelerated atoms was determined by the absorption of ultraviolet radiation. In both cases the energy of the fast atoms did not exceed 1 keV, and the question of their origin remained open. Charge exchange of accelerated ions in the working gas in the gun was indicated as a possible cause for the appearance of fast atoms in the plasma blob only in [1].

The density of atoms in a hydrogen blob moving at a speed of about 10^8 cm/sec was determined in this investigation by methods of passive corpuscular diagnostics. Such a blob had an ion density on the order of $4 \cdot 10^{12}$ cm^{-3} and an energy of about 160 J at a distance of 180 cm from the gun.

The experiments were conducted on the "INES" device, which is described in [3]. The capacitance of the bank in the gun discharge circuit was 32 μF, and the bank voltage was 20 kV. One cm^3 of hydrogen at a pressure of 4 atm (gage) was admitted to the interelectrode space by a pulsed valve. The time delay between the actuation of the spark gaps in the pulsed valve circuit and the actuation of those in the gun circuit was 150 μsec. The gas entered the interelectrode space through openings in the inner electrode.

The experiments were conducted with two guns, which differed in the location of these openings. In the gun I the distance from the center of the openings to the end of the center electrode was 80 mm, and in II it was 30 mm. The speed of the plasma blob was determined by time-of-flight with two diamagnetic loops. The fast atoms in the plasma blob were stripped by a gas target, and the resulting ionic current was registered on a detector. The detector was placed at a distance of 6 m from the plasma gun, where the low plasma density ($n_i = n_e \approx 10^9$ cm^{-3}) permitted separation of ions and electrons by an electric field. The appreciable length of the flight path permitted independent measurement of the atomic speed according to time-of-flight.

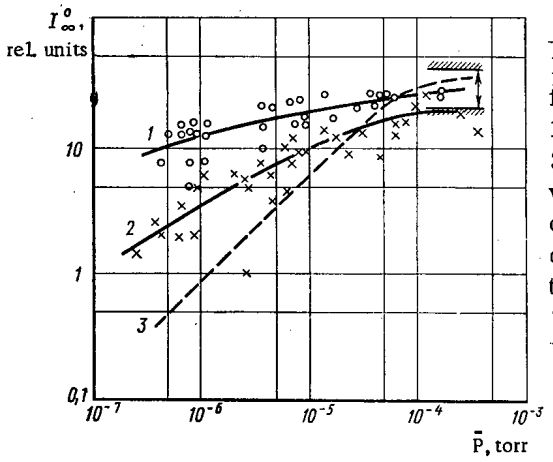

Fig. 1. Dependence of fast-atom flux on residual gas pressure: 1) for plasma gun I; 2) for gun II; 3) calculated for charge exchange with hydrogen molecules. The double arrow indicates the range of experimental flux values obtained after charge exchange in a "thick" magnesium target.

Translated from Atomnaya Énergiya, Vol. 31, No. 2, pp. 165-166, August, 1971. Original article submitted November 11, 1970.

The plasma blob with a velocity of about 10^8 cm/sec was passed through a charge-exchange target, which could be a supersonic jet of magnesium vapor or residual gas in the vacuum chamber of the device, and then the magnitude of the fast-atom flux was measured at various target parameters.

Figure 1 shows the dependence of the fast-atom flux on the pressure of residual gas in the vacuum chamber.

The gas pressure was averaged along the plasma blob trajectory. The range of atomic flux values observed after the plasma blob passed through a "thick" magnesium vapor target are also shown in Fig. 1. It is evident that all the curves have a tendency toward saturation, and the equilibrium fluxes for hydrogen and magnesium targets are in reasonable agreement. The dashed curve gives the theoretical dependence of the atom flux on the pressure. It was obtained using the following parameters: the equilibrium atomic current $I^0_\infty = 36$ (relative units); the neutral fraction resulting from charge exchange of 5 keV protons in molecular hydrogen $\Phi^0_\infty = 0.9$ [4]; and the charge-exchange cross section $\sigma_{10} = 8 \cdot 10^{-16}$ cm^2 [5]. Curves 1 and 2 were obtained with plasma guns I and II, respectively, without a guiding magnetic field. It can be seen that for plasma gun II the atomic current at a residual gas pressure of $5 \cdot 10^{-7}$ torr was less than 10% of the equilibrium current. At the same pressure the value for plasma gun I was about 35%.

The experimental conditions of curves 1 and 2 differ only in the location of the gas ports on the inner electrode of the gun. Therefore only the gun itself can be responsible for the difference in composition of the fast plasma blob. This conclusion agrees with the hypothesis mentioned above [1], according to which one can expect an increase in the fast-atom flux with an increase in distance of the gas ports from the end of the inner electrode.

Thus, with a suitable choice of geometry and working regime of the coaxial plasma gun, it is possible to generate hydrogen atoms with a speed of about 10^8 cm/sec, and their number, measured in the axial region at 6 m from the gun, can reach 35% of the total number of particles in the fast plasma blob.

LITERATURE CITED

1. É. P. Kruglyakov, V. K. Malinovskii, and Yu. N. Nesterikhin, Magnetohydrodynamics [in Russian], Vol. 1 (1965), p. 80.
2. P. Gloersen, Phys. Fluids, 12, 945 (1969).
3. K. B. Kartashev et al., Zh. Éksp. Teor. Fiz., 59, 779 (1970).
4. V. A. Oparin et al., Zh. Éksp. Teor. Fiz., 52, 369 (1967).
5. P. Stier and C. Barnett, Phys. Rev., 103, 896 (1956).

NEWS

XXIX SESSION OF THE LEARNED COUNCIL OF THE JOINT INSTITUTE FOR NUCLEAR RESEARCH

V. A. Biryukov

The XXIX regularly scheduled session of the Learned Council of the Joint Institute for Nuclear Research [JINR] was held October 27-30, 1970, in Dubna. Opening the session, the Institute's director, Academician N. N. Bogolyubov, delivered a report on how the decisions and resolutions of the Learned Council had been fulfilled. One of the events of paramount importance in the past year was the signing at Dubna, on June 18, 1970, of an agreement on scientific and technical collaboration between the USSR State Committee on Peaceful Uses of Atomic Energy and the Joint Institute for Nuclear Research. The parties to this agreement will jointly develop scientific and technical collaboration in the field of nuclear physics, ensuring effective utilization of the accelerators, reactors, experimental data processing equipment, and other research facilities at their disposal, and will collaborate in devising new equipment for those purposes. The agreement signed expands the opportunities of the Institute in the area of scientific collaboration with national physics centers throughout the Soviet Union, as well as in terms of the participation of specialists from member-nations of JINR in the scientific research programs drawn up by Soviet institutes.

N. N. Bogolyubov also mentioned some measured taken in the course of bringing the preparatory phase of the new five-year developmental program of the Institute to fruition. These include, in the first instance, work on developing a material groundwork for research on new acceleration techniques, building a new powerful pulsed reactor, and developing the computer complex of the JINR. Work has been carried out on preparations for rebuilding and redesigning the Institute's most prominent physics research facilities, the synchrocyclotron, the heavy-ion accelerator, and the synchrophasotron proton synchrotron.

Professor D. I. Blokhintsev gave a report on scientific research activities in progress at the Theoretical Physics Laboratory in the course of the past year. The laboratory's scientists have approached the problem of introducing an electromagnetic field and verifying gage invariance in the theory of weak interactions, within the framework of nonlocal and nonlinear quantum field theory. A combination of the methods of renormalizations and nonlocal methods made it possible to construct the scattering matrix.

Scattering of strongly interacting high-energy particles was investigated on the basis of the method of functional integration, in efforts to develop an approximation of rectilinear paths for finding the asymptotic aspects of amplitudes and cross sections of elastic and inelastic processes.

Many of the research findings are in agreement with conclusions inferred from the droplet model of the nucleus and from the model of coherent states. A model of coherent states for describing elastic and inelastic collisions of hadrons at high energies was formulated at the laboratory. These results were received with keen interest when they were reported at the International Conference on High-Energy Physics held in Kiev.

Prediction of the existence of a new region of deformed neutron-deficient nuclides in the neighborhood of $A \simeq 100$ was ventured in 1969. These calculations stimulated the setting up of experiments. Experimental data obtained in Berkeley during the past summer and confirming those calculations became available, with the new region of deformed nuclides $A \simeq 100$ detected experimentally.

Experimental indications as to the existence of excited states, with the equilibrium deformation differing from the equilibrium deformation of nuclides in the ground states, began to make their appearance. (We note that no such difference is found in the case of most known nuclides.) The existence of that type of states had been predicted by the theoretical physicists of the Theoretical Physics Laboratory back in 1966.

Translated from Atomnaya Énergiya, Vol. 31, No. 2, pp. 167-170, August, 1971.

The balance sheet on research work completed at the High Energies Laboratory was reported on by Professor A. M. Baldin. The research program at the accelerator of the High-Energy Physics Institute [IFVÉ] at Serpukhov included studies of pp-scattering and pd-scattering in the energy range from 8 to 70 GeV. The experiments confirmed the earlier fact of narrowing of the pp-scattering diffraction cone; the results of measurements of the ratio α_{pp} = Re A/Im A are in agreement with the predictions of Regge pole theory with branch cuts. The study of pd-scattering showed that the diffraction cone narrows down and that α_{pd} behaves in conformity with the conclusions of dispersion relations. IFVÉ physicists worked shoulder-to-shoulder with Bulgarian, Polish, and Vietnamese scientists on these experiments. After the computer-linked magnetic spark spectrometer had been through comprehensive adjustments and testing, a working exposure was taken with a liquid-hydrogen target, and preliminary results were obtained in studies of the regeneration of $K_L^0 \rightarrow K_S^0$-mesons over the range of momenta from 14 to 38 GeV/c.

A round of research projects on investigation of small-angle elastic π–p-scattering at the proton synchrotron has been completed. The real parts of the scattering amplitudes, which correspond to predictions based on the theory of dispersion relations, were measured. These data are unique in the 2-7 GeV energy range. A new method utilizing a gas Cerenkov differential hodoscope was applied to high-precision measurements of total π^-p-interaction cross sections at pion momenta in the range from 3.88 to 6.03 GeV/c. The systematic bias in the experiments was found to be at most about 20 μb, and the total error about 50 μb.

Studies of neutral bosons decaying to π^0-mesons and γ-photons were included in the work with the xenon bubble chamber. A study of the interactions between negative pions and protons at 5 GeV/c momentum was conducted with the aid of a one-meter liquid-hydrogen bubble chamber. Over three thousand six-prong events were detected on plates taken with this bubble chamber, in joint work with physicists of the German Democratic Republic. Distributions of events with respect to reaction channels, the cross sections of the reactions, the momentum and angular distributions of secondary particles, distributions of effective masses, and also cross sections of some of the resonances, were found in the course of these investigations.

The data obtained in the laboratory on the production cross section of the η^0-meson in the reaction $\pi^-p \rightarrow \eta^0 n$ (pion momentum 7 GeV/c) were indicative of the absence of any plateau in the differential cross section for the momentum transfer range $0 \leq |t| \leq 0.24$ (GeV/c)^2, and of a change in slope in the transition to lower transmitted momenta $|t| \leq 0.02$ (GeV/c)^2. The study of radiative decays of boson resonances is being conducted with the aid of a total-absorption spectrometer and spark chambers.

One outstanding achievement of the laboratory research team was the attainment of deuteron acceleration to 11 GeV energy on the proton synchrotron. Preliminary experiments on acceleration of α-particles were also staged.

Professor V. P. Dzhelepov reported on work completed at the Nuclear Problems Laboratory. A search for new types of fermion interactions is underway at the synchrocyclotron, and possible violations of the law of conservation of leptonic charge are being studied. The magnetic spark spectrometer took 300,000 plates containing information on rare mesonic decay events, over the course of the elapsed year. The upper limit of the relative probability of the very rare decay process $\mu^+ \rightarrow e^+e^+e^-$ was diminished to one-twentieth the figure held to in earlier available data, as a result of those experiments. The new value is $R \leq 6.2 \cdot 10^{-9}$ (at 90% confidence level). In the case of another rare process $\pi^+ \rightarrow e^+e^+e^-\nu$, the upper limit of the relative probability is set at $R \leq 3.4 \cdot 10^{-8}$.

The process of inverse electroproduction of pions $\pi^-p \rightarrow e^+e^-n$ at 275 MeV energy was observed for the first time on record. This experiment was undertaken with the purpose of investigating the electromagnetic structure of the pion and nucleons in the region of timelike transmitted momenta. As a result of analyzing 55 events involving the reaction under study, the differential cross section for emission of electrons at energies E > 40 MeV at a 90° angle to a beam of pions was studied ($d^2\sigma/d\Omega_1 d\Omega_2 = (3.0 \pm 0.8) \cdot 10^{-33}$ cm^2/sr^2). An estimate of the electromagnetic form factors of proton and pion in the timelike region of momentum transfer was made.

The first stage of a program of measurements of the ep-scattering cross section at 4.13 GeV was undertaken at the electron synchrotron in Erevan. This work is being carried out with the aid of a unique arrangement including semiconductor counters, and physicists from Erevan and Bucharest are participating in the work. Estimates of the proton radius yield the value 0.96 ± 0.08 f.

A one-meter propane bubble chamber irradiated at the proton synchrotron site by pions of momentum 5 GeV/c figures in continuing research on rare processes of formation of particles and resonances, with decay products containing the π^0-meson and γ-photons. A new resonance has been discovered in the system $\pi^-\gamma$, with mass 275 MeV. At the present time, the study is being extended to about 40 reactions accompanied by the production of Λ, Σ^0, K^0, $\tilde{K}^0$, π^0, and other particles in different combinations of two, three, or four such particles, and the cross sections of those reactions are being studied. This is a difficult undertaking in measurements based on hydrogen bubble chambers.

Emission of charged particles in muon capture on the nuclei ^{28}Si, ^{32}S, ^{40}Ca, and ^{64}Cu is being investigated with the object of shedding light on the mechanism underlying absorption of negative muons. A system of scintillation detectors and silicon surface-barrier detectors is used for that purpose. Separation of the charged particles formed by masses was achieved for the first time. The measured energy spectra decline exponentially and extend out to 50 MeV. The data obtained argue in favor of the cluster mechanism of muon absorption in the surface layer of the nucleus.

The reporter also provided information on new developments in physics research equipment. The facility known as YaSNAPP-1 (for nuclear spectroscopy on a beam of protons), for research with short-lived isotopes, was successfully run through its physical startup in the laboratory. A spectrometer with a projection spark chamber operating at high pressure was put into operation; this spark chamber had been proposed and designed at JINR. A more effective method of extracting protons from a synchrocyclotron, resulting in doubling of the proton beam intensity, was worked out and realized in practice. Work is continuing on preparations for the rebuilding of the synchrocyclotron.

The Vice-Director of the Institute, Professor A. Michul, informed the Learned Council of the progress of work on the JINR research program based on the Serpukhov accelerator.

Studies of photographic emulsions irradiated in a beam of high-energy negative pions are being conducted in seventeen laboratories in member-nations of JINR. Equipment is being installed for irradiation of photographic emulsions in a strong pulsed magnetic field.

After the expansion system had been rebuilt and other improvements had been made, stable operating conditions were achieved on the two-meter propane bubble chamber. A working exposure of the chamber was begun on a beam of negative particles of 40 GeV/c momentum. Installation of a two-meter liquid-hydrogen bubble chamber was completed. Control and thermostating systems, etc., were built into this facility, which was subjected to hydrogen tests. A particle separated-particles channel was installed at the accelerator working with this bubble chamber, and the magnet was rigged into place.

The Institute's scientists have prepared several experiments for the Serpukhov accelerator. A search for new heavy particles and antinuclei is being undertaken with the participation of IFVÉ scientists and GDR [East German] scientists. Equipment for experiments designed to search for the Dirac monopole has now been almost completely installed. A complex facility for investigation of πe-scattering with the object of determining the form factor of the negatively charged pion is being adjusted. Polish, Rumanian, and American scientists are taking part in this work, jointly with IFVÉ and JINR physicists. A team of IFVÉ and JINR physicists has begun investigations of K^0-meson interference in the light of K^0-decay.

Other experiments are also being prepared, including investigations of polarization phenomena in pion–nucleon scattering, and work is continuing on the building of the large general-purpose magnetic spectrometer.

Development of the collective method of acceleration is still underway at the Institute. V. P. Sarantsev reported on adjustments and physical tests of a section of the high-current linear accelerator built at the Institute. A gas-focused electron beam with 600 A current was accelerated to 350 keV energy. An accelerating section with thermal resonators was assembled.

Many of the work projects in progress have been linked to theoretical research on such problems as the stability of a storage ring, radiation in transitional structures, and focusing.

The first experiments involving acceleration of α-particles on a model of a collective accelerator demonstrated the need to improve the vacuum in the adherer chamber. Subsequent work resulted in attainment of a $5 \cdot 10^{-8}$ torr vacuum. Several runs of α-particle acceleration were then carried out. Measurements revealed that the energy of the accelerated α-particles was in excess of 20 MeV. The number of

particles impinging on the target during the exposure time was $3 \cdot 10^9$ to $5 \cdot 10^9$ in different measurement runs. These experiments proved that it is possible in principle to design an accelerator based on the collective method of acceleration.

The bulk of the work being done in the Laboratory of Computer Techniques and Automation has been directed at broadening the computer and data-processing facilities and capabilities of the Institute, and also at improving existing computers to make more effective use of them in research work. This work was reported on by Professor M. G. Meshcheryakov. New computers have been commissioned at the laboratory: the BÉSM-4 and several smaller machines of various types. Work is continuing on development of a system linking the central BÉSM-6 digital computer to peripheral computers. A design project of a multicomputer system for write-in and read-out of information in and out of a BÉSM-6 computer through the agency of TPA machines situated in the measuring centers of the various laboratories is being developed and realized in practice in joint work with the Central Physics Research Institute of Hungary.

Some of the machines are being modernized: the rapid-access memory has been expanded and special communications channels have been set up linking the system with experimental equipment, data-processing systems with multidimensional analyzers using computer rapid-access memory banks and standard storage devices are being introduced.

As a result of improvements in the FORTRAN translator and in the Dubna monitor system used in the BÉSM-6 computer system, translation has been speeded up by a factor of 1.5. The printing speed was doubled with the delivery of a modernized dispatcher. The Dubna monitor system developed at the laboratory is now being used to set up data-processing systems in some other institute in JINR member-nations.

The HDP automatic scanner for processing chamber plates has been through the stage of comprehensive adjustments and is being tested with real plates taken with a hydrogen bubble chamber. The development of most of the electronic circuitry for the modules of the Spiral'nyi Izmeritel' [Spiral Measurer] automatic scanner has been completed, and tests have been carried out on the optical–mechanical subassemblies of the system. Two large examination and measurement tables set on line with the TPA computer have been introduced into experimental operation.

Development of methods for visual display of data in computer readout has been given considerable attention in the laboratory's program of research. At the present time, several computers are equipped with oscillographs featuring a light pencil for data display, and more sophisticated models of data display arrangements are being developed. A data display panel developed for the ÉLT automatic unit working in unison with the magnetic drum of the BÉSM-4 computer was put into service, and opened up the possibility of processing plates with visual monitoring of the process.

An extensive line of work has been completed at the laboratory on compiling computer programs, first of all for large bubble chambers and physics research facilities operated on line with digital computers in real time.

Academician I. M. Frank reported on the completion of redesign and modernization work on the basic research facilities at the Neutron Physics Laboratory. An average power output of 25 kW was achieved with the laboratory's new reactor, and this is ten times higher than the output of the laboratory's previous reactor. A particle injector, a 30 MeV linear electron accelerator, was commissioned, and a system comprising a pulsed fast reactor plus the injector was put into service.

The startup of this new system made it possible to extend the study of α-decay of resonant states of nuclei. An improved procedure was used in measurements of 11 resonances of the isotope target ^{147}Sm and 2 resonances of the target ^{145}Nd. Partial α-transitions to the ground state and several excited states of parent nuclides were observed. An analysis was carried out, for the first time, of a score of partial widths (in groups of two tens).

Measurements of transmission and radiative capture of neutrons in uranium-238 were carried out for resonances of energies up to 1200 eV. These experiments were completed on a single detector, which is a new variant of the 260 liter methylborate liquid scintillation detector. The data obtained, in contrast to existing literature data, indicate constant radiation widths for the several resonances of uranium-238. The Doppler effect on uranium-238 was investigated in work done jointly at the Power Physics Institute [FÉI] (Obninsk) and at the Central Nuclear Research Institute (Rossendorf, German Democratic Republic). Characteristics of the temperature dependence of the transmission function were measured, and are important for fast reactor safety design.

Investigations of the ne-interaction are undergoing further development at the laboratory by a new technique: observation of neutron diffraction on a tungsten-186 single crystal.

Procedures and equipment for studying neutron diffraction in condensed media immersed in an externally applied high-intensity magnetic field are being improved. The measurements with hematite are continuing. The spectra of inelastic noncoherent scattering in several molecular crystals have been measured with an inverse-geometry spectrometer. Magnetic materials are undergoing continuing study with the aid of inelastic neutron scattering.

A channel of ultracold neutrons has been set up and put into service at the IBR-30 pulsed fast reactor for the purpose of developing experiments now in progress at the laboratory. Investigations of the yield of ultracold neutrons on different converters at different temperatures have begun.

Work connected with the design of the new IBR-2 fast power reactor with an injector is being continued, and programs of physics research using that reactor-injector system are being prepared. The building and accessories complex for the IBR-2 reactor are being designed.

Results of research completed at the Nuclear Reactions Laboratory were reported by Academician G. N. Flerov. Several experiments have been carried out in the laboratory in searches for superheavy elements in nature. Searches for new transuranium elements in lead glass and in galenite were conducted in a salt mine at depths of 40 m and 320 m water equivalent, under very low background conditions. Searches for a natural emitter were conducted in various minerals by the method of large proportional counters. About 10 tons of concretions have been obtained from various regions of the Pacific Ocean. Measurements carried out with these specimens by the method of dielectric detectors indicate a possible content of naturally occurring spontaneously fissioning emitter.

Improvements have been carried out on the design of a source of zinc ions at the laboratory, and experiments were set up to synthesize superheavy isotopes with atomic numbers in the neighborhood of 125.

Experiments on the synthesis and investigation of physical and chemical properties of element 105 have been successfully completed. When ^{243}Am was irradiated with accelerated ^{22}Ne ions, an emitter of spontaneous fission fragments with a half-life 1.8 ± 0.6 sec was recorded. The yield of the isotope corresponds to a production cross section of $5 \cdot 10^{-34}$ cm^2. A study of the angular distribution of the recoil nuclei, and control experiments, showed that the new isotope has the atomic number 105. An investigation of the excitation function provided independent confirmation of that finding. The most probable mass number of the new element is 261. An improved experimental arrangement was brought into play in studies of the α-decay of isotopes of the new element. Results of an analysis of amplitude–time correlations provide some basis for inferring that the α-decay of the nuclides ^{260}105 and ^{261}105 was actually observed. In experiments designed for chemical identification of element 105, success was obtained in recording 18 atoms of the new element. Its properties are close to those predicted for the element eka-tantalum.

A gas-filled mass separator was used in searches for a new phenomenon: proton decay of nuclei from the ground state. Emitters of delayed protons were recorded in all instances when separated isotopes ^{96}Ru, ^{102}Pd, ^{106}Cd, and ^{112}Sn were irradiated by accelerated ^{32}S and ^{35}Cl ions, and these emitters were found to be unidentified isotopes of the rare earths. Investigations of spontaneously fissioning isomers are also being continued over a broad range of masses of nuclei.

Eleven new neutron-deficient nuclides of light elements were synthesized: ^{18}C, ^{20}N, ^{21}N, ^{22}O, ^{23}O, ^{24}O, ^{23}F, ^{24}F, ^{25}F, ^{25}Ne, and ^{26}Ne, and the regularities of the formation of these nuclides in reactions with heavy ions were investigated. Experimental proofs of the nuclear instability of ^{14}Be were forthcoming in experiments designed to search for the boundary of nuclear stability of nuclei superenriched with neutrons. A method developed at Dubna and based on utilization of thin semiconductor detectors ($\simeq 10\ \mu$) of high energy resolution, and a magnetic analyzer, was employed in those experiments.

A separate report by Professor A. Michul dealt with international collaboration between JINR and other scientific research centers. Over the course of the year, the laboratories of the Institute have conducted about 250 scientific projects in joint work with research centers in JINR member-nations. A total of 250 Institute specialists have traveled to member-nations to do joint work, give lectures, and participate in conferences, and 160 scientists have been assigned to other countries for varying periods of work. JINR has accepted 360 scientists from JINR member-nations and 150 scientists from other nations. The colleagues of the Institute have acted as participants in 60 international and national scientific conferences and

gatherings held in the USSR, Poland, the German Democratic Republic, Hungary, Rumania, France, Italy, and other countries, including the XV International Conference on High-Energy Physics in Kiev, which was the largest gathering of physicists staged during 1970.

THE IV ALL-UNION CONFERENCE ON HEAT EXCHANGE AND HYDRAULIC RESISTANCE

E. V. Firsova and B. L. Paskar'

The IV All-Union Conference on heat exchange and hydraulic resistance in two-phase flow in the elements of power machinery and apparatus was held in Leningrad in January, 1971. The 650 delegates participating in the conference represented 123 scientific research organizations, institutions of higher learning, factories, electric power stations, and design engineering enterprises.

The participants in the plenary meeting heard reports by B. S. Petukhov on "Heat exchange in turbulent flow of a liquid in a single-phase near-critical region," by V. M. Borishanskii on "Current ideas concerning the thermal design of a steam-generating surface," and by M. E. Deich on "Characteristics of the flow of two-phase media in flow-through parts of turbines."

The work of the conference was divided into two sections: 1) heat exchange and hydrodynamics in boiling, condensation, and evaporation: heat exchange and hydrodynamics in the near-critical region; 2) heat exchange and hydrodynamics in organized two-phase flow, and heat exchange crises.

A distinguishing feature of the conference was that a limited number of reports were heard at the meetings. These reports were in the nature of surveys of fundamental problems: a) hydrodynamic characteristics in two-phase flow in channels of various shapes, and heat-exchange crises during boiling; b) theoretical and experimental investigations of boiling regimes, phase distribution, temperature fields, and true volumetric steam content values in nonequilibrium and equilibrium flows; investigation of the stability of two-phase flows; c) the temperature regime of a surface in the postcrisis region; d) thermal hydrodynamic characteristics of once-through potassium-vapor steam generators; e) the removal of small admixtures of condensing vapors from a current of inert gas (a series of investigations connected with the development of MGD installations), and others.

An important place in the program of the Conference was given to reports on the characteristics of high-speed nonequilibrium two-phase flows in the presence of condensation as related to stages of turbines operating with saturated and moist steam.

Of special interest were the reports devoted to heat-exchange crises in steam-generating channels and the calculation of the temperature regime of heat transfer surfaces in all zones of the precrisis region of a two-phase flow. The advances made in the investigation of two-phase flows of liquid-metal coolants have made it possible to work out designs for steam-generating channels with stable overheating. Such channels use special intensifiers by means of which the crisis regimes of operation can be avoided.

The reports presented gave reason for optimism concerning the possibility of removing metallic impurities from a current of inert gas by condensation. It was shown that under optimum conditions of operation it is possible to condense and remove up to 70% of the metallic impurity.

The reports were followed by a discussion. It provided an opportunity for a broader exchange of views on difficult problems and for the coordination of scientific research among various organizations.

Translated from Atomnaya Énergiya, Vol. 31, No. 2, p. 170, August, 1971.

II ALL-UNION CONFERENCE ON CHARGED-PARTICLE ACCELERATORS

V. S. Rybalko

The II All-Union Conference on charged-particle accelerators was held in Moscow in November, 1970, under the joint auspices of the Academy of Sciences of the USSR and the USSR State Committee on the Peaceful Uses of Atomic Energy.

The conference attracted participation from 450-odd Soviet specialists representing 54 scientific research organizations, 13 specialists from other socialist countries, and 23 specialists from research centers in the capitalist countries. The agenda was crammed full of pertinent topics. A total of 175 reports and papers were submitted to the organizing committee, including 26 papers from foreign scientists. A total of 115 reports and papers were delivered at the sessions and seminars held during the conference. The scientific and engineering problems discussed in the field of accelerator practice and theory were grouped around the following basic trends deciding the topical agendas of the 12 plenary sessions scheduled at the conference: 1) comparative characteristics of accelerators of different types from the standpoint of physical experimentation; 2) the status of accelerators of different types, and designs and plans for new machines and redesign and rebuilding of existing machines; 3) direct-voltage accelerators, ion sources and electron sources; 4) electromagnets for accelerators and power supplies for accelerator electromagnets, magnetic measurements; 5) collective methods of acceleration; 6) superconducting elements in accelerators; 7) dynamics of particles in accelerators, storage rings, and colliding-beam machines (two sessions of these topics); 8) radio electronics of accelerators, systems for measuring beam parameters; 9) high-power radio electronic devices and accelerating systems; 10) targets, beam separation and beam transport, beam injection and extraction; 11) computer monitoring and control of accelerator performance.

Seven seminars were held parallel with the deliberations of the conference sessions, to provide time for detailed discussions of specific topics relating to collective methods of acceleration, scientific and engineering problems in the design and building of fast boosters, the utilization of superconductivity in linear electron accelerators, coherent beam instability in accelerators and storage rings, etc.

Modern trends in the development of accelerators are determined by the efforts of scientists to pursue investigations of fundamental processes in increasingly higher energy ranges and steadily smaller cross sections. These efforts on the part of physicists were demonstrated in a report by A. A. Komar devoted to analysis of possible trends in physics research on accelerators of the future.

The scientific feasibility of designing accelerators for energies of hundreds and thousands of billions of electron-volts is not open to doubt at the present time, and practical advances in the region of such higher energies is linked more and more intimately with the use of superconducting magnets.

There were several papers devoted to plans and designs for ultrahigh-energy proton accelerators.

A. A. Vasil'ev reported on the status of research and development work on cybernetic accelerators, and forthcoming applications of superconducting magnets in such machines. One negative feature of modern superconducting cableware is the need to greatly increase the duration of the cycle of magnetic field variation in order to minimize energy losses in the superconductor, and end up with a magnet cycle duration much shorter than that characterizing magnets using ordinary conductors. As the duration of the magnet cycle is lengthened, however, the cost of the accelerating system skyrockets upward, and the possibility of using proton synchrotrons as injectors appears on the horizon. Similar arguments were adduced in a paper by Prof. R. Martin (Argonne National Laboratory, USA), where it was noted that the intensity of accelerators of that type could attain levels of 10^{14} to 10^{15} protons per burst.

Translated from Atomnaya Énergiya, Vol. 31, No. 2, pp. 171-173, August, 1971.

There was no report at the conference on the status of work on the construction of the 200 GeV proton synchrotron at Batavia (USA); In a private talk, Prof. Martin presented a viewing of slide transparencies giving some idea of the fast pace of construction work on this accelerator.

Keen interest was shown in a report by N. A. Monoszon on the design characteristics of synchrotrons designed for energies from 35 to 350 GeV, with commutable superconducting dc magnets. This paper dealt with certain difficulties stemming from complications in the dynamics of particle motion and from the rigid tolerances imposed on magnet displacement, and these are problems which will have to be solved in the course of future research.

Experimental investigations of superconducting magnets with coils made of thin-core niobium–titanium alloy base wire, and also investigations of cryogenic magnets with coils made of ultrapure aluminum, are being conducted on a broad scale in many acceleration research centers and accelerator facilities.

Work is being done at Karlsruhe (West Germany) within the framework of a program of study of a second-line 300 GeV accelerator (a CERN machine), in which the energy of the accelerated protons is to be 600 to 1000 GeV, which is to be achieved by replacing the conventional magnets with superconducting magnets. Pulsed superconducting dipole magnets with fields up to 50 kG are being fabricated and investigated at Karlsruhe, as well as cryogenic magnets with iron yokes and fields to 40 kG.

The next goal on the superconductivity research agenda at Rutherford Laboratory (Britain) concerns development of a redesign and modernization project for the 7 GeV accelerator, with the object of increasing the accelerator energy to 25 GeV while retaining the same machine radius.

A doublet of superconducting quadrupole lenses with aperture radius 10 cm and gradient 3.5 kG/cm has been fabricated at Saclay (France), and is being used effectively in the focusing system handling meson beams.

Soviet scientists reported on calculations and experiments centered around the design of superconducting magnets, and determination of losses in superconductors immersed in pulsed magnetic fields.

The conference audience displayed no less interest in reports on plans for improvements in existing accelerators, improved operational reliability of existing accelerators, and higher beam intensities.

A report presented by Yu. M. Ado et al. announced that the world's largest proton synchrotron, the IFVÉ 76 GeV machine, has been operating stably for the past year at a mean accelerated beam intensity of $7.5 \cdot 10^{11}$ protons per burst. The utilization factor of the accelerator for physical experiments has hovered around 82%. This attests to the high reliability of the accelerator and its multiplicity of auxiliary and accessory systems. A plan is being worked out to achieve substantial increases in the intensity of the accelerated beam (up to $5 \cdot 10^{13}$ protons per burst) on the basis of using an intermediate 1.5 GeV booster accelerator. Separate reports dealt with the development of the various systems for this booster accelerator.

E. A. Myae reported on research conducted at the IFVÉ accelerator to look into the possibility of going past the parametric resonance region by way of an incoherent coulomb shift of the betratron oscillations. It was demonstrated experimentally that this approach would not involve exorbitant particle losses when careful correction is made for resonance perturbations (narrowing the existing resonance bandwidth by one order of magnitude).

A new pulsed injector has been developed at the site of the world's largest linear electron accelerator, the 22 GeV Stanford (USA) machine, and high power klystrons (30 MW tubes) have been developed for the system. The possibility of replacing the existing accelerating waveguides by superconducting components, which could mean increasing the electron energy to 100 GeV when working with a duty factor of 6%, or continuous operation with the electron energy at about 25 GeV, is being examined.

G. S. Kazanskii shed light on several topics associated with the conversion of the JINR proton synchrotron ("synchrophasotron") to deuteron acceleration. Acceleration of deuterons to such high energies (on the order of 11 GeV) was achieved for the first time anywhere in the world, and this will unquestionably expand the experimental capabilities available to high-energy physics. The possibility of accelerating α-particles and heavier ions on the synchrophasotron machine is also being examined.

Slow extraction of a beam of electrons with a stretching time of 2.5 msec was achieved at the Erevan electron synchrotron.

Experiments using a nonlinear regenerative system of beam extraction were conducted at the synchrocyclotron of the Physicotechnical Institute of the USSR Academy of Sciences [FTI AN SSSR] (Leningrad), and high extraction efficiency (25%) was achieved in combination with excellent extracted beam quality.

Work on redesigning the 680 MeV synchrocyclotron is in progress at JINR, with the object of converting the machine to a high-current synchrocyclotron with spatially varied magnetic field. Two reports were presented to the conference dealing with simulation of the magnetic and radio-frequency systems of the high-current synchrocyclotron.

Of the papers devoted to low-energy accelerators, the one that excited the greatest interest was submitted by V. A. Slobodyanyuk, dealing with a project for a continuous-wave microtron of 12 MeV energy for the Power Physics Institute (FÉI). The radio-frequency power source for this machine will be a novel magnetron type oscillator, known as a nigatron with 150 kW power. This accelerator is simple in design and will prove useful in the study of the structure of the atomic nucleus, and in radiation physics research.

Considerable attention was given, in the deliberations of the conference, to scientific and engineering problems concerning penetration into the region of ultrahigh interaction energies via the colliding-beam method. Here we may mention the reports submitted by the Institute of Nuclear Physics of the Siberian Division of the USSR Academy of Sciences [IYaF SO AN SSSR], and in particular a communication delivered by R. A. Salimov on the building of an experimental facility for work on electron cooling on the VÉPP-3 storage ring system.

A report submitted by Prof. W. Entschke (CERN director) and read by F. Ferger, dealing with the physics program for proton storage rings, presented an idea of colliding-beam experiments which will be underway as part of the CERN program in the near future. A proton beam injection energy of 15 GeV has been selected for adjustments of the storage rings, since that would not require corrections of the magnetic field of the storage rings.

Topics relating to new systems of centralized digital monitoring and control of accelerators, methods for measuring phase volume and space-time characteristics of beams, noncontacting measurements of beam current using the Hall effect, and similar topics, were discussed at the session devoted to the radio electronics of particle accelerators.

As usual, a large number of reports were presented on the dynamics of particles in accelerators and storage rings, so that two sessions had to be set aside for reading them. Here we may mention the reports by V. A. Teplyakov on high-frequency quadrupole focusing in linear accelerators; by V. V. Petrenko on longitudinal compression of bunches; by M. Barton on instabilities in the radio-frequency system of the Brookhaven synchrotron due to beam loading features, and so forth. Some of the results dealt with theoretical investigations of space charge effects and special features of particle dynamics in specific accelerators. Numerical methods for simulating the motion of particles in accelerators by means of electronic computers figured prominently in these papers, alongside analytical techniques.

Computational techniques and computer mathematical simulation of the magnetic fields of iron magnets and ironless magnets also occupied a prominent place in the discussion of accelerator design. These topics were aired at a session devoted to electromagnets in accelerators. The topical content of the other reports read at that session dealt with features of the power supplies systems for the electromagnets, particularly the electromagnets employed in fast boosters, and also equipment for taking magnetic measurements.

Several interesting papers were submitted on accelerating systems. V. M. Pirozhenko delivered a report on investigations of a new $\pi/2$-wave accelerating structure, in the form of a resonator cavity with conducting disks and diaphragms. As the experiments revealed, the proposed structure is vastly superior to known accelerating structures in terms of the degree of coupling between different cells, and also in terms of the magnitude of the shunt impedance where it is practically on the same level of quality as other familiar structures. This type of structure can be used in high-energy linear proton accelerators, and specifically in meson factories.

A. I. Kvasha reported on the results of experiments probing compensation of fall-off in the accelerating field in the linac injector of the Serpukhov synchrotron. Total compensation of the power carried off by a beam with current to 80 mA/burst and burst duration to 40 μsec was achieved.

A method of coherent acceleration of ions with the aid of electron rings, proposed by Academician V. I. Veksler, has now become a basic trend of research in the field of new acceleration techniques. Experimental work aimed at devising accelerator facilities based on that principle is being pursued intensively not only in the USSR, but in many foreign laboratories as well. Naturally, discussion of topics relating to collective methods of acceleration took up a large part of the conference deliberations. V. P. Sarantsev gave an account of the latest achievements in this comparatively young branch of accelerator engineering in his report entitled "Collective ion accelerators – a new tool in the physics of elementary particles." Experimental work on a model of a collective accelerator is continuing at JINR. Following the successful acceleration of nitrogen ions a year ago, a decision was made to attempt acceleration of α-particles. This necessitated refashioning the gas evacuation and admission system. All systems in the model are now ready for the experiments on acceleration of α-particles. By mid-1971, installation of the radio-frequency system for accelerating electron rings on thermal resonators will be completed. We would also mention some reports on a new type of electron accelerator, the 3.5 MeV linear induction accelerator with maximum pulsed current 2 kA. Impressive progress has been recorded in devising the component systems for the future high-power accelerator dubbed the kol'tsetron ["ringatron"]. An average ion-accelerating field of ≈ 2 MeV/cm will be achieved in the cryogenic radio-frequency section that has been developed for this system. Superconducting resonators and solenoids establishing a longitudinal magnetic field of ≈ 20 kG are being used.

G. Peterson reported on the program drawn up at the Lawrence Radiation Laboratory (Berkeley, USA) on electron ring accelerators, and W. Heintz gave an account of work underway on electron ring accelerators at Karlsruhe (West Germany). Some interesting theoretical work on synchrotron radiation by electron rings and on coupling resonances of transverse oscillations in annular beams was reported by C. Pelligrini (Frascati, Italy) and by D. G. Koshkarev, respectively.

A large number of reports was presented at the session on direct-acting accelerators, ion sources, and electron sources. Some topics of importance in accelerator work, dealing with production of high-intensity ion and electron beams, beams of polarized ions, stable operating conditions for high-current direct-acting pulsed accelerators, etc., were discussed.

Plans for general improvements and reliability improvements in large accelerations are to an increasing extent featuring automatic control systems and automatic monitoring systems incorporating general-purpose computers and control computers. A special session was devoted fully to discussion of computerized automation of accelerators at this conference, for the first time.

A. A. Kuz'min reported on the principle underlying the automation of the Serpukhov accelerator. A functional principle allowing for automation of individual systems without disturbing the performance of the accelerator when these individual systems are joined together into a unified complex controlled by a central computer has been proposed. V. I. Kolosov reported on planned automation of the linear accelerator of the Physics and Engineering Institute of the Ukrainian SSR Academy of Sciences (FTI AN USSR). The accelerator is to be automated in three stages. In the first stage, centralized control of accelerator systems by means of the Dnepr-2 computer will be instituted. The second stage envisages use of the computer to maintain beam parameters at set point, test out prognosis and diagnostic programs. In the third stage, there is to be a gradual change-over to fully automated control with a self-adaptive program.

Yu. S. Kuz'min gave an account of an automatic complex for control of a model of a 1 GeV cybernetic accelerator at the RAI AN SSR Institute. Here functional monitoring of the accelerator parameters and control of the performance of automatic correction systems will be handled by two general-purpose Dnepr-1 digital computers. The information obtained will also be written into storage units on magnetic tapes, and in case of need these records will be available for transfer to a No. 6 high-speed computer for more complex processing.

The conference proceedings took place in a cordial and friendly setting, and numerous private talks and meetings in the corridors contributed to broadening of businesslike scientific ties between scientists of the different countries present. A visit to the principal accelerator centers of the Soviet Union was arranged for the foreign participants at the conference.

ACCELERATORS IN THE NATIONAL ECONOMY AND IN MEDICINE

L. G. Zolinova

By joint decision of the Academy of Sciences of the USSR and the USSR State Committee on the Peaceful Uses of Atomic Energy, the I All-Union Science and Engineering Conference on the use of charged-particle accelerators in the national economy and in medicine was held in Leningrad in February, 1971. There were 400 or so participants at the conference from various districts of the Soviet Union and from the socialist countries.

A total of 120 papers were discussed, their contents being distributed over the following headings: 1) designs and parameters of accelerators developed by different organizations for practical applications; 2) industrial radiation processes realized with the aid of accelerators; 3) use of accelerators in medicine, in biology, and in agriculture.

Industrial plants and scientific research agencies in our country have developed and have built accelerators (betatrons, linear accelerators, microtrons, neutron generators, resonant transformers, and so forth), and these sources can be used in various branches of industry.

Table 1 lists some information on some of the accelerators whose characteristics were discussed at the conference.

Industrial radiation processes, nondestructive flaw detection, and activation analysis were among the conference topics. The reports discussed research findings on applications of accelerators in realizations of industrial technology, in such processes as: curing of glass fiber reinforced plastics, production of rubber grades with special surface properties, and production of wares made from irradiated polyethylene.

Some of the papers dealt with radiation flaw detection of steel parts and structures. It was reported, in one of these papers, that regular use of a betratron facility for transmission flaw detection at the Barnaul boiler works has resulted in a drastic improvement in the quality of the equipment manufactured at that plant, so that the users of this equipment can count on annual savings totaling about 500,000 rubles. The reports also brought out the fact that the use of linear accelerators for radiography greatly shortens exposure time and makes it possible to obtain x-ray plates when inspecting steel parts and structures 400 mm

TABLE 1. Microtron Characteristics

Accelerator	Wave length, cm	Electron energy, MeV	Beam current, μA	Output power, W	Application
Flaw-detection microtron	10	10	50	500	Flaw detection (2000 R/m/min)
Tikker microtron	10	5—20	100—25	500	Research, activation analysis
Radiological microtron	10	30	15		Medical radiology (350 R/m/min)
The same	3	16	2	100	The same
Élektronika microtron	5	10	1 — (5)	200	Research
FÉI microtron	20	15	2 000	20 000	"

Translated from Atomnaya Energiya, Vol. 31, No. 2, pp. 173-176, August, 1971.

TABLE 2. Characteristics of Linear Accelerators

Type of accelerator	Energy of accelerated electrons, MeV	Energy control range, MeV	Average power output, kW	Intensity of bremsstrahlung (unfiltered) at distance 1 meter from target, mR/m	Intensity of bremsstrahlung (filtered) at distance of 1 meter from target, R/m	Remarks
LUÉ-8-5	8	4—12	5—7		—	For sterilization of medical wares, in radiation chemistry
LUÉ-8-5V	8	8—10	5		—	
LUÉ-15-10	13	5—15	To 10		—	
LUÉ-10/1	10	3—10	—	2 000	—	Nondestructive testing
LUÉ-15/15	15	5—15	—	10 000	—	The same
U-13*	10	5—10			—	Scientific research
U-18†	2	—			—	
LUÉ-5	5	—			To 200	Therapy of malignant neoplasms and medico-biological research
LUÉ-25	25	10—25			600—800	The same

* Current in pulse to 50 mA.

† Current in pulse to 250 mA.

TABLE 3. Characteristics of Betatrons

Type of betatron	Peak energy of accelerated electrons (MeV)	Intensity of bremsstrahlung at distance of 1 meter from target, r/m	Remarks
B-15 (TPI)	14,2	5	Activation analysis
LUCh (TPI)	24,5	500	The same
B-25/30	24	40	" "
B-30	28,5	30	" "
PMB-6	2—6	20	Nondestr. test.
B-1M-45	45	125	Nondestr. test.
B-5M-25	25	60—80	Medicine
B-50	50	800	Research

thick in times from 10 sec to 10 min. It has also been possible to inspect steel parts and structures up to 600 mm thick by transmission of x-rays in a practically acceptable time period (from 15 min to 1.5 h). The sensitivity of the radiographic method of flaw detection using linear accelerators is about 1%.

Note was made of the effectiveness of using accelerators for activation analysis of oxygen content and nitrogen in nonferrous metals and semiconducting materials, with the aid of the NG-150 neutron generator.

Several thousand analyses were run on an automated facility designed by GIRIDmet, NIIEFA, and FIAN. A sensitivity of 10^{-4} to $5 \cdot 10^{-4}$ wt. % was obtained in determinations of oxygen and nitrogen, with reproducibility of results to within 1 to 20% for contents from 0.1 to $5 \cdot 10^{-4}$ wt. %. Savings resulting from the regular use of one such facility at a titanium—magnesium plant totaled 500,000 rubles annually.

Other papers reported on the use of accelerators for inspection of welded joints in piping of large diameter, and also for inspection of electron-beam welding work (where the electron beam is the sole source of heat, so that welds can be made over a broad range of thicknesses from tenths to hundredths of a millimeter, and joining virtually any materials), and for the study of stability of semiconductor products to irradiation.

Use of Accelerators in Agriculture, Biology, and Medicine

A whole group of papers was devoted to the applications of accelerators for processing grain with dosages of 10 to 20 krad. It was reported that facilities for destroying insect infestation of grain based on the ÉLT-1 and ÉLIT-1 accelerators have been developed. (The Institute of Nuclear Physics of the Siberian Division of the USSR Academy of Sciences [IYaF SO AN SSSR] developed these facilities.) Work is in progress on irradiating potato tubers (using the KGÉ-2.5 and ÉG-5-É accelerators) for the purpose of presowing stimulation of the potato and preventing germination of tubers during long-term storage. Results of this research provide evidence that electron irradiation of potato seed and commodity potatoes using electrons of comparatively low energies (0.7 to 1.0 MeV) shows rather excellent promise as a practical application. One interesting feature of this type of irradiation is that only the surface parts of the potato tuber

TABLE 4. Characteristics of High-Power Direct-Voltage Electron Accelerators

Type of accelerator	Energy, MeV	Average beam power, kW	Pulsed beam power, kW
RTD-1*	1	3	18
Élektron	0,7	7	7
ÉLIT-1†	1	8	10 000
ÉLIT-3†	2,5	10	40 000
TÉUS-1.5	1,2	150	
KGÉ-2.5	2,5	20	20

*Resonant transformer.

† Electronic pulse transformer.

become affected by the irradiation, to a depth of about 4 mm. When tubers are irradiated with dosages of 10 to 20 krad, the storage times of the potatoes can be extended impressively, all the way till the next crop is ready, because germination processes are inhibited by the radiation treatment. At the present time, the most highly developed process is irradiation of potatoes for long-term storage.

Applications of accelerators in medicine, a topic quite popular among the participants of the conference, was the subject of a report by N. N. Aleksandrov (Scientific Research Institute for Oncology and Medical Radiology, Minsk). It was pointed out in this report that one of the basic principles in the radiation therapy of malignancies is the trend toward bringing about conditions to maximize the concentration of absorbed energy of ionizing radiation in the tumor while minimizing the effect exerted by that radiation on healthy tissues and organs. Practice has shown that best clinical results are secured through combined treatment of malignant tumors where irradiation is carried out before the surgical operation and after it. However, when treating cancer in some organs and tissues, it is possible to use the ionizing radiations with no surgical intervention at all. Electron accelerators producing powerful beams of electrons and x-rays have been used successfully in radiation therapy of cancers.

There are now over ten medical accelerators in the USSR capable of generating fast electrons and bremsstrahlung. The peak electron energy attainable with those accelerators ranges from 4 to 45 MeV. Foreign accelerators exhibit more or less the same range of energies.

In discussing the problem of how to integrate electron accelerators into radiation therapy practice, there is some significance in the question of preference in the selection of a betatron or a linear accelerator. Comparative estimates of the advantages gained in using the LUÉ-25 medical linear accelerator and the Siemens 42 MeV betatron have been made. One clear advantage of the linear accelerator is that it is possible to attain high values for the bremsstrahlung dose rate, with smooth variation of the limiting energy of that radiation over a broad range. Control of bremsstrahlung energy is difficult to achieve in practice with a betatron, since the dose rate at the betatron exit declines abruptly in response to a fall-off in the energy of electrons impinging on the target.

As a comparative estimate of data obtained in tests of these machines in Belorussia has shown, each of the machines has its own advantages and disadvantages. We may also note that the basic criteria for judging the effectiveness of their use, as governed by both the physical properties of the radiation generated and by the performance of the machines under conditions where large numbers of patients have to be treated, are quite similar. Although it had been assumed earlier that many of these criteria were inherent only in betatrons (reliability in service, fidelity of data in dosimetric measurements, availability of technical know-how and servicing equipment), there is now every reason to assume that these characteristics as found in linear accelerators will come close to their counterparts in betatrons.

An important survey of the research done at Minsk is provided by the results of a comparison of methods for generating large radiation fields with the aid of those machines. Large fields of electron radiation are generated in all existing accelerators by scattering the electron beam on foils. But these fields are brought about with the aid of electromagnetic lenses in the case of the LUÉ-25 linear electron accelerator designed at the D. V. Efremov Scientific Research Institute for Electrophysical Equipment [NIIÉFA]. The investigations revealed that a decrease of electron energy occurs in the first method (i.e., when foils are used). The fact that this decrease in energy is different under different radiation conditions is also of great importance. For example, the use of different radiation fields may bring about a decrease in radiation energy over a range from 0.1 to 1.5-2.5 MeV. In other words, when different fields are used in radiation therapy, even at the same energy of the electrons striking the foil, electrons having different energies will reach the patient. Moreover, there will be a broadening of the energy distribution of the electrons, which will result in a change in the dose distribution in the object irradiated. Another important fact to consider is that the presence of scattering foils will increase the admixture of bremsstrahlung in the electron beam. In that respect the method of electron-optics shaping of fields, which is the one used in the Soviet LUÉ-25 electron accelerator, shows greater promise, even though it requires more careful adjustment of the system.

The results of practical work allow us to state that the use of radiations generated in electron accelerators satisfies the requirements of radiation teletherapy quite thoroughly. But data accumulated in clinical radiology and oncology pose new problems before designers of radiological equipment.

The problem faced by designers is how to design new accelerators which will be automated to a significant extent, and which will feature general-purpose devices for irradiating different organs and achieving many distinct variants of irradiation settings. At the present time, NIIÉFA designers are engaged in development work on accelerators meeting that description.

In addition to electron accelerators capable of generating powerful beams of electrons and x-rays, a method of radiation therapy using a high-energy proton beam, somewhere of the order of 100 to 200 MeV, is being developed in the Soviet Union.

Other topics such as radiation safety, high-flux dosimetry, and so on, were discussed in some of the reports.

THE FRANCO-SOVIET COLLOQUIUM ON FAST-REACTOR TECHNOLOGY

Yu. E. Bagdasarov and O. D. Kazachkovskii

The Franco-Soviet Colloquium on Fast-Reactor Technology was held on November 18 and 28, 1970, at Saclay and Cadarache. The program of the Colloquium also included familiarization of the Soviet delegation with the Rhapsodie reactor, with the Phoenix reactor (now under construction), sodium stands for the thermophysical investigation of various technological problems, and tests of equipment used at the Chatou, Grand-Quevilly and Renardier reactors.

The Soviet delegation included O. D. Kazachkovskii, A. K. Kruglov, L. A. Alekhin, Yu. E. Bagdasarov, D. S. Yurchenko, V. P. Kevrolev, V. V. Kurilkin, and A. N. Egorov. French experts who presented reports and participated in the discussions included Carle, Robin, Leduc, Goujin, Delisle, Cauvin, Gajac, Zalessky, and others.

Among the questions discussed the most interesting ones are the following.

1. Experience with the testing of various models of sodium–water–steam boilers; the development of designs for steam boilers to be used in the Phoenix reactor and future atomic power stations with fast reactors; experimental and calculated investigation of processes taking place in the second loop when large-scale breaks occur in the heat transfer tubes; the experimental study of small leaks. It was noted that when proper steps are taken to remove the products of the water–sodium reaction, a large leak in one of the tubes does not lead to failure in the adjacent ones. A physical and mathematical description of the processes taking place in such a case was given. It was shown that the calculated and experimental curves of the variation in the main parameters (pressure, temperature) at characteristic points of the loop (the site of the leak and the buffer volume) are in satisfactory agreement with one another. Also noted was a trend toward full-scale testing of steam-generator modules on high-power test stands, and the search for and introduction of new steam-generator structural materials which would be resistant to corrosion both in water and in sodium containing a high percentage of sodium–water reaction products.

2. The development of high-powered atomic power stations using fast reactors: the economic optimization of active zones, the basic choices for the design and arrangement of the first loop, and the optimum parameters of an atomic power station. A characteristic of the French studies was that the parameters were optimized only with respect to the cost of the electrical energy generated (the problems of obtaining a maximum possible reproduction factor and minimum doubling time were considered secondary). Optimization in the Soviet Union, as is known, is based not only on the cost criterion but also on the value of the doubling time.

3. Experience in designing, testing, and operating the main technological equipment: pumps, heat exchangers, and the armature.

Contradictory trends were noted in the methods of compensation for temperature expansion in the tubes with respect to the shells of the intermediate heat exchangers. While in the USSR and most other countries this difference in expansion values is compensated by curving the tubes, French spacialists consider it possible to leave the heat exchange tubes straight. This appears possible because the maximum temperature difference between the structural elements not only in stationary processes but also in any possible transitional processes, according to the calculations cited, does not exceed 24°C. Thermal tests of shell-and-tube heat exchangers conducted in France showed very good agreement (within about 1%) between the experimental and calculated heat transfer coefficients. Valves for sodium loops with a freezing belt around the coupling were found to operate satisfactorily. Speakers emphasized the desirability of designing pumps with two intake tubes.

Translated from Atomnaya Énergiya, Vol. 31, No. 2, pp. 176-178, August, 1971.

4. Experience with fuel-element operation in the BR-5 and Rhapsodie reactors. The highly satisfactory operation of uranium monocarbide fuel elements in the BR-5 reactor and oxide fuel elements in the Rhapsodie reactor was noted. As is known, long experience with the operation of the BR-5 reactor using oxide fuel (first charge), which has a burnup value of up to 7%, provided the necessary data for designing the fuel elements of the BN-350 and BN-600 reactors. Favorable experience with oxide fuel accumulated in the Rhapsodie reactor supports the conclusions arrived at on the basis of operation of the BR-5.

In the Soviet report, based on operation of the BR-5 reactor, it was pointed out that 0Kh16N15 M3B steel had been found to be much better for use in the shells of monocarbide fuel elements than 0Kh18N9T steel.

It was noted that the activity buildup curves for the loops of the BR-5 and Rhapsodie reactors after rupture of the hermetic seal in fuel elements were very similar. The nature of the failure of oxide fuel element shells in both reactors and the composition of the impurities in the gas blanket were also almost identical.

5. Experience with the operation of the Rhapsodie reactor and start-up and testing operations on the BOR-60 reactor. The satisfactory operation of the Rhapsodie reactor made it possible to plan and apply a number of measures and alterations by means of which in the near future, after replacement of the fuel assemblies, the reactor power can be raised to 38-42 MW. Experience with the operation of the recharging machinery of the Rhapsodie reactor indicated that it would be desirable to construct multipurpose machinery. At present the functions of this machinery are divided among three much simpler and much more effective devices (for removing spent assemblies, charging the reactor with fresh fuel, and recharging operations related to experiments).

Experience with start-up and testing operations and with physical and technological investigations on the BOR-60 reactor confirmed the acceptability of the engineering decisions made during the design stage and the possibility of raising the yield to the nominal parameters.

6. Experience with the construction and installation of atomic power stations using the BN-350 and Phoenix fast reactors. The construction of the Phoenix atomic power station is progressing at a rapid rate. The construction work is about 80% finished. At the same time, the main equipment is being installed: all three reactor vessels (the primary hull and two safety tanks) are in place, and drainage tanks for the sodium of the first and second loops have been installed. Current plans call for filling the first loop with sodium and beginning the start-up operations during the second half of 1972. As is known, in the case of the Soviet BN-350 power reactor, it is expected that the bulk of the installation work will be completed in 1971 and start-up operations will begin at the end of the year.

A great deal of work is being done in France to produce reliable steam generators for atomic power stations using fast reactors. This is because steam generators are one of the main sources of trouble leading to a reduction of the station's operational readiness. Specialists at Saclay are engaged in the constructive development of various types of steam generators. For example, steam generator models are being tested on stands at Grand-Quevilly, Chatou, and Renardier, thermohydraulic processes are being studied on experimental installations at Chatou, studies on small water and steam leaks into the sodium in the intertube spaces of steam generators are being conducted, and methods for indicating these leaks are being worked out at Cadarache and Chatou; work is being done at Cadarache to check the stability of the heat-transfer bundles of the models and natural modules under conditions simulating serious breaks in the loops, with water mixing with the sodium at rates of up to 17 kg/sec of water.

In the summer of 1970 a 50 MW gas-heated test stand for investigating steam generators was put into operation at Renardier. The outlet temperature is 600°C (650°C is allowable for short periods). Two pumps are installed in the first loop. The stand is equipped with two bypasses, one of which has an air-type heat exchanger capable of removing up to 50 MW. It can be used for investigating steam generators under conditions of rapid change in sodium temperature (up to 150° in 10 sec). The stand is loaded with 105 tons of sodium. A cyclone separator with a capacity of about 20 m^3 is used for removing the products of the sodium–water reaction. The water part of the stand is capable of accepting steam at 160 atm and 565°C and simulating all the sections of the steam generator (heating, evaporation, superheating, intermediate superheating). After several stages of steam throttling the heat is dissipated in a cooling tower.

When the Soviet delegation visited the test stand, three modules of the Phoenix reactor steam generator had already been operating for 800 h at nominal parameters.

At Cadarache 60 experiments were conducted with slow leaks of water into the sodium and two experiments with steam entering the sodium. The water and steam parameters and the materials and geometry were chosen to be close to these characteristics of the steam generators of the Phoenix reactor. However, the final results and the processing of the data are not yet complete. The preliminary conclusions are the following: a water leakage rate of 0.04 kg/min or less is not dangerous, the steam generator can operate with such a leakage rate without significant corrosion for at least several hours. The results of two experiments with leakage of steam at 500°C and 170 atm into sodium at a temperature of 500°C indicated that the injection of steam at a rate of about 1 kg/min produces an opening in the target tube (situated about 15 mm away) in 3 min. The sodium volume of the stand for investigating small leaks is 3 m^3.

In addition to the already published results of studies of large water leaks into sodium on models, six full-scale experiments have recently been conducted directly on the stationary module of a steam generator of the Phoenix reactor. The module is situated next to the building used for studying water flow into sodium, in an open area without any protective enclosure, and is hooked up to the systems in the building by appropriate connecting lines. In each experiment, water at an average rate of about 17 kg/sec was emitted for 15-20 sec from a special fast-opening valve on the hull of the module; the stream of water was directed at a heat-transfer tube. No bursting or significant damage to the steam generator tubes occurred in any of the experiments; the reaction-product removal system operated satisfactorily.

On the basis of the Colloquium and the visit to the French research centers, the following general conclusions may be drawn.

1. The main research work on atomic power being conducted by the French Atomic Energy Commission is concentrated on the solution of problems related to fast reactors; financial support is being allocated accordingly.

2. The only type of fast reactor being considered in the development of the power-generation prototypes is a reactor with a sodium coolant and integral arrangement of the equipment in the first loop.

3. The French Atomic Energy Commission is cooperating very closely with the EDF: fast reactors are being developed according to programs worked out jointly by the two organizations. The EDF is independently engaged in a broad program of design work and scientific research on the use of sodium and the testing of technological equipment using sodium.

4. A great deal of attention is being devoted to the exchange of experience in the construction of fast reactors and to the popularization of this branch of power engineering. One indication of this is the French Atomic Energy Commission's plan to convene a meeting of representatives of leading countries to discuss problems of fast-reactor power station development; the meeting will be held at Aix-en-Provence prior to the Fourth International Conference at Geneva.

5. Previously announced plans for constructing and putting into operation a number of important installations relating to fast-reactor problems will be completed either on or before the published dates (the Rhapsodie, the Phoenix, and the 50 MW test stand), thanks to the careful organization of work and the prompt delivery of equipment produced by French industry.

THE USE OF NUCLEAR METHODS FOR MEASUREMENT AND CONTROL OF ENVIRONMENTAL POLLUTION

L. V. Artemenkova

An International Atomic Energy Agency symposium on the use of nuclear methods for measurement and control of environmental pollution was held in Salzburg on October 26-30, 1970; about 200 experts, representing more than 30 countries and many international organizations (WHO, WMO, and others), participated. Also attending were scientists from the Soviet Union and other socialist countries. Fifty-five reports were read, touching on nearly all possible spheres of application of nuclear methods to the measurement of environmental pollution: measurement of pollutant concentration in the atmosphere, identification of pollutants in water, the movement of pollutants in water and soil, tracer methods in the study of effluents, nuclear methods and ecosystems, and sludge and sewage processing.

The application of nuclear methods to the control of environmental pollution began about 15 years ago. The perfection and automation of measuring devices made it possible for sanitary specialists to use these devices widely.

Considered at the symposium were problems in the use of neutron activation analysis, tracers, radioisotope detectors, and other means (x-ray fluorescence methods, electron capture detectors, etc.) to control concentrations of harmful substances; and some aspects of the application of powerful sources of ionizing radiation to sewage processing and decontamination were also discussed.

Nearly half of the reports were related to the use of activation analysis, primarily neutron activation analysis, for the measurement and control of harmful impurities in water, soil, and air.

The procedure for studying the composition of a sample of the environment by activation analysis consists of the following stages: collecting the sample; preparation of specimens for irradiation; irradiating a specimen; measuring the induced activity by the method of comparison with a known specimen or by γ-spectrometry. Before the latter stage, sometimes chemical separation and sample aging are used to increase sensitivity.

Some possible uses for neutron activation analysis in the study of aerosol particles are shown in Table 1.

Scintillation detectors, semiconducting Ge(Li)-detectors, and multichannel analyzers (4096 channels) are used to record γ-spectra. In some work there is a trend towards the use of computers for processing data coming directly from the detector units or from multiple analyzers. In processing results, a library of standard spectra is used, and use of background spectra from the specimen backings is also known, but the backing (e.g., an aerosol filter) must be chosen with consideration of the tasks facing the investigators. The use of activation analysis permits the measurement of ultra-small quantities of aerosols (up to 10^{-9} g/m^3).

Several reports dealt with the use of neutron activation analysis to detect mercury in water, biological specimens, soils, and plants. The danger from mercury entering water reservoirs in the form of wastes from chemical and cellulose and paper manufacturing was noted.

It was noted that neutron activation analysis has good prospects for use in the study of trace elements in petroleum products and in sea and ocean pollution, as well as for tracing the cycles of elements contained in pesticides and herbicides.

Translated from Atomnaya Énergiya, Vol. 31, No. 2, pp. 178-180, August, 1971.

TABLE 1. Use of Neutron Activation Analysis in the Study of Aerosol Particles in the Air

Investigator (publication date)	Purpose of study	Sample equipment	Flux, neutrons/cm^2/sec	Irradiation time	Analysis method	Elements identified	Concentration, mg/m^3
Fraind (1961)*	Concentration of radioactive particles in the stratosphere	Impactor and filter on U-2 aircraft	$\sim 10^{-12}$	Various	Comparison method	Ni, Pb, Co, Mn, Cr, Cu, Fe, Zn, Co	
Tarras (1962)	Commercial use of stable tracers and neutron activation analsis		$5 \cdot 10^{-13}$	4 days		Ag, Ho, Sm	
Parkinson (1963)	Study of aerosol particles	Pump, Whatman filter 41	$1{,}8 \cdot 10^{11}$	3—100 min	Analysis of decay, activity, photopeak curves‡	Al, Ba, Cl, I, Mg, Mn	
Doke (1963)	Halogen geochemistry	Grid of silver rods	$\sim 10^{13}$	20 min	Comparison method‡	Br, Cl, I	
Gardon (1964)	Study of aerosols	Pump, ether-celluloid filter	$8{,}6 \cdot 10^{12}$	15 min	Comparison method†	Br Mn Na	0,22 0,04 0,51
Winchester (1965)	Halogen geophysics	Four-stage impactor	10^{13}	20 min	Comparison method†	Br Cl I	0,015 4,0 0,002
Lininger (1966)	Halogen and zinc geophysics	Four-stage impactor	10^{13}	20 min	Comparison method†	Br Cl I Pb	0,2 6,0 0,01 0,22
Li (1968)	Study of aerosols	Pump Millipore AA	$1{,}7 \cdot 10^{13}$	2—3 days	Comparison method	Ag As Br Ca Co Cu Fe Hg La Na Sb Sc Zn	$4{,}5 \times 10^{-2}$ $3{,}3 \times 10^{-2}$ 0,17 3,4 $5{,}2 \times 10^{-3}$ $2{,}5 \times 10^{-2}$ 0,65 $2{,}5 \times 10^{-4}$ $2{,}3 \times 10^{-5}$ 0,65 $4{,}9 \times 10^{-3}$ $6{,}8 \times 10^{-3}$ 0,33
Keri (1969)	Study of aerosols	Pump, filter	$1{,}2 \cdot 10^{13}$	5 min	GASP system†	Al Br Cl Mn Na V	0,3 0,04 2,0 0,03 0,8 0,015
Bro (1969)	Study of aerosols	Celluloid mesh X-1215-2	$2 \cdot 10^{13}$	1 min	Nelsen's system‡	Al Br Cl Mn Na V	2,0 0,17 3,0 0,6 0,4 0,06

*Completion date of study shown in parentheses.
† With chemical separation.
‡ Without chemical separation.

It was emphasized at the symposium that the use of tracers is of great value for obtaining information on the behavior and fate of substances polluting the atmosphere, water, and soil.

A method based on the isotope ratio of S^{32} and S^{34} is of interest. It is used to detect and trace the dispersion of sulfur dioxide in large cities and their surroundings. For studying the dispersion of flue gas emissions, Ar^{41}, Kr^{85}, and Xe^{133} are used as tracers.

For studying the dispersion of effluents and selecting locations for them, S^{35}, Br^{82}, and I^{131}, for example, may be used as tracers, as well as non-radioactive indium and iridium compounds and gold chlorides,

which can be activated later by neutrons. Methods of single and continuous injection of active isotopes into an aquatic environment were examined, as well as methods and apparatus for measuring an active tracer in water. The necessity of simultaneous measurement of current and wind velocity and determination of the location coordinates of the radiation detectors at the time of the measurements was noted.

Of special interest were the reports noting ways of processing some types of sewage by means of powerful sources of ionizing radiation.

SOVIET NUCLEAR POWER SPECIALISTS' TOUR OF THE NETHERLANDS AND BELGIUM

L. V. Komissarov

In September, 1970, a group of Soviet specialists in the field of nuclear reactor physics and technology visited the Netherlands and Belgium and became acquainted with scientific centers and universities conducting research in reactor physics, heat transfer, and hydrodynamics. The delegation also visited two operational atomic power plants and several factories and businesses involved in the planning, manufacture, and testing of atomic power plant equipment.

In the Netherlands the Soviet specialists visited the Reactor Center of the Netherlands at Petten, the Technological University at Eindhoven, laboratories of the KEMA firm at Arnhem, the Technical High School at Delft, the Netherlands' first atomic power plant at Dodenvard, and a high-pressure vessel factory owned by the RDM firm (Rotterdam). In Belgium the delegation visited the nuclear division of the ACEC firm at Charleroi, the French–Belgian SENA atomic power plant at Ardennes, the Center for Nuclear Research at Mol, and the Belgianuclaire firm at Brussels.

The Soviet specialists became acquainted with work on the following problems: 1) thermohydrodynamics design and experimentation; 2) atomic power plant safety design research; 3) reactor physics experimentation on critical assemblies and physical designs; and 4) equipment use and repair at operational atomic power plants.

1. Thermohydrodynamic reactor design at the ACEC and Belgianuclaire firms is based on the analysis of the spatial distribution of mass flow rate, steam content, pressure, temperature, and enthalpy of the coolant throughout the reactor by means of HAMBO or KOBPA programs and the like. To determine the critical parameters (heat flux, steam content) of the design, an unfavorable combination of such factors as reactor power, fuel consumption, temperature, and coolant velocity, as well as possible errors in the equations used, is assumed. But even in this case, there is no assurance that the safety margin determined will be sufficient, since the equations used do not completely account for the conditions of a real structure. In this connection the method proposed by Hoppe (of Belgianuclaire) for determining the safe operating conditions for a reactor is of some interest. The method is based on a detailed statistical analysis of experiments on ultimate loads and permits the probability of occurrence of a heat transfer crisis at any power level in the active zone to be determined for concrete conditions.

A multitude of experimental studies is performed to test and correct thermal and hydrodynamic designs. Much attention is given to the study of the hydrodynamics of single-phase and two-phase flows. At the Technological University of Eindhoven, flow mixing between separate streams in a group of rods is studied under natural and forced circulation. Two-phase flow and the distribution of phases in a group as a function of pressure, flow rate, and underheating of the coolant at the intake is studied at a station with up to 2 MW of power in a research section up to 4 m long at a pressure of up to 300 kg/cm^2. In the laboratory there is a low-pressure loop (10 kg/cm^2) for studying flow mixing in channels.

The flow stability of boiling water in parallel channels under natural and forced circulation is similarly studied. It has been found that mixing between neighboring streams in each phase occurs in an independent manner: the mixing of the steam phase is subject to the Fick law, while the mixing of the liquid phase is determined by the pressure differential between the streams (this differs in principle from the representations of the well-known HAMBO program).

Translated from Atomnaya Énergiya, Vol. 31, No. 2, pp. 180-182, August, 1971.

At the ACEC firm's station, a study of the critical heat flow has been done at a pressure of 157 kg /cm^2 in a flow rate range of 2.5 to 25 million kg/m^{2}h, with input heat contents of more than 200 kcal/kg and steam contents of up to 15% by weight. The experimental results are in agreement with the well-known Tong formula.

At RCN, a study is being done on heat exchange crises in rod groups 1 m long with 0 to 11°C of underheating and a steam content of up to 10%. Experiments are performed on an 850 kW station, allowing thermal loads up to 300 W/cm^2 to be created with coolant temperatures up to 350°C, pressures of up to 260 kg /cm^2, and flow rates of up to 4 kg/sec. At this station, rods were tested under crisis conditions for 300 h (the crisis was characterized by a surface temperature jump of about 100°C).

Extremely interesting experimental studies of volume compensators have been done by a laboratory at Delft University, which has the largest experimental base for these purposes in Western Europe and America. Attempts are being made in the laboratory to achieve characteristics of the steam volume compensators such as would permit a sharp change in the reactor load from 100 to 30% of the nominal power for a volume of water in the volume compensator equal to 10% of the volume of the first circuit and a 1 : 1 ratio of the water and steam volumes in the volume compensator.

2. Atomic power plant safety design studies are being conducted by the ACEC firm. Two basic emergencies are being considered for PWR-type reactors: rupturing of the primary coolant pipes and rupturing of the steam pipes. The studies are applicable to operational reactors (BR = 3, SENA) as well as the atomic power plants under construction at Douel and Tiange.

Emergencies involving rupture of the primary circuit pipes are analyzed in the following manner. A special computer program calculates the changes in coolant mass flow rate and pressure with respect to time and reactor volume (1000 volume points). The results of the calculations are used to determine the forces from the escaping steam jet acting on the internal structures of the reactor and on the external equipment. The data on changes in the coolant flow rate, pressure, and steam content are used to calculate the fuel element envelope temperature, allowing for reaction of the zirconium with water. Also calculated for such an emergency is the strength of the reactor housing walls and safety envelope.

The second emergency – steam pipe rupture – is examined for the end of a run with no boron in the coolant (the composition with the greatest temperature coefficient of reactivity); in addition, it is assumed that one of the most effective regulatory devices is not inserted into the active zone. The program calculates the parameters which characterize the occurrence of a heat exchange crisis in a region where there is no absorbent. Also examined are the mechanical forces occurring in the fuel assemblies when the fuel elements are cooled by water from the steam generators.

3. The delegation became acquainted with work being done on the "Stek" (RCN), "Afina" (the University at Eindhoven), and "Venus" (Mol) critical assemblies.

The "Stek" critical assembly was built mainly for integral measurements of neutron capture cross sections for fission products and materials used in fast reactors. The reactor oscillator method is used for the measurements. The fast neutron zone is located in the center of the assembly and consists of graphite blocks interbedded with layers of metallic uranium (90% U^{235}). Various uranium–carbon atomic ratios (1 : 21, 1 : 33, 1 : 45, 1 : 68, 1 : 92) may be realized to obtain various fast neutron spectra. A ring-shaped zone of thermal neutrons serves as a neutron source for the fast zone. Interpretation of the experiments with the oscillator substantially depend on the neutron spectrum, so the assembly has the equipment necessary to measure the spectrum by various methods: by the activation of Na^{23}, Mn^{55}, Cu^{63}, Mo^{98}, La^{109}, W^{186}, and Au^{197}; by measuring the relative U^{235} and U^{238} fission rates in depleted and enriched foils; by measuring the reaction rate by means of track detectors; and also by the boron filter method from recoil protons and their time of flight.

Fuel samples from HFR "DRAGON" reactors and samples of different isotopes will be used in the experiments. The maximum activity of the samples is 10,000 Ci.

Comparison of the measured effects of the sample reactivities with the calculations will make it possible to pinpoint the microscopic cross sections of the fission products. To obtain more reliable data, it is proposed to use the latest statistical methods to process the experimental results, together with a small computer connected directly to the transducers in the critical assembly.

"Athena" is a research reactor of the "Argonaut" type with a power of up to 10 kW; its active zone consists of two rectangular uranium–water lattices, separated by an internal graphite reflector. There are six horizontal channels, a water basin, and a graphite thermal column. It is proposed to conduct studies on the following topics: a) a detailed study of the physical parameters of the reactor for the purpose of developing rules for safe use in work using both active zones aswell as only one of them; b) perfection of reactor control. Practical use of a multiple point dynamic model is planned for the reactor control system, and also planned are obtaining control information from analysis of neutron noise, developing a control system using information on the economics of the fuel cycle, optimal burning, etc., and also a study of the safety aspects of the reactor when an electronic computer is used for control; c) a study of the Doppler effect in fast neutron spectra with sample temperatures up to 1200°C; d) a study of shielding. The purpose of the experiments is to develop a design model which may be used to predict the optimum weight, cost, volume, etc., of the shielding. Work on the reuse of plutonium in thermal reactors at the Belgian reactor center is of interest. A broad experimental program for the study of the physical characteristics of plutonium-enriched fuel was planned. A large part of the program consists of critical experiments on the "Venus" assembly, which was used earlier for experiments within the frame of the Anglo–Belgian "Vulcan" project. In the experiments stainless steel-jacketed fuel rods 50 cm long are used with various amounts of U^{235} and plutonium enrichment. The first step in the experiments consists of determining the critical masses of the active zones of various configurations, depending on the lattice spacing and the type of fuel. The effects of local irregularities in the lattice (water gaps, absorbers, etc.) are studied, and the distribution of energy production is also measured. The experimental results are used to develop design programs. Experiments are planned with moderator water poisoned with boric acid, and in simulating the working temperature by interspersing thin aluminum rods between the fuel elements.

4. Of great interest to the members of the delegation at Dodenvard was a system for taking measurements inside an atomic power plant reactor. To record the neutron flux in the active zone of the reactor there are 18 channels containing miniature movable fission chambers 5 cm long and 3 mm in diameter. The chamber readings are periodically transmitted to a computer center at Arnhem, where they are processed and compared with the results of the calculated distribution of the energy production field during fuel burning. On this basis, the regulator rod position is corrected in order to limit the fuel temperature, which is the determining parameter in this reaction. An experimental fuel assembly is being prepared at the atomic power plant which will be fitted with transducers to measure flow rate, steam content, temperature, and neutron flux.

At the SENA atomic power plant, an interesting report was presented on experience with repairing reactor equipment after a serious emergency following destruction of the heat shield by vibration caused by hydraulic instability in the coolant flow. During the repairs the shield was completely removed from the vessel, while the reactor pit was repaired by replacing its reinforcements.

During the excursion the delegation visited a factory of the RDM firm which produces high pressure reactor vessels. A vessel is presently being constructed with an internal diameter of 4.8 m, a height of 20 m, and a weight of 400 tons. The shop is equipped to construct a vessel 10 m in diameter, 25 m tall, and weighing up to 1200 tons. The firm has experience in transporting vessels by sea and by highway. A film was shown on the transportation of a vessel 4.8 m in diameter weighing 350 tons on the mountain roads of Spain.

BRIEF COMMUNICATIONS

In February, 1971, an All-Union Science and Technology Seminar on "Nuclear Physical Methods and Apparatus for Qualitative Analysis" was held at the Exhibition of Achievements of the National Economy of the USSR.

The wide acceptance of nuclear physical methods of analysis in geological investigations, prospecting for valuable minerals, and for composition control at nonferrous and ferrous metal refineries, and in the chemical, petrochemical, and petroleum refining industries and other branches of the national economy, was noted in the reports and papers. Representatives of the All-Union Scientific Research Institute of Radiation Technology reported on revised methods and apparatus for express analysis of geological samples and technological specimens and on the successful use of commercial equipment for analysis of element composition. Among these are measurement systems such as the K-1, K-2, NAR-1, NAR-2, and the "Multiplier," which may find wide application in various branches of the national economy.

A large number of reports was concerned with methods and apparatus for x-ray analysis. It was noted that x-ray methods and apparatus have found wide application for analysis of element composition of rocks and ores and their refinement products, and in geological searches and prospecting for nonferrous and ferrous metallurgy, the chemical industry, and other branches of industry. Industry has taken over the production of needed analytical apparatus: Mineral-3, Ferrit, Mayak, Gagara, Spektr, and others.

* * *

In February, 1971, a seminar was held in Kiev on the topic "The Status and Prospects of Applications of Radioisotope Technology by the Plants and Organizations of Kiev." Seminar participants became acquainted with mass-produced instruments for control and automation of technological production processes and with experiences in their application in industrial plants. They saw the operation of a UDAR-5 following content gage and a PR-1024 radioisotope densimeter.

* * *

In February, 1971, a conference of specialists from member nations of Comecon was convened in Dresden on the problems of producing short-lived isotopes, isolated from fission products, in those countries. The results of technical-economic studies on the production of generators for Technetium-99, Iodine-132, Xenon-133, Strontium-89, Yttrium-91, Niobium-95, and others, were examined at the conference. Also considered were possible production volumes to meet the requirements of Comecon member nations for these isotopes, and the technical characteristics of isotope production.

* * *

In January, 1971, a conference of specialists from Comecon member nations was convened in Warsaw on the production of isotope products, in accordance with the working plan of the Comecon Standing Commission on Peaceful Uses of Atomic Energy. Evaluated at the conference were the results of technical-economic studies of the production of the following vital products in Comecon member nations: reactor isotopes (Phosphorus-32, Sulfur-35, Iodine-131, Gold-198); sealed radiation sources (α-, β-, γ-, and Bremsstrahlung sources); and medical applicators. The requirements of Comecon member nations for this production were considered for the 1971-1975 period as well as the production capabilities of the countries, and quantitative parameters and technical characteristics of the products. Proposals were prepared for specialization of the production of these products.

At the same time, a coordinating conference of specialists from the Polish People's Republic and the USSR was held in accordance with an agreement for a program of research on methods of measuring radiophysical parameters of sealed β- and γ-radiation sources. The program provides for the Polish People's

Translated from Atomnaya Énergiya, Vol. 31, No. 2, p. 182, August, 1971.

Republic and the USSR to submit research materials to one another, acquaint each other's specialists with the methods and equipment developed in each country, etc. The final result of this research will be the development of recommendations for the standardization of measurement methods for Comecon member nations.

* * *

In December, 1970, a working conference of representatives of four nuclear data centers was convened in Vienna at the International Atomic Energy Agency. The centers represented were: the National Center for Neutron Cross Sections (Brookhaven, USA); the Center for Compilation of Neutron Data (Saclay, France); the International Atomic Energy Agency Nuclear Data Section (Vienna, Austria); and the Center for Nuclear Data (Obninsk, USSR).

At the present time these four centers are collaborating in collecting information on neutron cross sections (each center in its own geographical zone), codification of the data in one format (ÉKSFOR) interchangeable throughout the entire system, and regular exchange of information in the form of magnetic computer tapes. The following problems were considered at this conference: 1) development of the collection and exchange of experimental data; technical problems of the exchange; additions to the ÉKSFOR system; 2) publication and distribution of a bibliographical reference book for SINDA; 3) the problem of exchanging approximate data, including the problems of formats for approximate neutron data; 4) the agenda of a future international conference in Vienna on approximation methods; 5) the collection and evaluation of nuclear data for problems unrelated to the construction of fission reactors, in particular, data for problems of safeguards, for future thermonuclear reactors, and data on nuclear structure and nuclear reactions.

* * *

In accordance with an Agreement on Cooperation between the State Committee for the Use of Atomic Energy of the USSR and the Atomic Energy Commission of Denmark, a delegation of Danish specialists on atomic waste disposal problems was in the Soviet Union in February 1971.

Members of the delegation visited the Institute of Physical Chemistry of the Academy of Sciences of the USSR, the Zagorsk disposal station, the Moscow decontamination station, the Atomic Energy Pavilion at the Exhibition of Achievements of the National Economy of the USSR, and the Scientific Research Institute for Atomic Reactors. After completion of the visit, the delegation was received by the State Committee for the Use of Atomic Energy.

GROWING CRYSTALS FROM SOLUTION

By T. G. Petrov, E. B. Treivus,
and A. P. Kasatkin

Scientific Research Institute for the Earth's Crust and Crystallography Section Leningrad University, USSR

Translated from Russian by **Albin Tybulewicz**
Editor, "Soviet Physics — Semiconductors"

This highly practical and detailed handbook describes all the major methods of growing crystals from solutions with temperatures up to 100°C at atmospheric pressure. Following a brief review of the theory of crystal growth, the authors describe the technical equipment of a crystallization laboratory, operational procedures, measures for avoiding anomalies in growing crystals, and selection of optimal conditions.

---

106 pages CB Special Research Report 1969 $17.50

PLENUM PUBLISHING CORPORATION
Plenum Press • Consultants Bureau • IFI/Plenum Data Corporation
227 WEST 17th STREET, NEW YORK, N. Y. 10011

In United Kingdom: Plenum Publishing Co. Ltd., Donington House, 30 Norfolk Street, London, W.C. 2.

EFFECTS OF ELECTROMAGNETIC FIELDS ON LIVING ORGANISMS

By **A. S. Presman**
Department of Biophysics
Moscow University

Translated from Russian

Provides the first complete review of both experimental and theoretical data concerning the effects of electromagnetic fields of different frequencies on various organisms, ranging from protozoa to man. Comprehensive in its treatment, the volume surveys the effects of such fields at the molecular, cellular, organic and organismic levels of organization. A pioneer in the field, it focuses on formulating and substantiating the influence of electromagnetic fields of infralow, low, and radio frequencies on life. This innovative and lucid work will be valuable to medical, agricultural and biological research as well as to the solution of some problems of bionics. An extensive bibliography is included.

Approx. 300 pages PP 1970 $25.00

PLENUM PUBLISHING CORPORATION
Plenum Press • Consultants Bureau • IFI/Plenum Data Corporation
227 WEST 17th STREET, NEW YORK, N. Y. 10011

In United Kingdom: Plenum Publishing Co. Ltd., Donington House, 30 Norfolk Street, London, W.C. 2.